



DEVELOPMENT AND *MASH* TL-4 EVALUATION OF TxDOT RUBBER MOUNTED SINGLE SLOPE BARRIER



Crash testing performed at:
TTI Proving Ground
3100 SH 47, Building 7091
Bryan, TX 77807

Test Report 0-6895-R1

Cooperative Research Program

TEXAS A&M TRANSPORTATION INSTITUTE

COLLEGE STATION, TEXAS

TEXAS DEPARTMENT OF TRANSPORTATION

in cooperation with the
Federal Highway Administration and the
Texas Department of Transportation
<http://tti.tamu.edu/documents/0-6895-R1.pdf>

1. Report No. FHWA/TX-18/0-6895-R1		2. Government Accession No.		3. Recipient's Catalog No.	
4. Title and Subtitle DEVELOPMENT AND <i>MASH</i> TL-4 EVALUATION OF TXDOT RUBBER MOUNTED SINGLE SLOPE BARRIER				5. Report Date Published: April 2019	
				6. Performing Organization Code	
7. Author(s) Akram Y. Abu-Odeh, Michael S. Brackin, Nathan D. Schulz, James C. Kovar, Raissa D. Ferron, Sanjida Ahsan, Michael Rung, Wanda L. Menges, and Darrell L. Kuhn				8. Performing Organization Report No. Report 0-6895-R1	
9. Performing Organization Name and Address Texas A&M Transportation Institute College Station, Texas 77843-3135				10. Work Unit No. (TRAVIS)	
				11. Contract or Grant No. Project 0-6895	
12. Sponsoring Agency Name and Address Texas Department of Transportation Research and Technology Implementation Office 125 E. 11th Street Austin, Texas 78701-2483				13. Type of Report and Period Covered Technical Report: July 2015–February 2018	
				14. Sponsoring Agency Code	
15. Supplementary Notes Project performed in cooperation with the Texas Department of Transportation and the Federal Highway Administration. Project Title: Development of Low-Maintenance Cost Median Barriers with Enhanced Safety Features URL: http://tti.tamu.edu/documents/0-6895-R1.pdf					
16. Abstract <p>Median barriers are used as a separation between two opposing traffic lanes on divided highways. Typically, rigid median barriers are made of reinforced concrete using safety or single slope profiles. These barriers are positively constructed as an integral part of the roadway through starter bars or other construction means. A damaged rigid median barrier typically requires lane closures, which results in congestion in addition to costs associated with the repair of the damaged section.</p> <p>Texas A&M Transportation Institute (TTI) researchers designed a new generation of median barriers for Texas Department of Transportation (TxDOT) through computer simulation and state of the art optimization technologies to maximize the performance of the barrier in terms of safety, while incorporating low-maintenance cost features in the design. TTI researchers reviewed traditional and non-traditional construction material and technologies for use in this new design. Full-scale crash testing was conducted according to the latest version of American Association of State Highway and Transportation Officials <i>Manual for Assessing Safety Hardware (MASH)</i> standards to validate the crashworthiness of the system.</p> <p>The TxDOT Rubber Mounted Single Slope Barrier performed acceptably for <i>MASH</i> TL-4.</p>					
17. Key Words Longitudinal Barrier, Median Barrier, Low Maintenance Cost, Concrete Barrier, Crash Testing, Roadside Safety			18. Distribution Statement No restrictions. This document is available to the public through NTIS: National Technical Information Service Alexandria, Virginia http://www.ntis.gov		
19. Security Classif.(of this report) Unclassified		20. Security Classif.(of this page) Unclassified		21. No. of Pages 290	22. Price

DEVELOPMENT AND MASH TL-4 EVALUATION OF TXDOT RUBBER MOUNTED SINGLE SLOPE BARRIER

by

Akram Y. Abu-Odeh, Ph.D.

Research Scientist

Texas A&M Transportation Institute

Michael S. Brackin, Ph.D., P.E.

Instructional Assistant Professor

Zachry Department of Civil Engineering

Nathan D. Schulz

Associate Transportation Researcher

Texas A&M Transportation Institute

James C. Kovar, E.I.T.

Associate Transportation Researcher

Texas A&M Transportation Institute

Raissa D. Ferron, Ph.D.

Associate Professor, Civil, Architectural, and Environmental Engineering

University of Texas at Austin

Sanjida Ahsan

Graduate Research Assistant, Civil, Architectural, and Environmental Engineering

University of Texas at Austin

Michael Rung

Technical Staff Assistant V, Center for Transportation Research

University of Texas at Austin

Wanda L. Menges

Research Specialist

Texas A&M Transportation Institute

and

Darrell L. Kuhn, P.E.

Research Specialist

Texas A&M Transportation Institute

Report 0-6895-R1

Project 0-6895

Project Title: Development of Low-Maintenance Cost Median Barriers
with Enhanced Safety Features

Performed in cooperation with the
Texas Department of Transportation
and the

Federal Highway Administration

Published: April 2019

TEXAS A&M TRANSPORTATION INSTITUTE
College Station, Texas 77843-3135

DISCLAIMER

This research was performed in cooperation with the Texas Department of Transportation (TxDOT) and the Federal Highway Administration (FHWA). The contents of this report reflect the views of the authors, who are responsible for the facts and the accuracy of the data presented herein. The contents do not necessarily reflect the official view or policies of the FHWA or TxDOT. This report does not constitute a standard, specification, or regulation. The researcher in charge of this project was Akram Y. Abu-Odeh. The United States Government and the State of Texas do not endorse products or manufacturers. Trade or manufacturers' names appear herein solely because they are considered essential to the object of this report.

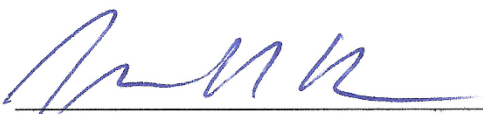
TTI PROVING GROUND DISCLAIMER

The results of the crash testing reported herein apply only to the article being tested.




Wanda L. Menges, Research Specialist
Deputy Quality Manager


Darrell L. Kuhn, Research Specialist
Quality Manager


Matthew N. Robinson, Senior Research Specialist
Technical Manager

ACKNOWLEDGMENTS

This research project was conducted under a cooperative program between the Texas A&M Transportation Institute, the Texas Department of Transportation, and the Federal Highway Administration. The TxDOT project manager for this research was Wade Odell, Research and Technology Implementation. Technical support and guidance were provided by Christopher Lindsey (Design Division). The authors acknowledge and appreciate their assistance. The authors acknowledge the computational support provided by the Texas A&M High Performance Research Computing (HPRC) (<http://hprc.tamu.edu/>). The authors appreciate the HPRC facility assistance. The authors also wish to thank the assistance of Jeff Hirsch, Melissa Martinez, and Nataly de la Fuente.

The research team acknowledges the support of different suppliers and producers: Genan Inc for their generous donation of recycled tire rubber samples, Texas Lehigh for cement, ABC polymers, Forta corporation, Concrete Fiber Solution (CFS), FRC industries for fibers. Headwater Inc. for fly ash, Martin Marrietta for aggregates (both coarse and fine), L&M supplier for the geogrids.

We also thank undergraduate research assistants, Mr. Dan Sin and Ms. Jessica Milligan for their support, hard work, and dedication to the project.

Support for Texas Department of Transportation facility at Cedar park with flexural testing setup is highly appreciated, especially Ms. Rachel Cano for her assistance and coordination in performing flexural testing and all other staff at Cedar Park TxDOT facility who helped us in this process.

Sincere gratitude is also extended to Dr. Tom Juenger for making the spectrophotometer available for project use.

TABLE OF CONTENTS

	Page
List of Figures	xiii
List of Tables	xxii
Chapter 1: Introduction	1
Chapter 2: Review of Concrete Barrier Shapes	3
2.1 The Single Slope Barrier Profile.....	3
2.1.1 TTI Test 420020-9b	4
2.1.2 Simulation of TTI Test 420020-9b	5
2.1.3 TTI Test No. 9-1002-3 Pan Form— <i>MASH</i> 3-11	5
2.1.4 <i>MASH</i> Test 4-11 Simulation of the Texas SSTR.....	8
2.1.5 <i>MASH</i> 4-10 Test of the Texas Single Slope Barrier	12
2.2 <i>MASH</i> Evaluation of the California Department of Transportation (Caltrans) 60G Barrier	14
2.2.1 <i>MASH</i> Test 4-10 of the Caltrans Type 60G Barrier.....	14
2.2.2 <i>MASH</i> Test 4-11 of Caltrans Type 60G Barrier.....	16
2.2.3 MwRSF Hybrid Concrete Barrier with Rubber and Steel Posts.....	19
2.3 Augmenting the Concrete Barrier with Elastic Rubber Fender	20
2.4 Conclusion	21
Chapter 3: Identification and Characterization of Materials	23
3.1 Identification of Candidate Material	23
3.2 Literature Review on Candidate Material	23
3.2.1 Geogrid	23
3.2.2 Recycled Tire Rubber	24
3.2.3 Class F Fly Ash (F-ash)	26
3.2.4 Reclaimed Asphalt Pavement (RAP).....	26
3.2.5 Fiber	27
3.3 Material Properties and Characterization.....	28
3.3.1 Aggregates	28
3.3.2 Fiber	28
3.3.3 Geogrid	30
3.4 Summary of Literature Review.....	30
3.5 Mortar and Concrete Evaluation.....	30
3.5.1 Testing and Evaluation Methods	31
3.5.2 Initial Phase Testing Results.....	34
3.5.3 Second Phase Testing Results.....	45
3.5.4 Selection of Concrete Mixtures for Field Bogie Testing	47
3.5.5 Additional Tasks Performed	48
3.6 Conclusions on Material Testing and Evaluation	52
Chapter 4: Design Process	53
4.1 Pickup Truck Median Barrier	53
4.1.1 Four 40-ft Segments Configuration	53
4.1.2 Four 40-Ft Segments – Two Rubber Fenders	54
4.1.3 Four 40-Ft Segments – Three Rubber Fenders	59
4.1.4 Three 60-Ft Segments – Two Rubber Fenders	64

TABLE OF CONTENTS (CONTINUED)

	Page
4.1.5 Three 60-Ft Segments – Three Rubber Fenders	69
4.2 SUT Median Barrier	74
4.2.1 Two 40 Ft Segment – Three Rubber Fenders	74
4.2.2 Two 60-Ft Segments – Three Rubber Fenders	79
4.3 Simulations of Recommended Design Concepts	84
4.3.1 Simulation: Critical Impact Point 1-ft Offset.....	85
4.3.2 Simulation: Critical Impact Point 3-Ft Offset.....	88
4.3.3 Simulation: Critical Impact Point 5-Ft Offset.....	92
4.4 Summary of Critical Impact Simulations	96
4.5 Recommended System Design	97
Chapter 5: Bogie Testing.....	99
5.1 Bogie Testing – Phase I	99
5.1.1 Test Article Design and Construction.....	99
5.1.2 Weather Conditions:	101
5.1.3 Test Vehicle	101
5.1.4 Test No. 468957-B4.....	101
5.1.5 Test No. 468957-B5.....	105
5.1.6 Test No. 468957-B6.....	107
5.1.7 Test No. 468957-B7	110
5.1.8 Summary – Bogie Testing Phase I.....	113
5.2 Bogie Testing – Phase II.....	117
5.2.1 Test Article Design and Construction.....	117
5.2.2 Test Vehicle	118
5.2.3 Test No. 468957-B8 – Class C Concrete	119
5.2.4 Test No. 468957-B9 – PR5FCR5F Concrete.....	124
5.2.5 Test No. 468957-B10 – CR10F-Gnet Mix Concrete	129
5.2.6 Summary – Bogie Testing Phase II	134
5.3 Summary and Conclusions	136
Chapter 6: System Details.....	139
6.1 Test Article and Installation Details	139
6.2 Material Specifications	140
Chapter 7: Test Requirements and Evaluation Criteria.....	145
7.1 Crash Test Matrix	145
7.2 Evaluation Criteria	147
Chapter 8: Test Conditions.....	149
8.1 Test Facility	149
8.2 Vehicle Tow and Guidance system.....	149
8.3 Data Acquisition Systems	149
8.3.1 Vehicle Instrumentation and Data Processing	149
8.3.2 Anthropomorphic Dummy Instrumentation	150
8.3.3 Photographic Instrumentation and Data Processing	151

TABLE OF CONTENTS (CONTINUED)

	Page
Chapter 9: MASH Test 4-10 (Crash Test No. 468958-3)	153
9.1 Test Designation and Actual Impact Conditions	153
9.2 Weather Conditions	153
9.3 Test Vehicle	153
9.4 Test Description	154
9.5 Damage to Test Installation	154
9.6 Damage to Test Vehicle.....	155
9.7 Occupant Risk Factors	156
Chapter 10: MASH Test 4-11 (Crash Test No. 468958-2)	159
10.1 Test Designation and Actual Impact Conditions	159
10.2 Weather Conditions	159
10.3 Test Vehicle	159
10.4 Test Description	160
10.5 Damage to Test Installation	160
10.6 Damage to Test Vehicle.....	162
10.7 Occupant Risk Factors	162
Chapter 11: MASH Test 4-12 (Crash Test No. 468958-1)	167
11.1 Test Designation and Actual Impact Conditions	167
11.2 Weather Conditions	167
11.3 Test Vehicle	167
11.4 Test Description	168
11.5 Damage to Test Installation	168
11.6 Damage to Test Vehicle.....	171
11.7 Occupant Risk Factors	172
Chapter 12: Studies of Coatings	175
12.1 Background Study on Coatings	175
12.2 Coating Performance Evaluation	175
12.2.1 Water Absorption.....	176
12.2.2 Surface Color Measurement	178
12.3 Conclusion on Studies on Coatings	179
Chapter 13: Summary and Conclusions	181
13.1 Assessment of Crash Test Results	181
13.2 Conclusions.....	181
Chapter 14: Implementation Statement	187
References	191
Appendix A. Material Source, Type, and Physical Properties	197
Appendix B: Bogie Testing Phase I	201
B.1 Test Article Details	201
B.2 Material Certification Documents.....	207
Appendix C. Details Of The Pipe Cylinders For Nose Of Bogie	209
Appendix D. Test Article Details – Bogie Testing Phase II	211
Appendix E. Details of the TxDOT Rubber Mounted Single Slope Barrier	213
Appendix F. Supporting Certification Documents	217

TABLE OF CONTENTS (CONTINUED)

	Page
Appendix G. MASH Test 4-10 (Crash Test No. 468958-3)	223
G.1 Vehicle Properties and Information	223
G.2 Sequential Photographs.....	226
G.3 Vehicle Angular Displacement	229
G.4 Vehicle Accelerations	230
Appendix H. MASH Test 4-11 (Crash Test No. 468958-2)	237
H.1 Vehicle Properties and Information	237
H.2 Sequential Photographs.....	241
H.3 Vehicle Angular Displacement	243
H.4 Vehicle Accelerations	244
Appendix I. MASH Test 4-10 (Crash Test No. 468958-1)	251
I.1 Vehicle Properties and Information	251
I.2 Sequential Photographs.....	253
I.3 Vehicle Angular Displacement	255
I.4 Vehicle Accelerations	256
Appendix J. Recommended TxDOT Rubber Mounted Single Slope Barrier	263

LIST OF FIGURES

		Page
Figure 2.1.	Common New Jersey Shape (Left) and F-Shape (Right) Concrete Barriers.....	3
Figure 2.2.	Texas Single Slope (Left) and Caltrans (Right) Barrier Profiles.....	4
Figure 2.3.	Sequences Showing SUT Impacting a 36-inch Tall Texas SSTR.....	5
Figure 2.4.	Sequential Photo Comparison between Test and Simulation of <i>MASH</i> Test 4-12 (SUT) Test of Texas 36-inch SSTR.	6
Figure 2.5.	Summary of Results for <i>MASH</i> Test 3-11 on TxDOT Pan-Formed Bridge Rail.....	7
Figure 2.6.	Sequential Comparison of Pan Form Test (Right) and Simulation (Left) under <i>MASH</i> Test 3-11 Impact Conditions.....	8
Figure 2.7.	Longitudinal Acceleration for <i>MASH</i> Test 3-11 on TxDOT Pan-Formed Bridge Rail.....	9
Figure 2.8.	Lateral Acceleration for <i>MASH</i> Test 3-11 on TxDOT Pan-Formed Bridge Rail.....	10
Figure 2.9.	Angular Displacements for <i>MASH</i> Test 3-11 on TxDOT Pan-Formed Bridge Rail.....	10
Figure 2.10.	Longitudinal Acceleration History from Simulated <i>MASH</i> Test 4-11 of Texas SSTR.....	11
Figure 2.11.	Lateral Acceleration History from Simulated <i>MASH</i> Test 4-11 of Texas SSTR.....	11
Figure 2.12.	Angular Displacement History from Simulated <i>MASH</i> Test 4-11 of Texas SSTR.....	11
Figure 2.13.	Sequential Simulation Images of <i>MASH</i> Test 4-10 of Texas SSTR.....	12
Figure 2.14.	Longitudinal Acceleration History from Simulated <i>MASH</i> Test 4-10 of Texas SSTR.....	13
Figure 2.15.	Lateral Acceleration History from Simulated <i>MASH</i> Test 4-10 of Texas SSTR.....	13
Figure 2.16.	Angular Displacement History from Simulated <i>MASH</i> Test 4-10 of Texas SSTR.....	14
Figure 2.17.	Sequential Simulation Images of <i>MASH</i> Test 4-10 of Caltrans 60G Barrier.....	15
Figure 2.18.	Acceleration and Euler Angles Histories from Simulated <i>MASH</i> Test 4-10 of Caltrans Type 60G Barrier.....	16
Figure 2.19.	Sequential Simulation Images of <i>MASH</i> Test 4-11 (Pickup) of Caltrans 60G Barrier.....	17
Figure 2.20.	Acceleration from Simulated <i>MASH</i> Test 4-11 of Caltrans Type 60G Barrier.....	18
Figure 2.21.	Euler Angles Histories from Simulated <i>MASH</i> Test 4-11 of Caltrans Type 60G Barrier.....	19
Figure 2.22.	Concrete Beam Barrier with Alternating Steel and Rubber Post from MwRSF.....	19
Figure 2.23.	Single Slope Barrier with Two Rubber Fenders.....	20

LIST OF FIGURES (CONTINUED)

	Page
Figure 2.24. Close-up Details of Single Rubber Fender Inserted within the Concrete Barrier.	21
Figure 3.1. Images for Uniaxial, Biaxial, and Triaxial Geogrid.	23
Figure 3.2. Fibers Selected for Screening Study.	29
Figure 3.3. Biaxial Geogrid Aperature Dimensions.	30
Figure 3.4. Load-Deflection Curve for Gnet.25 Sample.	34
Figure 3.5. Experimental Set-Up for Impact Testing.	35
Figure 3.6. 28 Days-Flexural Toughenss Results for Geogrid Samples.	39
Figure 3.7. 28-Days Flexural Strength Test Results for Geogrid Samples.	39
Figure 3.8. Number of Blows to Initial Crack Data Comparison for Geogrid Samples and Control.	40
Figure 3.9. Initial Screening 28-Days Compressive Strength Test Results for Rubber Series.	41
Figure 3.10. Load-Deflection Curve for Control Concrete and PR10F and PR20F under Flexural Loading.	41
Figure 3.11. Initial Screening 28-Days Flexural Toughness Test Results for Rubber Series.	42
Figure 3.12. Initial Screening 28-Days Flexural Strength Test Results for Rubber Series.	42
Figure 3.13. Initial Screening 28-Days Compressive Strength of RAP Series.	43
Figure 3.14. Initial Screening 28-Days Flexural Strength of RAP Series.	44
Figure 3.15. Initial Screening 28-Days Flexural Toughness of RAP Series.	44
Figure 3.16. Initial Screening 28-Days Impact Resistance of RAP Series.	45
Figure 3.17. Comparison Plots of Concrete Mixture Characteristics.	47
Figure 3.18. Bulk Resistivity Test Results for Cores Collected from Barriers Tested in Bogie Impact Field Test.	48
Figure 3.19. Images of Crack Pattern and Maximum Crack Width Measurement of CR10FGnet, Control, and PR5FCR5F Mixtures after Field Bogie Impact Test.	50
Figure 3.20. Drop Analysis on Surface of Rubber using ImageJ Plugin.	51
Figure 4.1. Four – 40-ft Segments Configuration.	53
Figure 4.2. Three – 60-ft Segments Configuration.	53
Figure 4.3. Lateral Force on Barrier 2 (Four 40-ft Segments – Two Rubber Fenders).	54
Figure 4.4. Lateral Force on Barrier 3 (Four 40-ft Segments – Two Rubber Fenders).	54
Figure 4.5. Deflection at Joint 1 (Four 40-ft Segments – Two Rubber Fenders).	55
Figure 4.6. Deflection at Joint 2 (Four 40-ft Segments – Two Rubber Fenders).	55
Figure 4.7. Deflection at Joint 3 (Four 40-ft Segments – Two Rubber Fenders).	56
Figure 4.8. Deflection of Barrier System (Four 40-ft Segments – Two Rubber Fenders).	56
Figure 4.9. Vehicle Interaction with Barrier (Four 40-ft Segments – Two Rubber Fenders).	56
Figure 4.10. Vehicle Angular Displacement (Four 40-ft Segments – Two Rubber Fenders).	57

LIST OF FIGURES (CONTINUED)

		Page
Figure 4.11.	Vehicle Longitudinal Acceleration Trace (Four 40-ft Segments – Two Rubber Fenders).....	58
Figure 4.12.	Vehicle Lateral Acceleration Trace (Four 40-ft Segments – Two Rubber Fenders).....	58
Figure 4.13.	Vehicle Vertical Acceleration Trace (Four 40-ft Segments – Two Rubber Fenders).....	58
Figure 4.14.	Lateral Force on Barrier 2 (Four 40-ft Segments – Three Rubber Fenders).	59
Figure 4.15.	Lateral Force on Barrier 3 (Four 40-ft Segments – Three Rubber Fenders).	59
Figure 4.16.	Deflection at Joint 1 (Four 40-ft Segments – Three Rubber Fenders).....	60
Figure 4.17.	Deflection at Joint 2 (Four 40-ft Segments – Three Rubber Fenders).....	60
Figure 4.18.	Deflection at Joint 3 (Four 40-ft Segments – Three Rubber Fenders).....	61
Figure 4.19.	Deflection of Barrier System (Four 40-ft Segments – Three Rubber Fenders).....	61
Figure 4.20.	Vehicle Interaction with Barrier (Four 40-ft Segments – Three Rubber Fenders).....	61
Figure 4.21.	Vehicle Angular Displacements (Four 40-ft Segments – Three Rubber Fenders).....	62
Figure 4.22.	Vehicle Longitudinal Acceleration Trace (Four 40-ft Segments – Three Rubber Fenders).....	63
Figure 4.23.	Vehicle Lateral Acceleration Trace (Four 40-ft Segments – Three Rubber Fenders).....	63
Figure 4.24.	Vehicle Vertical Acceleration Trace (Four 40-ft Segments – Three Rubber Fenders).....	63
Figure 4.25.	Lateral Force on Barrier 1 (Three 60-ft Segments – Two Rubber Fenders).....	64
Figure 4.26.	Lateral Force on Barrier 2 (Three 60-ft Segments – Two Rubber Fenders).....	64
Figure 4.27.	Deflection at Joint 1 (Three 60-ft Segments – Two Rubber Fenders).....	65
Figure 4.28.	Deflection at Joint 2 (Three 60-ft Segments – Two Rubber Fenders).....	65
Figure 4.29.	Deflection of Barrier System (Three 60-ft Segments – Two Rubber Fenders).....	66
Figure 4.30.	Vehicle Interaction with Barrier (Three 60-ft Segments – Two Rubber Fenders).....	66
Figure 4.31.	Vehicle Angular Displacements (Three 60-ft Segments – Two Rubber Fenders).....	67
Figure 4.32.	Vehicle Longitudinal Acceleration Trace (Three 60-ft Segments – Two Rubber Fenders).....	68
Figure 4.33.	Vehicle Lateral Acceleration Trace (Three 60-ft Segments – Two Rubber Fenders).....	68
Figure 4.34.	Vehicle Vertical Acceleration Trace (Three 60-ft Segments – Two Rubber Fenders).....	68
Figure 4.35.	Lateral Force on Barrier 1 (Three 60-ft Segments – Three Rubber Fenders).....	69
Figure 4.36.	Lateral Force on Barrier 2 (Three 60-ft Segments – Three Rubber Fenders).....	69

LIST OF FIGURES (CONTINUED)

		Page
Figure 4.37.	Deflection at Joint 1 (Three 60-ft Segments – Three Rubber Fenders).....	70
Figure 4.38.	Deflection at Joint 2 (Three 60-ft Segments – Three Rubber Fenders).....	70
Figure 4.39.	Deflection of Barrier System (Three 60-ft Segments – Three Rubber Fenders).....	71
Figure 4.40.	Vehicle Interaction with Barrier System (Three 60-ft Segments – Three Rubber Fenders).....	71
Figure 4.41.	Vehicle Angular Displacements (Three 60-ft Segments – Three Rubber Fenders).....	72
Figure 4.42.	Vehicle Longitudinal Acceleration Trace (Three 60-ft Segments – Three Rubber Fenders).....	73
Figure 4.43.	Vehicle Lateral Acceleration Trace (Three 60-ft Segments – Three Rubber Fenders).....	73
Figure 4.44.	Vehicle Vertical Acceleration Trace (Three 60-ft Segments – Three Rubber Fenders).....	73
Figure 4.45.	Two 40-ft Segment Configuration.....	74
Figure 4.46.	Two 60-ft Segment Configuration.....	74
Figure 4.47.	Lateral Force on Barrier System (Two 40-ft Segment Configuration – Three Rubber Fenders).	75
Figure 4.48.	Deflection at Joint 1 (Two 40-ft Segment Configuration – Three Rubber Fenders).....	75
Figure 4.49.	Maximum Deflection of Barrier System (Two 40-ft Segment Configuration – Three Rubber Fenders).....	76
Figure 4.50.	Vehicle Interaction with Barrier System at Maximum Deflection (Two 40- ft Segments – Three Rubber Fenders).	76
Figure 4.51.	Vehicle Angular Displacement (Two 40-ft Segments – Three Rubber Fenders).....	77
Figure 4.52.	Vehicle Longitudinal Acceleration Trace (Two 40-ft Segments – Three Rubber Fenders).....	78
Figure 4.53.	Vehicle Lateral Acceleration Trace (Two 40-ft Segments – Three Rubber Fenders).....	78
Figure 4.54.	Vehicle Vertical Acceleration Trace (Two 40-ft Segments – Three Rubber Fenders).....	78
Figure 4.55.	Lateral Force on Barrier System (Two 60-ft Segments – Three Rubber Fenders).....	79
Figure 4.56.	Deflection at Joint 1 (Two 60-ft Segments – Three Rubber Fenders).....	80
Figure 4.57.	Maximum Deflection of Barrier System (Two 60-ft Segments – Three Rubber Fenders).....	80
Figure 4.58.	Vehicle Interaction with Barrier System at Maximum Deflection (Two 60- ft Segments – Three Rubber Fenders).	81
Figure 4.59.	Vehicle Angular Displacement (Two 60-ft Segments – Three Rubber Fenders).....	82
Figure 4.60.	Vehicle Longitudinal Acceleration Trace (Two 60-ft Segments – Three Rubber Fenders).....	82

LIST OF FIGURES (CONTINUED)

		Page
Figure 4.61.	Vehicle Lateral Acceleration Trace (Two 60-ft Segments – Three Rubber Fenders).....	82
Figure 4.62.	Vehicle Vertical Acceleration Trace (Two 60-ft Segments – Three Rubber Fenders).....	83
Figure 4.63.	Plan View of Impact Configurations.	84
Figure 4.64.	Elevation View of Impact Configurations.	84
Figure 4.65.	Plan View of Impact Configuration with 1-ft Offset.	85
Figure 4.66.	Elevation View of Impact Configuration with 1-ft Offset.	85
Figure 3.67.	Deflection at Joint 1: Impact 1 ft from Joint.	85
Figure 4.68.	Simulation Maximum Deflection at .0225 s.	86
Figure 4.69.	Vehicle Roll, Pitch, and Yaw Angles-1-ft Offset.	87
Figure 4.70.	Vehicle Longitudinal Acceleration-1-ft Offset.	87
Figure 4.71.	Vehicle Lateral Acceleration-1-ft Offset.	87
Figure 4.72.	Vehicle Vertical Acceleration-1-ft Offset.	88
Figure 4.73.	Plan View of Impact Configuration with 3-ft Offset.	88
Figure 4.74.	Elevation View of Impact Configuration with 3-ft Offset.	88
Figure 4.75.	Deflection at Joint: Impact 3 ft from Joint.	89
Figure 4.76.	Simulation Maximum Deflection at 0.023 s.	89
Figure 4.77.	Vehicle Roll, Pitch, and Yaw Angles-3-ft Offset.	90
Figure 4.78.	Vehicle Longitudinal Acceleration-3-ft Offset.	91
Figure 4.79.	Vehicle Lateral Acceleration-3-ft Offset.	91
Figure 4.80.	Vehicle Vertical Acceleration-3-ft Offset.	92
Figure 4.81.	Plan View of Impact Configurations with 5-ft Offset.	92
Figure 4.82.	Elevation View of Impact Configuration with 5-ft Offset.	92
Figure 4.83.	Deflection at Joint 1: Impact 5 ft from Joint.	93
Figure 4.84.	Simulation Maximum Deflection at 0.245 s.	93
Figure 4.85.	Vehicle Roll, Pitch, and Yaw Angles-5-ft Offset.	94
Figure 4.86.	Vehicle Longitudinal Acceleration-5-ft Offset.	95
Figure 4.87.	Vehicle Lateral Acceleration-5-ft Offset.	95
Figure 4.88.	Vehicle Vertical Acceleration-5-ft Offset.	96
Figure 5.1.	Single-Slope Median Barrier with Shear Fender Anchor Plate before Test No. 468957-B4.	100
Figure 5.2.	Bogie Vehicle before Test No. 468957-B4.	101
Figure 5.3.	Right Traffic Side of Barrier after Test No. 468957-B4.	102
Figure 5.4.	Center and Left Traffic Side of Barrier after Test No. 468957-B4.	102
Figure 5.5.	Traffic Face of Barrier after Test No. 468957-B4.	102
Figure 5.6.	Top of Barrier after Test No. 468957-B4.	103
Figure 5.7.	Field Side-Center of Barrier after Test No. 468957-B4.	103
Figure 5.8.	Bogie Vehicle after Test No. 468957-B4.	104
Figure 5.9.	Longitudinal Accelerometer Trace during Test No. 468957-B4.	104
Figure 5.10.	Impact Forces during Test No. 468957-B4.	105
Figure 5.11.	Impact Side of Barrier after Test No. 468957-B5.	105
Figure 5.12.	Field Side-Center of Barrier after Test No. 468957-B5.	106

LIST OF FIGURES (CONTINUED)

		Page
Figure 5.13.	Bogie Vehicle after Test No. 468957-B5.	106
Figure 5.14.	Longitudinal Acceleration during Test No. 468957-B5.	107
Figure 5.15.	Impact Force during Test No. 468957-B5.	107
Figure 5.16.	Impact Side of Barrier after Test No. 468957-B6.	108
Figure 5.17.	Field Side of Barrier after Test No. 468957-B6.	108
Figure 5.18.	Bogie Vehicle after Test No. 468957-B6.	109
Figure 5.19.	Longitudinal Acceleration during Test No. 468957-B6.	109
Figure 5.20.	Impact Force during Test No. 468957-B6.	110
Figure 5.21.	Impact Side of Barrier after Test No. 468957-B7.	111
Figure 5.22.	Field Side of Barrier after Test No. 468957-B7.	111
Figure 5.23.	Crack in Block after Test No. 468957-B7.	112
Figure 5.24.	Bogie Vehicle after Test No. 468957-B7.	112
Figure 5.25.	Longitudinal Acceleration during Test No. 468957-B7.	113
Figure 5.26.	Impact Force during Test No. 468957-B7.	113
Figure 5.27.	Bogie Vehicle before Testing.	118
Figure 5.28.	TxDOT Class C Concrete Barrier before Test No. 468957-B8.	119
Figure 5.29.	Right End and Field Side of Barrier after Test No. 468957-B8.	120
Figure 5.30.	Left End and Traffic Side of Barrier after Test No. 468957-B8.	120
Figure 5.31.	Traffic Face of Barrier after Test No. 468957-B8.	120
Figure 5.32.	Top of Barrier after Test No. 468957-B8.	121
Figure 5.33.	Field Side-Center of Barrier after Test No. 468957-B8.	121
Figure 5.34.	Bogie Vehicle after Test No. 468957-B8.	122
Figure 5.35.	Longitudinal Accelerometer Trace during Test No. 468957-B8.	123
Figure 5.36.	Impact Forces during Test No. 468957-B8.	123
Figure 5.37.	PR5FCR5F Mix Concrete Barrier before Test No. 468957-B9.	124
Figure 5.38.	Right End and Field Side of Barrier after Test No. 468957-B9.	125
Figure 5.39.	Left End and Traffic Side of Barrier after Test No. 468957-B9.	125
Figure 5.40.	Traffic Face of Barrier after Test No. 468957-B9.	125
Figure 5.41.	Top Field Side of Barrier after Test No. 468957-B9.	126
Figure 5.42.	Field Side-Center of Barrier after Test No. 468957-B9.	126
Figure 5.43.	Bogie Vehicle after Test No. 468957-B9.	127
Figure 5.44.	Longitudinal Accelerometer Trace during Test No. 468957-B9.	128
Figure 5.45.	Impact Forces during Test No. 468957-B9.	128
Figure 4.46.	CR10F-Gnet Mix Concrete Barrier before Test No. 468957-B10.	129
Figure 5.47.	Right End and Field Side of Barrier after Test No. 468957-B10.	130
Figure 5.48.	Left End and Traffic Side of Barrier after Test No. 468957-B10.	130
Figure 5.49.	Traffic Face of Barrier after Test No. 468957-B10.	130
Figure 5.50.	Top of Barrier after Test No. 468957-B10.	131
Figure 5.51.	Field Side-Center of Barrier after Test No. 468957-B10.	131
Figure 4.52.	Bogie Vehicle after Test No. 468957-B10.	132
Figure 5.53.	Longitudinal Accelerometer Trace during Test No. 468957-B10.	133
Figure 5.54.	Impact Forces during Test No. 468957-B10.	133
Figure 6.1.	Overall Details of the TxDOT Rubber Mounted Single Slope Barrier.	141

LIST OF FIGURES (CONTINUED)

		Page
Figure 6.2.	TxDOT Rubber Mounted Single Slope Barrier prior to <i>MASH</i> Tests 4-10 and 4-11.	142
Figure 6.3.	Straps Used on TxDOT Rubber Mounted Single Slope Barrier prior to <i>MASH</i> Test 4-12.....	143
Figure 7.1.	Target CIP for <i>MASH</i> Test 4-10 (Test No. 468958-3) on the TxDOT Rubber Mounted Single Slope Barrier.....	145
Figure 7.2.	Target CIP for <i>MASH</i> Test 4-11 (Test No. 468958-2) on the TxDOT Rubber Mounted Single Slope Barrier.....	146
Figure 7.3.	Target CIP for <i>MASH</i> Test 4-12 (Test No. 468958-1) on the TxDOT Rubber Mounted Single Slope Barrier.....	146
Figure 9.1.	TxDOT Rubber Mounted Single Slope Barrier/Test Vehicle Geometrics for Test No. 468958-3.....	153
Figure 9.2.	Test Vehicle before Test No. 468958-3.....	154
Figure 9.3.	TxDOT Rubber Mounted Single Slope Barrier after Test No. 468958-3.....	155
Figure 9.4.	Test Vehicle after Test No. 468958-3.....	156
Figure 9.5.	Interior of Test Vehicle for Test No. 468958-3.....	156
Figure 9.6.	Summary of Results for <i>MASH</i> Test 4-10 on the TxDOT Rubber Mounted Single Slope Barrier.....	158
Figure 10.1.	TxDOT Rubber Mounted Single Slope Barrier/Test Vehicle Geometrics for Test No. 468958-2.....	159
Figure 10.2.	Test Vehicle before Test No. 468958-2.....	160
Figure 10.3.	TxDOT Rubber Mounted Single Slope Barrier after Test No. 468958-2.....	161
Figure 10.4.	Damage to Barrier #1 after Test No. 468958-2.....	161
Figure 10.5.	Damage to Barrier #2 after Test No. 468958-2.....	162
Figure 10.6.	Test Vehicle after Test No. 468958-2.....	163
Figure 10.7.	Interior of Test Vehicle for Test No. 568958-2.....	163
Figure 10.8.	Summary of Results for <i>MASH</i> Test 4-11 on the TxDOT Rubber Mounted Single Slope Barrier.....	165
Figure 11.1.	TxDOT Rubber Mounted Single Slope Barrier/Test Vehicle Geometrics for Test No. 468958-1.....	167
Figure 11.2.	Test Vehicle before Test No. 468958-1.....	168
Figure 11.3.	TxDOT Rubber Mounted Single Slope Barrier/Test Vehicle after Test No. 468958-3.....	169
Figure 11.4.	Damage to Barrier #2 after Test No. 468958-3.....	169
Figure 11.5.	Damage to Barrier #3 after Test No. 468958-3.....	170
Figure 11.6.	Damage to Field Side of Barrier after Test No. 468958-3.....	171
Figure 11.7.	Test Vehicle after Test No. 468958-3.....	172
Figure 11.8.	Interior of Test Vehicle for Test No. 468958-3.....	172
Figure 11.9.	Summary of Results for <i>MASH</i> Test 4-10 on the TxDOT Rubber Mounted Single Slope Barrier.....	174
Figure 12.1.	Plots for Percent Absorbance at Discrete Time Intervals in Days for Samples (a) Control, (b) PR5FCR5F, and (c) CR10FGnet.....	177

LIST OF FIGURES (CONTINUED)

		Page
Figure 12.2.	Change in Percent Bulk Resistivity of Coated Samples Compared to No-Coat Samples at Day 31.....	178
Figure 12.3.	Visual Interpretation of Colors Measured on (a) FN Coated, (b) TPX Coated, and (c) Non-Coated PR5FCR5F Mixture Slab Surfaces.	179
Figure A.1.	Impact of Fiber Type on 7 Day Compressive Strength.	197
Figure A.2.	Sieve Analysis of Coarse and Fine Aggregate.....	198
Figure A.3.	Flexural Toughness Comparison between Rubberized Concrete Mixtures with and without Green-Net Fiber.	199
Figure A.4.	Effect of RAP Aggregate Size on Compressive Strength (from Huang et al. 2005).	200
Figure G.1.	Sequential Photographs for Test No. 468958-3 (Overhead and Frontal Views).....	226
Figure G.2.	Sequential Photographs for Test No. 468958-3 (Rear View).....	228
Figure G.3.	Vehicle Angular Displacements for Test No. 468958-3.....	229
Figure G.4.	Vehicle Longitudinal Accelerometer Trace for Test No. 468958-3 (Accelerometer Located at Center of Gravity).	230
Figure G.5.	Vehicle Lateral Accelerometer Trace for Test No. 468958-3 (Accelerometer Located at Center of Gravity).	231
Figure G.6.	Vehicle Vertical Accelerometer Trace for Test No. 468958-3 (Accelerometer Located at Center of Gravity).	232
Figure G.7.	Vehicle Longitudinal Accelerometer Trace for Test No. 468958-3 (Accelerometer Located Rear of Center of Gravity).	233
Figure G.8.	Vehicle Lateral Accelerometer Trace for Test No. 468958-3 (Accelerometer Located Rear of Center of Gravity).	234
Figure G.9.	Vehicle Vertical Accelerometer Trace for Test No. 468958-3 (Accelerometer Located Rear of Center of Gravity).	235
Figure H.1.	Sequential Photographs for Test No. 468958-2 (Overhead and Frontal Views).....	241
Figure H.2.	Vehicle Angular Displacements for Test No. 468958-2.....	243
Figure H.3.	Vehicle Longitudinal Accelerometer Trace for Test No. 468958-2 (Accelerometer Located at Center of Gravity).	244
Figure H.4.	Vehicle Lateral Accelerometer Trace for Test No. 468958-2 (Accelerometer Located at Center of Gravity).	245
Figure H.5.	Vehicle Vertical Accelerometer Trace for Test No. 468958-2 (Accelerometer Located at Center of Gravity).	246
Figure H.6.	Vehicle Longitudinal Accelerometer Trace for Test No. 468958-2 (Accelerometer Located Rear of Center of Gravity).	247
Figure H.7.	Vehicle Lateral Accelerometer Trace for Test No. 468958-2 (Accelerometer Located Rear of Center of Gravity).	248
Figure H.8.	Vehicle Vertical Accelerometer Trace for Test No. 468958-2 (Accelerometer Located Rear of Center of Gravity).	249

LIST OF FIGURES (CONTINUED)

	Page
Figure I.1. Sequential Photographs for Test No. 468958-1 (Overhead and Frontal Views).....	253
Figure I.2. Vehicle Angular Displacements for Test No. 468958-1.....	255
Figure I.3. Vehicle Longitudinal Accelerometer Trace for Test No. 468958-1 (Accelerometer Located at Center of Gravity).	256
Figure I.4. Vehicle Lateral Accelerometer Trace for Test No. 468958-1 (Accelerometer Located at Center of Gravity).	257
Figure I.5. Vehicle Vertical Accelerometer Trace for Test No. 468958-1 (Accelerometer Located at Center of Gravity).	258
Figure I.6. Vehicle Longitudinal Accelerometer Trace for Test No. 468958-1 (Accelerometer Located Rear of Center of Gravity).	259
Figure I.7. Vehicle Lateral Accelerometer Trace for Test No. 468958-1 (Accelerometer Located Rear of Center of Gravity).	260
Figure I.8. Vehicle Vertical Accelerometer Trace for Test No. 468958-1 (Accelerometer Located Rear of Center of Gravity).	261

LIST OF TABLES

	Page
Table 2.1. Occupant Risk Metrics from Simulated <i>MASH</i> Test 4-11 of the Texas SSTR.....	9
Table 2.2. Occupant Risk Metrics from Simulated <i>MASH</i> Test 4-10 of Texas SSTR.	13
Table 2.3. Occupant Risk Metrics from Simulated <i>MASH</i> Test 4-10 of Caltrans Type 60G Barrier.	15
Table 2.4. Occupant Risk Metrics from Simulated <i>MASH</i> Test 4-11 of Caltrans Type 60G Barrier.	18
Table 3.1. Source and Properties of Fibers Selected for Screening Study.....	29
Table 3.2. Biaxial Geogrid Properties Obtained from Manufacturer.	30
Table 3.3. Mixture Proportion for Control Concrete Barrier Mixture.	31
Table 3.4. Candidate Material Description and Mixture Proportion Designation Matrix.....	32
Table 3.5. First Phase Screening Test Summary for Fiber Series.....	36
Table 3.6. Net-Like Fiber Test Summary Data Evaluated for 0.25% Dosage of Fibers.....	36
Table 3.7. PVA Fiber Test Summary Added at Dosage of 0.25% by Volume of Mixture.....	37
Table 3.8. Comparison of Concrete Containing Corrugated Geogrid (Geogrid 1/2U) and Noncorrugated Geogrid (Geogrid 1/2U).	39
Table 3.9. Summary of Second Phase Test Results of Recycled Tire Rubber Series.	46
Table 3.10. Influence of Green-Net Fibers On Concrete Mixtures Containing Rubber Particles.....	46
Table 3.11. Comparison of Compressive Strength Test Results of Core and Lab Samples.	49
Table 4.1. TRAP Results – Occupant Safety Analysis (Four 40-ft Section with Two Rubber Fenders).....	57
Table 4.2. TRAP Results – Occupant Safety Analysis (Four 40-ft Section with Three Rubber Fenders).....	62
Table 4.3. TRAP Results – Occupant Safety Analysis (Three 60-ft Section with Two Rubber Fenders).....	67
Table 4.4. TRAP Results – Occupant Safety Analysis (Three 60-ft Section with Three Rubber Fenders).	72
Table 4.5. TRAP Results – Occupant Safety Analysis (Two 40-ft Section with Three Rubber Fenders).....	77
Table 4.6. TRAP Results – Occupant Safety Analysis (Two 60-ft Section with Three Rubber Fenders).....	81
Table 4.7. Summary of Results of Simulations.	83
Table 4.8. TRAP Summary Data of 1-ft Offset Simulation.....	86
Table 4.9. TRAP Summary Data of 3-ft Offset Simulation.....	90
Table 4.10. TRAP Summary Data of 5-ft Offset Simulation.....	94
Table 4.11. Summary of Critical Impact Point Configurations.	96
Table 5.1. Summary of Results for Test No. 468957-B4.	114

LIST OF TABLES (CONTINUED)

		Page
Table 5.2.	Summary of Results for Test No. 468957-B5.	115
Table 5.3.	Summary of Results for Test No. 468957-B6.	116
Table 5.4.	Summary of Results for Test No. 468957-B7.	117
Table 5.5.	Occupant Risk Factors for Test No. 468957-B8.	122
Table 5.6.	Occupant Risk Factors for Test No. 468957-B9.	127
Table 5.7.	Occupant Risk Factors for Test No. 468957-B10.	132
Table 5.8.	Summary of Results for Test No. 468957-B8.	134
Table 5.9.	Summary of Results for Test No. 468957-B9.	135
Table 5.10.	Summary of Results for Test No. 468957-B10.	136
Table 7.1.	Test Conditions and Evaluation Criteria Specified for <i>MASH</i> TL-4.	145
Table 7.2.	Evaluation Criteria Required for <i>MASH</i> TL-4 Tests.	147
Table 9.1.	Events during Test No. 468958-3.	154
Table 9.2.	Occupant Risk Factors for Test No. 468958-3.	157
Table 10.1.	Events during Test No. 468958-2.	160
Table 10.2.	Occupant Risk Factors for Test No. 468958-2.	164
Table 11.1.	Events during Test No. 468958-1.	168
Table 11.2.	Occupant Risk Factors for Test No. 468958-1.	173
Table 12.1.	Bulk Resistivity at Day 31 Measured at 10kHz.	178
Table 12.2.	L* Values at Day 60.	179
Table 13.1.	Performance Evaluation Summary for <i>MASH</i> Test 4-10 on the TxDOT Rubber Mounted Single Slope Barrier.	182
Table 13.2.	Performance Evaluation Summary for <i>MASH</i> Test 4-11 on the TxDOT Rubber Mounted Single Slope Barrier.	183
Table 13.3.	Performance Evaluation Summary for <i>MASH</i> Test 4-12 on the TxDOT Rubber Mounted Single Slope Barrier.	184
Table 13.4.	Assessment Summary for <i>MASH</i> TL-4 Testing on the TxDOT Rubber Mounted Single Slope Concrete Barrier.	185
Table A.1.	Material Nomenclature, Distributor, and Oxide Analysis.	197
Table A.2.	Material Source, Type, and Physical Properties of Aggregates.	198
Table A.3.	Performance of PVA Fibers at Dosage of 0.25% by Volume of Mixtures in Concrete.	198
Table G.1.	Vehicle Properties for Test No. 468958-3.	223
Table G.2.	Exterior Crush Measurements of Vehicle for Test No. 468958-3.	224
Table G.3.	Occupant Compartment Measurements of Vehicle for Test No. 468958-3.	225
Table H.1.	Vehicle Properties for Test No. 468958-2.	237
Table H.2.	Measurements of Vehicle Vertical CG for Test No. 468958-2.	238
Table H.3.	Exterior Crush Measurements of Vehicle for Test No. 468958-2.	239
Table H.4.	Occupant Compartment Measurements of Vehicle for Test No. 468958-2.	240
Table I.1.	Vehicle Properties for Test No. 468958-1.	251

CHAPTER 1: INTRODUCTION

A median barrier is a roadway safety and protective device installed between two opposing directions of traffic to reduce the severity of impact crashes between the two opposing directions of traffic (1). In addition, barriers provide continuous protection from any obstacle parallel to the traffic stream direction. Bligh, Miaou, Lord, and Cooner mentioned that fatality rate of cross median crashes is significantly higher compared to other types of crashes (2). Median barriers do not prevent crashes from occurring, rather the barrier changes the type of crash from a head-on cross median collision to a fixed object crash (where the fixed object is the median barrier) (3). Though it reduces the severity and involvement of the occupants traveling in the cross-traffic direction, impacting the barrier poses a safety threat to occupants of the crash vehicle as well as causes damage to the vehicle. The errant vehicle encroachment at the concrete barrier applies a high magnitude load with a short frame of time (i.e., an impact load). The rigid barrier returns reaction forces to the vehicle, and depending on the crash condition, these forces can cause severe injury to vehicle occupants and damage to the vehicle. Additionally, the barrier sustains damage and will require repair.

Regular concrete mixes do not possess material characteristics that significantly dampen or absorb the impact load of vehicular crashes; however, incorporation of material in concrete mixtures that increase impact absorbance capacity can enhance the safety performance of concrete barriers (4). The flexibility, ductility, toughness, and impact load absorption capacity of the material significantly dictates the injury severity of the driver and damage intensity of the vehicle and barrier itself (5, 6). Increase in flexural toughness will arrest and control propagation of cracks under flexural loading leading to better structural integrity and less damage in a crash event. If the barrier is flexible or includes materials with the capability to dampen impact loads, the reaction force to the crash vehicle will be reduced and the safety of vehicle occupants will be improved (7).

Considering the challenge of mitigating damage of the vehicle and concrete barriers, and injury severity of occupants associated with the crash, the Texas Department of Transportation (TxDOT) initiated Project 0-6895 with the objective to develop safer and lower maintenance requiring concrete barrier. In this report, safer refers to increased toughness and load absorbing capacity under the impact of the crash load so that reaction load on the vehicle and occupants will be less. In addition to safety, implementation potential based on availability and cost were also considered while prioritizing materials.

Researchers designed a new generation of median barriers for TxDOT through computer simulation. Researchers reviewed traditional and non-traditional construction material and technologies for use in this new design. Full-scale crash testing was then performed on the new design to evaluate the crashworthiness of the system.

CHAPTER 2: REVIEW OF CONCRETE BARRIER SHAPES

Concrete barriers provide positive rigid protection to errant roadway vehicles from hazards. Concrete barriers have different shapes and could be temporary or permanent in terms of installation. The barrier's performance upon impact depends on the vehicle type, impact speed, impact angle, and other variables (8). The concrete safety shape barrier is commonly known as the Jersey or New Jersey barrier and has a staged profile. This profile starts with a 3-inch vertical surface, then a slanted surface of 55° off horizontal level that goes vertically for 10 inches. Then, there is another slope break of 84° off horizontal level that goes vertically for 19 inches (8). The New Jersey profile has a height of 32 inches, and is shown in the left side of Figure 2.1. Another multistage concrete barrier, known as the F-Shape profile, is proven to exhibit an enhanced crash safety performance over the New Jersey profile. The F-Shape profile starts with a 3-inch vertical surface, then a slanted surface of 55° off horizontal level that goes vertically for 7 inches. Then, there is another slope break of 84° off horizontal level that goes vertically for 22 inches (8). The F-Shape profile has a height of 32 inches, and is shown in the right side of Figure 2.1.

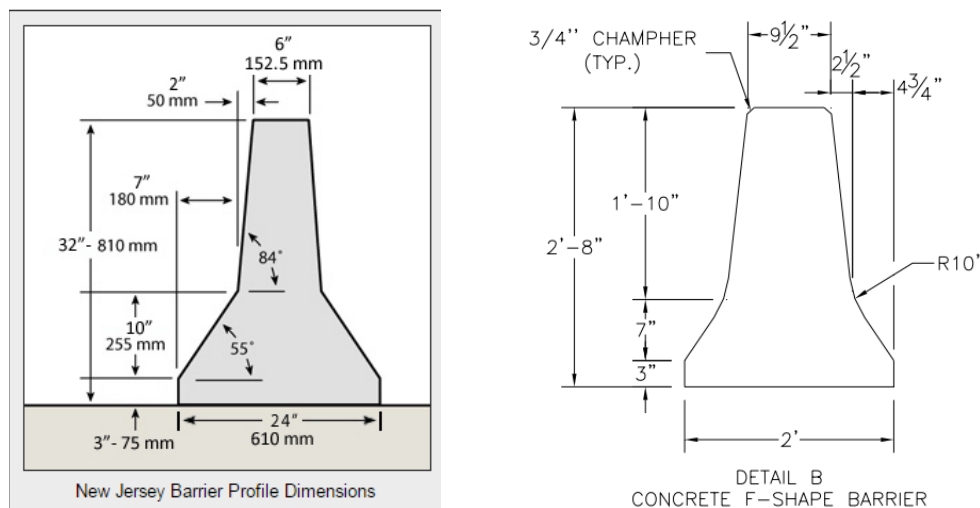


Figure 2.1. Common New Jersey Shape (Left) and F-Shape (Right) Concrete Barriers.

2.1 THE SINGLE SLOPE BARRIER PROFILE

The single slope barrier is a barrier with a constant slope on its sides. The slope is 10.8° for the Texas single slope barrier, and 9.2° for the Caltrans Type 60G barrier. Figure 2.2 shows both the Texas Single Slope Traffic Railing (SSTR) and Caltrans.

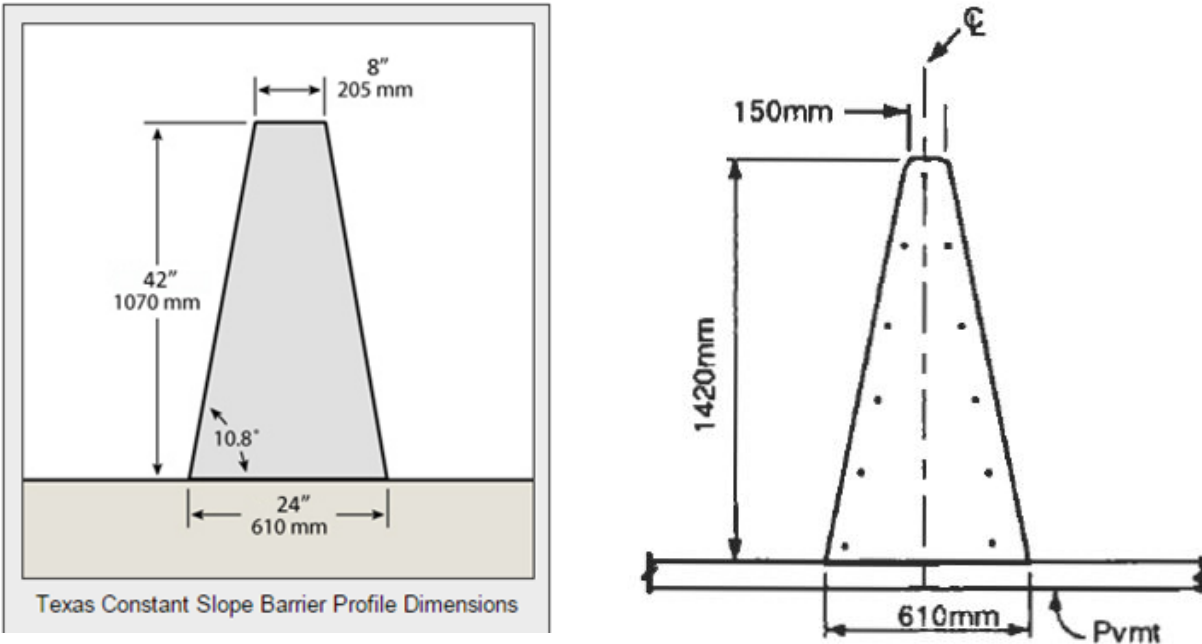


Figure 2.2. Texas Single Slope (Left) and Caltrans (Right) Barrier Profiles.

2.1.1 TTI Test 420020-9b

The objective of this project was to determine a minimum height for bridge rails and barriers to meet Test Level 4 (TL-4) of American Association of State Highway and Transportation Officials (AASHTO) Manual for Assessment of Safety Hardware (*MASH*) (9). *MASH* TL-4 specifies an impact speed of 56 mi/h compared to 50 mi/h per National Cooperative Highway Research Program (NCHRP) *Report 350* (10). The *MASH* Single Unit Truck (SUT) has a mass of 22,050 lb (10 000 kg) compared to 17,640 lb (8000 kg) per *NCHRP Report 350*. The impact angle remained at the previous value of 15°. Due to the increase in severity of *MASH*, there was a need to revise the minimum standards previously held. TTI researchers conducted a *MASH* TL-4 test with a 32-inch New Jersey barrier. The test with the 32-inch New Jersey barrier resulted in failure because the test vehicle rolled over the barrier. This indicates that a 32-inch rail height was not sufficient. TTI determined the minimum rail height by using LS-DYNA nonlinear finite element code as a simulation test bed (11). TTI researchers began testing barrier heights starting at 42 inches and decreasing them each time until they decided on 36 inches to use for the crash test.

The *MASH* TL-4 test was performed using a 36-inch single-slope barrier (SSTR) with an 11° slope on the traffic-side. There are many advantages to the SSTR compared to the New Jersey or the F-shape. The SSTR facilitates resurfacing because performance is not affected by the thickness of asphalt overlay. It is also more cost-effective than the other two shapes and does not need to be replaced as often. It has not been tested much with bigger trucks and tractors, which is one reason for the *MASH* TL 4.

During the test, a 22,150 lb SUT impacted the barrier at a speed of 57.2 mi/h and an angle of 16.1°. Figure 2.3 shows the truck impacting the barrier at 0.0 s and its position at 0.559 s. The SSTR was evaluated on the basis of three factors: structural adequacy, occupant risk, and post impact vehicle trajectory. Structural adequacy is how well the barrier withstood the

impact and how well it redirected the vehicle. Occupant risk evaluates any potential injury to the occupant, and post vehicle trajectory evaluates potential secondary impact, whether that be with another vehicle or the occupant.



Figure 2.3. Sequences Showing SUT Impacting a 36-inch Tall Texas SSTR.

No notable occupant compartment deformation from the test was noted, but the impact to the vehicle itself was significant. Damages included a left front tire blow-out and bumper deformity. Other damages included the left frame rail, front axle, front U-bolts and springs, front tire rod, steering rod, left rear U-bolts and springs, and drive shaft. All of these were deformed as a result of the test. This test was considered a success per *MASH* evaluation criteria.

2.1.2 Simulation of TTI Test 420020-9b

A finite element computer model was developed to simulate the 420020-9b test. The impact speed was 57.2 mi/h, and the impact angle was 16.1°. This matches the values provided in the crash test reports.

Comparison of the results from the 420020-9b test and finite element simulation yields an acceptable match. Figure 2.4 shows a photographic comparison of the simulation to its corresponding frame from the crash test footage. As seen in the comparison, from impact until 0.5 s (the end of available high-speed footage), the simulation and crash test exhibit some similar phenomena. This gives confidence in the behavior of the SUT model for future tasks of this project.

2.1.3 TTI Test No. 9-1002-3 Pan Form—*MASH* 3-11

The objective of this project was to determine if the single-slope barrier (SSTR) bridge rail on a pan-formed bridge deck would perform according to *MASH* performance criteria. Pan form girders (concrete slabs held together by a steel beam) in bridge decks were developed in the late 1940s to accommodate the need for low-cost bridges in rural areas in Texas. *MASH* Test 4-11 was performed on the barrier system. The test is a strength test used to determine the success of a barrier when impacted by a pickup truck. The test vehicle was a 2005 Dodge Ram 1500 quad-cab pickup weighing 5036 lb. The vehicle impacted the barrier at a speed of 63.8 mi/h and an angle of 24.8°. The crash test was evaluated on the basis of three factors: structural

adequacy, occupant risk, and post impact vehicle trajectory. This test was considered successful per *MASH* evaluation criteria. Figure 2.5 shows a summary of the crash test.

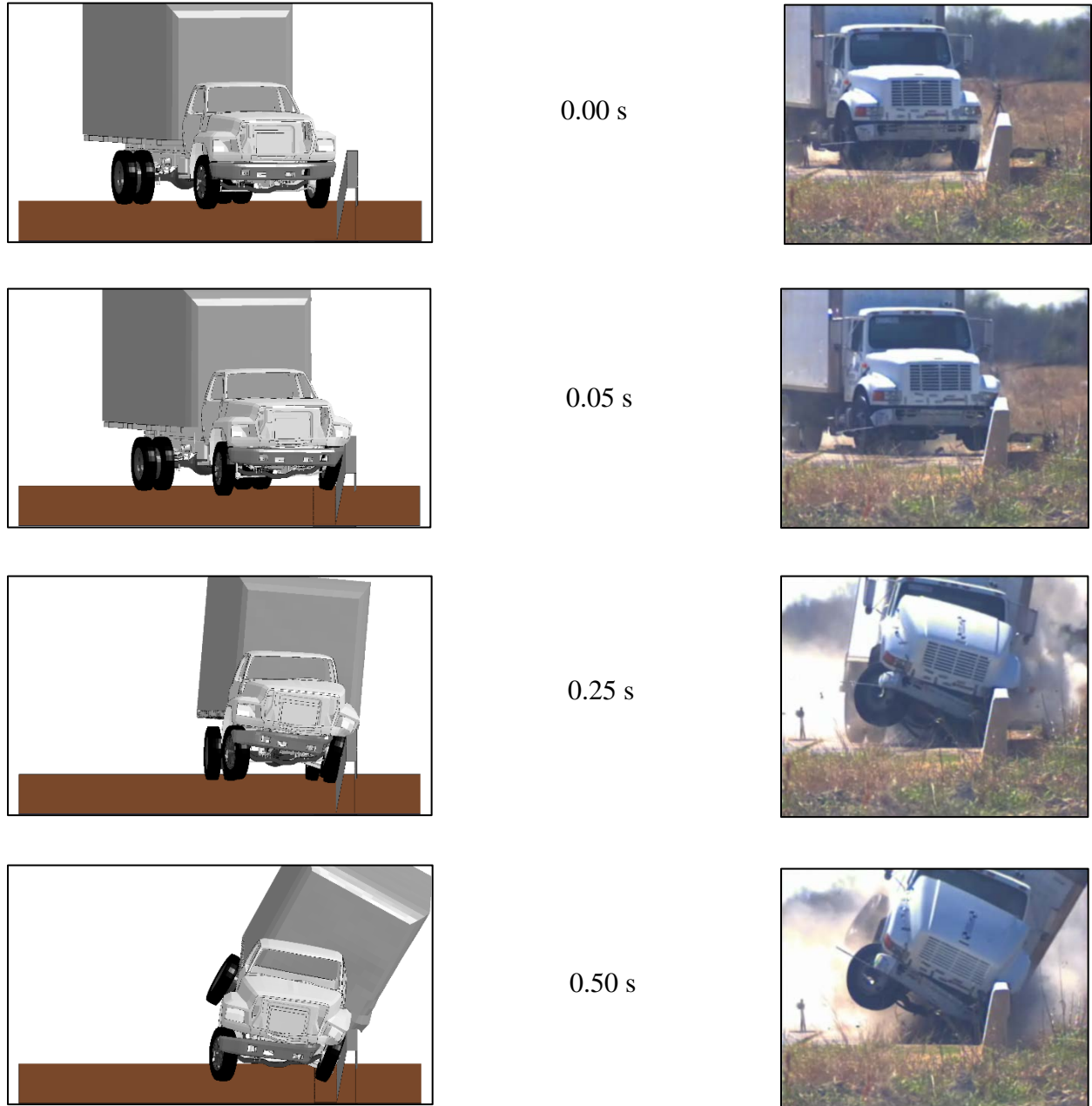


Figure 2.4. Sequential Photo Comparison between Test and Simulation of *MASH* Test 4-12 (SUT) Test of Texas 36-inch SSTR.

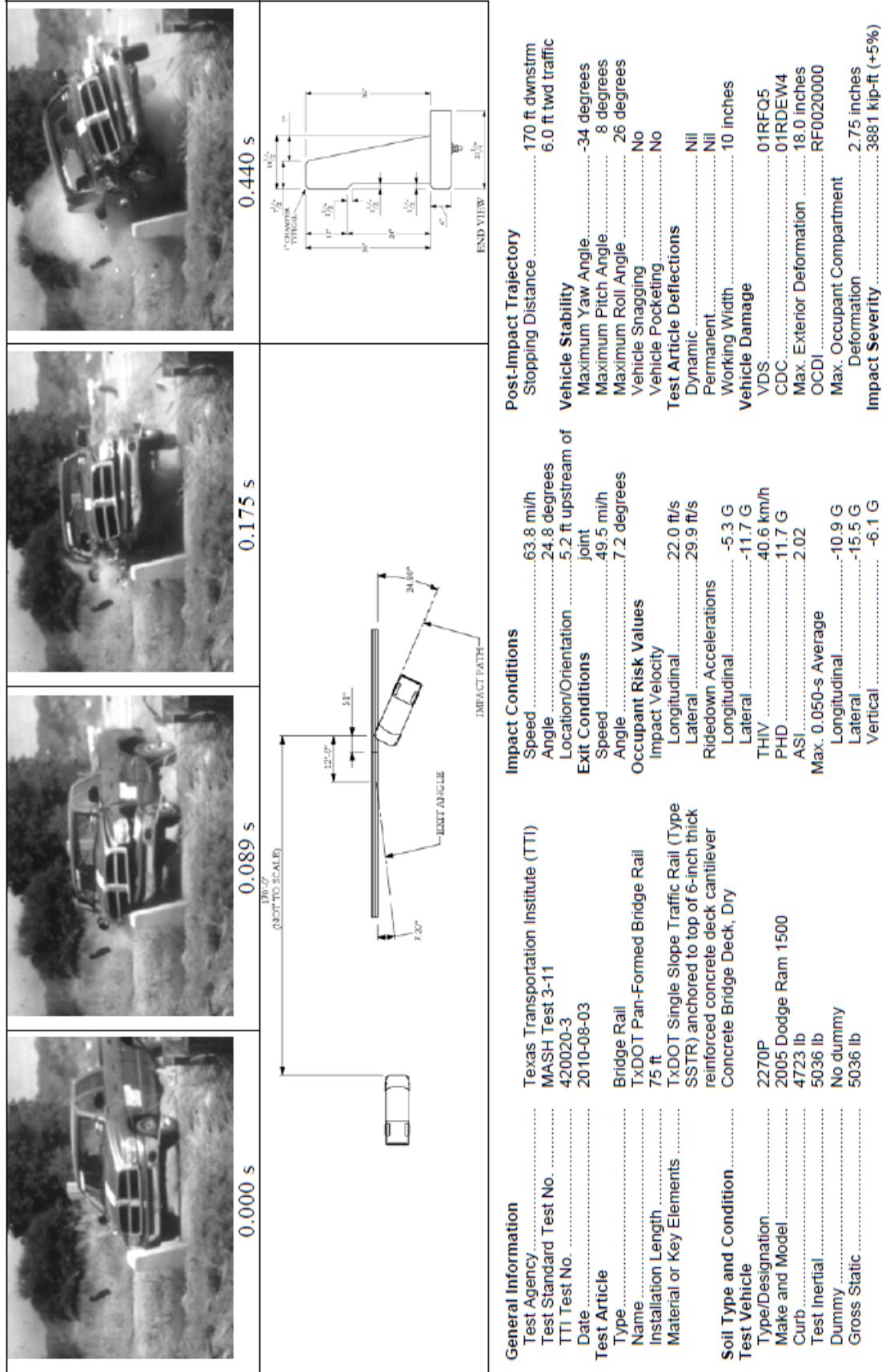


Figure 2.5. Summary of Results for MASH Test 3-11 on TxDOT Pan-Formed Bridge Rail.

2.1.4 MASH Test 4-11 Simulation of the Texas SSTR

MASH Test 4-11 is a length-of-need test condition that involves a quad-cab pickup truck (2270P) impacting the barrier at a speed of 62 mi/h and an angle of 25°. This simulation case was conducted with the modeled Texas SSTR as previously used in the simulations described in Section 2.1.2. The simulation vehicle had a speed of 63.8 mi/h and an angle of 24.8°, which replicated the 9-1002-3 crash test conditions.

Comparison of the results from the Pan Form Retrofit test and the finite element simulation point to a reasonable correlation. Figure 2.6 presents a photographic comparison of the simulation and the crash test. Table 2.1 shows the occupant risk values for the simulation. The X-acceleration, Y-acceleration, and the angular displacements for the crash test are shown in Figures 2.7 through 2.9, respectively.



Figure 2.6. Sequential Comparison of Pan Form Test (Right) and Simulation (Left) under MASH Test 3-11 Impact Conditions.

Table 2.1. Occupant Risk Metrics from Simulated *MASH* Test 4-11 of the Texas SSTR.

TRAP Results: Silverado into TxDOT SSTR	
<i>Impact Velocity, mi/h</i>	63.8
<i>Impact Angle (degrees)</i>	24.8
Occupant Risk Factors	
OIV (ft/s)	
x-direction	13.8
y-direction	26.6
Ride down Accelerations (g's)	
x-direction	5.4
y-direction	-24
Max Roll, Pitch, and Yaw Angles (degrees)	
Roll	32.4
Pitch	8.3
Yaw	-28.8

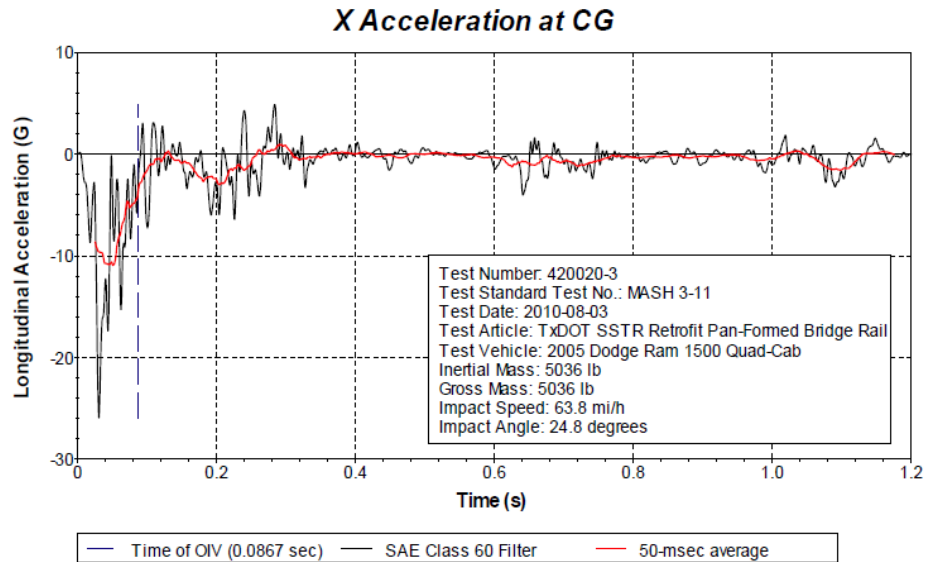


Figure 2.7. Longitudinal Acceleration for *MASH* Test 3-11 on TxDOT Pan-Formed Bridge Rail.

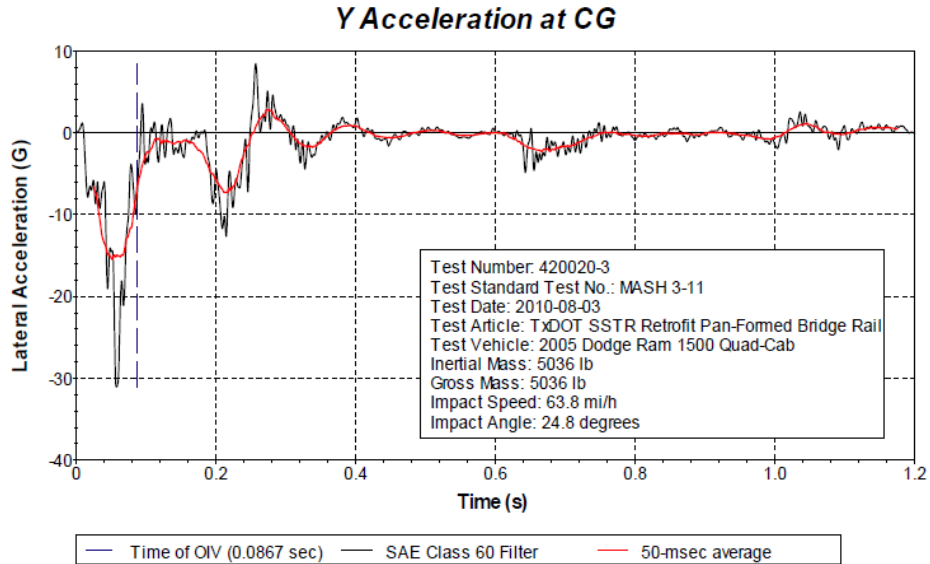


Figure 2.8. Lateral Acceleration for MASH Test 3-11 on TxDOT Pan-Formed Bridge Rail.

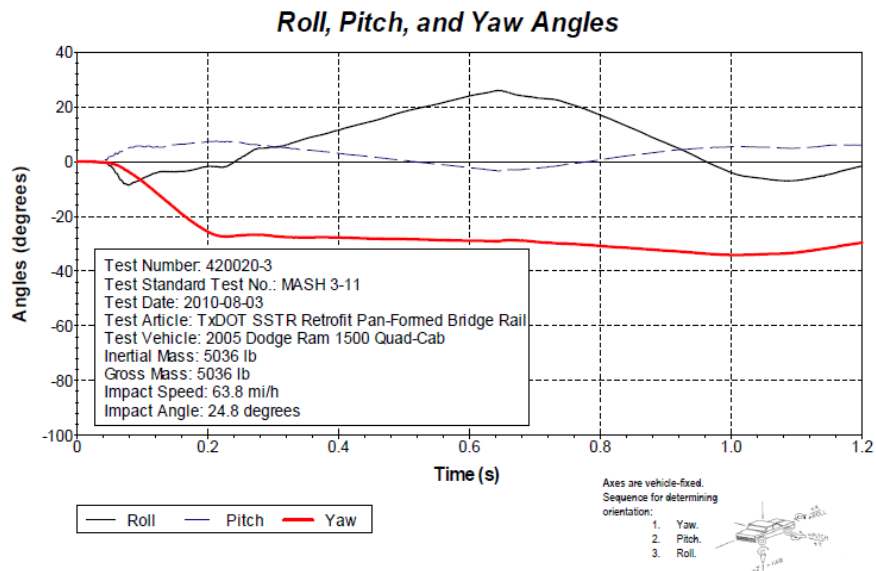


Figure 2.9. Angular Displacements for MASH Test 3-11 on TxDOT Pan-Formed Bridge Rail.

Figures 2.10 through 2.12 show corresponding accelerations from the simulations. Although these signals showed a reasonable correlation, lateral acceleration (side) is much higher in simulation than test at the point of back slap. This indicates a stiffer lateral stiffness of the rear suspension system in the model than the test vehicle. Hence, the results should be viewed with that in mind once the ride down values are compared.

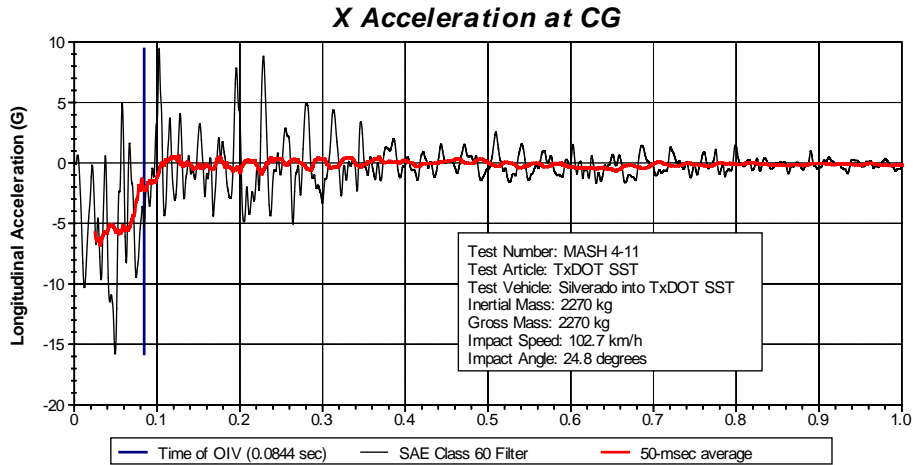


Figure 2.10. Longitudinal Acceleration History from Simulated *MASH* Test 4-11 of Texas SSTR.

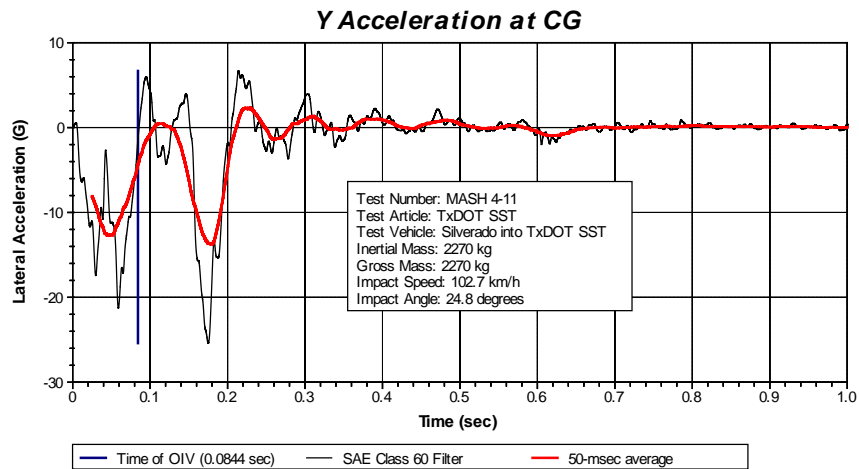


Figure 2.11. Lateral Acceleration History from Simulated *MASH* Test 4-11 of Texas SSTR.

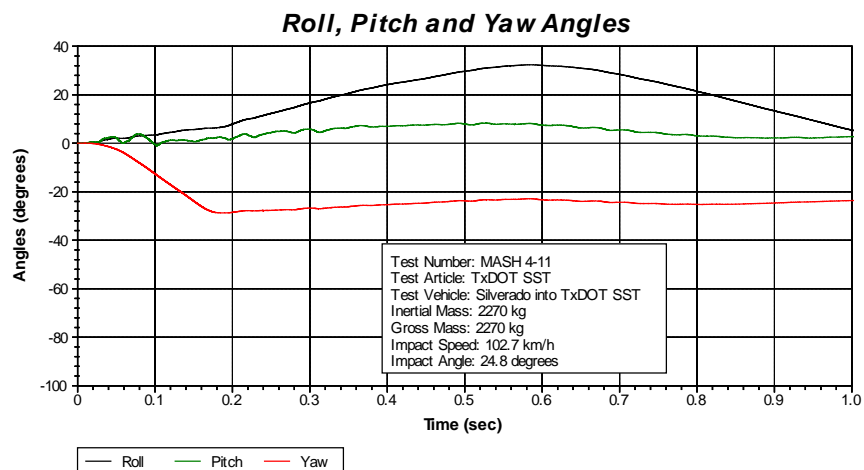


Figure 2.12. Angular Displacement History from Simulated *MASH* Test 4-11 of Texas SSTR.

2.1.5 MASH 4-10 Test of the Texas Single Slope Barrier

Although there is no known *MASH* Test 3-10 (or *MASH* Test 4-10) test to compare with simulation, researchers conducted a simulation of a *MASH* test 4-10. *MASH* Test 3-10 or 4-10 is defined as 1100C (2420 lb/1100 kg) passenger car impacting the critical impact point (CIP) of the length-of-need (LON) of the barrier at a nominal impact speed and angle of 62 mi/h and 25°, respectively. This test investigates a barrier's ability to successfully contain and redirect a small passenger vehicle.

Figure 2.13 shows the sequential images of the impact for the 1100C small car while Table 2.2 presents the simulation occupant risk metrics, and Figures 2.14 through 2.16 provide the acceleration and angular displacement histories. The simulation indicates that this test would be successful if it were to be conducted without quantifying the uncertainty in the simulation and testing.

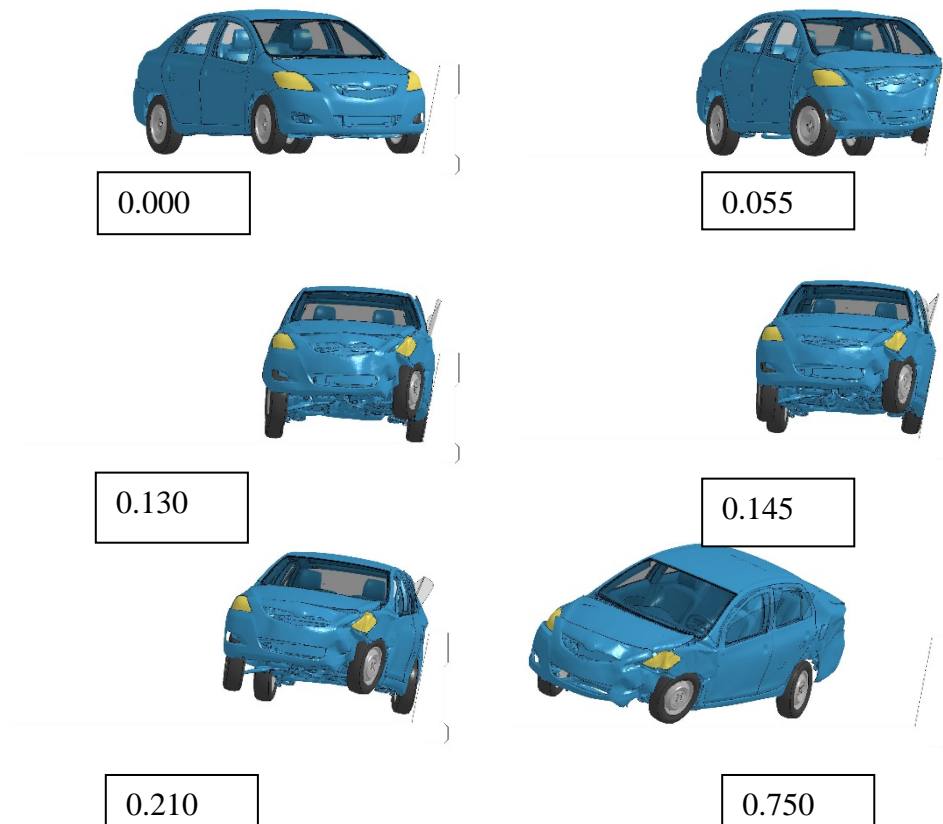


Figure 2.13. Sequential Simulation Images of *MASH* Test 4-10 of Texas SSTR.

Table 2.2. Occupant Risk Metrics from Simulated MASH Test 4-10 of Texas SSTR.

TRAP Results: Yaris into TxDOT SSTR	
Impact Velocity, mi/h	62.1
Impact Angle (degrees)	25
Occupant Risk Factors	
OIV (ft/s)	
x-direction	14.8
y-direction	30.8
Ridedown Accelerations (g's)	
x-direction	-4.5
y-direction	17.6
Max Roll, Pitch, and Yaw Angles (degrees)	
Roll	-34.3
Pitch	-6.3
Yaw	55.1

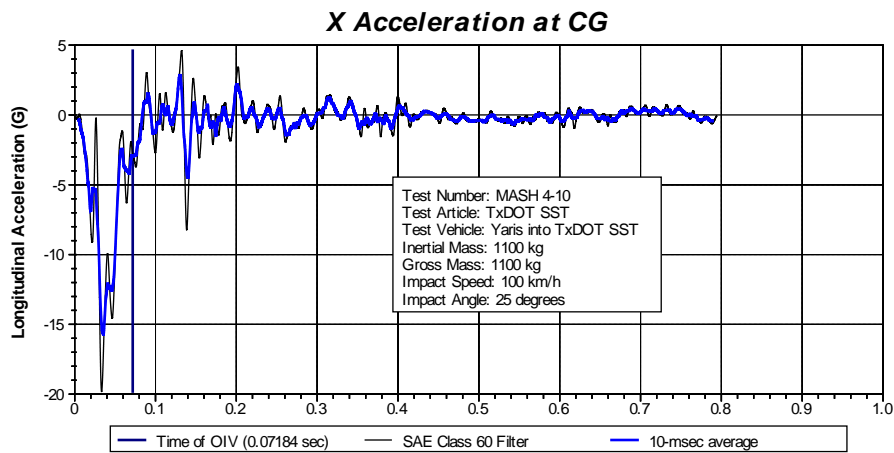


Figure 2.14. Longitudinal Acceleration History from Simulated MASH Test 4-10 of Texas SSTR.

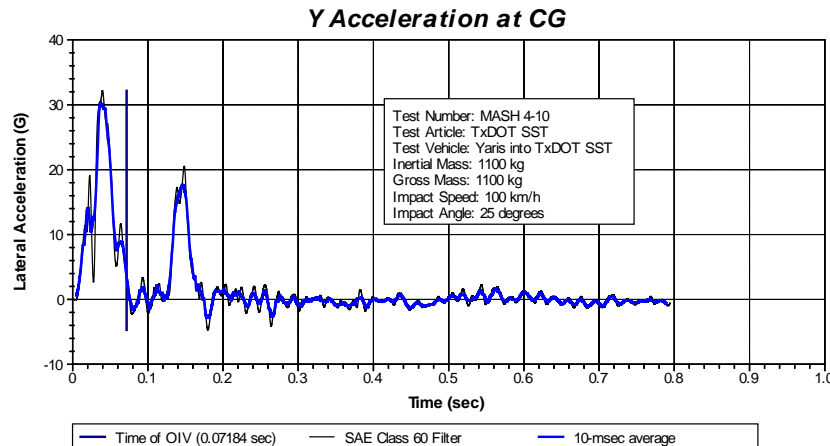


Figure 2.15. Lateral Acceleration History from Simulated MASH Test 4-10 of Texas SSTR.

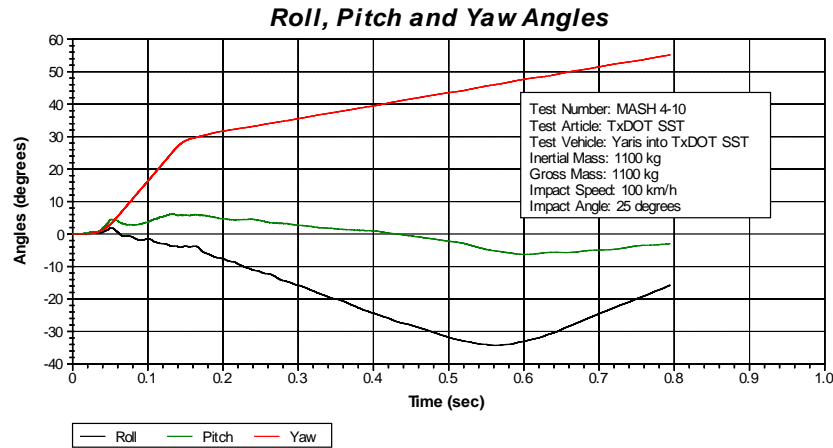


Figure 2.16. Angular Displacement History from Simulated *MASH* Test 4-10 of Texas SSTR.

2.2 *MASH* EVALUATION OF THE CALIFORNIA DEPARTMENT OF TRANSPORTATION (CALTRANS) 60G BARRIER

Researchers investigated the *MASH* performance of the 9.1° vertical face angle design of the Caltrans 60G through simulation to provide another data point for barrier shape performance since there are no known *MASH* tests of this barrier.

2.2.1 *MASH* Test 4-10 of the Caltrans Type 60G Barrier

Similar to the simulation conducted on the Texas SSTR, a simulation of *MASH* Test 4-10 was conducted for the Caltrans 60G barrier.

Figure 2.17 shows the sequential images of the impact for the 1100C small car. Table 2.3 presents the simulation occupant risk metrics, and Figures 2.18 provides the acceleration and angular displacement histories.

The simulation indicates that this test would be successful if it were conducted without quantifying the uncertainty in the simulation and testing. However, the ride down acceleration is 20 g for the Caltrans Type 60G barrier compared to 17.6 g for the Texas SSTR for the simulated *MASH* 3-10 test.

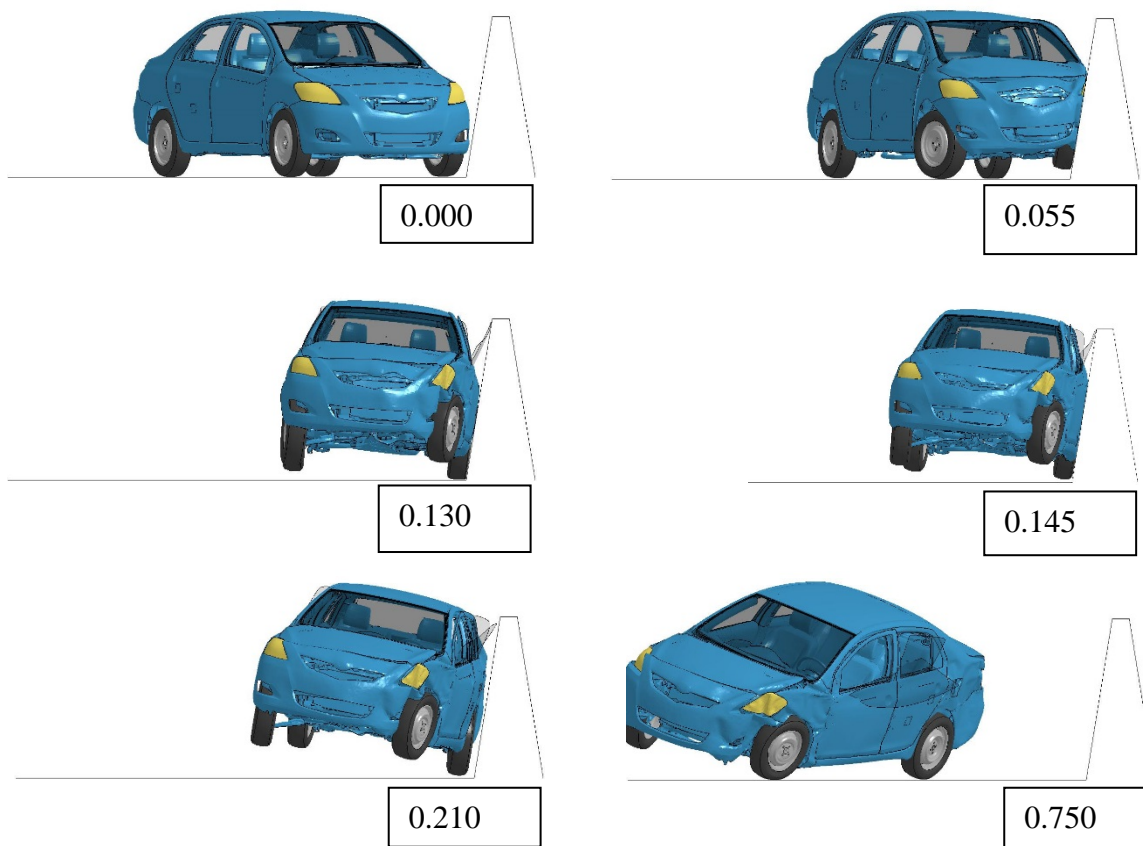


Figure 2.17. Sequential Simulation Images of MASH Test 4-10 of Caltrans 60G Barrier.

Table 2.3. Occupant Risk Metrics from Simulated MASH Test 4-10 of Caltrans Type 60G Barrier.

TRAP Results: Yaris into CalTrans 60G SST	
<i>Impact Velocity, mi/h</i>	62.1
<i>Impact Angle (degrees)</i>	25
Occupant Risk Factors	
OIV (ft/s)	
x-direction	15.1
y-direction	-31.2
Ride down Accelerations (g's)	
x-direction	-4.2
y-direction	20
Max Roll, Pitch, and Yaw Angles (degrees)	
Roll	-33.4
Pitch	-5.5
Yaw	54.4

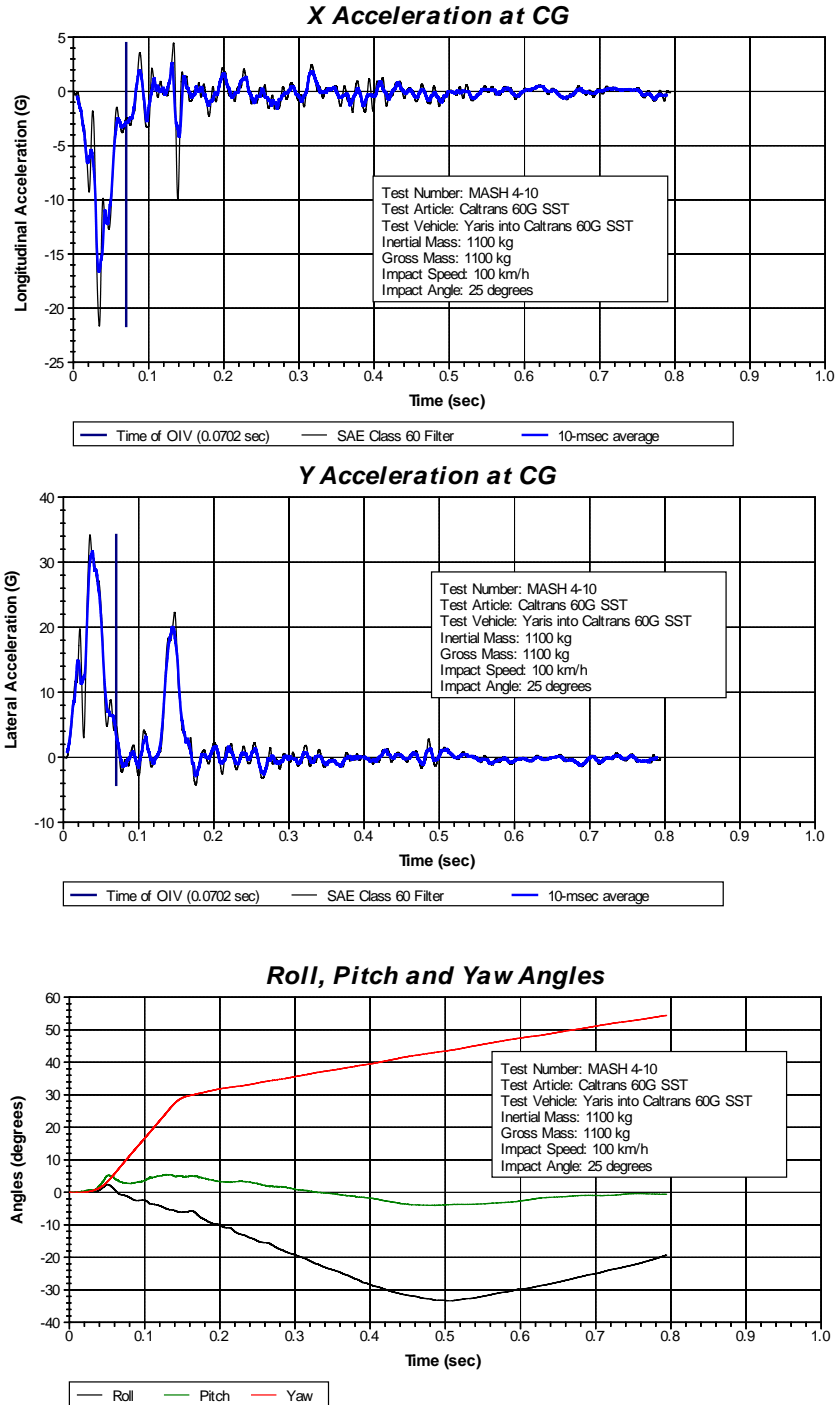


Figure 2.18. Acceleration and Euler Angles Histories from Simulated MASH Test 4-10 of Caltrans Type 60G Barrier.

2.2.2 MASH Test 4-11 of Caltrans Type 60G Barrier

MASH Test 4-11 simulation was conducted for the Caltrans Type 60G barrier. MASH Test 4-11 is a 2270P (5000 lb/2270 kg) pickup truck impacting the CIP of the LON of the barrier

at a nominal impact speed and angle of 62 mi/h and 25°, respectively. This test investigates a barrier's ability to successfully contain and redirect light trucks and SUVs.

Sequential images of this simulated impact is shown in Figure 2.19, while occupant risk metrics are presented in Table 2.4. The X, Y accelerations signals and angular displacements are plotted in Figures 2.20 and 2.21, respectively. Again, the simulations seem to present a stiff response of the pickup truck once a back slap occurred. Hence, an over the limit ride down acceleration value is obtained as an occupant risk indicator.

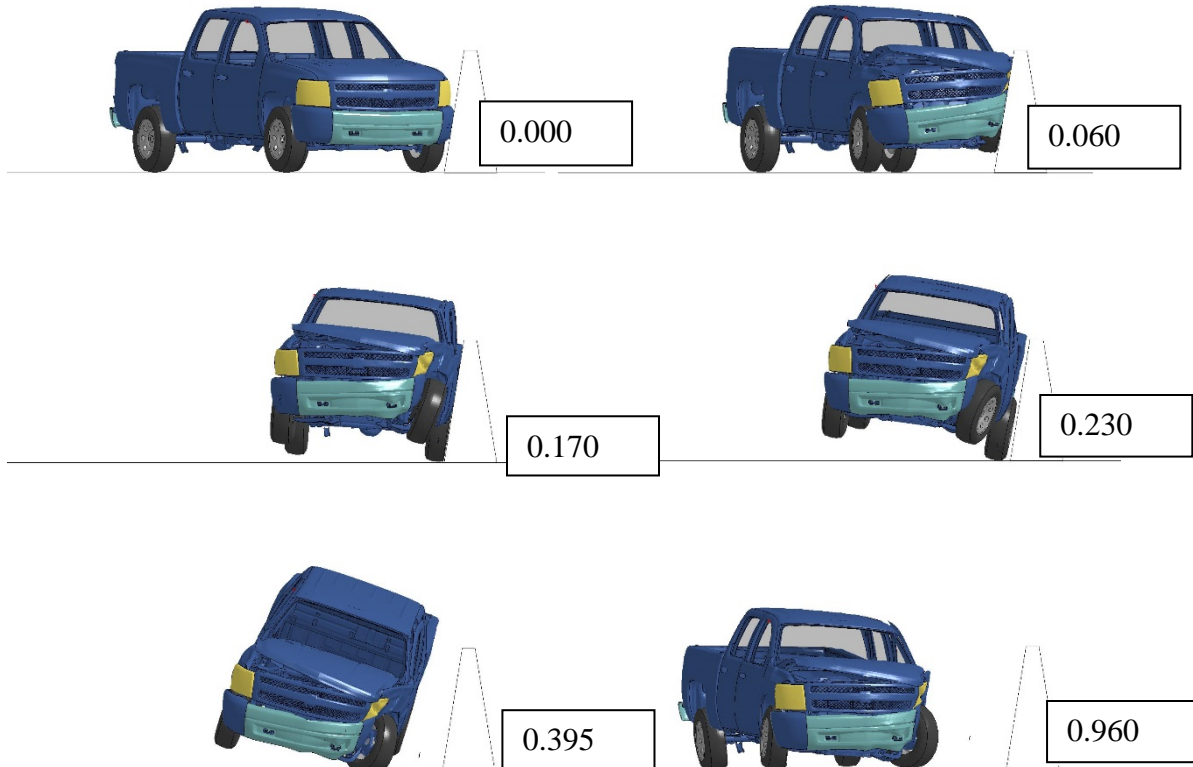


Figure 2.19. Sequential Simulation Images of MASH Test 4-11 (Pickup) of Caltrans 60G Barrier.

Table 2.4. Occupant Risk Metrics from Simulated *MASH* Test 4-11 of Caltrans Type 60G Barrier.

TRAP Results: Silverado into CalTrans 60G SST	
<i>Impact Velocity, mi/h</i>	62.1
<i>Impact Angle (degrees)</i>	25
Occupant Risk Factors	
OIV (ft/s)	
x-direction	12.5
y-direction	-25.6
Ridedown Accelerations (g's)	
x-direction	6.5
y-direction	21.8
Max Roll, Pitch, and Yaw Angles (degrees)	
Roll	-19.8
Pitch	-12.7
Yaw	30.3

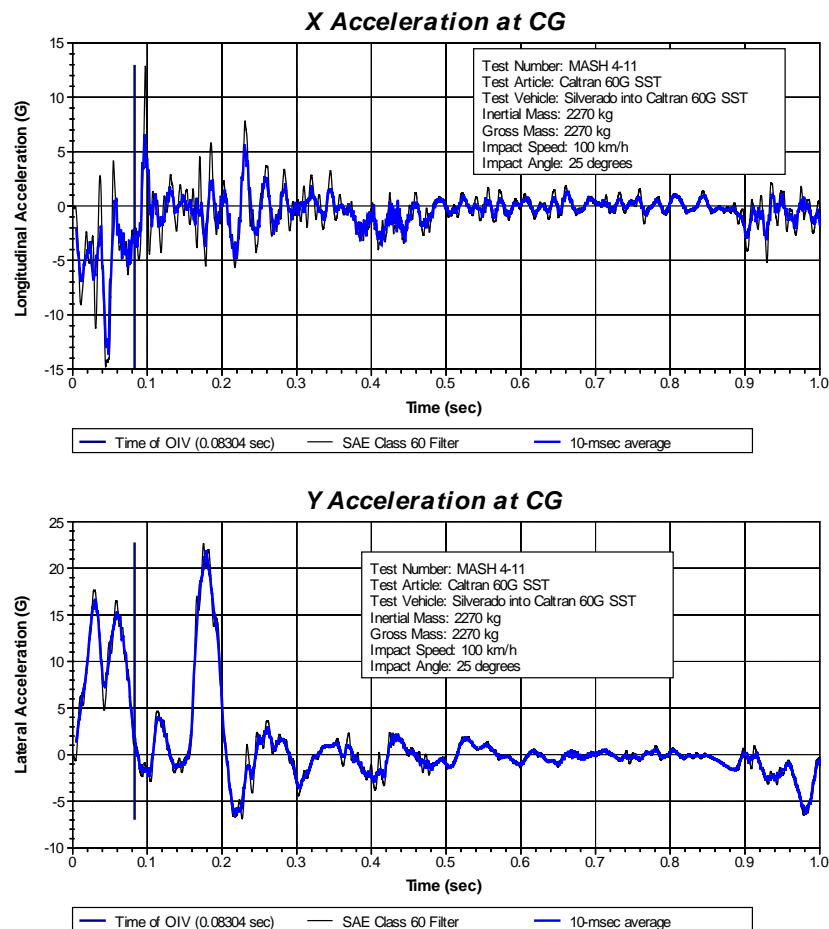


Figure 2.20. Acceleration from Simulated *MASH* Test 4-11 of Caltrans Type 60G Barrier.

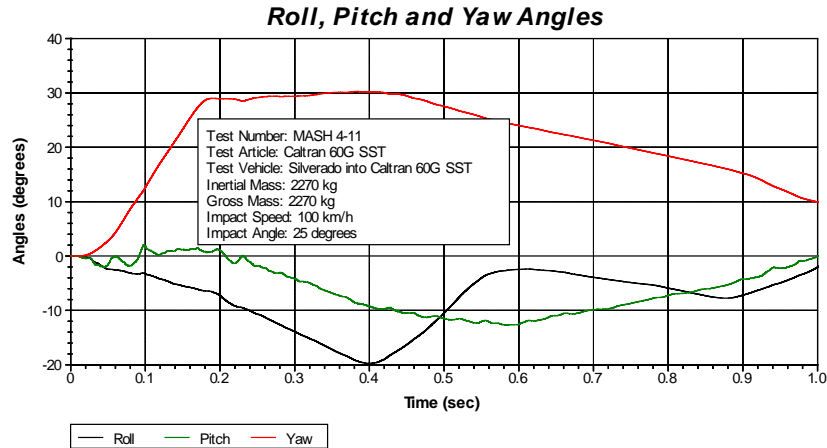


Figure 2.21. Euler Angles Histories from Simulated *MASH* Test 4-11 of Caltrans Type 60G Barrier.

2.2.3 MwRSF Hybrid Concrete Barrier with Rubber and Steel Posts

Researchers at the Midwest Roadside Safety Facility (MwRSF) developed a concrete barrier that employs precast concrete sections, steel rail on top, positively attached rubber footings, and sliding steel footings (12). Figure 2.22 shows this hybrid system. The rigid concrete barrier was designed to be a high containment longitudinal barrier. Elastomer (rubber) support posts, or shear fenders, were used to absorb energy by restoring their pre-crash position. This selection was based on restorability, resistance, flexibility, moldability, and successful performance in several safety tests. The shear fenders measured 11⁵/₈ inches × 10 inches × 15³/₄ inches and were attached to the concrete beam. They were also meant to extend the time of vehicle impact, thus reducing the force imparted to the vehicle.



Figure 2.22. Concrete Beam Barrier with Alternating Steel and Rubber Post from MwRSF.

A hybrid concrete beam with a steel tube combination rail was designed, and required to measure 36 inches or less in width, and the concrete rail must be at least 21½-inch width. These requirements are necessary to reduce the mass of the total system, and was also accomplished by using lightweight concrete, and placing vertical holes in the centerline of the beam. The top 6 inches of the beam was replaced with a mounted steel tube, creating a hybrid that met all necessary requirements. Adjustable continuity joint with steel angles were incorporated to achieve moment continuity. Steel skids were added to increase stability by restricting rotation and supporting the rail's weight, thus improving efficiency of the shear fenders.

The final barrier configuration is represented by a median barrier with total length 239 ft -11½ inches, and height of 38 ⅝ inches. Twelve precast reinforced concrete beams and upper tubes were used, with four elastomer posts spaced 60 inches apart, and two steel skids placed 120 inches apart, per beam.

This system performed successfully when tested per *MASH* TL-4. The authors presented it as a barrier with enhanced occupant risk values due to its ability to move. This system is not suitable for slip forming and requires additional details for joint connectivity and steel railing.

2.3 AUGMENTING THE CONCRETE BARRIER WITH ELASTIC RUBBER FENDER

Researchers developed a concept for slip form concrete barrier with rubber fenders placed inside using steel enclosure. The concept is shown in Figure 2.23 for the Texas SSTR.

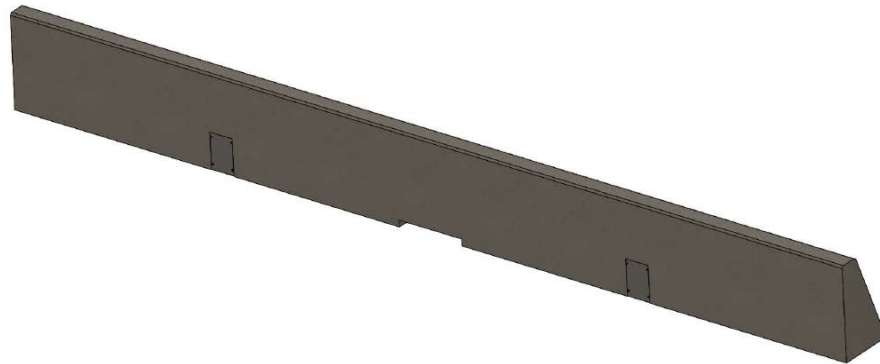


Figure 2.23. Single Slope Barrier with Two Rubber Fenders.

The steel enclosure allows for the slip form process and provides protection for the rubber fender during impact. Figure 2.24 shows a close-up view of this enclosure. The steel door is made transparent to show the inside of the enclosure.



Figure 2.24. Close-up Details of Single Rubber Fender Inserted within the Concrete Barrier.

2.4 CONCLUSION

Researchers recommend using the Texas SSTR as the barrier shape given its performance and adjustability for construction height. Common safety shapes such as the New-Jersey and the F-Shape affect the vehicular stability once impacted by potentially increasing the roll angle. Additionally, these profiles will be affected by the presence of pavement overlay. Hence, researchers recommend the use of elastic rubber parts to provide some level of flexibility to the barrier system. Adding such flexibility can potentially enhanced occupant risk values while reducing damage to the barrier upon impact by an errant vehicle.

CHAPTER 3: IDENTIFICATION AND CHARACTERIZATION OF MATERIALS

This chapter presents an overview of materials that were identified as potential materials that could be used to enhance the durability and safety concrete median barriers. The materials were identified based on a literature review, input from TxDOT officials, and previous experience of the research team.

3.1 IDENTIFICATION OF CANDIDATE MATERIAL

A list of candidate materials was generated based on a literature review, input from TxDOT officials, and previous experience of the researchers. The likely impact on concrete's toughness and impact resistance were the governing factors when considering the mechanical properties of the candidate materials. Additionally, ease of handling and cost were also taken into consideration since these both will impact the implementation potential. Below is a list of five different candidate materials that were selected with the goal of making the concrete barrier safer by enhancing the toughness and impact resistance of concrete:

1. Geogrid.
2. Recycled tire rubber.
3. Class F fly ash (F-ash).
4. Recycled asphalt pavement (RAP).
5. Fibers.

3.2 LITERATURE REVIEW ON CANDIDATE MATERIAL

In the following sub-sections, reasons for why a particular candidate material was included in the project matrix are provided, along with the general characteristics and properties of the candidate material.

3.2.1 Geogrid

Geogrid is a polymer mesh that is often used in geotechnical engineering applications as a ground stabilization technique to reinforce soils (13). Geogrids are commonly made from high density polypropylene and are classified as uniaxial, biaxial, and triaxial, depending on the opening area (see Figure 3.1).



Figure 3.1. Images for Uniaxial, Biaxial, and Triaxial Geogrid.

In concrete, geogrid's performance has been evaluated for concrete pavement overlay applications to arrest cracks in thin overlays, which is believed due to geogrid's effectively transferring tensile loading by acting as a continuous fiber (14). The geogrid changes the post cracking behavior of the concrete material under flexural loading and the resultant composite material demonstrates improved post-peak flexure loading response. Kim, Tang, and Chehab evaluated the response of geogrids for concrete overlay use under monotonic loading (15). Similar to the work of Chidambaram and Agarwal, post cracking ductility improved and an increase in flexural loading carrying capacity after peak strength was detected (16).

Meski and Chehab explored flexural behavior of concrete beams reinforced with different types of geogrid (e.g., uniaxial, biaxial, and triaxial) at different placement levels (17). Meski and Chehab observed enhanced post crack behavior and toughness in the post peak region. However, the performance of geogrids varied significantly with the configuration of the geogrid and placement level. Chidambaram and Agarwal evaluated geogrid's performance as shear load bearing components rather than using them as flexural load bearing components. Though Chidambaram and Agarwal focused primarily on shear strength and failure patterns under shear, they also observed the flexural behavior of the material. The sample containing the geogrid showed better tension bearing capacity compared to the control mixture. Zakaria, Sharif, and Hong performed flexural testing in lightweight concrete containing a geogrid (oil palm shells were used as the lightweight aggregates in this research) and observed an enhancement in tensile loading capacity of samples containing the geogrid as compared to the control sample without the geogrid (18).

Confinement from the geogrids is also likely to play a role in arresting crack propagation rate under impact and tensile loading (19). Under impact loading, concrete material is exposed to high tensile loading within a very short time span. Geogrid is expected to perform well in impact by restraining the material with confinement. Zakaria et al. also performed impact testing on similar samples and observed better impact performance of concrete slabs with geogrids compared to concrete slabs with no geogrids.

In view of geogrid's potential to enhance toughness and confining property under tensile loading, this material was selected as a candidate for the project study and analysis.

3.2.2 Recycled Tire Rubber

Tire rubber disposal is a global problem. It has been estimated that over 2 billion tires are stockpiled in the United States and around 100 million tires are generated every year globally. With this huge disposal load, end of life management of tire rubber has become a challenging issue worldwide. A major portion of disposed rubber goes into landfills after use. As rubber is not biodegradable, disposal generates severe environmental concern along with being a fire hazard and serving as a breeding ground for vermin. Research on inclusion of tire rubber as a partial replacement for fine and coarse aggregates in cement composites has shown promising results (20-25). Due to the high energy absorbance capacity, rubber material is particularly suitable for noise and shock reduction barrier application. Based on this unique characteristic when added to the cement composites, researchers have recommended exploring the applicability of rubber in concrete barriers (5, 6, 24).

Rubber is a chemically inert, flexible material with high energy absorbing capacity. These properties reflected as advantages for rubber to be used in cement composites for

enhanced mechanical properties such as fracture toughness, impact resistance, and durability, such as resistivity to chloride ingress, freeze-thaw, and acid attack. Inclusion of tire rubber in concrete materials (i.e., rubberized concrete) showed significant enhancement in impact resistance compared to control mixtures in previous studies (26, 5). In addition, when rubber was incorporated as a replacement for mineral aggregate, ductile failure was observed rather than brittle failure due to the better crack propagation resistivity of the rubber and the higher amount of plastic energy absorbed as compared to control mixes (20, 24). Furthermore, rubberized cement composites showed better resistivity in chloride ion penetration acid attack and freeze-thaw than its control, which is attributed to the chemical inertness and hydrophobicity features of the rubber (19, 27, 28). However, the performance varies significantly with the dosage, gradation, and shape of the tire particles.

Variables responsible for rubberized cement composite performance includes, but is not limited to, replacement type, replacement dosage, size, and shape of rubber. Recycled tire rubber is commercially available in coarse and fine forms, with sizes ranges from 0.075 mm to 5 mm. Depending on the size, rubber has been incorporated as partial replacement of cement, coarse and/or fine aggregates. Utilization of fine powdered rubber is not a viable replacement of cement as rubber possesses no cementitious properties and is chemically inert to adhere to aggregates. Therefore, almost all previous research focused on incorporating rubber as a partial replacement of coarse and fine aggregates (22, 23). Gupta, Sharma, and Chaudhary investigated use of rubber particles 2-5 mm in length, up to 25 percent by volume replacement of fine aggregate, and observed increased impact resistance with the increase in rubber content (29). Topçu and Avcular and Eldin and Senouci stated similar conclusions derived from their results (5, 6, 20). In general, higher dosages of rubber led to improved impact resistance. Taha et al. observed impact resistance and toughness enhancement of rubberized cement composite with the addition of chipped (5-20 mm) and crumb (1-5 mm) tire particles as volume replacement of coarse and fine aggregates, respectively (24). Twenty-five percent rubber content was observed as the optimal content from a toughness and impact resistance perspective in the work of Taha et al. Tantala, Lepore, and Zandi reported 10 percent rubber dosage as optimum for toughness enhancement (30). Here, similar sizes of crumb rubber were incorporated as Taha et al., but replaced the coarse aggregate fraction with the crumb rubber rather than the fine aggregates. From the literature, increase of impact resistance and toughness with the increase in rubber content have been observed.

Though rubber is a potential candidate in terms of impact resistance, toughness, and some other durability properties, inclusion of rubber in cement composites has shortcomings as well. With the increase in rubber percentage, compressive and flexural strength decreases (20, 24, 5, 6). Irrespective of the size of rubber and replacement type, compressive and flexural strength always decreases. Rubber is a flexible material and the difference in deformability of rubber compared to cement composite, along with the low cement-rubber bond strength, were reported to be key attributes in the compressive strength reduction (24). However, decrease in compressive strength was reported not to be significant with up to 5 percent addition of rubber by volume (31). Therefore, research and material testing are required to optimize dosage of rubber for augmented performance of rubber for concrete barrier application. If rubber performance is adequate in developing a safer barrier, it will not only be beneficial environmentally by reducing rubber landfill load, but also it will aid in lowering the consumption rate of virgin aggregates which is economical and cost effective.

Considering the economic and environmental benefits along with enhanced composite performance, crumb and fine tire rubber particles were selected as candidate materials to be evaluated for this project use.

3.2.3 Class F Fly Ash (F-ash)

Class F fly ash is a pozzolanic material-waste product from the coal power industry and used as a partial replacement of cement in the concrete industry. It reduces the heat of hydration and improves durability of the concrete mixtures. Typical replacement range of cement with fly ash is 15-25 percent by volume. Utilization of high volume of fly ash (HVFA) (>50 percent replacement by volume) has gained research interest to be included in concrete materials as it is a low-cost waste material replacing high-cost cement and exhibits better durability performance compared to control concrete.

Inclusion of high volume fly ash with low water/cement ratio can produce moderate and high strength concrete mixtures (21). Siddique, Mehta and Langley, and Huang et al. investigated the mechanical properties of concrete including high volume (>50 percent replacement) of Class F fly ash as a replacement of cement (32, 33, 21). All the studies reported satisfactory performance of HVFA mixtures at early days (7-28 days), and in some cases better performance compared to control mixes in terms of compressive strength at a later age. Huang et al. incorporated Class F fly ash up to 80 percent, and Mehta and Langley up to 50 percent, in concrete mixtures and observed that with low water/cement ratio and loss of ignition (LOI), compressive strength of HVFA is suitable enough to use in concrete construction. Malhotra and Mehta reported that flexural and tensile performance for HVFA mixtures improve over time (34).

Due to its low heat of hydration, HVFA is a primary choice of material for mass concrete construction since thermal cracking is reduced. Several case studies reported the use of HVFA for massive construction, and all studies revealed satisfactory performance of HVFA concrete mixtures in terms of strength and good performance in durability properties (34, 33, 28). Considering the prospects of producing durable concrete with low cost and more resistance to thermal cracking, fly ash can be listed as a candidate material for the project. However, performance of HVFA concrete varies with the properties not limited to age, water/cement ratio, and LOI. With the selection of compatible properties to get the desired mechanical and durability performance, HVFA has the prospect for utilization in concrete barrier use. A Class F fly ash with low LOI was involved in the study.

3.2.4 Reclaimed Asphalt Pavement (RAP)

Reclaimed asphalt pavement is materials reclaimed and recycled from a rehabilitated or newly constructed asphalt pavement site. Reclaimed material consists of fine and coarse aggregates with asphalt film on the surface. Asphalt surfacing exists in nearly 94 percent of the U.S. paved roads (35). According to an asphalt pavement industry survey, the U.S. produced around 76.5 million tons of RAP in 2016 (36). RAP is mostly utilized in asphalt pavement industries for base stabilization or as replacement of virgin aggregates in new mixtures. Due to RAP's likely performance of enhancing ductility and toughness with the asphalt film coating the aggregates (37), research has been done to incorporate RAP in concrete mixtures (38, 39, 40).

With proper screening and utilization, RAP may serve as a potential alternate of virgin aggregate in Portland concrete mixtures with improved performance.

It was reported by several researchers that inclusion of RAP in concrete improves ductility and post cracking behavior of concrete. Concrete has limited performance in terms of flexure and tension due to its brittleness property. Delwar, Mostafa, and Ramzi conducted research on strain behavior of concrete mixtures with RAP and concluded that ductility of concrete improved as RAP failed at a higher strain rate compared to control (38). A study conducted by Hassan et al. to investigate the feasibility of utilizing RAP in concrete showed that RAP enhanced ductility of concrete (39). Hossiney et al. focused their research on effect of RAP on modulus of elasticity along with the strength properties of concrete (37). They reported a decrease in strength and modulus of elasticity and deduced that RAP improved flexibility of concrete by decreasing modulus of elasticity of material. Huang et al. investigated behavior of concrete with respect to toughness and brittle failure (40). Their conclusion was in agreement with other researchers in terms of enhancing ductility of concrete mixtures using RAP. Their observation was that the asphalt film on the surface of aggregates blunted and arrested microcrack growth and thus improved toughness and ductility. All literature supported the fact that inclusion of RAP decreases the strength and stiffness, however increases toughness and ductility. In view of the performance review of past literature and additional benefits of adding the recycling option for RAP as an alternate source of aggregates for concrete with lower cost, RAP was considered as a viable material to incorporate in this research with the focus on optimized performance in terms of toughness, strength, and ductility for concrete barrier use.

3.2.5 Fiber

Fibers are used as small reinforcing materials to improve crack resistance of concrete. Concrete exhibits excellent performance in compression. However, concrete performance is limited in withstanding tensile and flexural loading. Reinforcing characteristics of fiber arrest and control the growth and propagation of crack by bridging (41) and pull-out mechanisms (42); fiber also improves flexural and tensile performance and structural integrity of concrete mixtures.

Inclusion of short fibers in concrete improves flexural toughness and impact resistance of concrete composites (43, 44, 45). Research has been performed to evaluate the effect of fiber properties including, but not limited to, different types, dosages, and geometry. Numerous research has been conducted on steel fiber as steel fiber is one of the commonly used fibers in the concrete industry. Steel fibers exhibited improved impact resistance with steel fiber dosage ranges from 0.1-2 percent by volume of mixture (43,46, 42). In addition, with improvement of toughness with pullout mechanism, steel fibers showed enhancement in toughness and post peak behavior of concrete (47, 43). Research on synthetic fibers such as polypropylene, polyvinyl alcohol, and polyamide also reported improvement in toughness (48, 49, 50) and impact resistance of fiber reinforced concrete (51). Synthetic fiber requires lower dosage compared to steel fibers, and typical dosage for synthetic fiber ranges from 0.01-0.5 percent by volume of concrete (52). Though natural fibers are being successfully used in other composites, it is not so popular in concrete due to concerns of corrosion of the fibers in the alkaline environment of concrete. Carbon nanofiber (CNF) and nanotubes (CNT) are two emerging types for fibers that exhibited excellent performance in toughness and ductility enhancement (53). CNT and CNF arrests development of microcracks, and thus demonstrates significant improvement in concrete

toughness, ductility, and impact resistance. Though concrete can be made using small dosages of CNT and CNF (53), it is not economical to use because of high material acquisition cost.

In addition to enhancing mechanical properties of concrete mixtures, fibers aid in improvement in durability properties. Incorporation of short length fibers, specially the synthetic fibers, decreases permeability, plastic and drying shrinkage, and carbonation depth (54). In light of the above, fiber was listed as a candidate material to be utilized for project use.

3.3 MATERIAL PROPERTIES AND CHARACTERIZATION

The materials for the concrete mixture was selected based on a mixture proportion that is currently in use in *MASH* TL-4 barriers used on TxDOT roadways (9). A *MASH* TL-4 barrier is a barrier type that satisfies the requirement of TL-4 of the AASHTO *MASH* Cement and Cementitious material.

Texas Lehigh cement conforming to ASTM C150 Type I/II was used in the majority of mixtures. Texas Lehigh cement conforming to ASTM C150 Type III was used for the mixtures for the fly ash material series only. The fly ash was a Rockdale Class F fly ash sourced from Headwaters Resources, Inc. Information on chemical and physical properties of the Portland cement and fly ash used in this project was obtained from the suppliers (see Table A.1 in Appendix A). Both of the Portland cements had a specific gravity of 3.15 and the fly ash had a specific gravity of 2.19.

3.3.1 Aggregates

One virgin fine aggregate source and virgin crushed stone was used for all the mixtures. Specific gravity and absorption capacity of the aggregates were determined in accordance to ASTM C127 and ASTM C128. Source, type, and physical properties of the aggregates are tabulated in Table A.2 in Appendix A. Sieve analysis was performed in accordance to ASTM C136 for the traditional (i.e., concrete sand and #67 river gravel) aggregates. Figure J.2 in Appendix A shows the sieve analysis results for virgin coarse and fine aggregates. In this project, both crumb and fine rubber particles were utilized individually or in combination as replacement of coarse and fine aggregates for performance evaluation. The rubber aggregate particles were supplied in size fractions; therefore, no sieve analysis was performed for the rubber. A #5-8 sieve size (2.36-4mm) and #20 sieve (0.841mm) size rubbers were received for the project use. The material properties for the rubber aggregates were provided by the supplier.

3.3.2 Fiber

A variety of commercial fibers are available for concrete. Initial selection of fiber was conducted on the basis of material type, length, and cost of the fibers. Fiber classification with respect to material type includes natural, synthetic, steel, glass, carbon nanofiber,s and carbon nanotubes. Natural and glass fibers were not incorporated in this study due to potential corrosion of fibers when exposed to the alkaline environment of concrete. Under the synthetic series, polypropylene, polyvinyl alcohol, and nylon fibers were selected for screening tests. Carbon nanofiber and nanotubes have proven to be promising candidates in enhancing toughness and ductility of cementitious material (55). However, the carbon nanofiber and nanotubes were excluded from the fiber list for project use due to its high added cost per unit volume of mixture.

The maximum length of fiber was restricted to 1 inch for proper dispersion of fibers in 4×4×14 beam samples. Based on the criteria mentioned above with suggestion from the manufacturer companies; the fibers tabulated in Table 3.1 were selected for performance evaluation.

Table 3.1. Source and Properties of Fibers Selected for Screening Study.

Fiber Name	Supplier	Length (in)	Material	Form	Specific Gravity	Tensile Strength
Nylo mono	Forta	¾	Nylon	Monofilament	1.14	140 ksi
Mono 150	FRC Industries	¾	Polypropylene	Monofilament	0.91	40-50 ksi
Ultra-net	Forta	¾	100% virgin Polypropylene	Fibrillated	0.91	83-96ksi
Super-net	Forta	¾	100% virgin Polypropylene	Fibrillated	0.91	83-96 ksi
Green-net	Forta	¾	100% Recycled Polypropylene	Fibrillated	0.91	83-96 ksi
CFS 100-S	CFS	1	Steel	Deformed mono fiber	7.86	Exceeds ASTM A820 specs
PVA RECS15	Nycon	0.375	Polyvinyl alcohol	Monofilament	1.3	240 ksi

Information was obtained on fiber geometry (e.g. length, type single, fibrillated) and material property (e.g. tensile strength) from the material supplier. Table 3.1 lists fiber details, and Figure 3.2 provides pictures of the fibers.

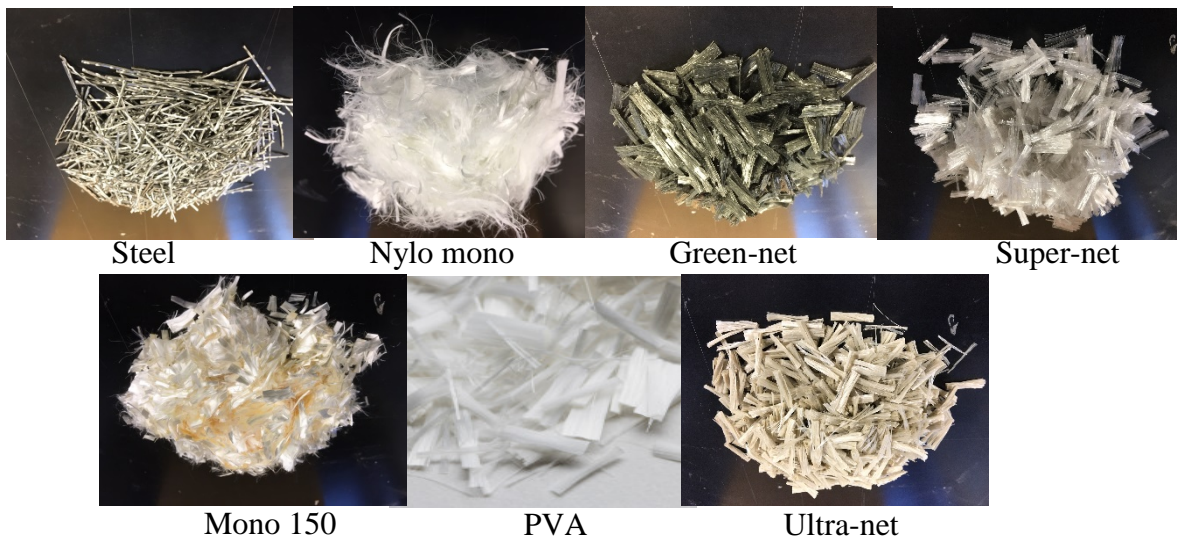


Figure 3.2. Fibers Selected for Screening Study.

3.3.3 Geogrid

A high density polypropylene structure geogrid was used in this work. Geogrid performance varies with the orientation of the grids with respect to applied load. Therefore, biaxial geogrids with square openings was selected to eliminate the variability of directional load distribution. A polypropylene biaxial geogrid was received from L&M Supply Company. Table 3.2 lists the aperture size and tensile strength information obtained from the supplier, and Figure 3.3 shows a photo of the geogrid.

Table 3.2. Biaxial Geogrid Properties Obtained from Manufacturer.

Property	BX12 type 2
Aperture Dimensions (Nominal)	1.0 × 1.3 inches
Flexural Stiffness	750,000 mg-cm
Minimum Rib Thickness (Nominal)	0.05 × 0.05 inches
Tensile Strength @ 2% Strain	410 × 620 lb/ft
Tensile Strength @ 5% Strain	810 × 1340 lb/ft
Ultimate Tensile Strength	1310 × 1970 lb/ft

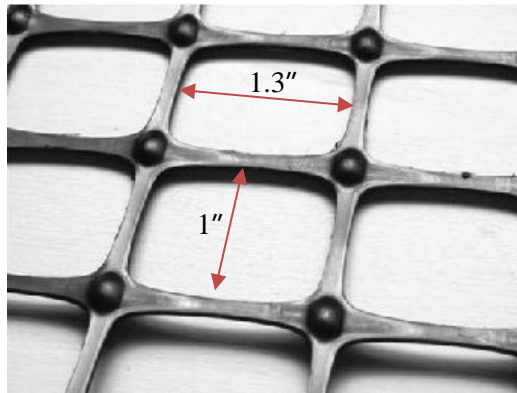


Figure 3.3. Biaxial Geogrid Aperture Dimensions.

3.4 SUMMARY OF LITERATURE REVIEW

The previous sections presented a summary of the background study and property analysis of material that were considered for use in this project. Candidate materials were identified considering the likely behavior of the material, cost, and ease of construction. The results from this phase of the study was vital to shortlist candidate materials for the test matrix.

3.5 MORTAR AND CONCRETE EVALUATION

The next sections include testing and evaluation of control concrete mixtures and concrete blends with the candidate materials discussed in the previous sections to observe the performance of mixtures.

The base mixture (aka the control) was designed based on a *MASH* TL-4 concrete median barrier mixture proportion that is currently in use on TxDOT roadways. The mixture proportion for the control mix is tabulated in Table 3.3. In the test mixtures, the mixture proportion was adjusted depending on the material series tested. For the geogrid and fiber material series, the materials were incorporated in an addition basis. Recycled tire rubber and RAP were incorporated as volume and weight replacement of aggregate, respectively; fly ash was included as volume replacement of cement. Table 3.4 shows the material proportion matrix.

Table 3.3. Mixture Proportion for Control Concrete Barrier Mixture.

Component	Amount (lb/yd³)
Type I/II Cement	424
Fly Ash	142
#67 River Gravel	1886
Concrete Sand	1324
Water	250

Referring to the control concrete mixture design, water to cement ratio for all mixes was 0.44, coarse to fine aggregate ratio by weight was 1.4, and replacement of cement by Class F fly ash was 25 percent by volume. A mid-range water reducer was utilized to attain a 3-inch minimum slump for acceptable workability. Batching, mixing, and curing of concrete were performed conforming to ASTM C192/C192M.

3.5.1 Testing and Evaluation Methods

3.5.1.1 Compressive Strength

Control concrete mixtures and alternate material incorporated blends were tested according to ASTM C39, and the compressive strength was evaluated at 7 and 28 days. Except for the mixtures containing fibers, three 4×8-inch cylinders were cast and evaluated at each specific age. For better dispersion and orientation of fibers, 6×12-inch cylinders were prepared and tested for those mixtures. The compressive strength testing data was analyzed to check whether the data fell within the maximum permissible range according to ASTM C39 specification. As per ASTM C39 specification, if any sample data was dispersed more than 8.7 percent from the average, the data was discarded and the average of two samples were recorded. If any of the two data points deviated more than 7.6 percent of the average of the two data points, then compressive strength data for all three specimens for the mixtures were discarded and new samples were prepared and tested.

3.5.1.2 Flexural Strength

Flexural strength and toughness were determined by performing a four-point bending test similar to ASTM C1609 on 4×4×14-inch beams.

Table 3.4. Candidate Material Description and Mixture Proportion Designation Matrix.

Material Series	Material Type	Material Description	Content Used/Approach	Mixture Designation
Recycled tire rubber aggregate	Powder rubber	#20 sieve (0.8mm) Scrap tire rubber particles ranging from 0.2-0.8mm	10% or 20% volumetric replacement of fine aggregate with powder rubber aggregate	Example: PR10F designates a mixture that contains 10% fine aggregate replacement with powder rubber
	Crumb rubber	#5-8 sieve (2-4mm) Scrap tire rubber particles ranging from 2-4mm	10% or 20% volumetric replacement of coarse aggregate with crumb rubber aggregate	Example: CR10C designates a mixture that contains 10 % coarse aggregate replacement with crumb rubber
	Powder rubber/crumb rubber hybrid	#20 sieve and #5-8 sieve	10% or 20% volumetric replacement of fine aggregate with powder and crumb rubber	Example: PR5FCR5F designates a mixture that contains 5% replacement of fine aggregate with powder rubber and 5% replacement of fine aggregate with crumb rubber for a total rubber replacement content of 10%
	Powder rubber/crumb rubber hybrid	#20 sieve and #5-8 sieve	10% or 20% volumetric replacement of fine and coarse aggregate with powder and crumb rubber	Example: PR5FCR5C designates a mixture that contains 5% replacement of fine aggregate with powder rubber and 5% replacement of coarse aggregate with crumb rubber for a total replacement content of 10%
RAP	Coarse	≥#4 sieve (4.75mm) Recycled asphalt pavement passing 3/4 in and retained on #4 sieve (4.75mm)	25 or 50% mass replacement of coarse aggregate with coarse RAP	Example: RAPC25 designates a mixture that contains 25% replacement of coarse aggregate with coarse RAP
	Fine	< #4 sieve (4.75mm) Recycled asphalt pavement passing #4 sieve (4.75mm) and retained on #100 sieve (0.15mm)	25 or 50% mass replacement of fine aggregate with fine RAP	Example: RAPF25 designates a mixture that contains 25% replacement of fine aggregate with fine RAP

Table 3.4. Candidate Material Description and Mixture Proportion Designation Matrix (Continued).

Material Series	Material Type	Material Description	Content Used/Approach	Mixture Designation
Fiber	Polypropylene	Synthetic	Addition of 0.075% or 0.12% (based on mixture volume) of polypropylene fibers to the mixture	Example: Polypropylene0.12 designates a mixture that contains 0.12% of polypropylene fibers added to the mixture
	Nylon	Synthetic	Addition of 0.075% or 0.12% (based on mixture volume) of nylon fibers to the mixture	Example: Nylon0.12 designates a mixture that contains 0.12% of nylon fibers added to the mixture
	Polyvinyl alcohol (PVA)	Synthetic	Addition of 0.075% or 0.12% (based on mixture volume) of polyvinyl fibers to the mixture	Example: PVA0.12 designates a mixture that contains 0.12% of polyvinyl alcohol fibers added to the mixture
	Steel	Metallic	Addition of 0.75% (based on mixture volume) of steel fibers to the mixture	Example: Steel0.75 designates a mixture that contains 0.75% of steel fibers added to the mixture
Fly ash	F-ash	Supplementary cementitious material	50% replacement of cement by volume with class F fly ash	Example: Fash50 designates a mixture that contains 50% replacement of cement by class F fly ash
		Supplementary cementitious material	75% replacement of cement by volume with class F fly ash	Example: Fash75 designates a mixture that contains 75% replacement of cement by class F fly ash
Geogrid	Biaxial geogrid	as-received	Placement of as-received geogrid in 1 layer at either 1/3 or 1/2 level from bottom	Example: Geogrid1/3U designates a mixture that contains 1 layer of as-received geogrid placed at 1/3 level from bottom
		corrugated	Placement of corrugated geogrid in 1 layer at either 1/3 or 1/2 level from bottom	Example: Geogrid1/3C designates a mixture that contains 1 layer of corrugated geogrid placed at 1/3 level from bottom
			Placement of corrugated geogrid in 2 layers at 1/3 and 2/3 level from bottom	Example: Geogrid2LC designates a mixture that contains 2 layers of corrugated geogrids placed at 1/3 and 2/3 level from bottom

3.5.1.3 Flexural Toughness

As per ASTM C1609, flexural toughness was determined by calculating the area under the flexural testing load-deflection curve up to 0.08 inch deflection. Figure 3.4 shows a sample load-deflection curve **Error! Reference source not found.** The area under the curve was automatically calculated by the flexural testing device software. However, the machine was unable to capture the load-deflection data for the samples that exhibited brittle and abrupt failure, and provided incorrect toughness values. For these mentioned cases, the trapezoid method was incorporated to manually calculate the toughness value from the load-deflection curve.

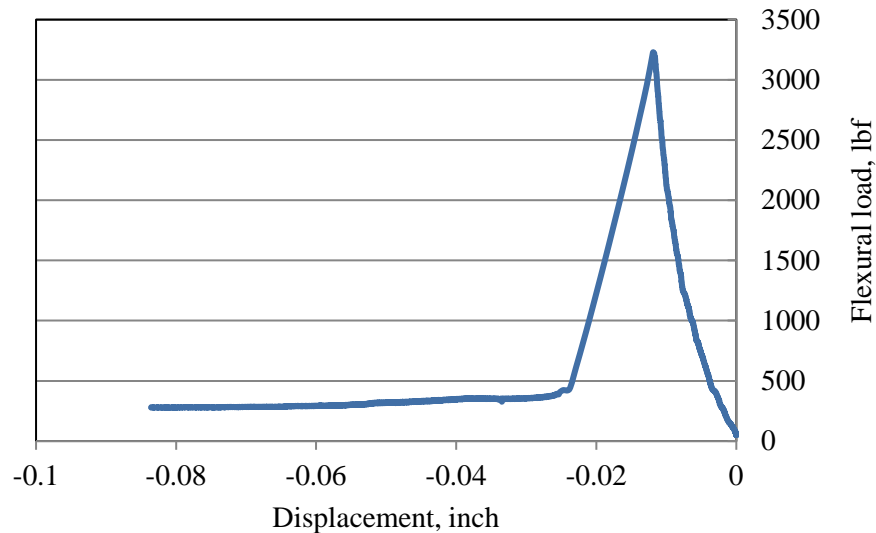


Figure 3.4. Load-Deflection Curve for Gnet.25 Sample.

3.5.1.4 Impact Resistance

Impact resistance test was performed in accordance to the drop weight test procedure proposed by ACI 544. However, it was revised so that the thicknesses of the concrete disk samples could be modified (see Figure 3.5). Eight identical 6.0-inch diameter and 2.5-inch thick cylindrical specimens were cut from two 6-inch diameter \times 12-inch high concrete cylinders. Then, using a standard proctor hammer of 10 lb weight with a drop of 18 inches, load was transferred to the sample through a steel ball at the center of the cut specimen. The hammer was dropped repeatedly, and the number of blows required to achieve the first visible crack and ultimate failure for the specimen were recorded.

3.5.2 Initial Phase Testing Results

Following is a summary of the initial set of screening studies that were conducted to assess the effectiveness of the candidate materials:

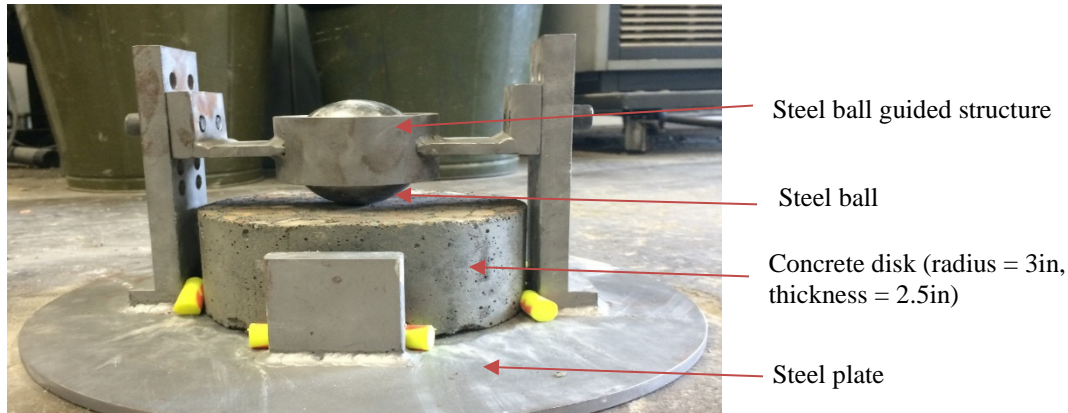


Figure 3.5. Experimental Set-Up for Impact Testing.

3.5.2.1 Fibers

- a) Fiber concrete mixtures were prepared by adding the fibers to concrete. In the literature, typical fiber volumes range from as low as 0.05–0.6 percent for synthetic fibers (52) to 0.1–2 percent for steel fibers (47). Therefore, in this project 0.12 and 0.75 percent dosages were selected for initial screening for synthetic and steel fibers, respectively. The 7-day compressive strength results for the control mixture and fiber mixtures are provided in Figure A.1 in Appendix A.
- b) With respect to the monofilament fibers, NyloMono and Mono150 (see Table 3.1) fiber test results were almost similar except for the failure type exhibited at the time of flexural testing. ***Mono150 showed better toughness, i.e. flexural failure was more abrupt for the concrete containing Nylo mono as compared to the concrete containing Mono150 (see Table 3.5).*** These fibers were all evaluated at a dosage of 0.12 percent by volume.
- c) ***Among net-like fibers, Green-net performed the best overall.*** Note, the dosage of the fibers was set to 0.12 percent.
- d) Comparison of the best performing monofilament fiber (Mono150) with net-like fibers (i.e., Green-net, Super-net, Ultra-net) (see Table 3.5) showed the concrete containing the 0.12 percent by volume. Mono150 fiber depicted better toughness than the concrete containing the 0.12 percent by volume net-like fibers, however, the Mono150 fiber concrete mixture had significantly higher reduction in flexural strength as compared to the Green-net fibers (see Table 3.6). Thus, it was decided to investigate further the influence of the net fibers and Mono150 and ***Nylo-Mono was removed from the matrix.***
- e) Thus, another set of tests was performed for all the net-like fibers by increasing the dosage to 0.25 percent by volume of mixtures in order to see whether the toughness could be improved. It was found that the Green-net fiber performed the best comparing all the parameters. ***Therefore, Green-net was chosen for the next phase and Mono150 was tabled.***
- f) Another monofilament fiber, polyvinyl alcohol (PVA), was procured by the research team. Since this fiber was procured after the initial set of screening tests was performed at 0.12 percent, the research team decided to evaluate this fiber at 0.25 percent fiber volume dosage in order to compare the results of the net-like fibers that were evaluated

at 0.25 percent fiber volume. The performance showed the PVA was comparable to the Green-net fiber (see Table 3.7), however, the fiber was not cost effective compared to polypropylene fiber (PVA cost twice as much as the polypropylene fiber per pound).

Therefore, PVA was not chosen for further evaluation.

- g) Table 3.5 provides a cost analysis and 28-day strength performance comparison of fiber reinforced concrete mixtures as compared to the control concrete. The steel fiber performed the best in improving strength and toughness; however, the **steel fiber was withdrawn from further evaluation** due to concerns with handling the fibers during concrete processing, corrosion concerns, and cost.

Table 3.5. First Phase Screening Test Summary for Fiber Series.

Product	Dosage	Price Per Pound, \$*	Cost Increase Per Cubic Yard	Measured Change in 28 day Compressive Strength	Measured Change in 28 day Flexural strength	Measured Change in 28 day Toughness	Change in impact load absorbance up to initial crack
Ultra-net	0.12% by vol	8	15.1	-0.4	-22.4	2.2	-21.429
Green-net	0.12% by vol	8	15.1	3.9	4.3	18.8	7.14286
Super-net	0.12% by vol	8	15.1	2.5	6.3	-6.4	7.14286
Mono 150	0.12% by vol	4.5	8.8	2.8	-23.3	27.9	-7.1429
CFS	0.75% by vol	0.6	48	10	24	54.8	60.2041

*Price per pound is a ballpark number provided by the supplier

Table 3.6. Net-Like Fiber Test Summary Data Evaluated for 0.25% Dosage of Fibers.

	Compressive strength, psi	Flexural strength, psi	Flexural toughness, lbf-in	Number of blows for initial crack to occur	Number of blows for failure to occur
Control	6094	788	17	14	15
Ultra-net	5380	572	71	19	21
Green-net	5611	768	82	19	24
Super-net	5538	783	64	20	27

Table 3.7. PVA Fiber Test Summary Added at Dosage of 0.25% by Volume of Mixture.

	Compressive strength, psi	Flexural strength, psi	Flexural toughness, lbf-in	Number of blows for initial crack to occur	Number of blows for failure to occur
Control	6094	788	17	14	15
PVA.25	6135	762	50	16	21
Gnet.25	5611	768	82	19	24

3.5.2.2 F-Ash

Rate of strength gain of concrete mixtures with HVFA is slower compared to the control composite. Siddique incorporated 50 percent Class F fly ash by volume in a Type I cement concrete mixtures and observed 38 percent reduction in compressive strength compared to the control (32). Huang, Shu, and Cao reported that 80 percent by volume of class F fly ash decreased the compressive strength from 34.5 MPa to 25 MPa (56). This is even with a water/cement adjustment to compensate for the reduced strength gain. The water/cement ratio for the control mixture was 0.60, and it was reduced by 20 percent to 0.48 for the 80 percent HVFA. Therefore, a Type III cement was utilized in this work to aid in early strength gain for the F-ash mixture.

- (a) F-ash material series at both 50 and 75 percent replacement level of cement showed lower values of compressive strength compared to the control concrete. Reduction in 28-days compressive strength for Fash50 and Fash75 were approximately 20 and 35 percent, respectively (see Table A.3 **Error! Reference source not found.** in Appendix A).
- (b) Performance of the F-ash series was not satisfactory in flexural toughness and strength. Test results showed that the Fash50 blend depicted 40 percent reduction in flexural toughness compared to the control blend, and 15 percent reduction in flexural strength value as compared to the control mixture. Fash75 experienced more than 50 percent reduction in flexural strength. Bilodeau and Malhotra incorporated HVFA in Type III cement concrete mixtures (57). The research showed that HVFA mixtures could achieve flexural strength close to the control if the water/cement ratio was decreased to 33 percent from the control (0.48 percent).
- (c) Impact testing on F-ash series samples showed significant reduction in impact absorbance.

It is evident that compressive and flexural performance of F-ash was poor compared to the control. If the water/cement ratio was reduced, then it might have helped to achieve flexural strengths similar to the control. However, reduction in water/cement to a very low value would create consolidation and workability issues during the construction. An increase in curing time above 28 days could enhance performance of F-ash series. However, it would not be convenient for the construction purposes to increase curing time. Therefore, this material series was not considered for further evaluation and discarded from second phase testing.

3.5.2.3 Geogrid

As-received geogrids were placed at different placement levels and evaluated.

- a) Overall performance of concrete containing geogrids showed 4-5 times increase in toughness (see Figure 3.6) as compared to the control concrete, except in the case of the sample containing the geogrid placed at one-third from the bottom of the sample. This sample had a reduction in flexural strength and the lowest improvement in toughness when compared to the other geogrid placement level tests. It could be due to bond-slip effect between geogrid and concrete under tensile loading.
- b) Another set of tests in which the surfaces of the geogrids were brushed with a steel brush to roughen the surface (aka corrugate) were conducted. However, as seen in Figure 3.6, the corrugated geogrids did not perform better than the as-received, non-corrugated geogrids—which could be due a weakening in the geogrids from the abrasion process to make the corrugations.
- c) Flexural strength data followed the same trend as the toughness behavior (compare Figures 3.6 and 3.7). Among all the samples in the geogrid series, both corrugated and non-corrugated geogrid position midway (i.e., 1/2-depth) were comparable in flexural strength and improved in toughness, and shown separately in Table 3.8.
- d) Impact performance of concrete samples with geogrids were improved compared to the control concrete. The number of blows required for initial crack of the samples was recorded (see Figure 3.8). The test method associated here can be associated with high dispersion of data, and Geogrid 1/3U and Geogrid2LU samples showed high standard error. The data trend showed that non-corrugated geogrid samples provided higher impact resistance values compared to corrugated samples. However, recording of the number of impact blows data for failure was difficult to determine. This was due to the fact that the number of blows to failure should be recorded when the samples completely break, and any broken part touching the side bars of the impact testing device. Specimens with geogrids held the cracked pieces together even though the disks were completely cracked. In general, approximately 15-20 additional blows from initial cracking was required for geogrid samples to propagate the crack throughout the disk samples.
- e) Geogrid samples showed improved performance in flexure. However, **considering the difficulty in placement of geogrid in concrete barrier formwork, this material series was not considered for the final material selection phase.**

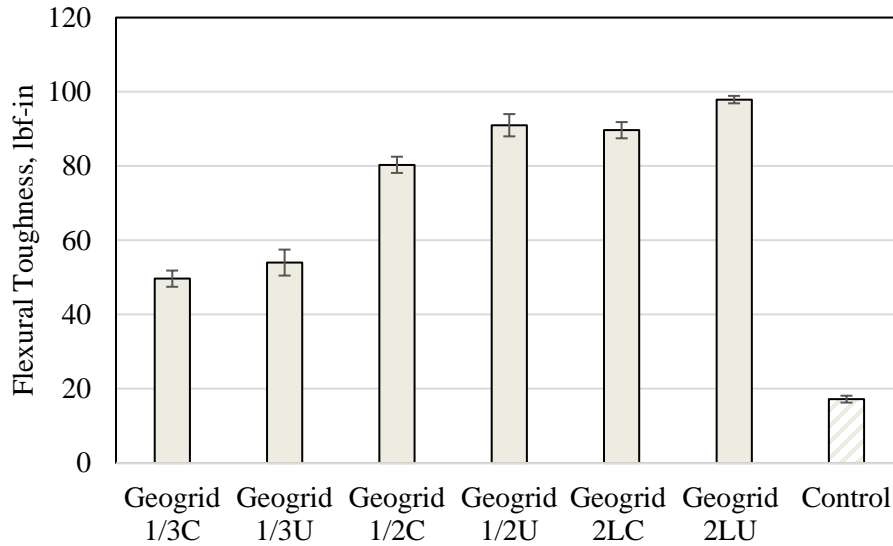


Figure 3.6. 28 Days-Flexural Toughness Results for Geogrid Samples.

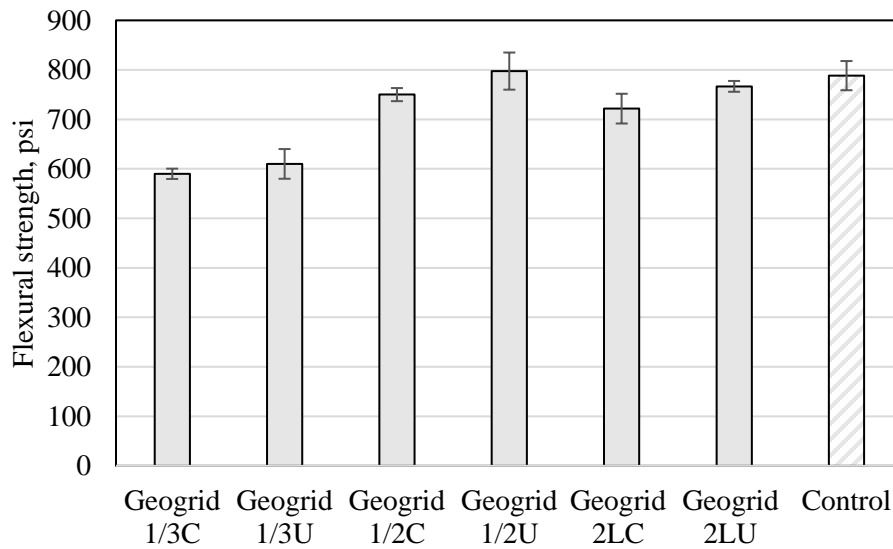


Figure 3.7. 28-Days Flexural Strength Test Results for Geogrid Samples.

Table 3.8. Comparison of Concrete Containing Corrugated Geogrid (Geogrid 1/2U) and Noncorrugated Geogrid (Geogrid 1/2U).

Geogrid was placed in 1-layer placement at 1/2 from bottom surface of the sample.

	Flexural strength	Flexural toughness
Mixture ID	psi	lbf-in
Control concrete	788	17
Geogrid 1/2U	798	91
Geogrid 1/2C	750	80

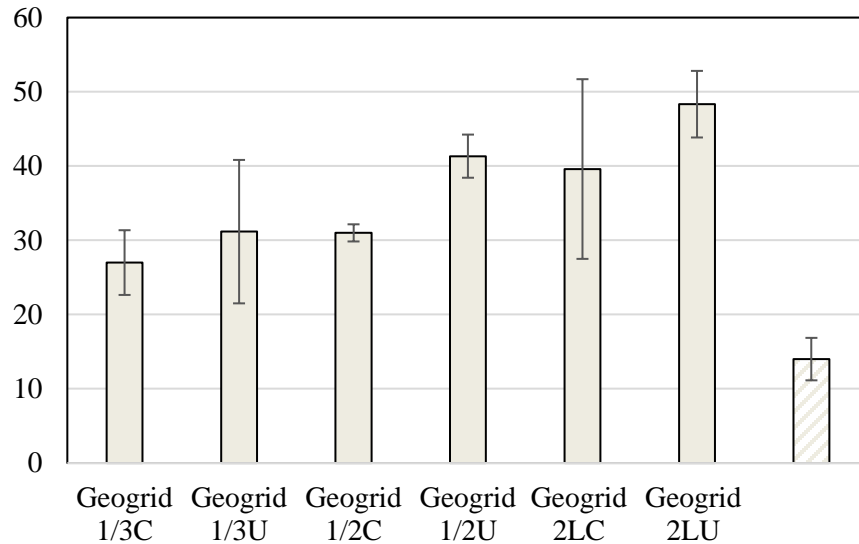


Figure 3.8. Number of Blows to Initial Crack Data Comparison for Geogrid Samples and Control.

3.5.2.4 Rubber

- a) Compressive strength testing results were evaluated for rubber as replacement of fine, coarse, and both fine and coarse aggregate with fine and crumb rubbers. Figure 3.9 summarizes the 28-day results. Inclusion of rubber reduced compressive strength of concrete mixtures. With the increase in rubber content, decrease in compressive strength was observed. Combination of powdered and crumb rubber performed better compared to other rubberized concrete mixtures. A concrete barrier requires a minimum of 4000 psi strength. **Therefore, it was decided to limit the rubber content to 10 percent replacement for the next phase testing.**
- b) Recycled tire rubber was used as a partial replacement of fine and coarse aggregate, and diverse performance in flexural testing was observed (see Figure 3.10). Initial screening was conducted starting with 10 percent and 20 percent by volume replacement of fine and coarse aggregates by powdered rubber and crumb rubber, respectively. The concrete containing 10 percent rubber particles all showed similar behavior in toughness regardless of the type of rubber particles (i.e., crumb or powdered) it contained (see Figure 3.11). At 20 percent replacement, flexural strength decreased, but as evident in Figure 3.10, toughness increased (see change in post-peak behavior in the control mixture versus the PR20F mixture).
- c) Initial testing of the rubber series depicted that inclusion of rubber decreased compressive and flexural strength, but improved toughness (see Figure 3.9, Figure 3.12, and Figure 3.11). Rubber dosage at 20 percent showed significant reduction (35-50 percent) in both compressive and flexural strength. Therefore, the next phase testing of rubberized concrete was performed at a rubber dosage of 10 percent by volume. In addition, only fine aggregate replacement by both crumb and powdered rubber was evaluated since the as-received rubber size of the crumb and powdered rubber was more consistent to that of a fine aggregate than a coarse aggregate. Siddique and Naik reported that crumb and powdered rubber sizes from

0.075 mm-5 mm performed better in strength testing as a replacement of fine aggregates rather than when it was used as a replacement of coarse and fine (22, 23). Consequently, the next phase of rubber testing comprised inclusion of both crumb and powdered rubber as a replacement of fine aggregate only.

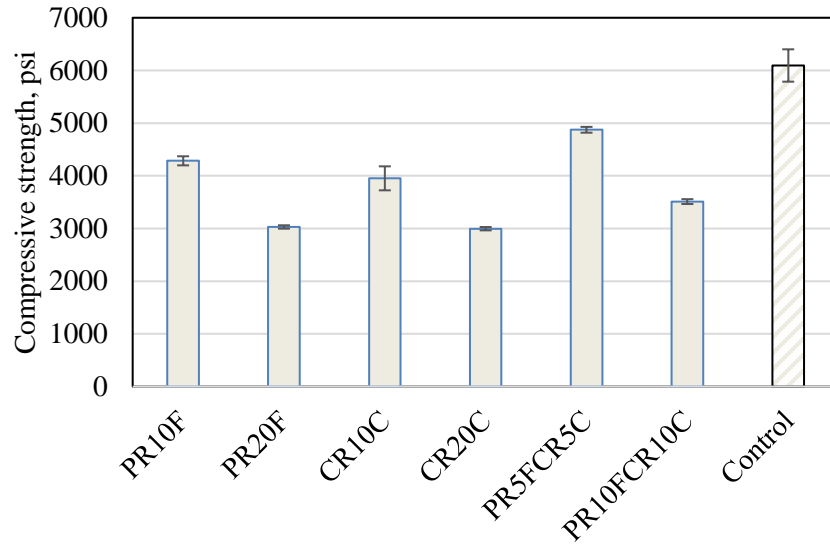


Figure 3.9. Initial Screening 28-Days Compressive Strength Test Results for Rubber Series.

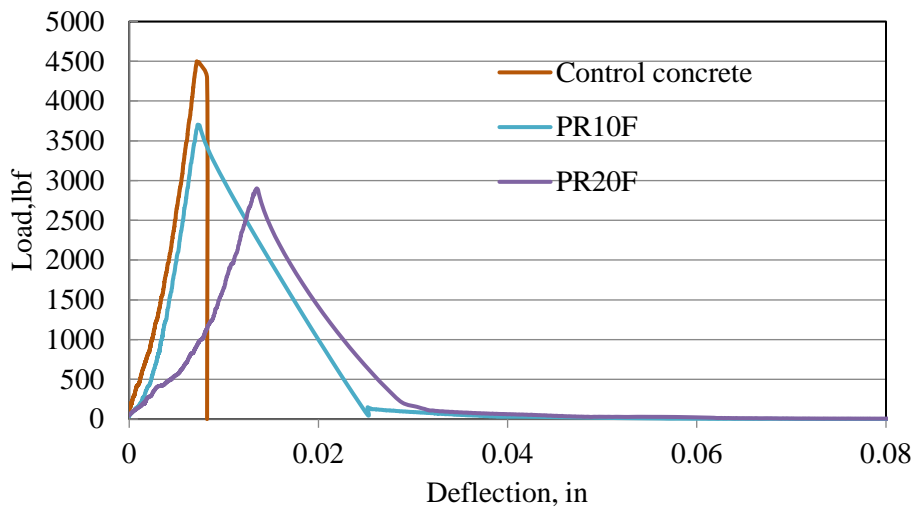


Figure 3.10. Load-Deflection Curve for Control Concrete and PR10F and PR20F under Flexural Loading.

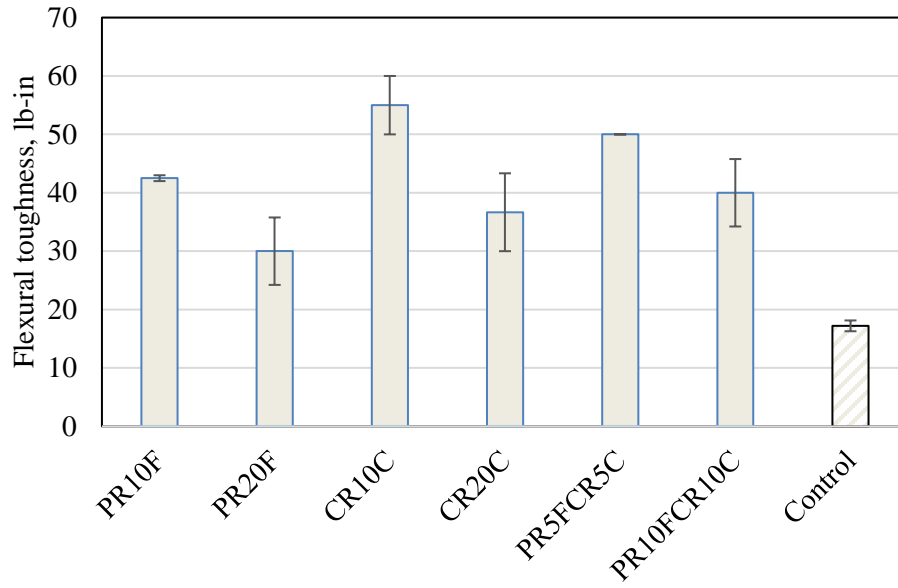


Figure 3.11. Initial Screening 28-Days Flexural Toughness Test Results for Rubber Series.

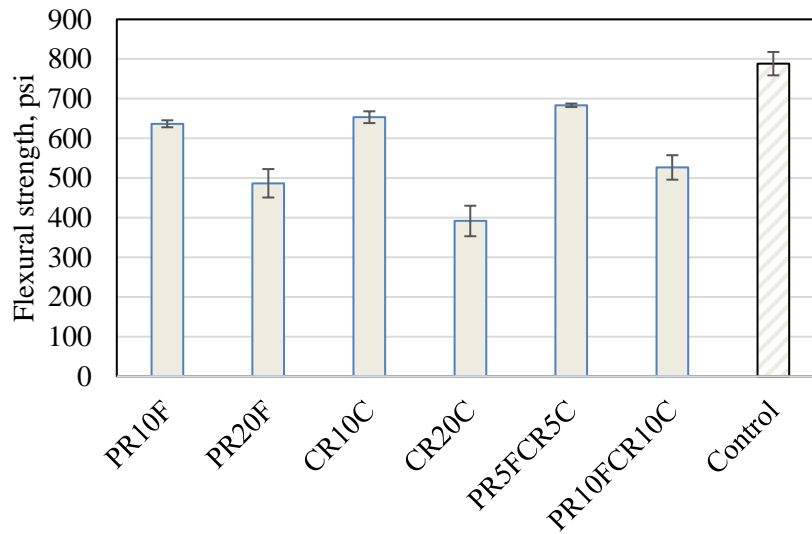


Figure 3.12. Initial Screening 28-Days Flexural Strength Test Results for Rubber Series.

3.5.2.5 Reclaimed Asphalt Pavement (RAP)

RAP was screened and material retaining on #4 sieve was used as a coarse aggregate replacement; material passing #4 sieve and retained on #100 sieve was incorporated as fine aggregate replacement. The replacement was conducted on a mass replacement basis. The initial screening testing mixtures for RAP were RAPC25 and RAPF25 (note, RAPC25 corresponds to 25 percent of coarse aggregate with RAP material retained on the #4 sieve, whereas RAPF25 corresponds to 25 percent replacement of fine aggregate with RAP materials passing the #4 sieve and retained on #100 sieve).

- a) Figure 3.13 shows the recorded 28-day compressive strength test results for RAPC25 and RAPF25. It was observed that concrete containing coarse RAP provided better compressive strength compared to concrete containing fine RAP. The RAP series overall showed reduction in compressive strength compared to the control. Decrease in compressive strength with the increase in RAP content was reported by Hassan et al., Huang et al., and Hossiney et al. (39, 40, 37). In addition, the study conducted by Huang et al. showed that addition of fine RAP depicted higher reduction compared to coarse RAP (see Figure A.4 in Appendix A).
- b) Flexural strength and flexural toughness performances of the RAP series were evaluated and plotted in Figures 3.14 and 3.15, respectively. RAPC25 depicted almost the same flexural strength as the control (2 percent reduction compared to control), but had a higher toughness value compared to the control (35 percent increase as compared to the control). Whereas, RAPF25 showed approximately 20 percent reduction in flexural strength and almost the same value of toughness compared to the control. Therefore, increase in RAP decreased flexural strength and enhanced or maintain similar values of toughness as the control for the materials and replacement dosages evaluated in this work. A similar conclusion was drawn by Hassan et al. and Huang et al. (39, 40).
- c) Impact test results for the RAP series showed that on average RAPC25 absorbed more energy compared to the other two mixtures before the initial crack occurred (see Figure 3.16). Post initial crack behavior was comparable for all mixtures. High variance was associated with the impact test results. High dispersion in data collected using a drop weight test was reported in several studies (58, 59).

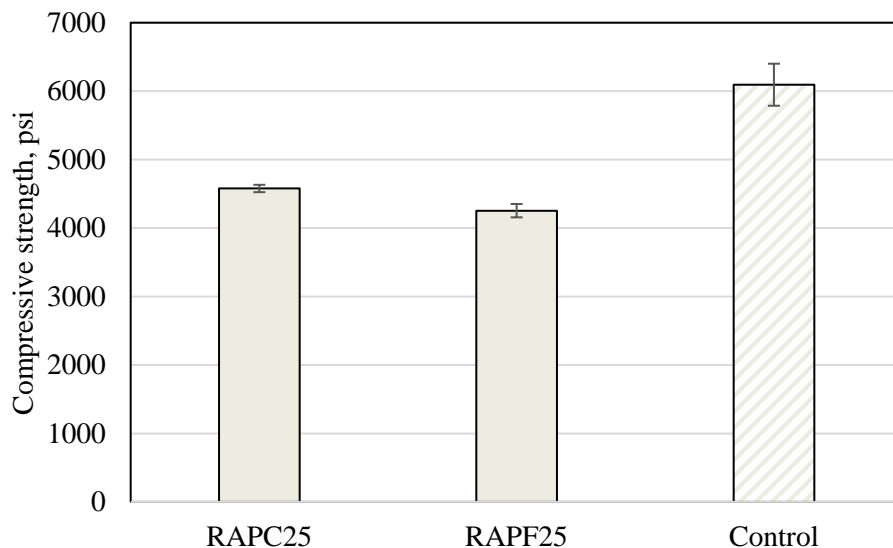


Figure 3.13. Initial Screening 28-Days Compressive Strength of RAP Series.

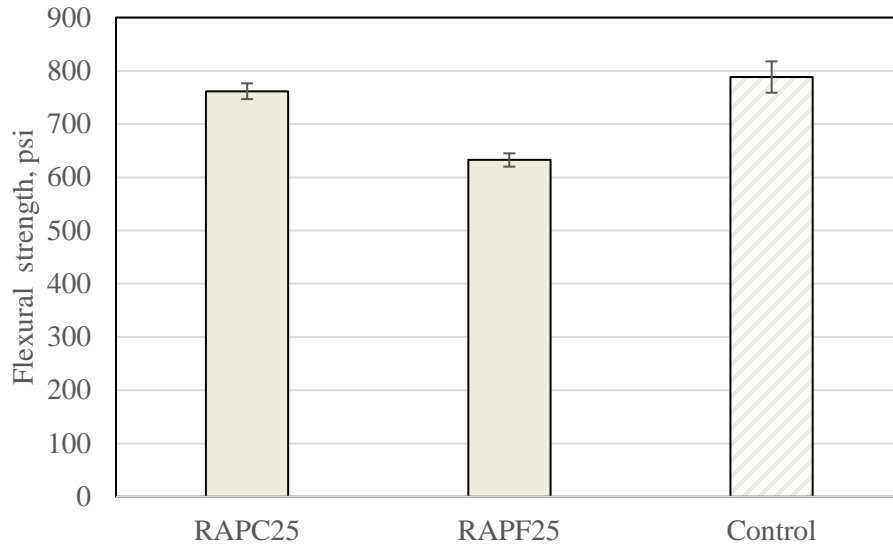


Figure 3.14. Initial Screening 28-Days Flexural Strength of RAP Series.

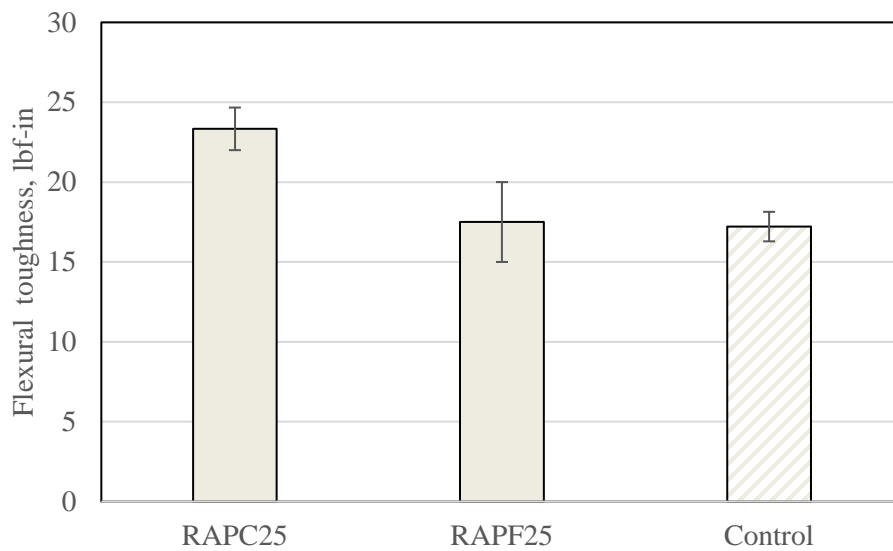


Figure 3.15. Initial Screening 28-Days Flexural Toughness of RAP Series.

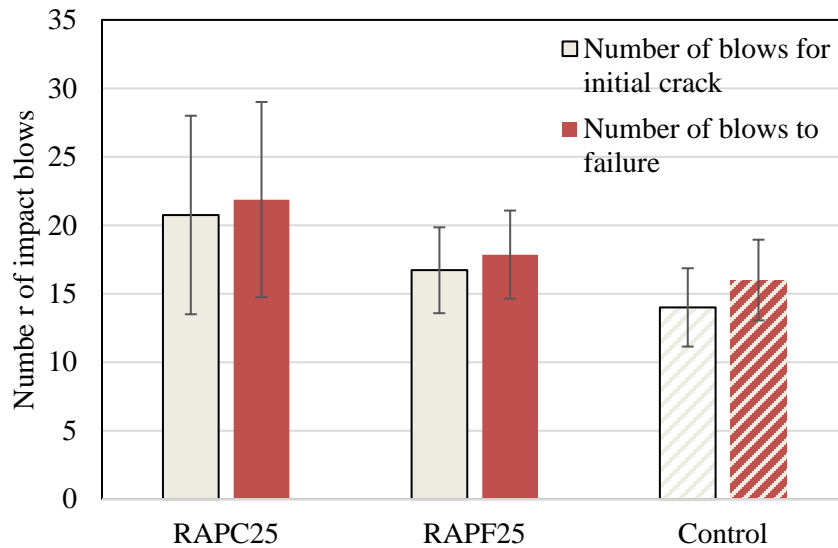


Figure 3.16. Initial Screening 28-Days Impact Resistance of RAP Series.

Based on the performance discussed above, **RAPC25 mixture was considered for the final evaluation and comparison study**. Increase in RAP percentage results in decrease in compressive strength. Blend mixtures of coarse and fine RAP performance have been reported to perform worse than only coarse RAP or only fine RAP concrete mixtures (Huang et al. and see Appendix A); thus, increasing the RAP content and using coarse and fine RAP blends were not pursued in this research.

3.5.3 Second Phase Testing Results

Additional testing (hence called the second phase) was conducted to evaluate the impact of using crumb rubber as a fine aggregate replacement (note, previously the crumb rubber was used as a coarse aggregate replacement). Table 3.9 summarizes the results. The table revealed that rubberized concrete with crumb rubber exerted almost 1.5-2.5 times improvement in impact resistance compared to the control concrete. Furthermore, compressive, flexural strength, and flexural toughness results were satisfactory and similar for all the rubber samples. It was also observed that the difference between initial crack to occur and failure to occur was one to three blows for the crumb rubber samples. It could be inferred that inclusion of rubber in concrete aided in absorbing more energy in impacts compared to the control until initial crack occurred. After initial crack occurrence, crumb rubber particles failed to arrest and control the propagation of cracks, and thus the samples failed to withstand much impact load after the occurrence of the initial crack.

Concrete mixtures with rubber particles showed promising results in terms of impact resistance with respect to the control. However, a reduction in compressive and flexural strength also occurred, with no significant improvement in toughness. As fiber has the property to enhance toughness of concrete (see section 3.5.2.1), another set of impact test was conducted using a hybridization approach with concrete that included different percentages of rubber particles and a fixed percentage of Green-net fiber. Green-net fiber was specifically chosen as it

was the optimum fiber in terms of impact resistance and toughness. Table 3.10 tabulates the drop weight impact test results for rubber mixes with and without fibers.

Table 0.9. Summary of Second Phase Test Results of Recycled Tire Rubber Series.

	Compressive strength, psi	Flexural strength, psi	Flexural toughness, lbf-in	Number of blows for initial crack to occur	Number of blows for failure to occur
Control	6094	788	17	14	15
PR10F	4285	637	40	15	17
CR10F	4685	607	43	29	30
PR5FCR5F	4732	615	38	31	34

Table 3.10. Influence of Green-Net Fibers On Concrete Mixtures Containing Rubber Particles.

Mixture Type	Sample ID	No of Blow for Initial Cracking	No of Blow for Ultimate Failure	Difference in No. of Blows
Control	Control	14	15	1
Green-net fiber	Gnet.25	10	14	4
Rubber and Green-net hybrid*	PR5FGnet	10	17	7
	PR10FGnet	8	14	7
	CR5FGnet	16	19	4
	CR10FGnet	20	25	5
	PR5FCR5FGnet	17	22	5
	PR10FCR10FGnet	9	17	9
Rubber blend	PR5F	17	18	2
	PR10F	14	17	3
	CR5F	19	22	3
	CR10F	30	31	1
	PR5FCR5F	31	34	3
	PR10FCR10F	24	26	2

*All Green-net and rubber hybrid mixtures contained Green-net fiber at a dosage of 0.25% by volume; therefore, the percentage was removed from sample designation for rubber and Green-net hybrid blends.

It was evident that addition of fiber in rubberized concrete reduced the impact resistance of these mixtures. However, the difference in the number of blows between the initial crack and the number of blows for ultimate failure increased in the hybrid samples containing the Green-

net fibers as compared to samples without the fibers. This indicates that the toughness of the mixtures was enhanced with the addition of fiber in the rubberized concrete mixtures. Toughness measurement results shown in Figure A.3 in Appendix A showed agreement with this result.

3.5.4 Selection of Concrete Mixtures for Field Bogie Testing

Based on all the tests performed, all the mixtures (i.e., Control, Gnet.25, PR5F, PR5FCR5F, PR5FCR5FGnet, PR10F, PR10FGnet, CR10F, CR10FGnet, and CR10Gnet) were compared and two mixtures were selected among the mixtures to be recommended for field bogie testing. Figure 3.17 shows four graphs plotted to determine the two optimum mixtures: (a) toughness versus flexural strength, (b) toughness versus number of blows to occur first crack, (c) flexural strength versus number of blows to occur first crack and (d) compressive strength versus number of blows to occur first crack. In the plots, the yellow filled circle corresponds to the control mixture and the red and green filled circles corresponds to CR10FGnet and PR5FCR5F mixtures, respectively. Those two mixtures are recommended based on their overall performance on all the properties evaluated earlier in this chapter.

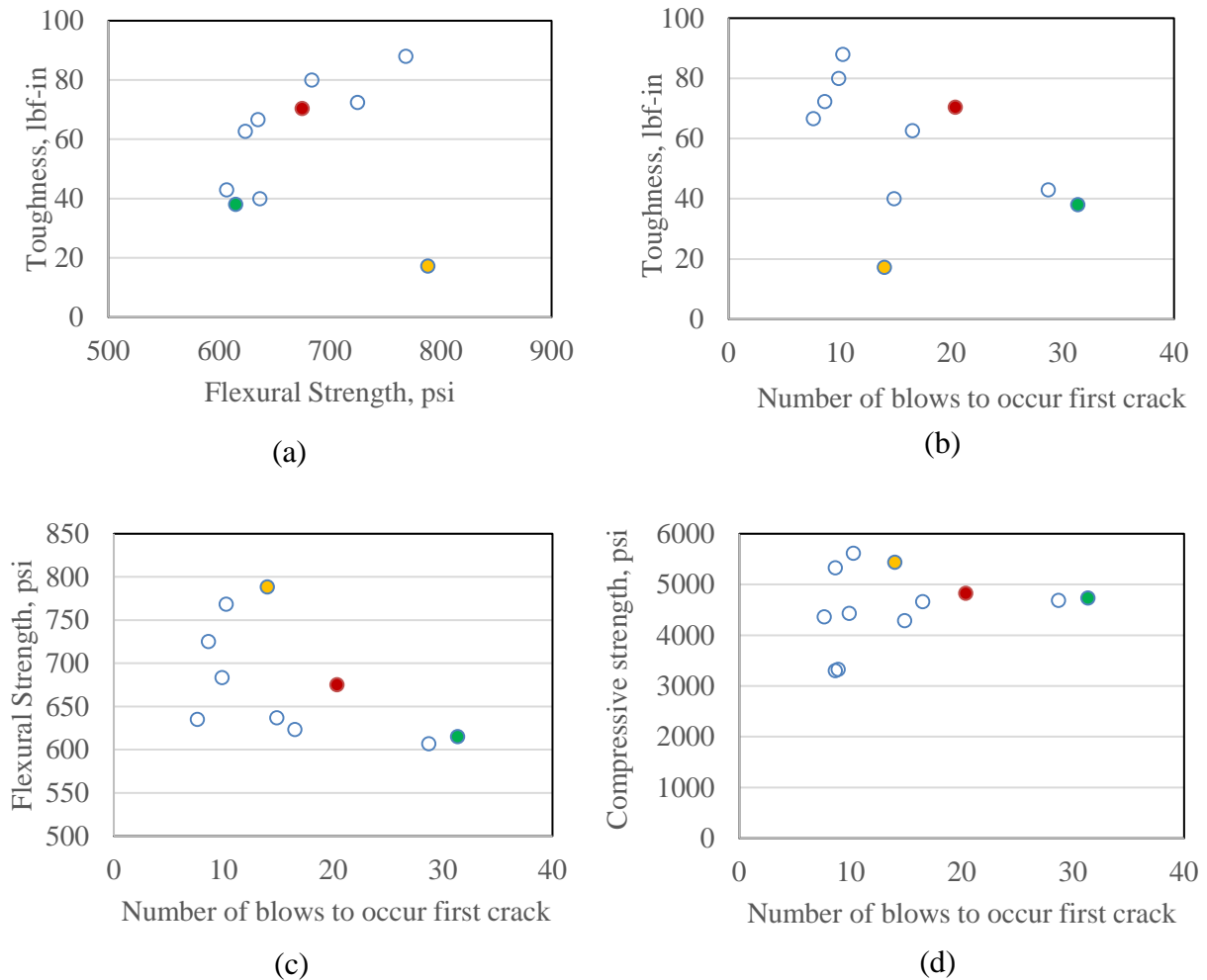


Figure 3.17. Comparison Plots of Concrete Mixture Characteristics.

3.5.5 Additional Tasks Performed

3.5.5.1 Analysis of Concrete Cores from Field Bogie Testing

Three 8-inch cylinder cores were collected from each of the median barriers used in bogie impact field tests. The cores were collected to perform comparative analyses on the samples. Resistivity test, visual inspection, and compressive strength test were performed on the cores. In addition, crack images were taken from the crash barriers after the bogie impact field testing was performed.

- a) Figure 3.18 shows the bulk resistivity test results for the cores collected from barriers tested in the bogie impact field tests. CR10FGnet has the lowest bulk resistivity compared to the control and PR5FCR5F. CR10FGnet cores contained gaps and large holes that are indicative of consolidation issues. The cores from the other two mixtures did not reveal any distress or holes.
- b) Compressive strength was performed on the core samples. The core from the CR10FGnet barrier displayed the lowest compressive strength values (see Table 3.11); the compressive strength of the core was significantly less than the samples that were made in the lab. This reduction in strength could have occurred due to the addition of an extra 25 gallons of water during mixing due to workability issues with CR10FGnet. As such, the considerable additional water likely affected the field impact test result since the laboratory performed impact and field test results varied significantly for this mixture.
- c) Figure 3.19 shows images of the crash barriers taken after field bogie test was performed to analyze crack pattern and crack opening. The crack pattern of the CR10FGnet mixture showed a zipper effect on the mixture. Impact loading induced zipper-like effect after initiation of the crack. Therefore, a single straight-line crack formation was observed. PR5FCR5F blend performed well in arresting the crack propagation; thus, thin width cracks with a branched pattern was observed for this mixture. Maximum crack opening for the control was smaller than CR10FGnet, but larger than PR5FCR5F mixture.

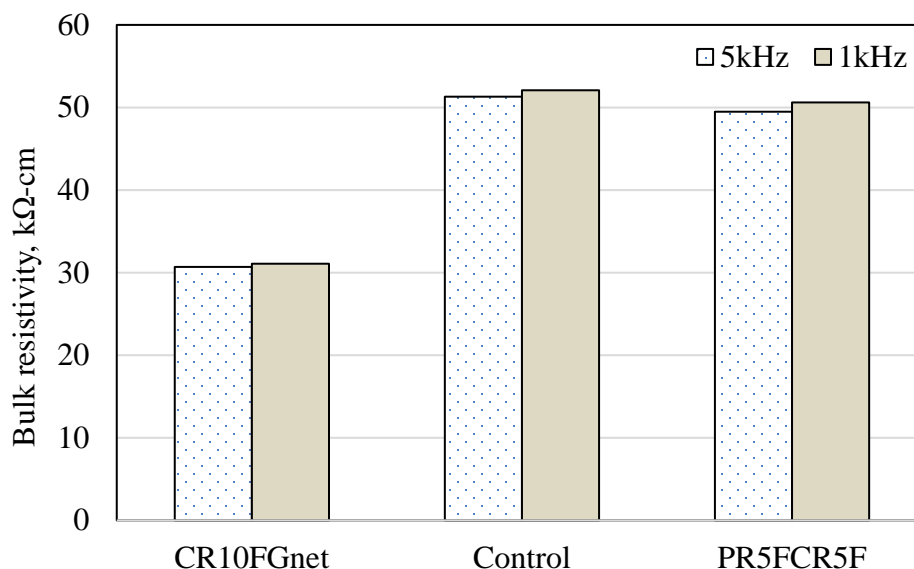


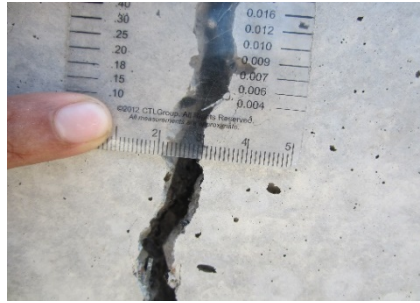
Figure 3.18. Bulk Resistivity Test Results for Cores Collected from Barriers Tested in Bogie Impact Field Test.

Table 3.11. Comparison of Compressive Strength Test Results of Core and Lab Samples.

	Core Compressive strength psi	Lab sample Compressive strength psi
Control	6120	6191
CR10FGnet	3849	4825
PR5FCR5F	4610	4731



(a) CR10FGnet crack pattern



(b) CR10FGnet maximum crack width measurement



(c) Control mixture crack pattern



(d) Control maximum crack width measurement



(e) PR5FCR5F crack pattern



(f) PR5FCR5F maximum crack width measurement

Figure 3.19. Images of Crack Pattern and Maximum Crack Width Measurement of CR10FGnet, Control, and PR5FCR5F Mixtures after Field Bogie Impact Test.

3.5.5.2 Recycled Tire Rubber Surface Treatment

Inclusion of rubber into concrete caused a reduction in compressive and flexural strength (see Table 3.9). Therefore, a chemical surface treatment was performed on the surface of the

rubber to improve bonding between cement and rubber, and thus enhance mechanical strength properties of rubberized concrete.

A two-step chemical process was performed to increase hydrophilicity of the rubber particles and adhesion bonding between the surface of rubber particles and paste. The first step involved a chlorination treatment on the surface of the rubber, and the second step included alteration of the surface using a sulfur donor. The rubber was cleaned with acetone before starting the chemical treatment process. Two percent trichloroisocyanuric acid dissolved in ethyl acetate was applied to the rubber surfaces for the first stage treatment process. Then the treated samples were heated with the chemicals, maintaining 65°C temperature for 6 hours. This process was followed by the second step treatment which involved an addition of 3-amino 1 propane sulfonic acid at a concentration of 0.5 mol/liter and exposed to heating at 145°C for 2 hours. The rubber samples were then directly incorporated to prepare mortar samples for mechanical strength evaluation.

Two sets of 2-inch mortar cube samples were cast, one containing treated rubber particles and the other containing untreated particles. Compressive strength testing was performed at 7 and 28 days as an indirect way to assess change in bond properties. Additionally, the change in contact angle of the water on the surface of the rubber was assessed. The contact angle technique was incorporated to determine the wettability of rubber. Images of 0.5µL water droplets on the surface the surface of rubber was captured, and the ImageJ software plugin was utilized to analyze and determine the wetting angle of rubber before and after treatment (see Figure 3.20). A decrease in the angle of contact between the rubber and water indicates an increase in hydrophilicity.

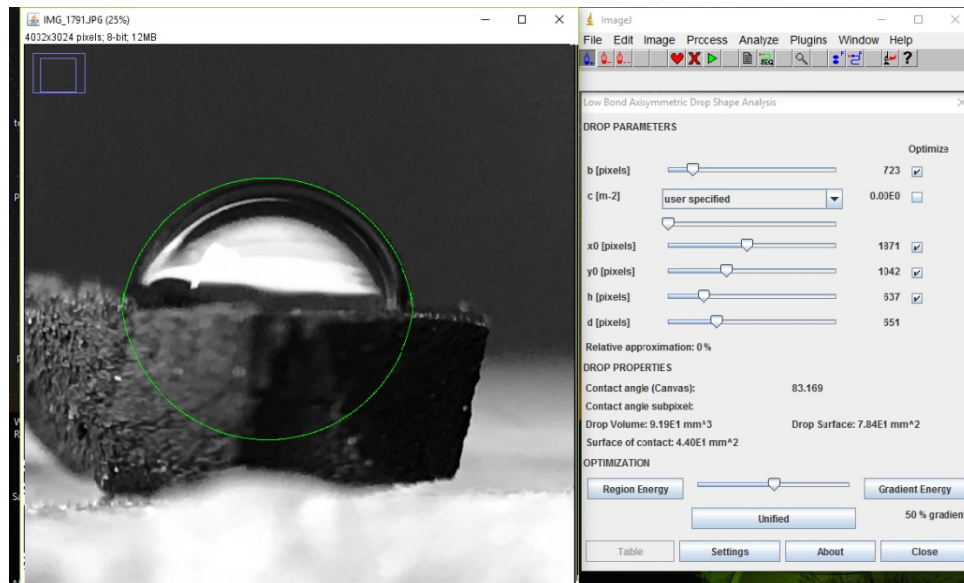


Figure 3.20. Drop Analysis on Surface of Rubber using ImageJ Plugin.

The chemical treatment resulted in improvement in compressive strength. Treated rubber samples containing mortar showed 15 and 18 percent increment on compressive strength for 5 percent and 10 percent replacement of fine aggregates, respectively, by rubber. Modulus of elasticity of the 5 percent and 10 percent treated samples dropped approximately 6 and 9 percent,

respectively, compared to the corresponding untreated samples. After treatment, the matrix might have become a bit more flexible with the treated rubber. After treatment, contact angle dropped from average of 108° to 72° when compared at 10 random readings taken at the surface of the rubber. Further investigation is needed to evaluate the impact of the treated rubber in other mechanical tests and in larger sized specimens.

3.6 CONCLUSIONS ON MATERIAL TESTING AND EVALUATION

The research in this chapter involved evaluating the feasibility of using different material systems to improve the performance of concrete barriers. The goal was to identify two mixtures that showed improved performance overall so that the concrete blend of the material series could be recommended for concrete barrier use. Based on the tests conducted in this chapter, the following main conclusions were drawn.

- a) Even though geogrid showed noteworthy improvement in toughness and impact resistance, it was not considered as a candidate for the recommended mixture list. It was not considered due to the potential difficulty in placing the material in the concrete barrier formwork with the reinforcement. The F-ash series overall performance was not satisfactory. Furthermore, it required more curing time and less water/cement ratio to exhibit improved performance, which was not feasible from a construction point of view.
- b) Green-net fiber at a dosage of 0.25 percent by volume of concrete blend, rubberized mixture contained 10 percent rubber as a volume replacement of fine aggregate, and coarse RAP as a 25 percent replacement of coarse aggregates were suggested from the initial screening for next phase testing.
- c) In the next phase testing, rubberized concrete mixtures that included 10 percent crumb or powdered, or combination of both, as a replacement of fine aggregates were evaluated. Based on the result, CR10F and PR5FCR5F were recommended for final evaluation. Gnet.25 and rubber combined mixtures were also evaluated in this phase with the purpose to overcome the shortcomings of concrete containing either rubber or fiber material series.
- d) Considering all the performance in initial screening and second phase testing, Control, Gnet.25, PR5F, PR5FCR5F, PR5FCR5FGnet, PR10F, PR10FGnet, CR10F, CR10FGnet, and CR10Gnet were selected for final evaluation. All the test results for the mentioned mixtures were compared, and CR10FGnet and PR5FCR5F mixtures were identified as optimum performance mixtures. These two mixtures were recommended to prepare full size concrete barriers for field bogie testing.

CHAPTER 4: DESIGN PROCESS

The design process consisted of determining barrier segment length and the frequency of rubber fenders placements based on the maximum barrier deflection and the lateral force exerted on the barrier by the impacting vehicle. All simulations were conducted with a rigid concrete model but with a calibrated rubber model to identify the influence of the rubber fenders on the system performance.

4.1 PICKUP TRUCK MEDIAN BARRIER

Four configurations of barrier segments and barrier lengths were simulated in this set of analyses with the pickup truck vehicle. There was a variation of two and three rubber fenders for the entire barrier system. In each simulation, there were expansion joint dowels between the barriers. The configurations of the segments that were simulated are as follows:

- Four 40-ft segments with two rubber fenders.
- Four 40-ft segments with three rubber fenders.
- Three 60-ft segments with two rubber fenders.
- Three 60-ft segments with three rubber fenders.

4.1.1 Four 40-ft Segments Configuration

For these simulations, the PVC pipe used in the expansion joint was enlarged to 1.5 times the size of the standard expansion joint (which is 1¼inch pipe), and the friction between the expansion dowel and the PVC was reduced to 0.01. Based on the results from all four runs, there was no major snagging that takes place at the joint between the barriers and the truck appears to be successfully redirected after impact. Figures 4.1 and 4.2 show the barrier set-up with the joints and barriers labeled.



Figure 4.1. Four – 40-ft Segments Configuration.

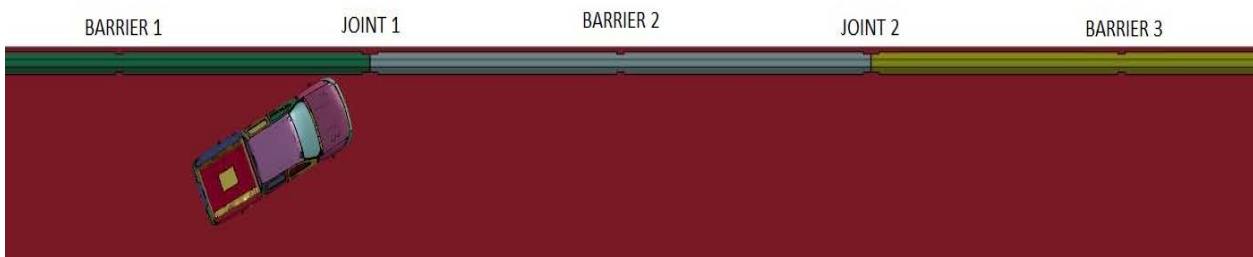


Figure 4.2. Three – 60-ft Segments Configuration.

In order to determine which configuration was the best option to use for full scale crash tests, data was extracted from the simulations and analyzed as seen in the following sections.

4.1.2 Four 40-Ft Segments – Two Rubber Fenders

4.1.2.1 Lateral Barrier Forces

The instantaneous and 50-millisecond (ms) average lateral force on each barrier were determined for the simulation impact. Figures 4.3 and 4.4 show the lateral force on barriers 2 and 3, respectively. No lateral force is shown for barriers 1 and 4 because there was no contact between these barriers and the vehicle during the simulation.

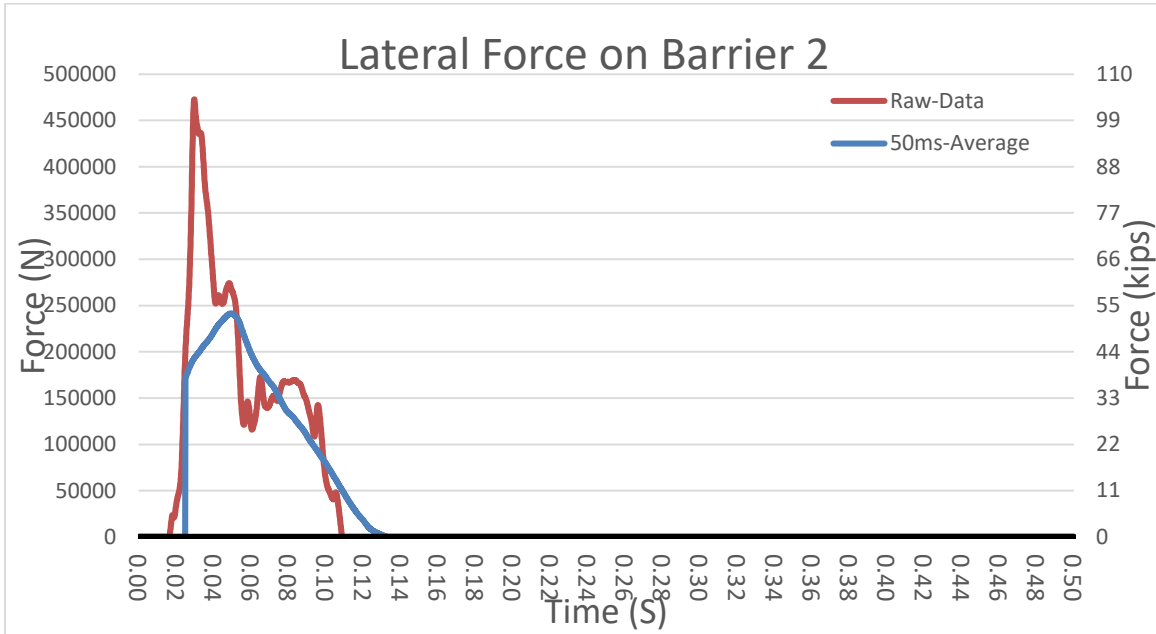


Figure 4.3. Lateral Force on Barrier 2 (Four 40-ft Segments – Two Rubber Fenders).

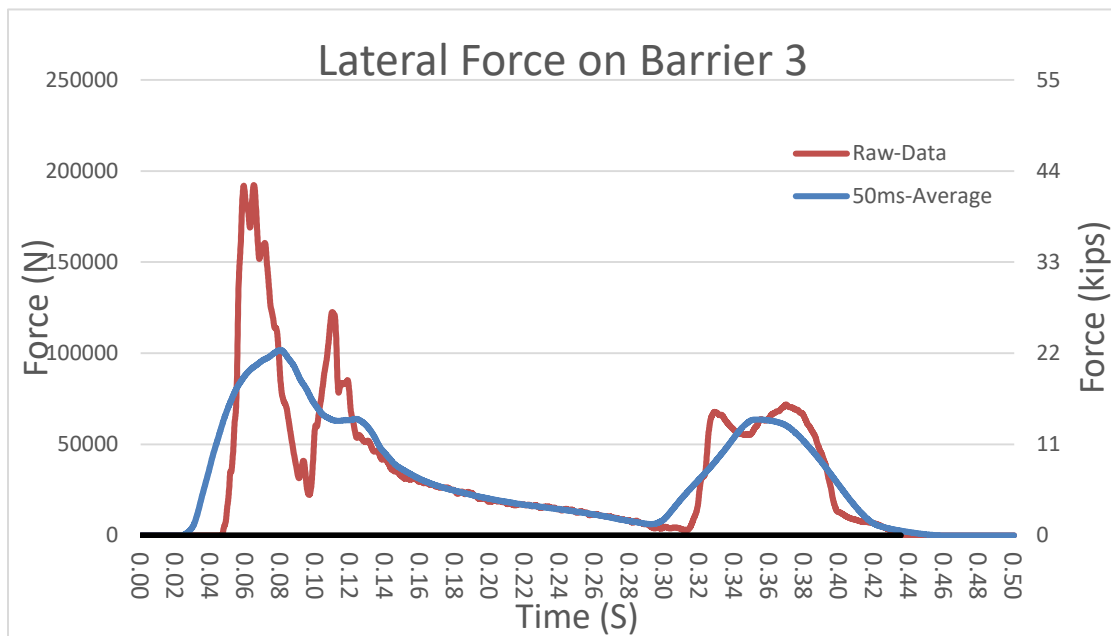


Figure 4.4. Lateral Force on Barrier 3 (Four 40-ft Segments – Two Rubber Fenders).

4.1.2.2 Joint Deflection/Deflected Shape

The lateral deflections on each barrier joint were determined for the simulation impact. Figures 4.5, 4.6, and 4.7 show the lateral deflection for joints 1, 2, and 3, respectively. The maximum deflection of the barrier system at 0.22 seconds (s) after impact is shown in Figure 4.8. Figure 4.9 shows the vehicle interaction at maximum deflection.

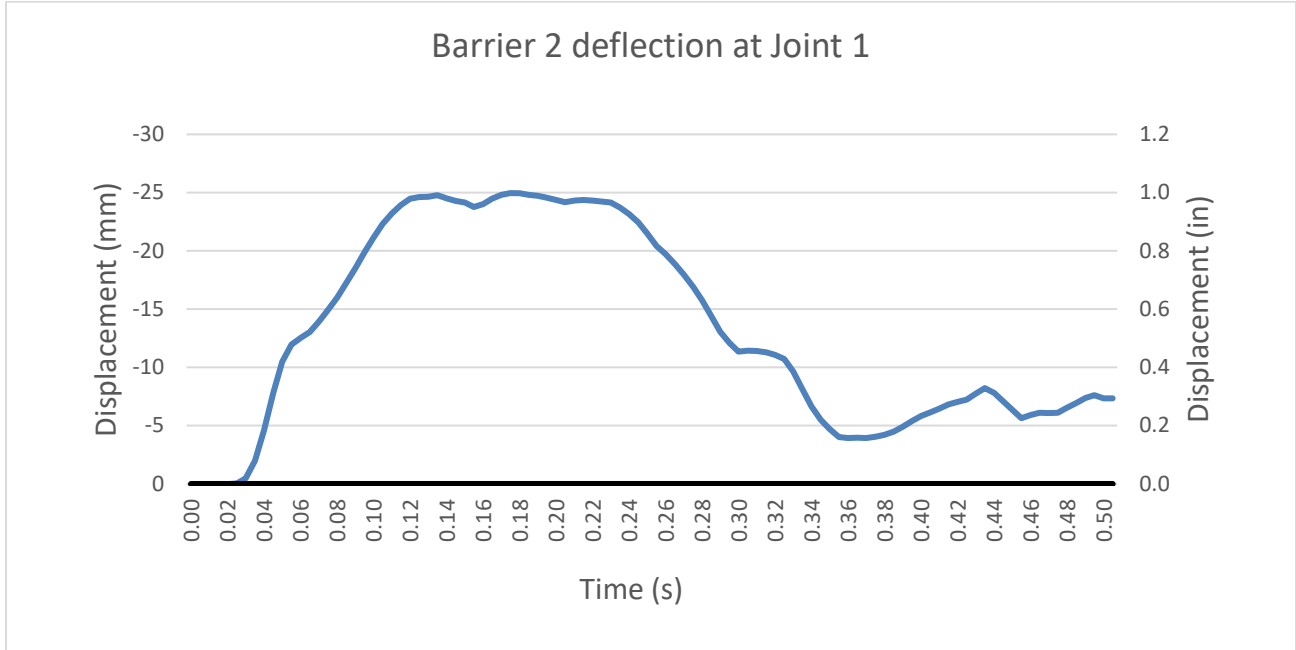


Figure 4.5. Deflection at Joint 1 (Four 40-ft Segments – Two Rubber Fenders).

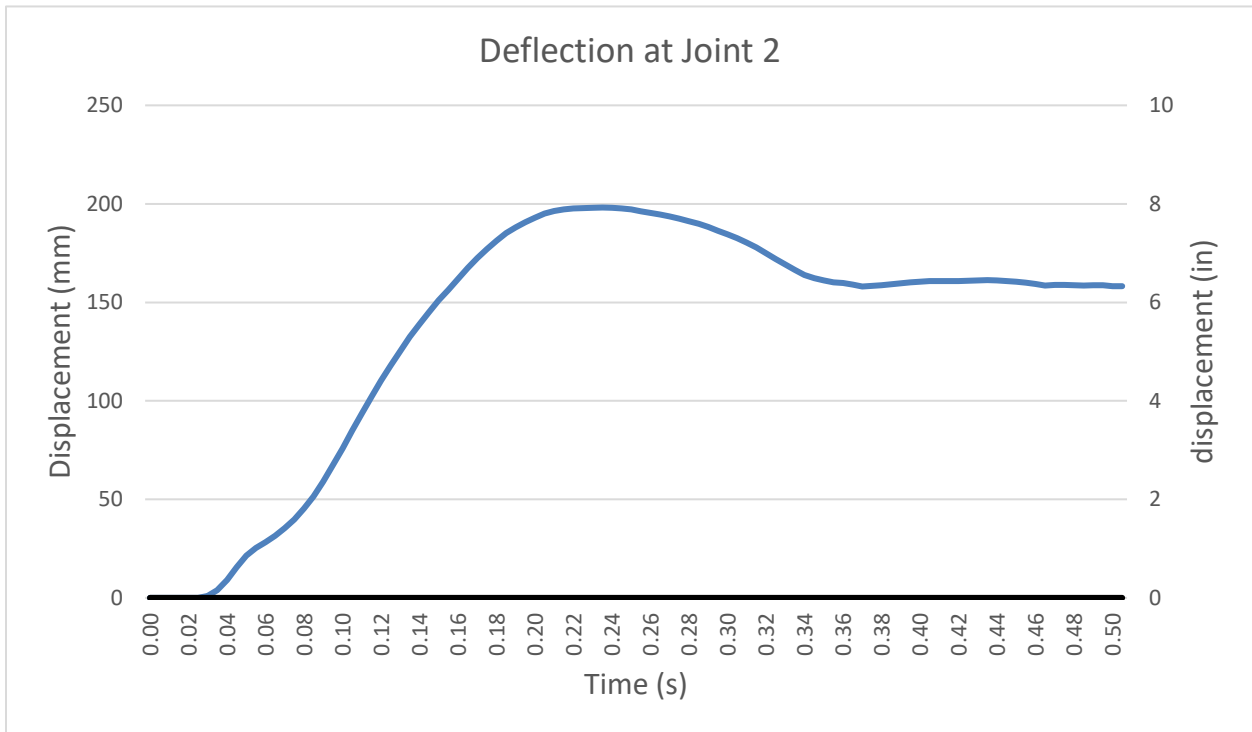


Figure 4.6. Deflection at Joint 2 (Four 40-ft Segments – Two Rubber Fenders).

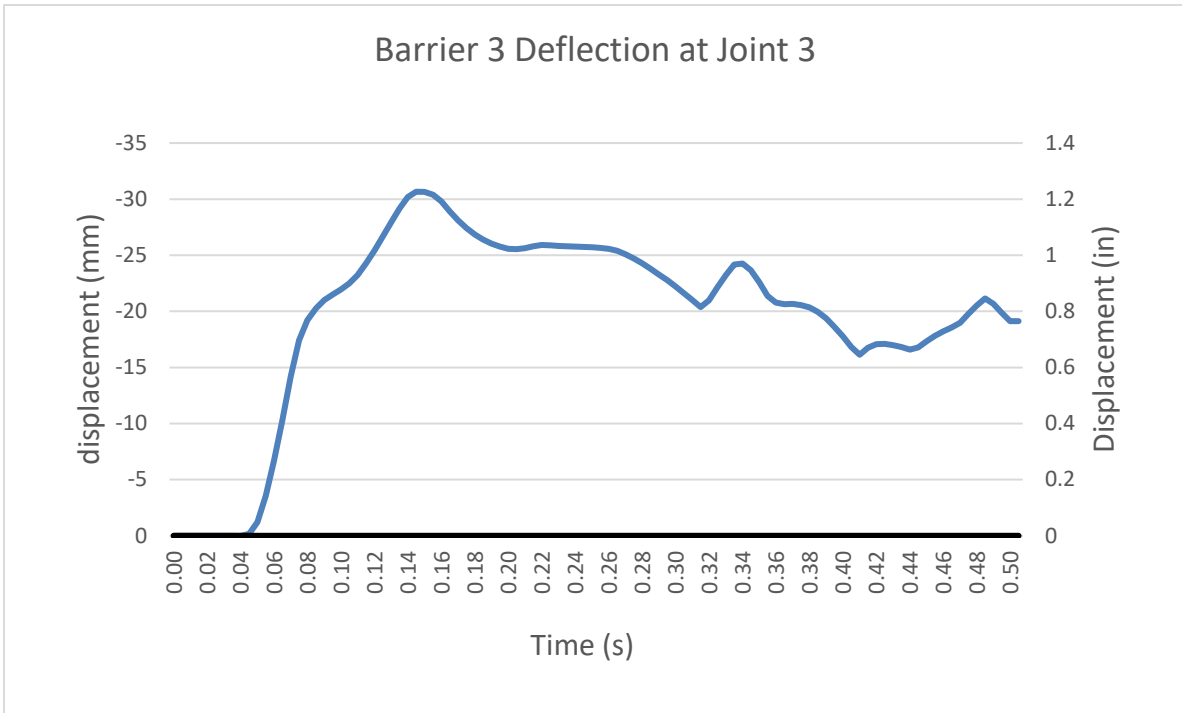


Figure 4.7. Deflection at Joint 3 (Four 40-ft Segments – Two Rubber Fenders).

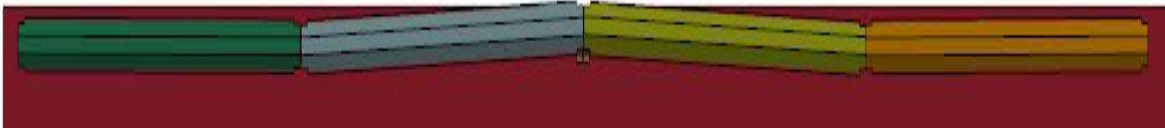


Figure 4.8. Deflection of Barrier System (Four 40-ft Segments – Two Rubber Fenders).

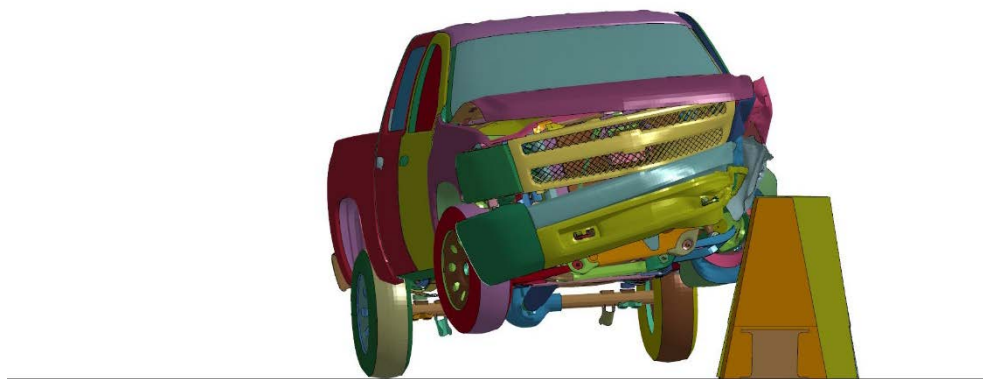


Figure 4.9. Vehicle Interaction with Barrier (Four 40-ft Segments – Two Rubber Fenders).

Accelerations at the vehicle center of gravity were tracked for evaluation of occupant risk. Table 4.1 presents the resulting occupant risk evaluation according to TRAP. Figure 4.10 shows vehicle angular displacements, and Figures 4.11 through 4.13 show vehicle acceleration versus time traces.

Table 4.1. TRAP Results – Occupant Safety Analysis (Four 40-ft Section with Two Rubber Fenders).

TRAP Results: MASH 2270P 4-40 ft Section with 2 Rubber Fenders	
<i>Impact Velocity, mi/h</i>	62.1
<i>Impact Angle (degrees)</i>	25
Occupant Risk Factors	
OIV (ft/s)	
x-direction	28.5
y-direction	20.9
Ridedown Accelerations (g's)	
x-direction	8.9
y-direction	6.4
Max Roll, Pitch, and Yaw Angles (degrees)	
Roll	4.0
Pitch	-4.8
Yaw	28.1

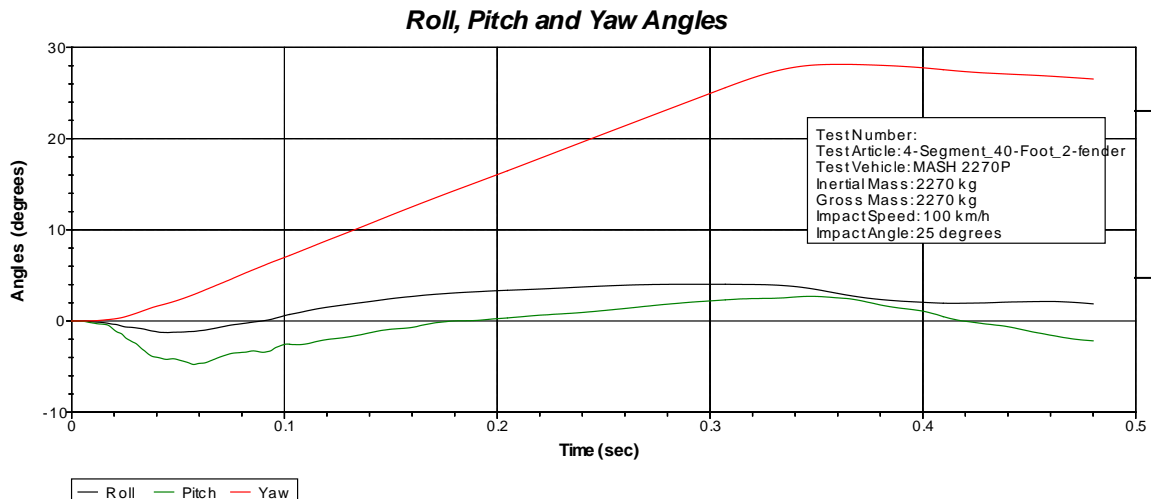


Figure 4.10. Vehicle Angular Displacement (Four 40-ft Segments – Two Rubber Fenders).

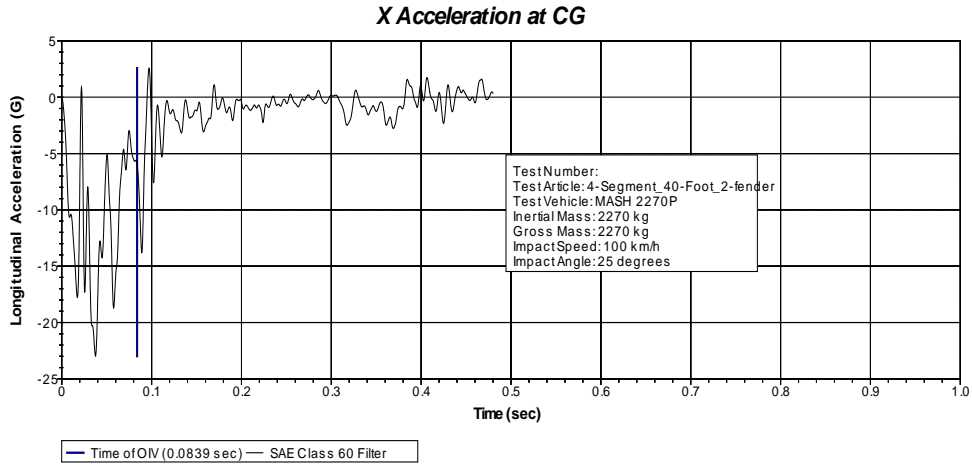


Figure 4.11. Vehicle Longitudinal Acceleration Trace (Four 40-ft Segments – Two Rubber Fenders).

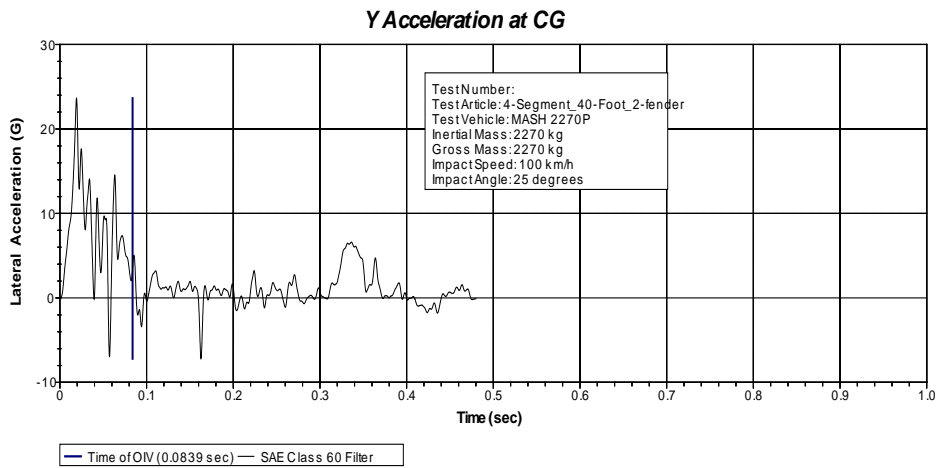


Figure 4.12. Vehicle Lateral Acceleration Trace (Four 40-ft Segments – Two Rubber Fenders).

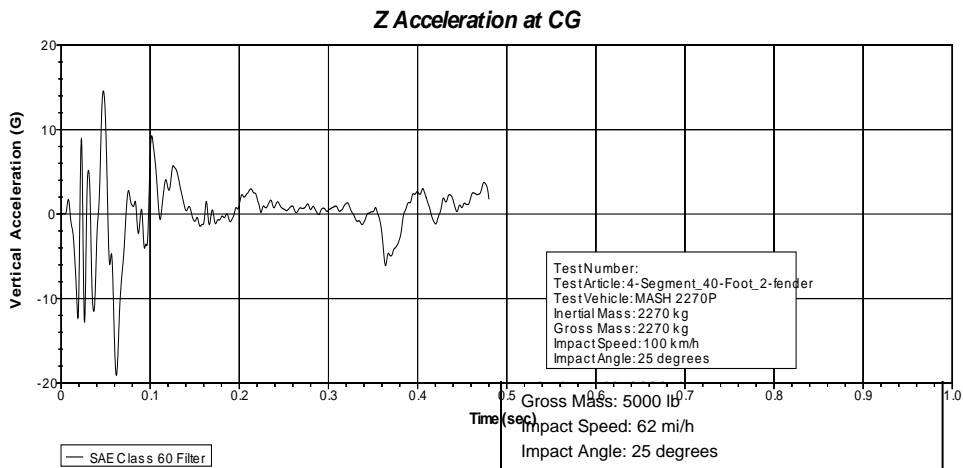


Figure 4.13. Vehicle Vertical Acceleration Trace (Four 40-ft Segments – Two Rubber Fenders).

4.1.3 Four 40-Ft Segments – Three Rubber Fenders

4.1.3.1 Lateral Barrier Forces

The instantaneous and 50-ms average lateral force on each barrier were determined for the simulation impact. Figures 4.14 and 4.15 show the lateral force on barriers 2 and 3, respectively. No lateral force is shown for barriers 1 and 4 because there was no contact between these barriers and the vehicle during the simulation.

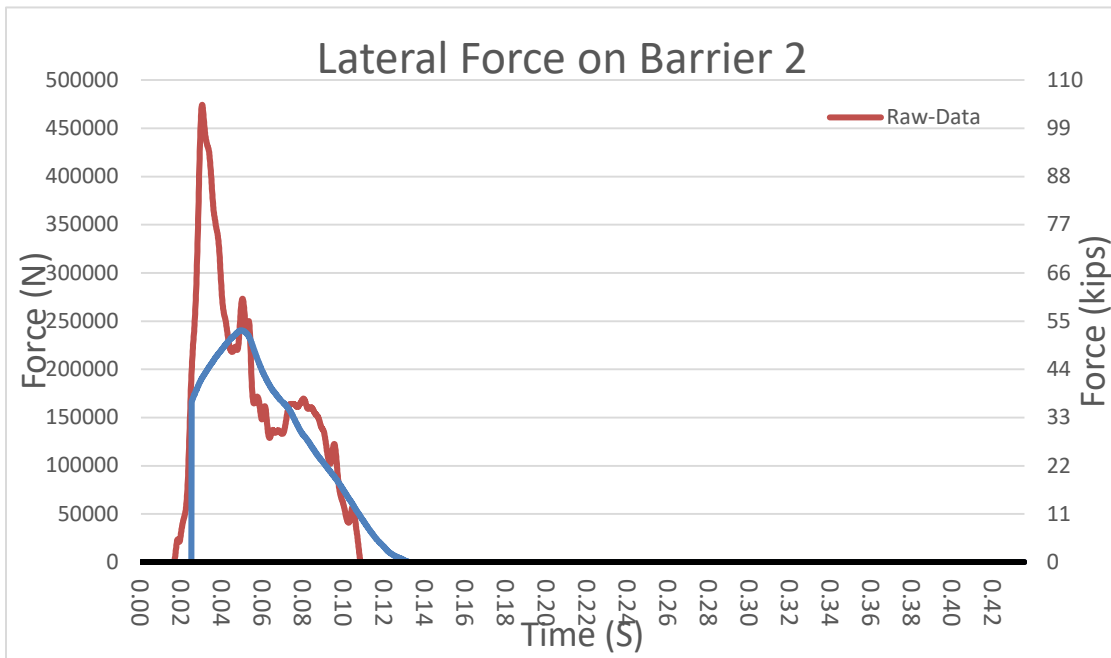


Figure 4.14. Lateral Force on Barrier 2 (Four 40-ft Segments – Three Rubber Fenders).

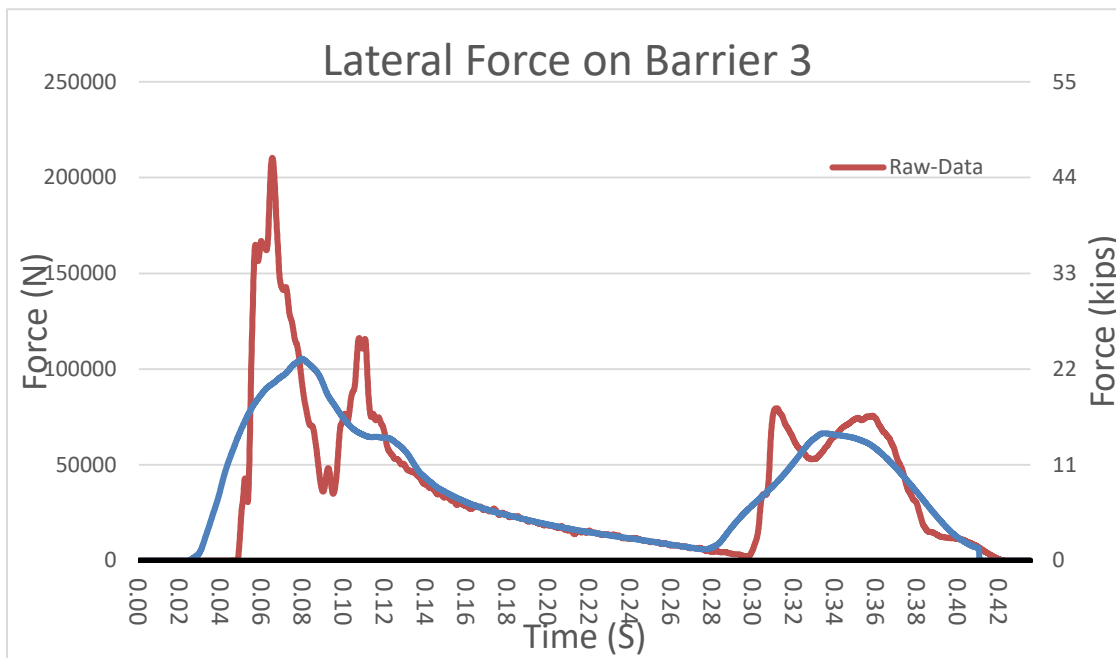


Figure 4.15. Lateral Force on Barrier 3 (Four 40-ft Segments – Three Rubber Fenders).

4.1.3.2 Joint Deflection/Deflected Shape

The lateral deflections on each barrier joint were determined for the simulation impact. Figures 4.16, 4.17, and 4.18 show the lateral deflection for joints 1, 2, and 3, respectively. The maximum deflection of the barrier system at 0.21 s after impact is shown in Figure 4.19. Figure 4.20 shows the vehicle interaction at maximum deflection.

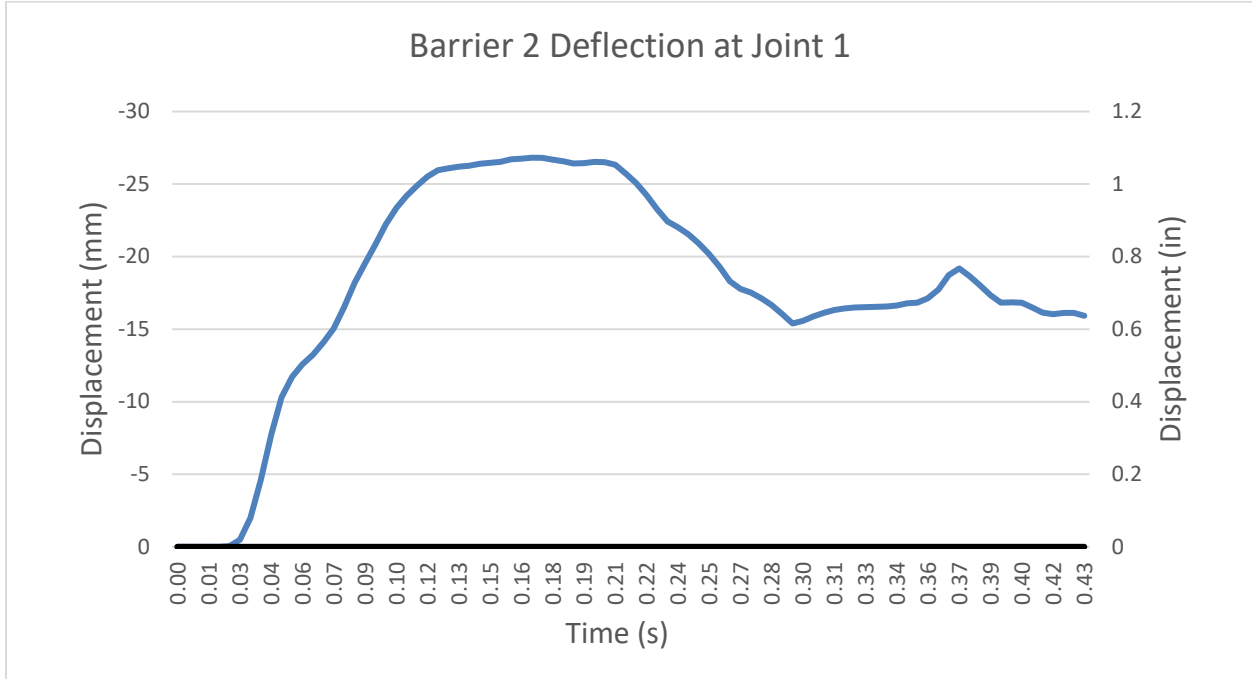


Figure 4.16. Deflection at Joint 1 (Four 40-ft Segments – Three Rubber Fenders).

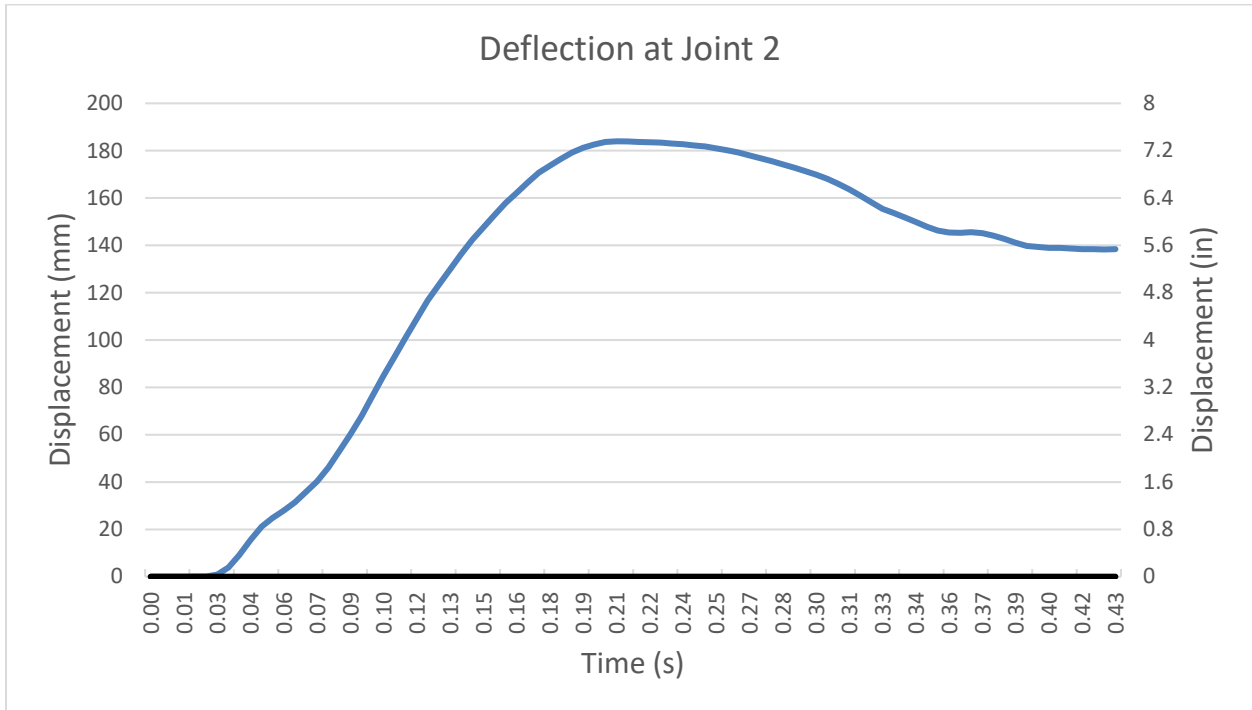


Figure 4.17. Deflection at Joint 2 (Four 40-ft Segments – Three Rubber Fenders).

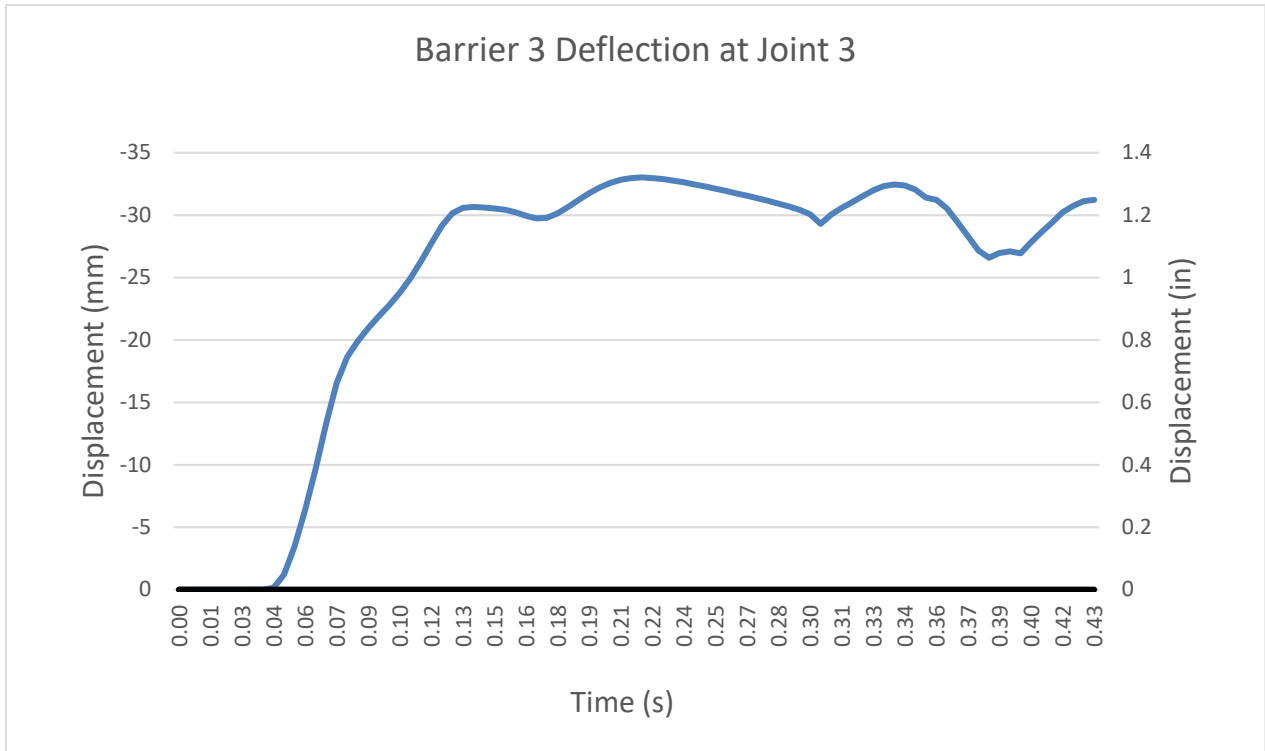


Figure 4.18. Deflection at Joint 3 (Four 40-ft Segments – Three Rubber Fenders).

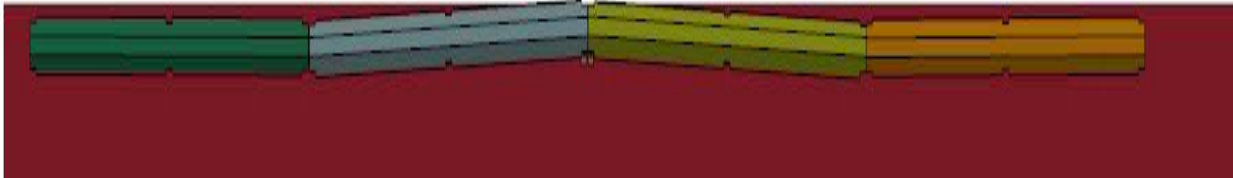


Figure 4.19. Deflection of Barrier System (Four 40-ft Segments – Three Rubber Fenders).



Figure 4.20. Vehicle Interaction with Barrier (Four 40-ft Segments – Three Rubber Fenders).

Accelerations at the vehicle center of gravity were tracked for evaluation of occupant risk. Table 4.2 presents the resulting occupant risk evaluation according to TRAP. Figure 4.21 shows vehicle angular displacements, and Figures 4.22 through 4.24 show vehicle acceleration versus time traces.

Table 4.2. TRAP Results – Occupant Safety Analysis (Four 40-ft Section with Three Rubber Fenders).

TRAP Results: MASH 2270P 4-40 ft Section with 3 Rubber Fenders	
<i>Impact Velocity, mi/h</i>	62.1
<i>Impact Angle (degrees)</i>	25
Occupant Risk Factors	
OIV (ft/s)	
x-direction	32.2
y-direction	20.9
Ridedown Accelerations (g's)	
x-direction	6.5
y-direction	6.2
Max Roll, Pitch, and Yaw Angles (degrees)	
Roll	4.4
Pitch	-4.7
Yaw	28.1

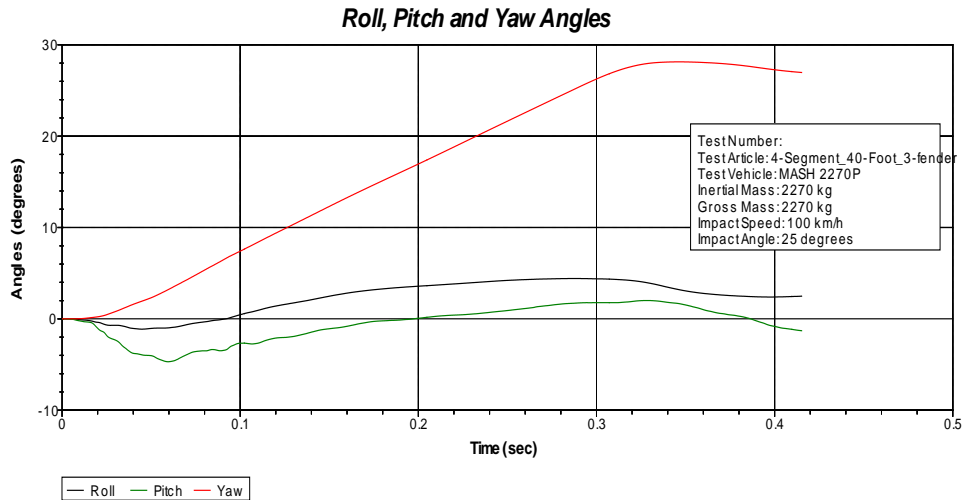


Figure 4.21. Vehicle Angular Displacements (Four 40-ft Segments – Three Rubber Fenders).

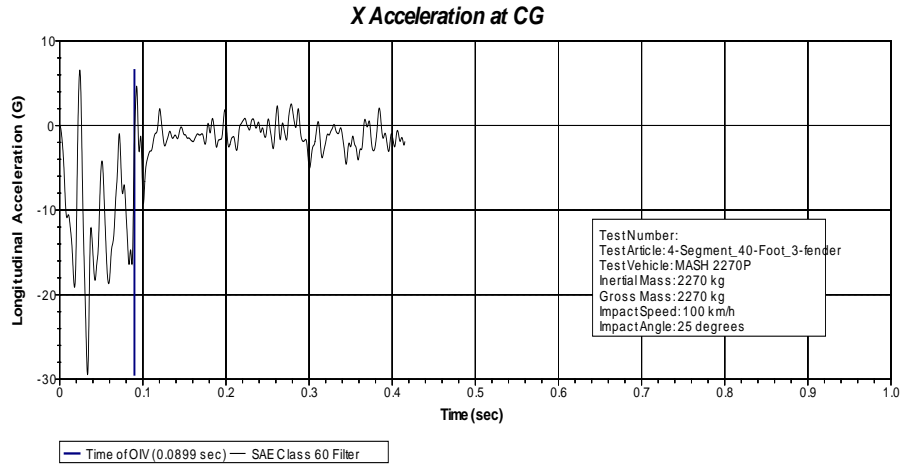


Figure 4.22. Vehicle Longitudinal Acceleration Trace (Four 40-ft Segments – Three Rubber Fenders).

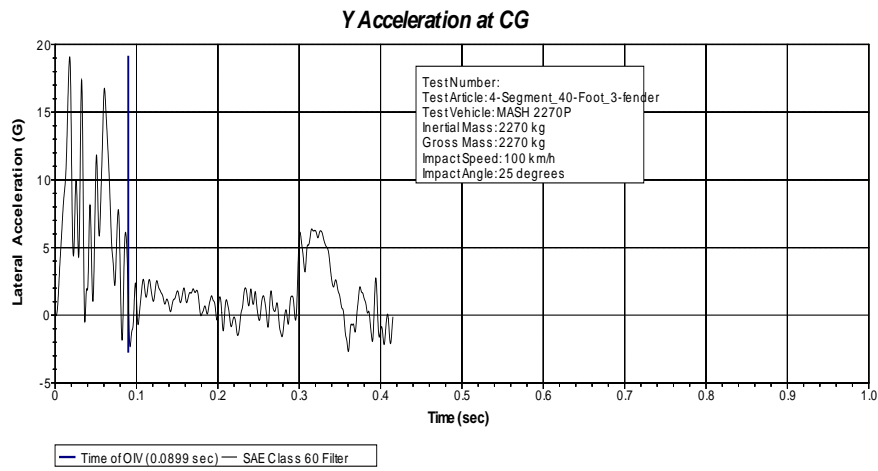


Figure 4.23. Vehicle Lateral Acceleration Trace (Four 40-ft Segments – Three Rubber Fenders).

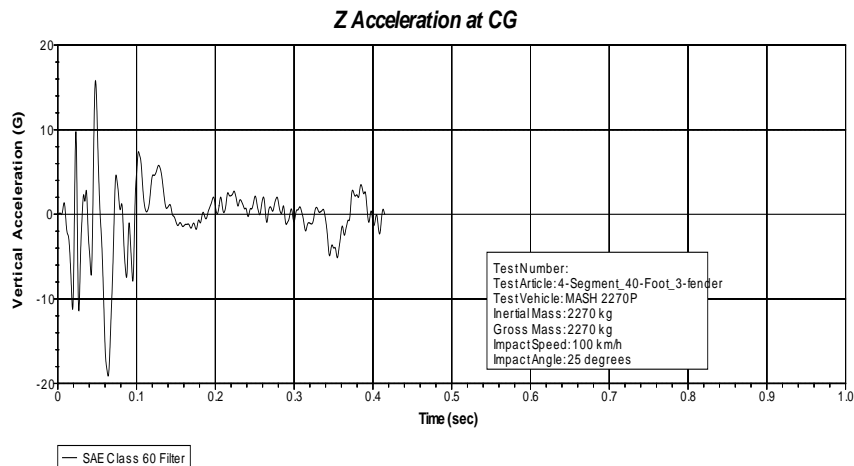


Figure 4.24. Vehicle Vertical Acceleration Trace (Four 40-ft Segments – Three Rubber Fenders).

4.1.4 Three 60-Ft Segments – Two Rubber Fenders

4.1.4.1 Lateral Barrier Forces

The instantaneous and 50-ms average lateral force on each barrier were determined for the simulation impact. Figures 4.25 and 4.26 show the lateral force on barriers 1 and 2, respectively. No lateral force is shown for barrier 3 because there was no contact between the barrier and the vehicle during the simulation.

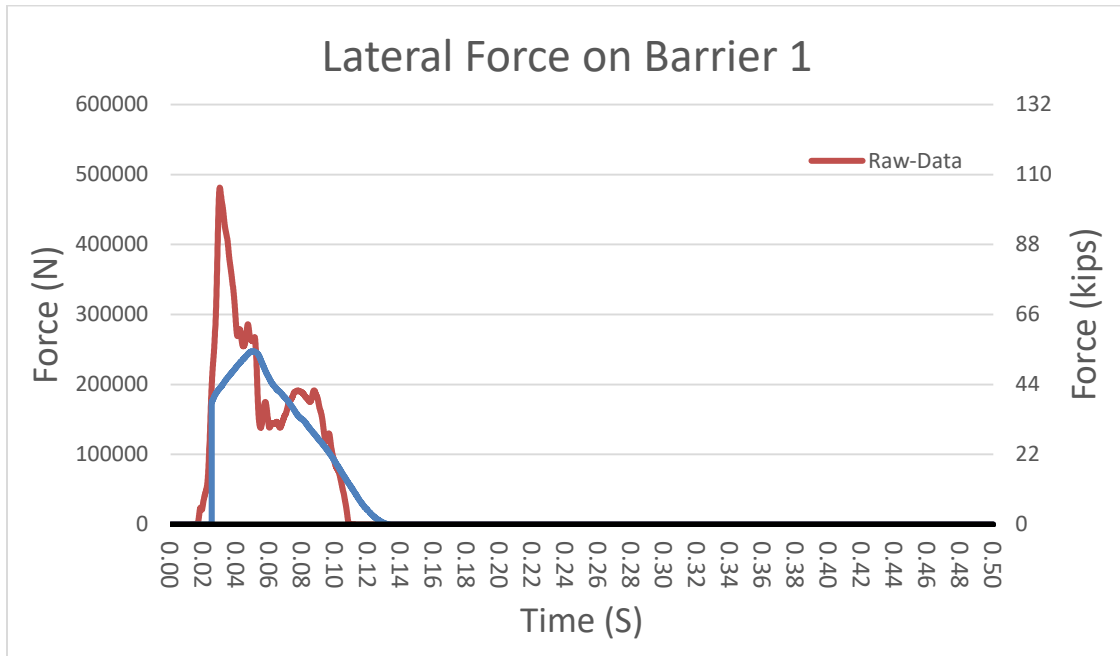


Figure 4.25. Lateral Force on Barrier 1 (Three 60-ft Segments – Two Rubber Fenders).

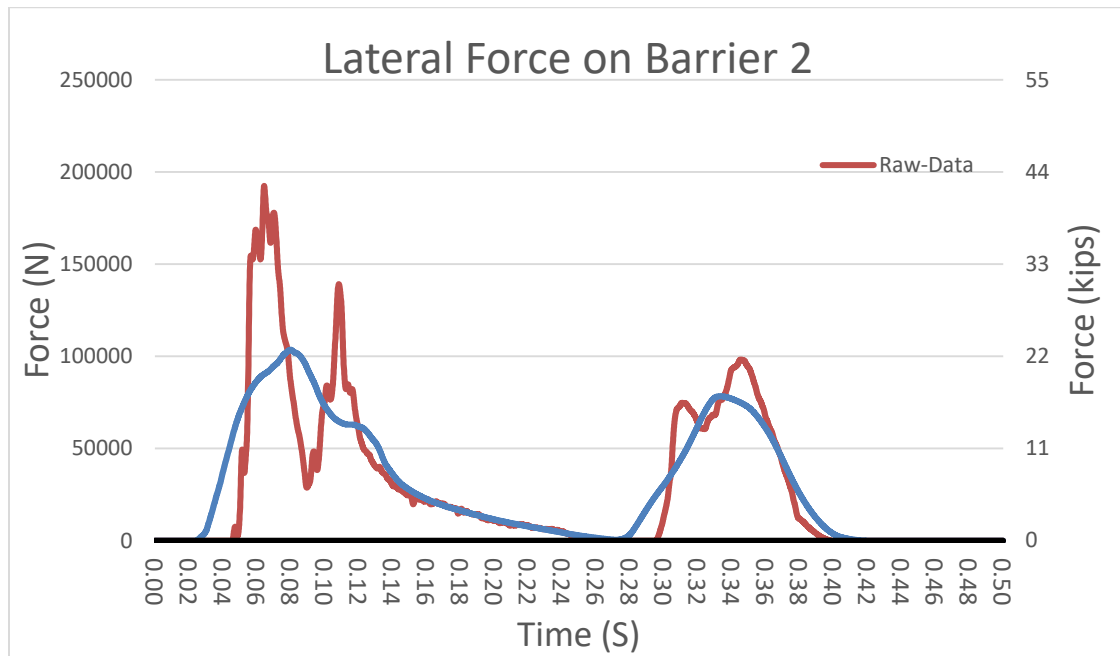


Figure 4.26. Lateral Force on Barrier 2 (Three 60-ft Segments – Two Rubber Fenders).

4.1.4.2 Joint Deflection/Deflected Shape

The lateral deflections on each barrier joint were determined for the simulation impact. Figures 4.27, and 4.28 show the lateral deflection for joints 1, and 2, respectively. The maximum deflection of the barrier system at 0.2 s after impact is shown in Figure 4.29. Figure 4.30 shows the vehicle interaction at maximum deflection.

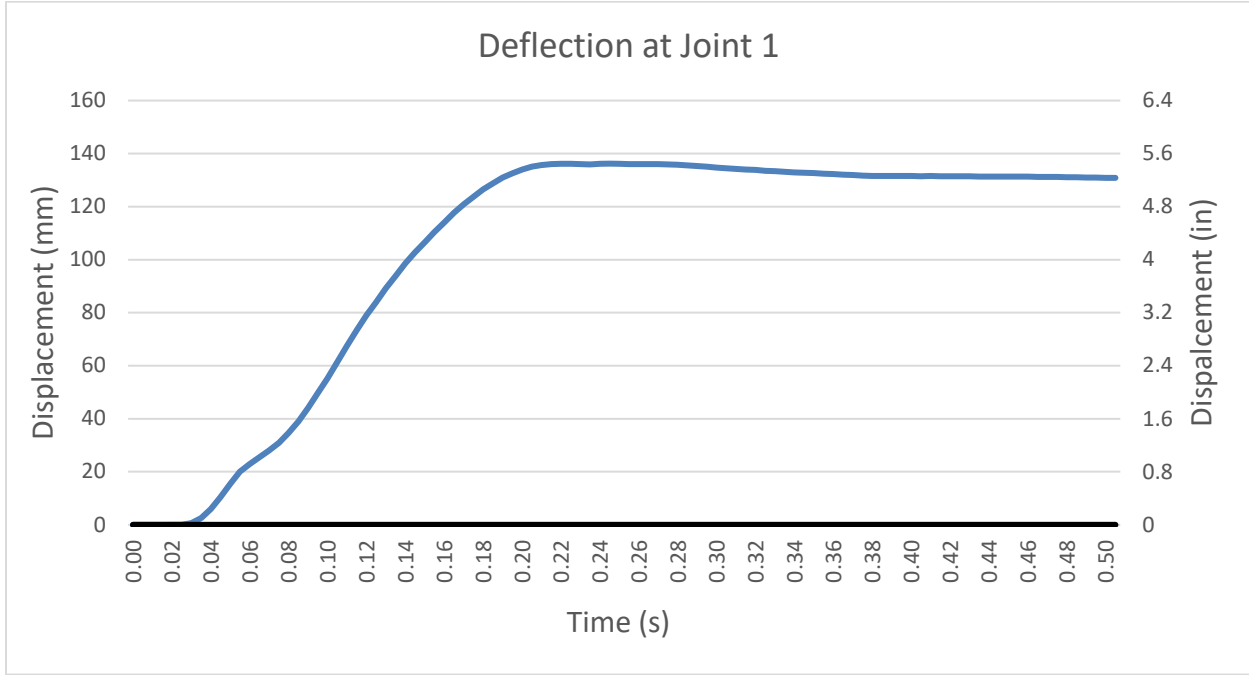


Figure 4.27. Deflection at Joint 1 (Three 60-ft Segments – Two Rubber Fenders).

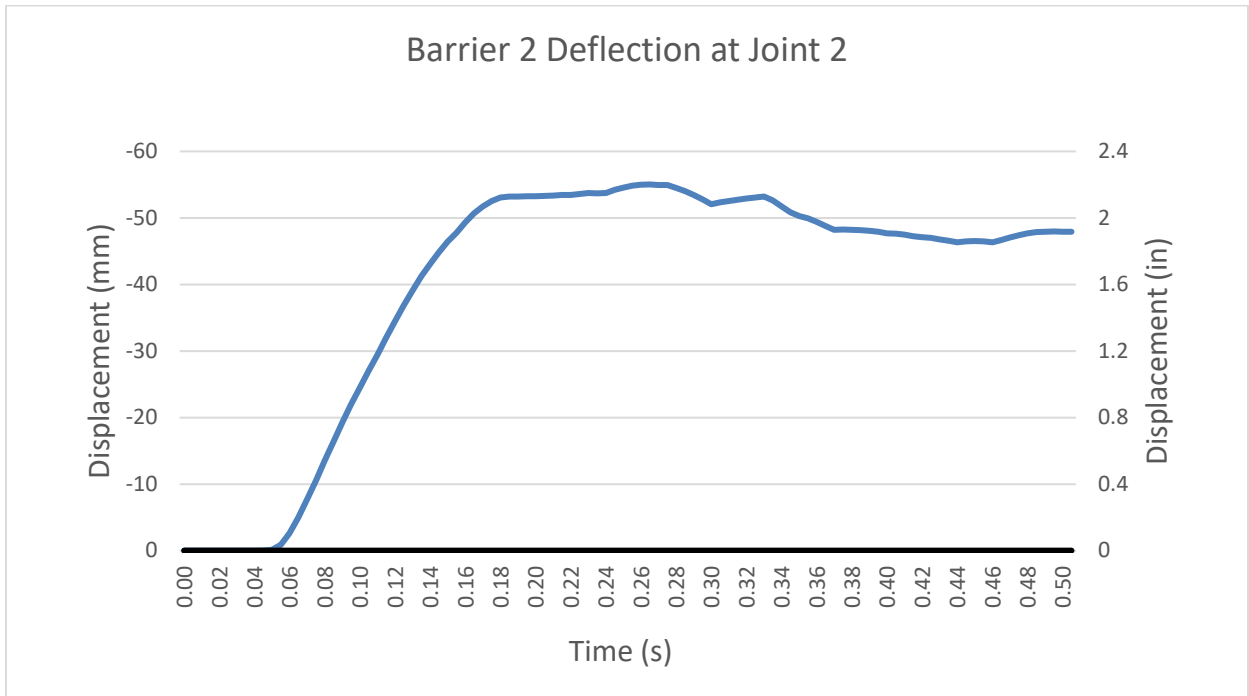


Figure 4.28. Deflection at Joint 2 (Three 60-ft Segments – Two Rubber Fenders).



Figure 4.29. Deflection of Barrier System (Three 60-ft Segments – Two Rubber Fenders).

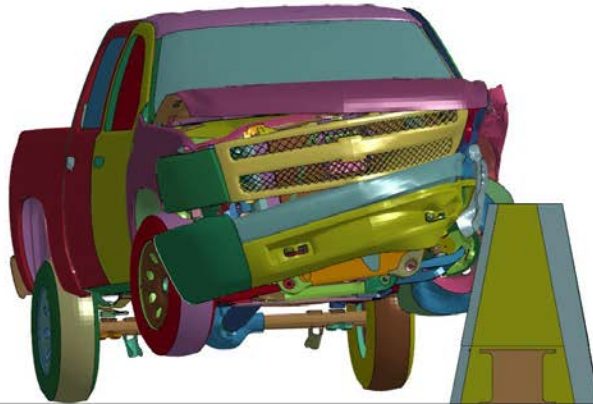


Figure 4.30. Vehicle Interaction with Barrier (Three 60-ft Segments – Two Rubber Fenders).

Accelerations at the vehicle center of gravity were tracked for evaluation of occupant risk. Table 4.3 presents the resulting occupant risk evaluation according to TRAP. Figure 4.31 shows vehicle angular displacements, and Figures 4.32 through 4.34 show vehicle acceleration versus time traces.

Table 4.3. TRAP Results – Occupant Safety Analysis (Three 60-ft Section with Two Rubber Fenders).

TRAP Results: MASH 2270P 3-60 ft Section with 2 Rubber Fenders	
<i>Impact Velocity, mi/h</i>	62.1
<i>Impact Angle (degrees)</i>	25
Occupant Risk Factors	
OIV (ft/s)	
x-direction	29.0
y-direction	-23.6
Ridedown Accelerations (g's)	
x-direction	5.1
y-direction	7.2
Max Roll, Pitch, and Yaw Angles (degrees)	
Roll	-7.9
Pitch	-5.1
Yaw	29.5

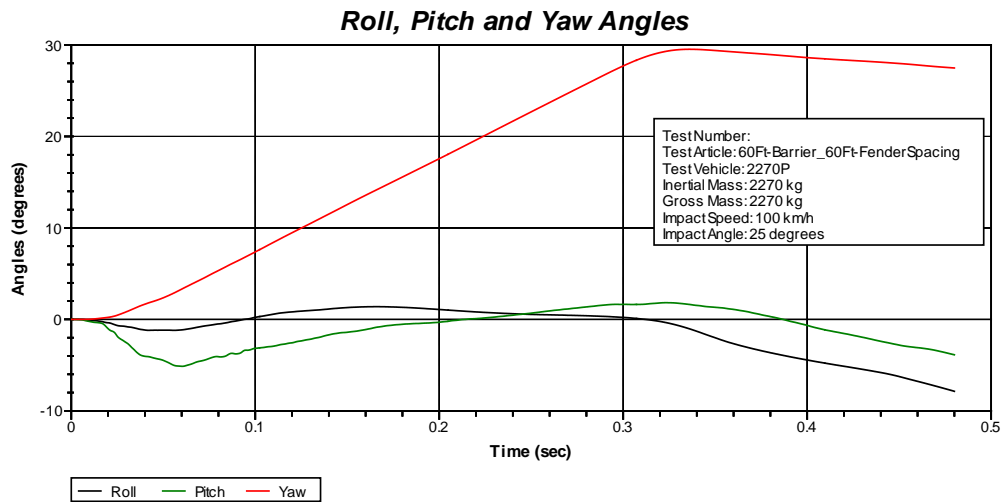


Figure 4.31. Vehicle Angular Displacements (Three 60-ft Segments – Two Rubber Fenders).

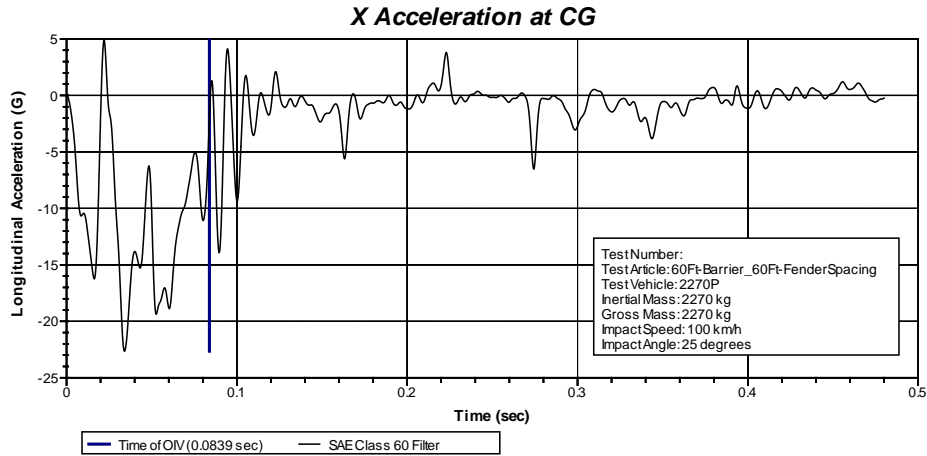


Figure 4.32. Vehicle Longitudinal Acceleration Trace (Three 60-ft Segments – Two Rubber Fenders).

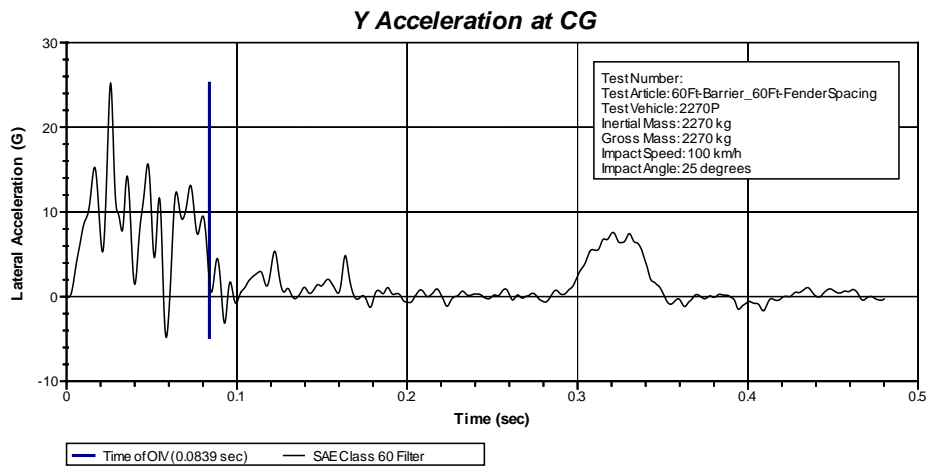


Figure 4.33. Vehicle Lateral Acceleration Trace (Three 60-ft Segments – Two Rubber Fenders).

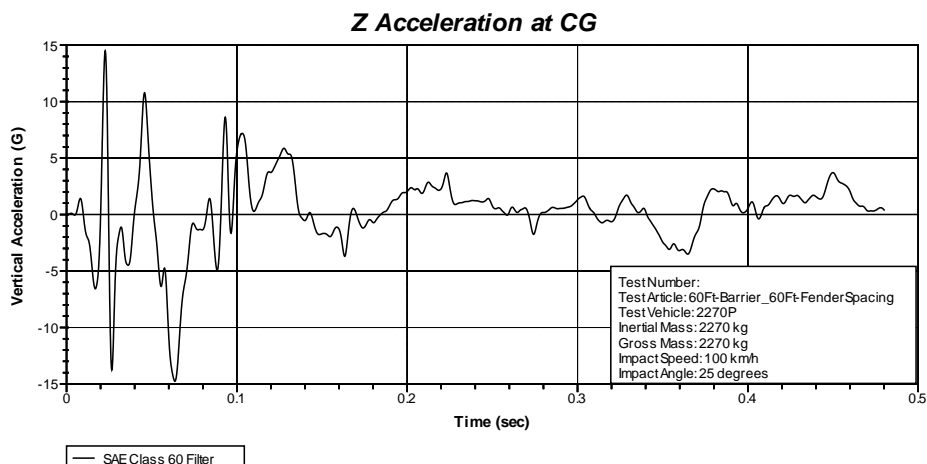


Figure 4.34. Vehicle Vertical Acceleration Trace (Three 60-ft Segments – Two Rubber Fenders).

4.1.5 Three 60-Ft Segments – Three Rubber Fenders

4.1.5.1 Lateral Barrier Forces

The instantaneous and 50-ms average lateral force on each barrier were determined for the simulation impact. Figures 4.35 and 4.36 show the lateral force on barriers 1 and 2, respectively. No lateral force is shown for barrier 3 because there was no contact between the barrier and the vehicle during the simulation.

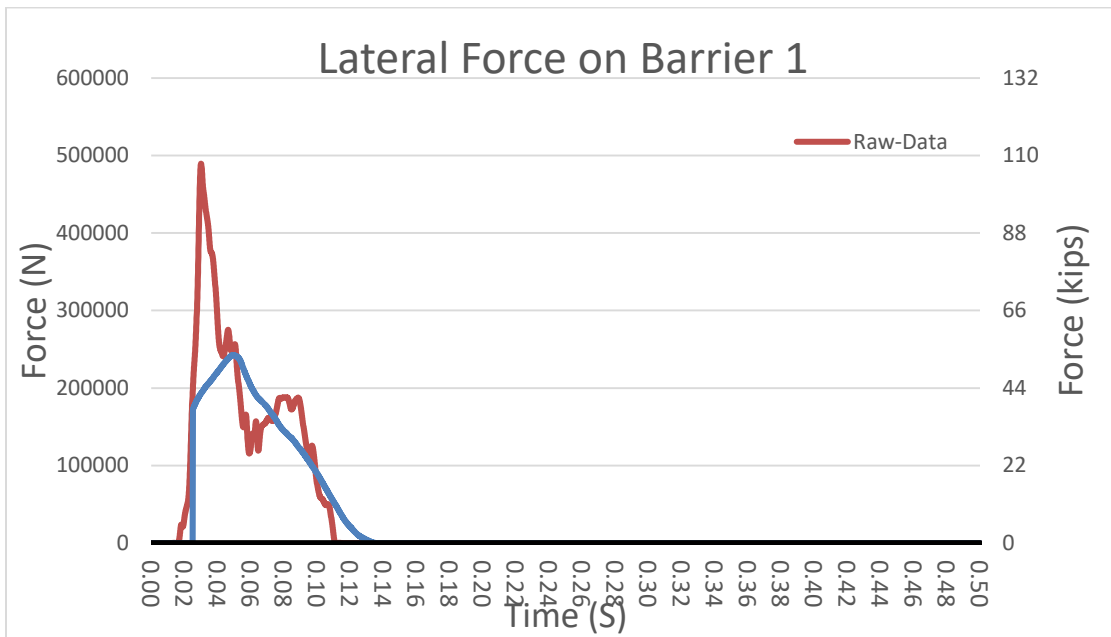


Figure 4.35. Lateral Force on Barrier 1 (Three 60-ft Segments – Three Rubber Fenders).

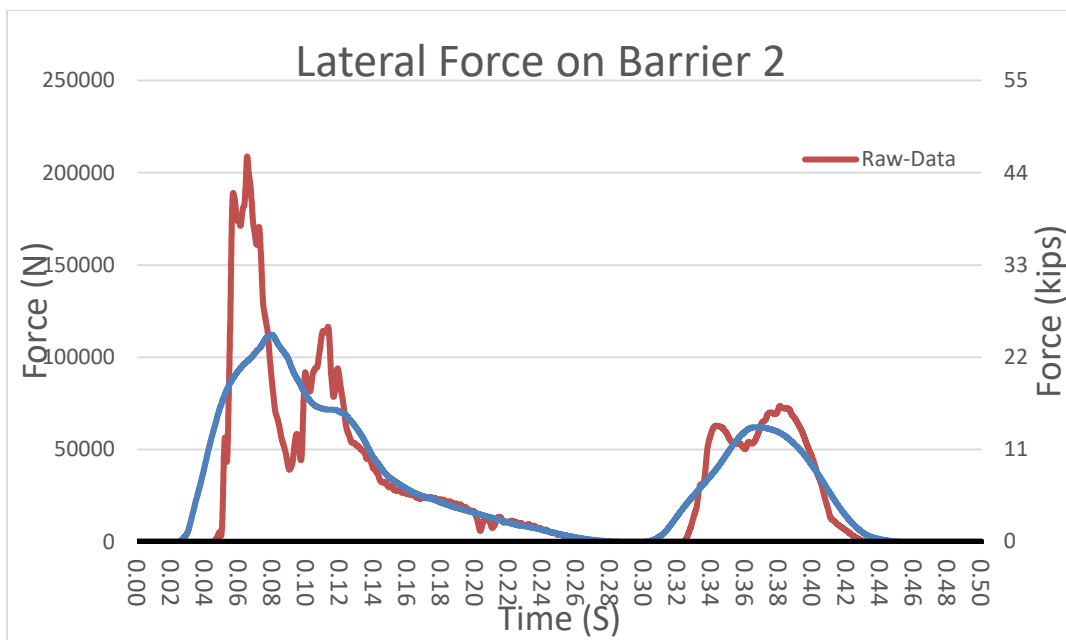


Figure 4.36. Lateral Force on Barrier 2 (Three 60-ft Segments – Three Rubber Fenders).

4.1.5.2 Joint Deflection/Deflected Shape

The lateral deflections on each barrier joint were determined for the simulation impact. Figures 4.37, and 4.38 show the lateral deflection for joints 1, and 2, respectively. The maximum deflection of the barrier system at 0.2 s after impact is shown in Figure 4.39. Figure 4.40 shows the vehicle interaction at maximum deflection.

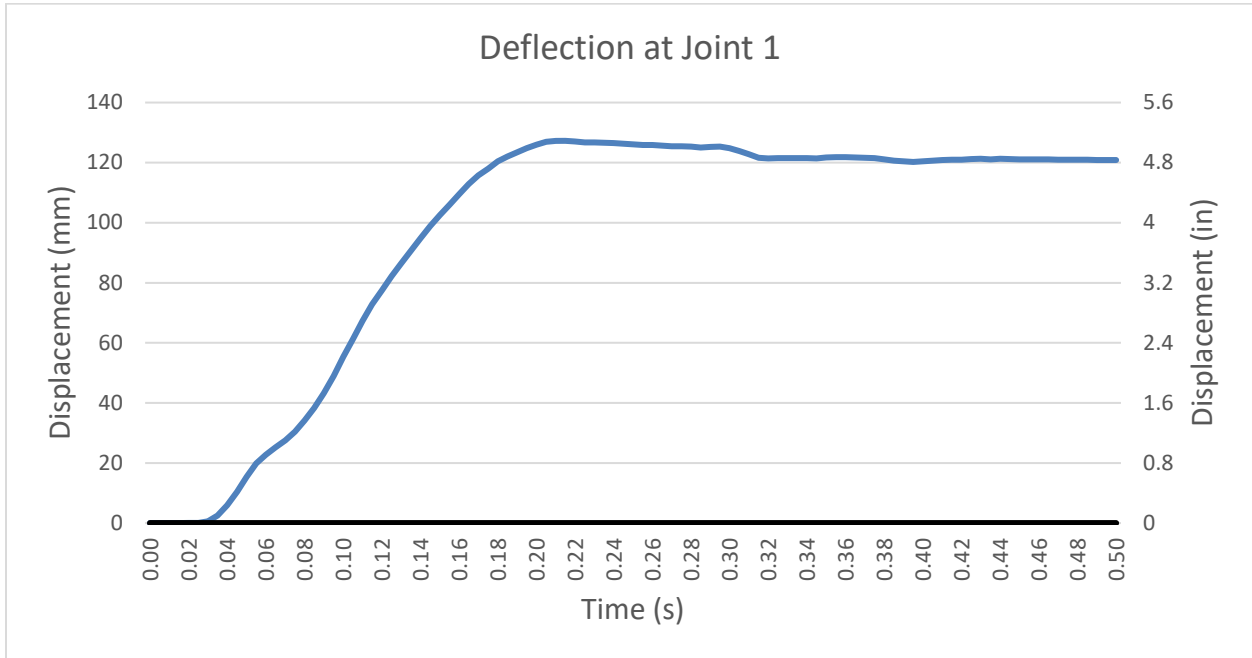


Figure 4.37. Deflection at Joint 1 (Three 60-ft Segments – Three Rubber Fenders).

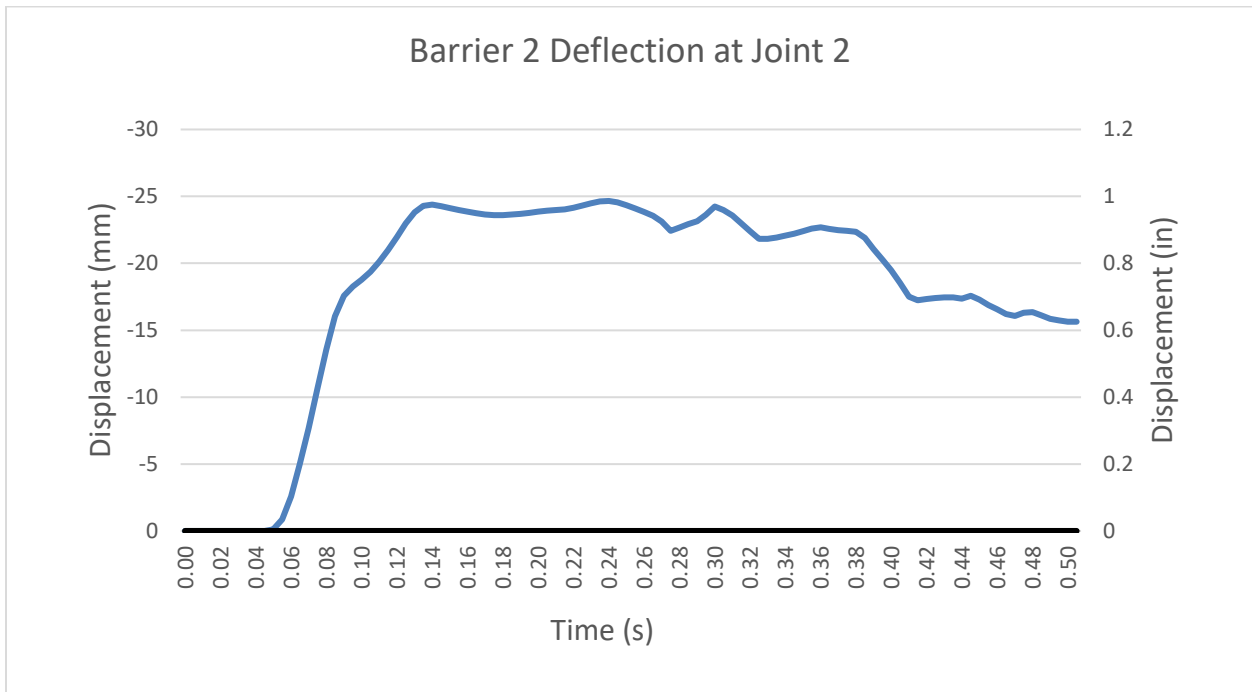


Figure 4.38. Deflection at Joint 2 (Three 60-ft Segments – Three Rubber Fenders).



Figure 4.39. Deflection of Barrier System (Three 60-ft Segments – Three Rubber Fenders).

LS-DYNA keyword deck by LS-PrePost
Time = 0.2

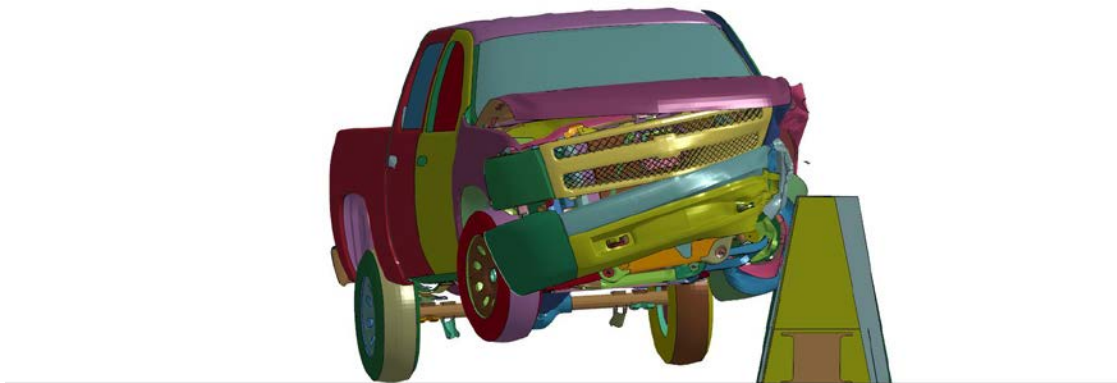


Figure 4.40. Vehicle Interaction with Barrier System (Three 60-ft Segments – Three Rubber Fenders).

Accelerations at the vehicle center of gravity were tracked for evaluation of occupant risk. Table 4.4 presents the resulting occupant risk evaluation according to TRAP. Figure 4.41 shows vehicle angular displacements, and Figures 4.42 through 4.44 show vehicle acceleration versus time traces.

Table 4.4. TRAP Results – Occupant Safety Analysis (Three 60-ft Section with Three Rubber Fenders).

TRAP Results: MASH 2270P 3 60-ft Section with 3 Rubber Fenders	
<i>Impact Velocity, mi/h</i>	62.1
<i>Impact Angle (degrees)</i>	25
Occupant Risk Factors	
OIV (ft/s)	
x-direction	25.9
y-direction	-25.6
Ridedown Accelerations (g's)	
x-direction	9.1
y-direction	-7.8
Max Roll, Pitch, and Yaw Angles (degrees)	
Roll	-4.4
Pitch	-5.2
Yaw	31

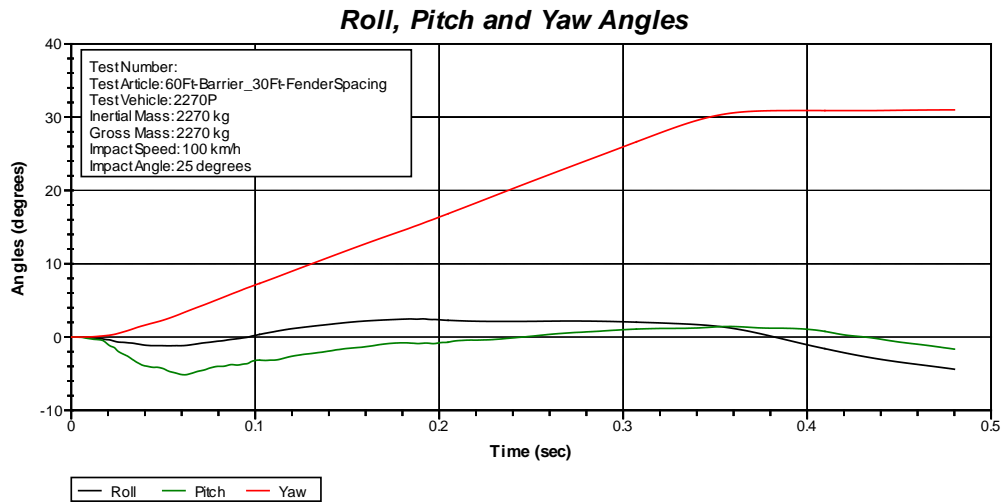


Figure 4.41. Vehicle Angular Displacements (Three 60-ft Segments – Three Rubber Fenders).

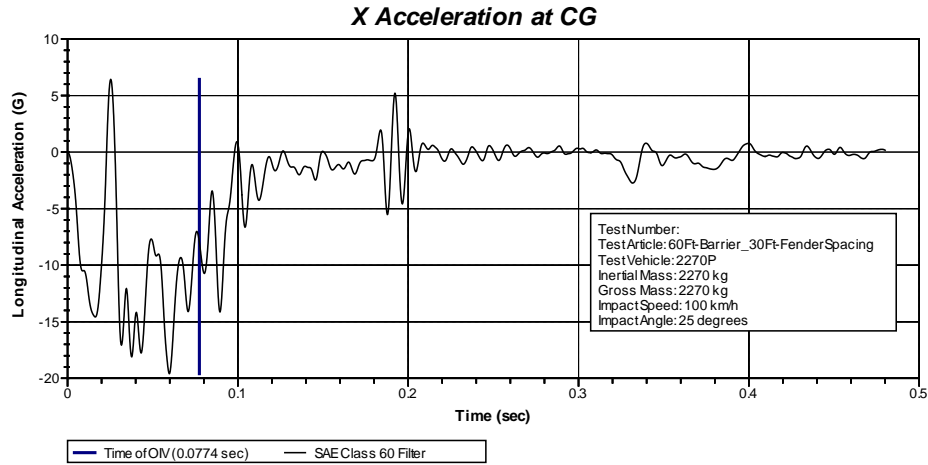


Figure 4.42. Vehicle Longitudinal Acceleration Trace (Three 60-ft Segments – Three Rubber Fenders).

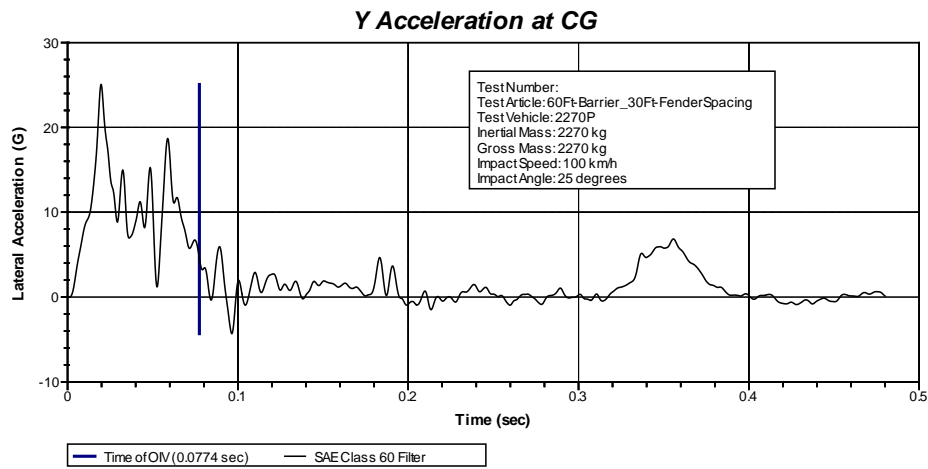


Figure 4.43. Vehicle Lateral Acceleration Trace (Three 60-ft Segments – Three Rubber Fenders).

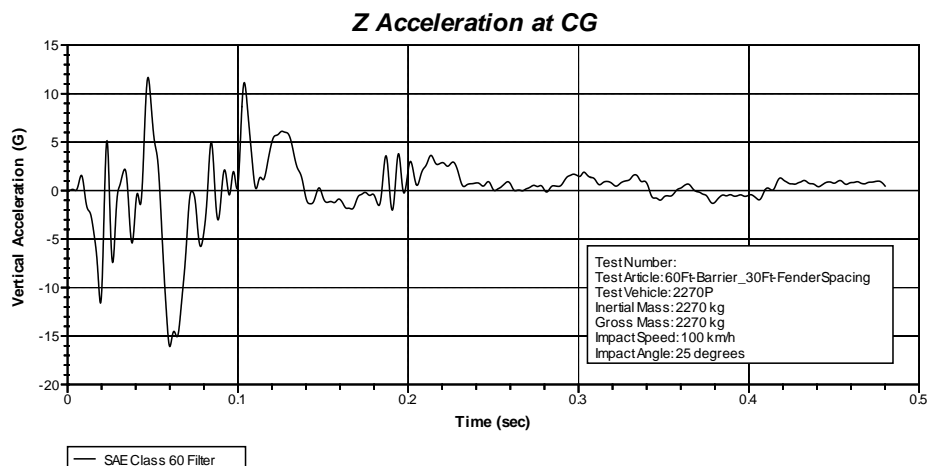


Figure 4.44. Vehicle Vertical Acceleration Trace (Three 60-ft Segments – Three Rubber Fenders).

4.2 SUT MEDIAN BARRIER

Two configurations of barrier segments and barrier lengths were simulated in this set of analyses with the SUT vehicle. There were three rubber fenders for the entire barrier system. In each simulation, there were expansion joint dowels between the barriers. The configurations of the barriers that were simulated are as follows:

- Two 40-ft segments with three rubber fenders.
- Two 60-ft segments with three rubber fenders.

Figures 4.45 and 4.46 show the two different configurations for the simulations. The only difference is the length of the barrier segments.

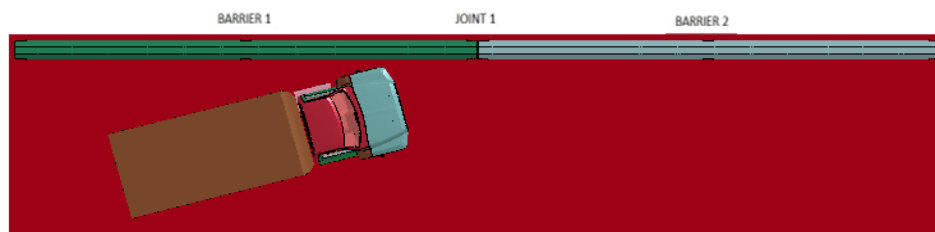


Figure 4.45. Two 40-ft Segment Configuration.

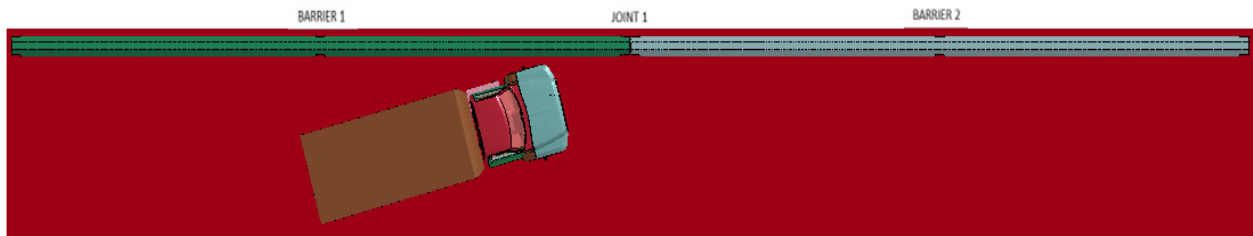


Figure 4.46. Two 60-ft Segment Configuration.

4.2.1 Two 40 Ft Segment – Three Rubber Fenders

4.2.1.1 Lateral Barrier Force

The instantaneous and 50-ms average lateral force on the barrier system were determined for the simulation impact. Figure 4.47 shows the lateral force on the barrier system.

4.2.1.2 Joint Deflection/Deflected Shape

The lateral deflections on the barrier joint was determined for the simulation impact. Figure 4.48 shows the lateral deflection for joint 1. The maximum deflection of the barrier system at 0.41 s after impact is shown in Figure 4.49. Figure 4.50 shows the vehicle interaction at maximum deflection.

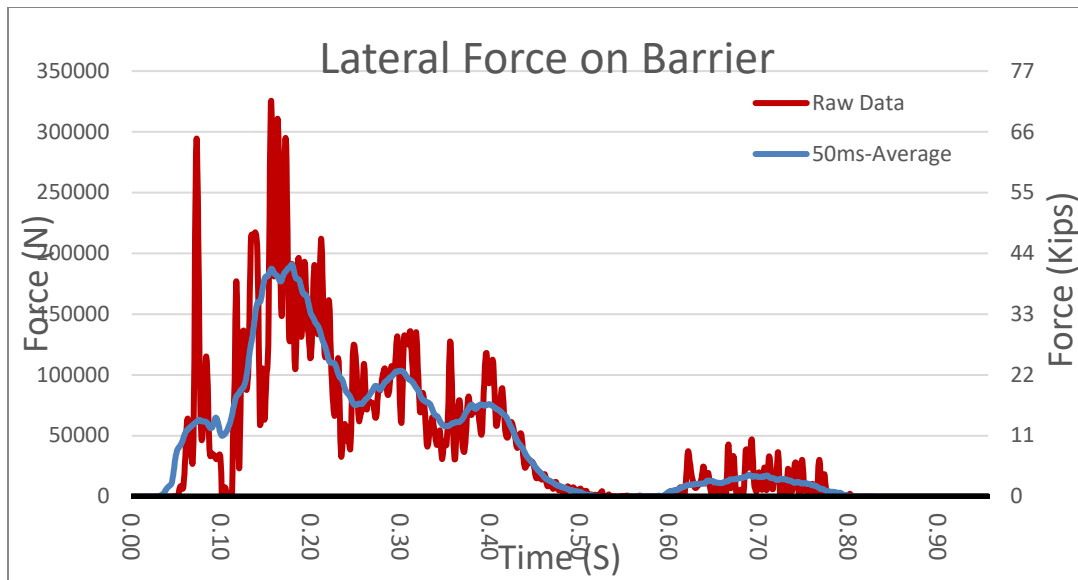


Figure 4.47. Lateral Force on Barrier System (Two 40-ft Segment Configuration – Three Rubber Fenders).

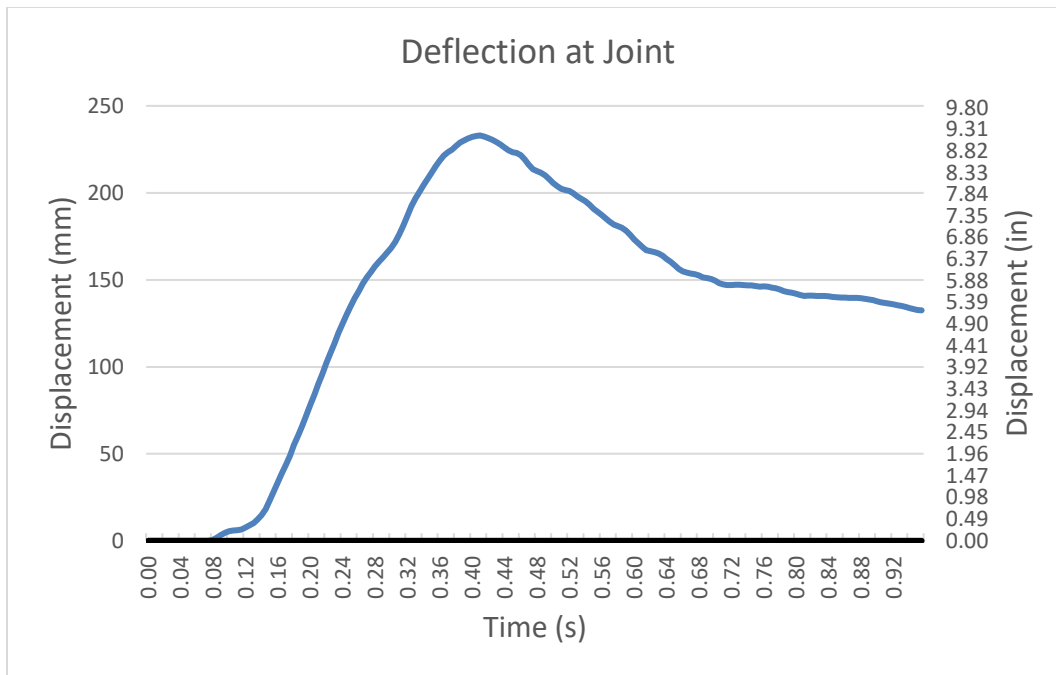


Figure 4.48. Deflection at Joint 1 (Two 40-ft Segment Configuration – Three Rubber Fenders).



Figure 4.49. Maximum Deflection of Barrier System (Two 40-ft Segment Configuration – Three Rubber Fenders).

LS-DYNA keyword deck by LS-PrePost
Time = 0.41

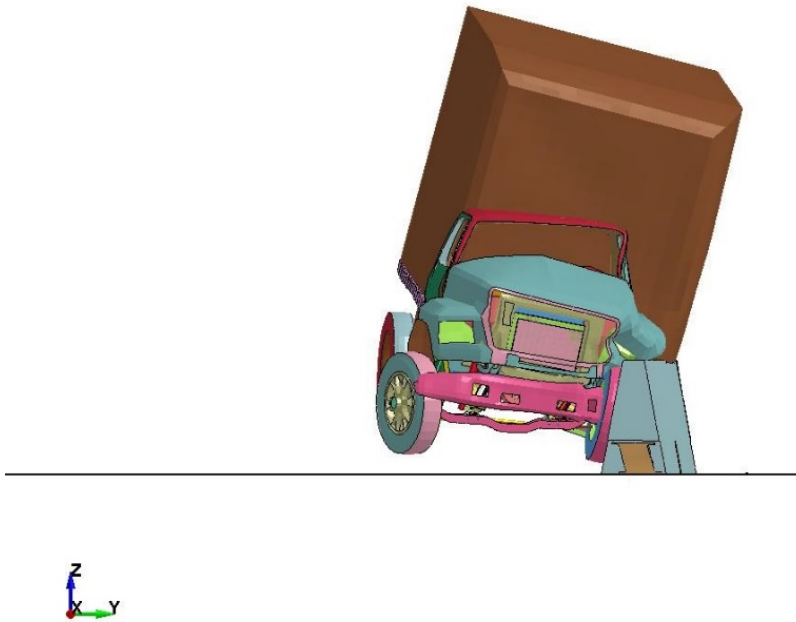


Figure 4.50. Vehicle Interaction with Barrier System at Maximum Deflection (Two 40-ft Segments – Three Rubber Fenders).

Accelerations at the vehicle center of gravity were tracked for evaluation of occupant risk. Table 4.5 presents the resulting occupant risk evaluation according to TRAP. Figure 4.51 shows vehicle angular displacements, and Figures 4.52 through 4.54 show vehicle acceleration versus time traces.

Table 4.5. TRAP Results – Occupant Safety Analysis (Two 40-ft Section with Three Rubber Fenders).

TRAP Results: MASH 1000S 2 40-ft Section with 3 Rubber Fenders	
<i>Impact Velocity, mi/h</i>	62.1
<i>Impact Angle (degrees)</i>	15
Occupant Risk Factors	
OIV (ft/s)	
x-direction	9.5
y-direction	18.7
Ridedown Accelerations (g's)	
x-direction	5.4
y-direction	7.2
Max Roll, Pitch, and Yaw Angles (degrees)	
Roll	-22.3
Pitch	-20.0
Yaw	21.4

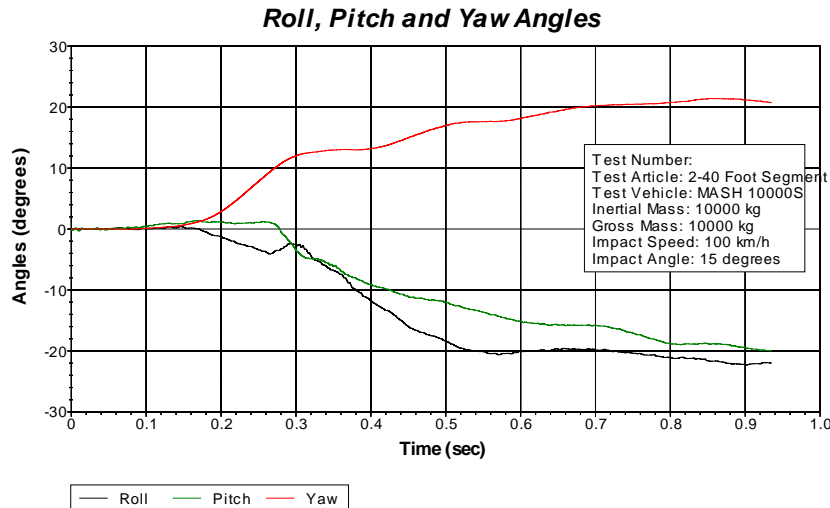


Figure 4.51. Vehicle Angular Displacement (Two 40-ft Segments – Three Rubber Fenders).

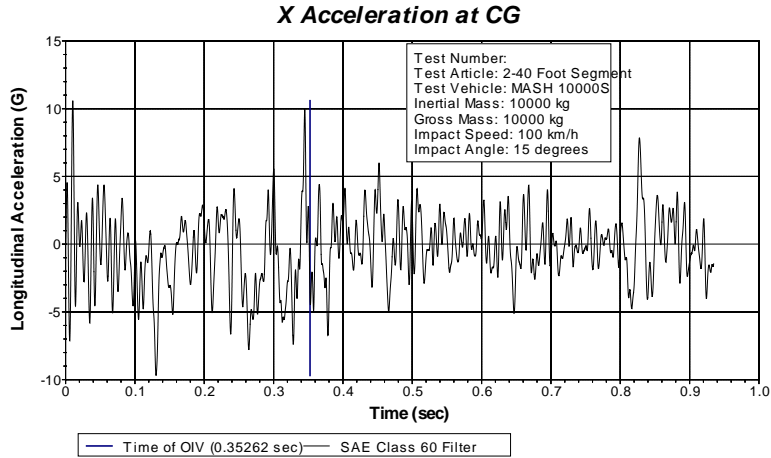


Figure 4.52. Vehicle Longitudinal Acceleration Trace (Two 40-ft Segments – Three Rubber Fenders).

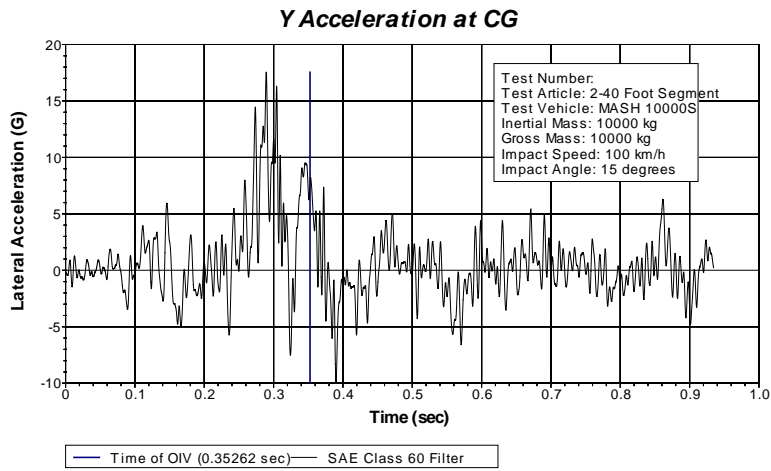


Figure 4.53. Vehicle Lateral Acceleration Trace (Two 40-ft Segments – Three Rubber Fenders).

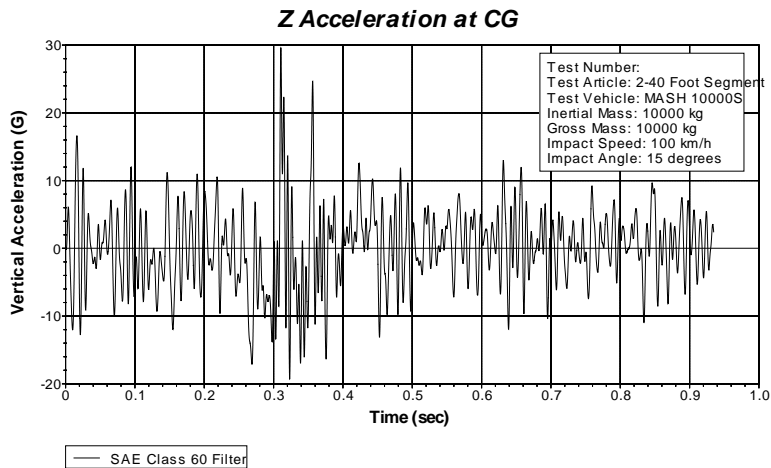


Figure 4.54. Vehicle Vertical Acceleration Trace (Two 40-ft Segments – Three Rubber Fenders).

4.2.2 Two 60-Ft Segments – Three Rubber Fenders

4.2.2.1 Lateral Barrier Force

The instantaneous and 50-ms average lateral force on the barrier system were determined for the simulation impact. Figure 4.55 shows the lateral force on the barrier system.

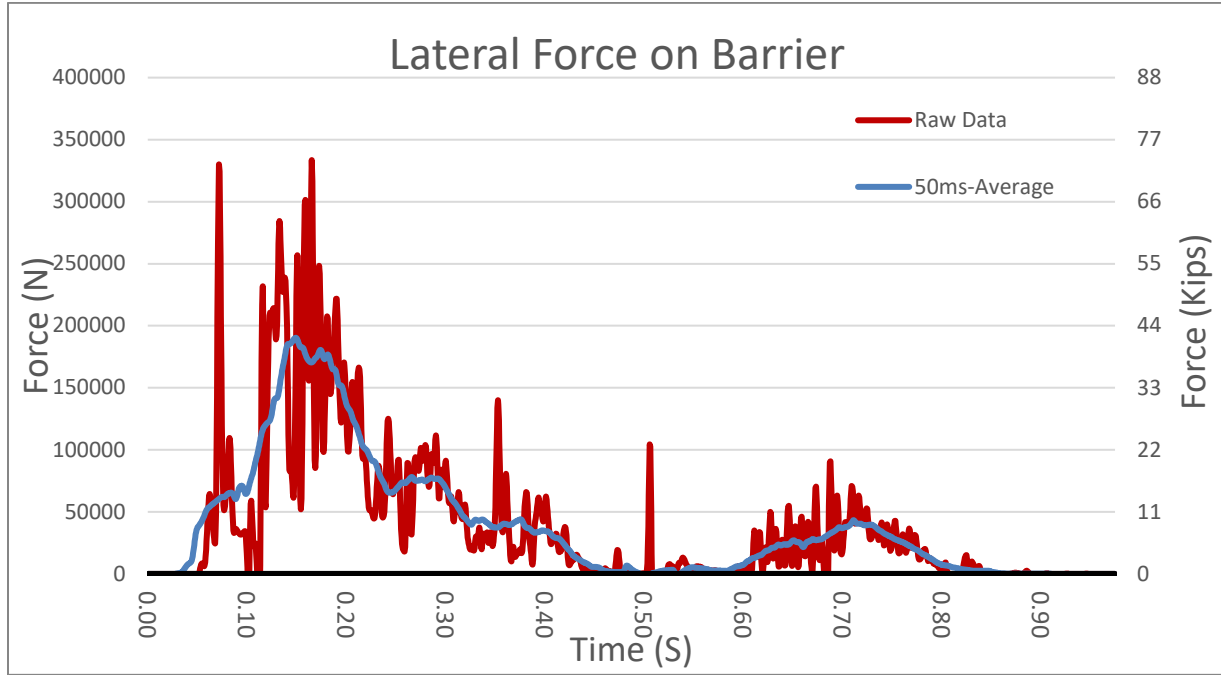


Figure 4.55. Lateral Force on Barrier System (Two 60-ft Segments – Three Rubber Fenders).

3.2.2.2 Joint Deflection/Deflected Shape

The lateral deflections on the barrier joint was determined for the simulation impact. Figure 4.56 shows the lateral deflection for joint 1. The maximum deflection of the barrier system at 0.37 s after impact is shown in Figure 4.57. Figure 4.58 shows the vehicle interaction at maximum deflection.

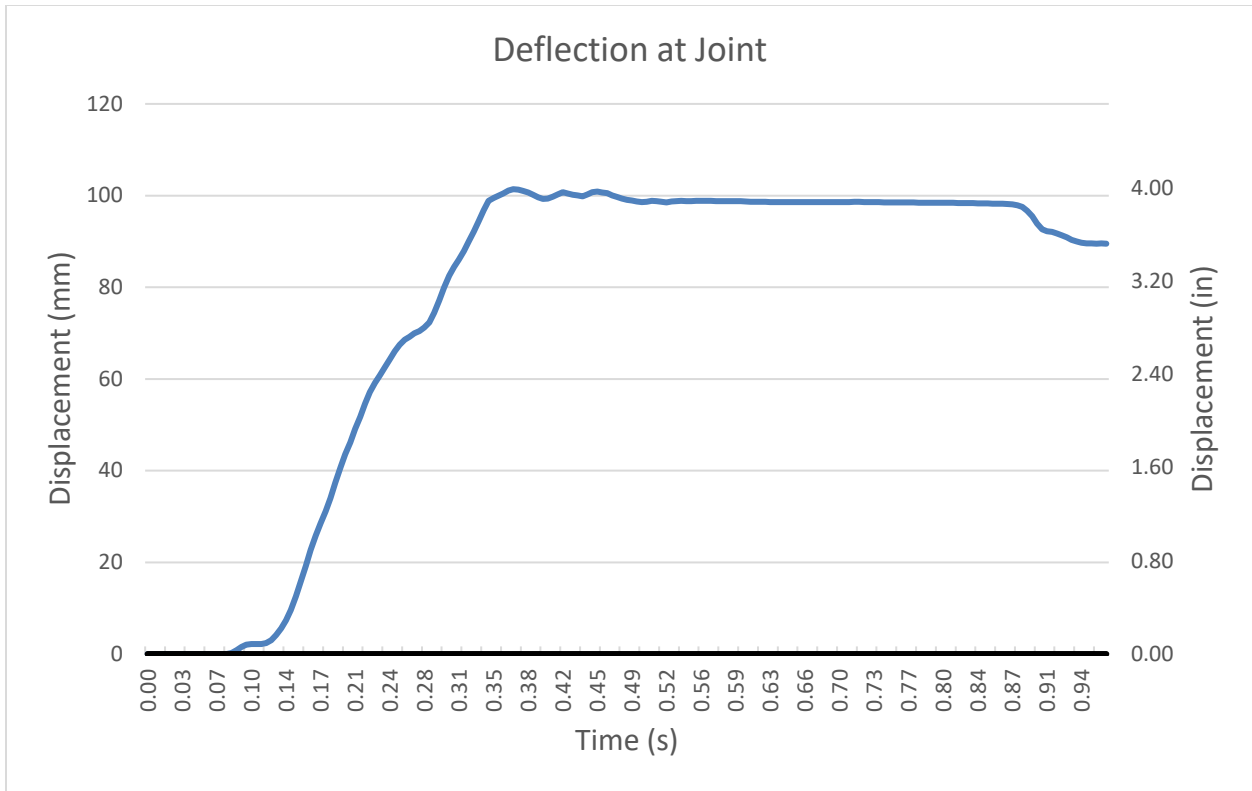


Figure 4.56. Deflection at Joint 1 (Two 60-ft Segments – Three Rubber Fenders).

LS-DYNA keyword deck by LS-PrePost
 Time = 0.37



Figure 4.57. Maximum Deflection of Barrier System (Two 60-ft Segments – Three Rubber Fenders).

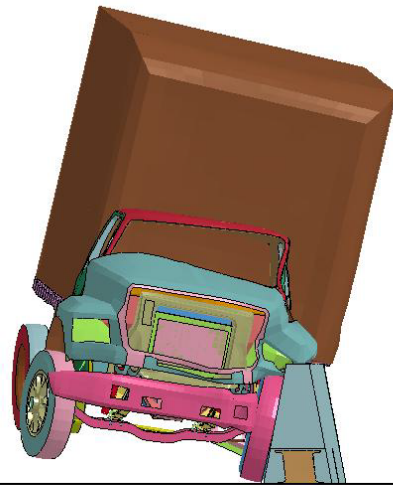


Figure 4.58. Vehicle Interaction with Barrier System at Maximum Deflection (Two 60-ft Segments – Three Rubber Fenders).

Accelerations at the vehicle center of gravity were tracked for evaluation of occupant risk. Table 4.6 presents the resulting occupant risk evaluation according to TRAP. Figure 4.59 shows vehicle angular displacements, and Figures 4.60 through 4.62 show vehicle acceleration versus time traces.

Table 4.6. TRAP Results – Occupant Safety Analysis (Two 60-ft Section with Three Rubber Fenders).

TRAP Results: MASH 1000S 2 60-ft Section with 3 Rubber Fenders	
<i>Impact Velocity, mi/h</i>	62.1
<i>Impact Angle (degrees)</i>	15
Occupant Risk Factors	
OIV (ft/s)	
x-direction	7.9
y-direction	20.3
Ridedown Accelerations (g's)	
x-direction	7.5
y-direction	5.4
Max Roll, Pitch, and Yaw Angles (degrees)	
Roll	-21.9
Pitch	-17.5
Yaw	22.3

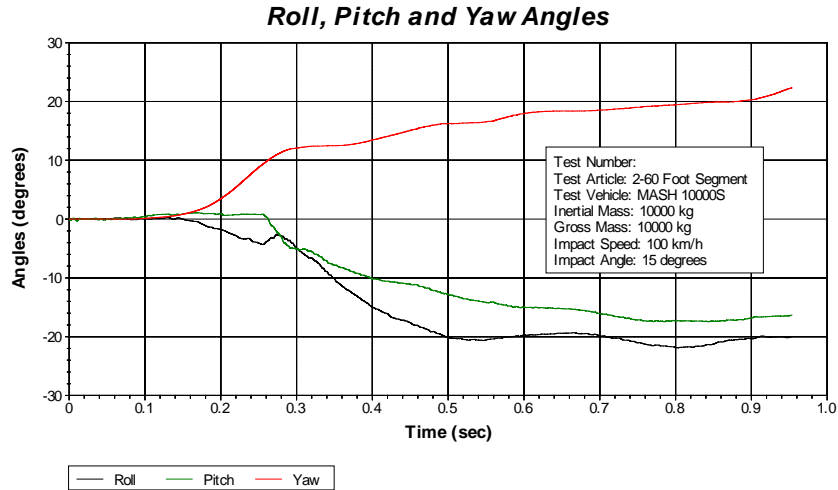


Figure 4.59. Vehicle Angular Displacement (Two 60-ft Segments – Three Rubber Fenders).

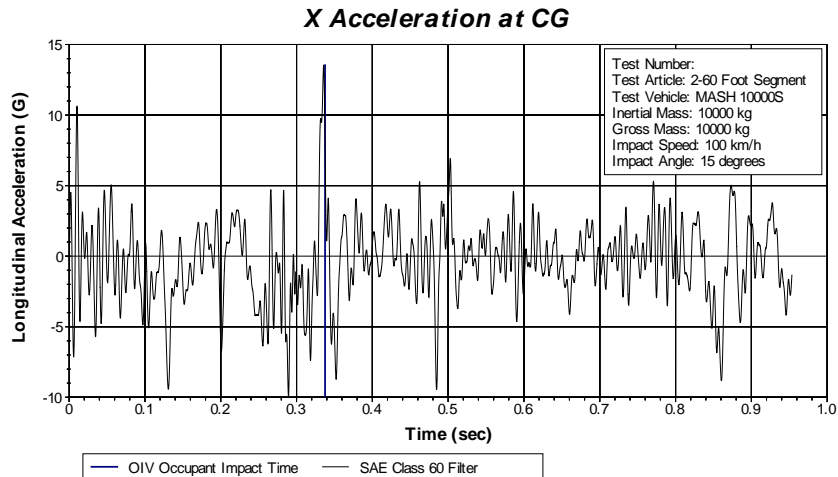


Figure 4.60. Vehicle Longitudinal Acceleration Trace (Two 60-ft Segments – Three Rubber Fenders).

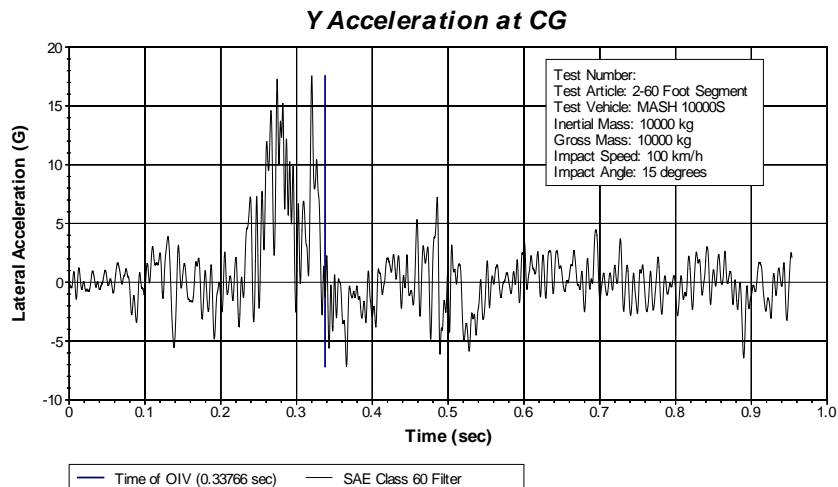


Figure 4.61. Vehicle Lateral Acceleration Trace (Two 60-ft Segments – Three Rubber Fenders).

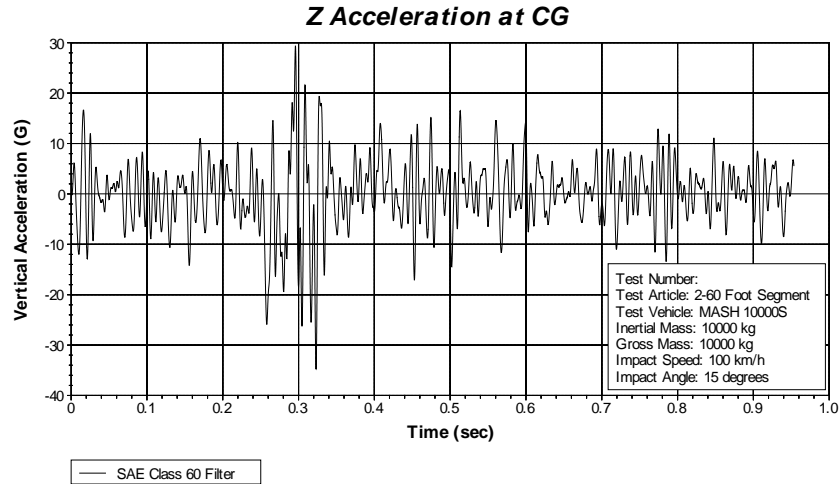


Figure 4.62. Vehicle Vertical Acceleration Trace (Two 60-ft Segments – Three Rubber Fenders).

In each simulation the impact vehicle was successfully contained and redirected. The OIV and ridedown accelerations were all below the maximum limits as specified in *MASH*. Table 4.7 shows the results for the seven different simulations that were conducted.

Table 4.7. Summary of Results of Simulations.

Case	Vehicle	Max Force 50-ms Average (kips)	Max Deflection (inches)	OIV (ft/s)	Ridedown Acceleration (g)
#1 4-40 ft Segment 3 Fenders	Pickup Truck	54.00	7.24	X= 32.2	X= -6.5
				Y= -20.9	Y= 6.2
#2 4-40 ft Segment 2 Fenders	Pickup Truck	54.30	7.80	X= 28.5	X= -8.9
				Y= -20.9	Y= 6.4
#3 3-60 ft Segment 3 Fenders	Pickup Truck	54.50	5.00	X= 25.9	X= -9.1
				Y= -25.6	Y= 6.3
#4 3-60 ft Segment 2 Fenders	Pickup Truck	55.60	5.36	X= 29.5	X= -5.1
				Y= -23.6	Y= 7.2
#5 2-40 ft Segment 3 Fenders	SUT	42.87	9.17	X= 31.2	X= 5.4
				Y= -18.7	Y= 7.2
#6 2-60 ft Segment 3 Fenders	SUT	42.77	4.00	X= 7.9	X= -7.5
				Y= -20.3	Y= 5.4

4.3 SIMULATIONS OF RECOMMENDED DESIGN CONCEPTS

Based on the simulation results, the recommended design system consisted of 60-ft barrier lengths and two rubber fenders for each barrier segment. The rubber fenders are located at the quarter points of each section. An analysis was conducted to determine the critical impact point for the barrier system.

Three different simulation configurations were used to determine the critical impact point. All three simulations impact barrier number one and are each offset a predetermined distance (1, 3, or 5 ft) upstream of joint number one. Figures 4.63 and 4.64 show all three configurations from a plan and elevation view.



Figure 4.63. Plan View of Impact Configurations.

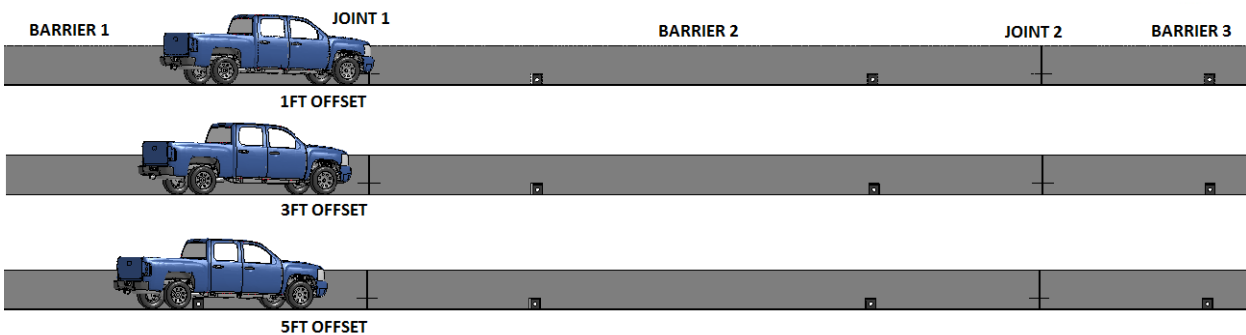


Figure 4.64. Elevation View of Impact Configurations.

4.3.1 Simulation: Critical Impact Point 1-ft Offset

4.3.1.1 Configuration: 1-ft Offset

The first simulation impacts barrier number one a distance of 1 ft upstream of the joint. For this simulation, all barriers are 60 ft long and each barrier has two rubber fenders. The rubber fenders are mounted a distance of 15 ft from the joints. Figures 4.65 and 4.66 show the 1-ft offset configuration in more detail.

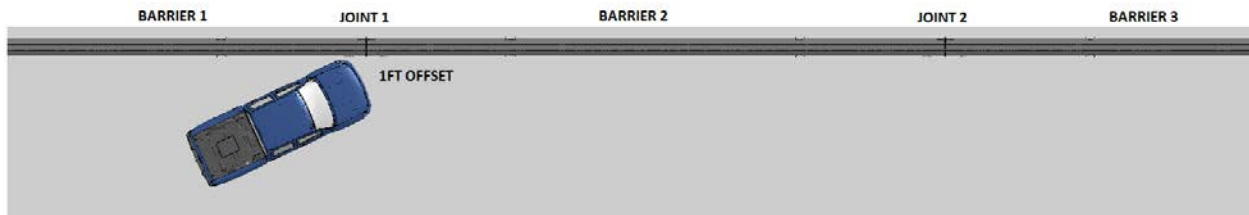


Figure 4.65. Plan View of Impact Configuration with 1-ft Offset.

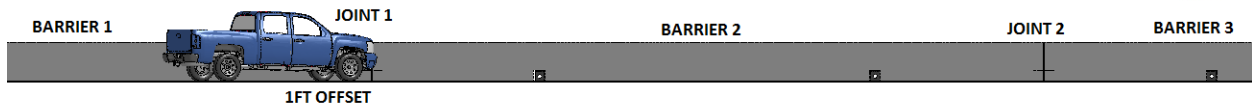


Figure 4.66. Elevation View of Impact Configuration with 1-ft Offset.

4.3.1.2 Maximum Deflection: 1-ft Offset

Deflection at joint number one is shown in Figure 4.67. The maximum deflection occurred at 0.225 seconds and was 4.71 inches. Figure 4.68 shows the simulation at time of maximum deflection.

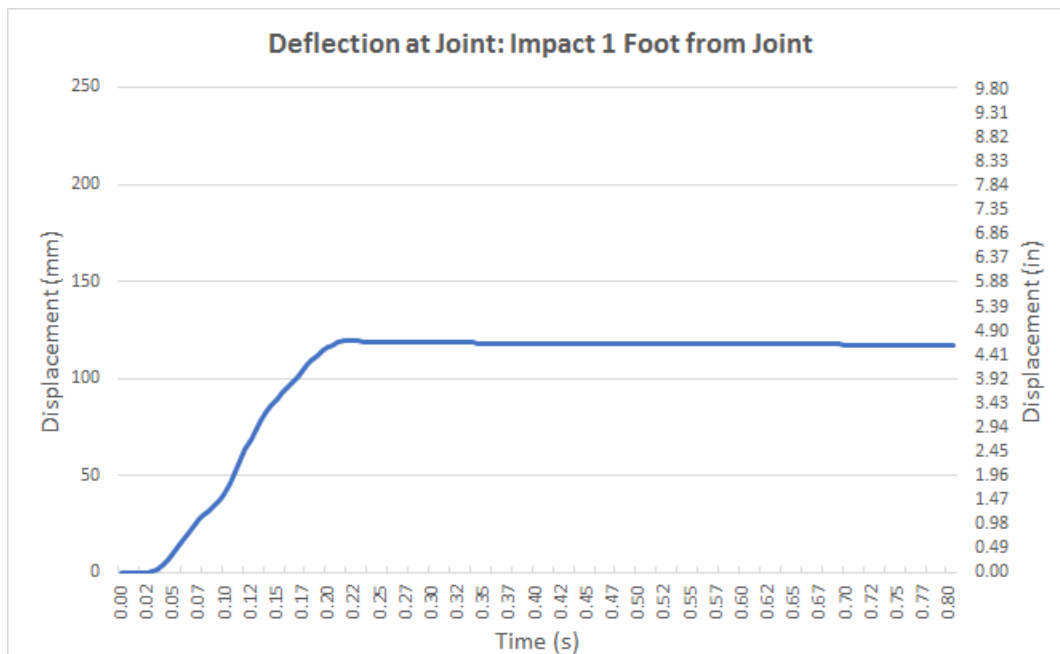


Figure 3.67. Deflection at Joint 1: Impact 1 ft from Joint.

Time = 0.225

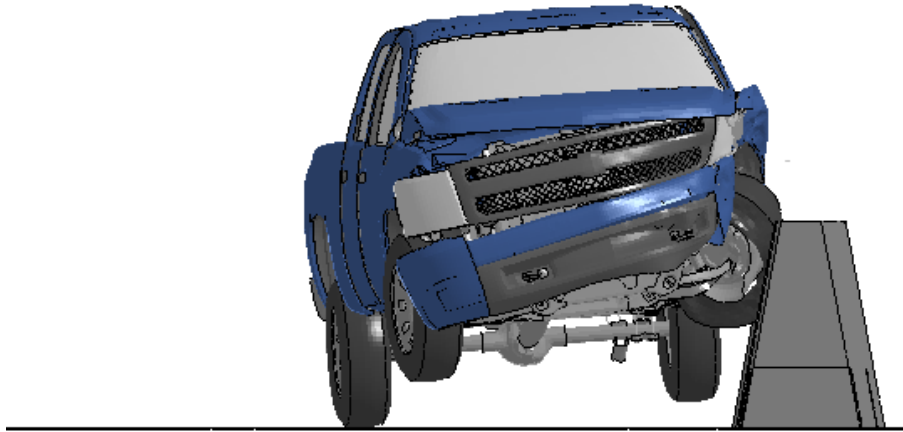


Figure 4.68. Simulation Maximum Deflection at .0225 s.

4.3.1.3 Occupant Risk: 1-ft Offset

Accelerations at the vehicle center of gravity were tracked for evaluation of occupant risk. Table 4.8 presents the resulting occupant risk evaluation according to TRAP. Figure 4.69 shows vehicle angular displacements, and Figures 4.70 through 4.72 show vehicle acceleration versus time traces.

Table 4.8. TRAP Summary Data of 1-ft Offset Simulation.

TRAP Results: Truck Median Barrier	
<i>Impact Velocity, mi/h</i>	62.1
<i>Impact Angle (degrees)</i>	25
Occupant Risk Factors	
Impact Velocity (m/s)	
x-direction	7.7
y-direction	-8.3
Ridedown Accelerations (g's)	
x-direction	-5.7
y-direction	6.6
Max Roll, Pitch, and Yaw Angles (degrees)	
Roll	5.1
Pitch	-10.9
Yaw	29.7

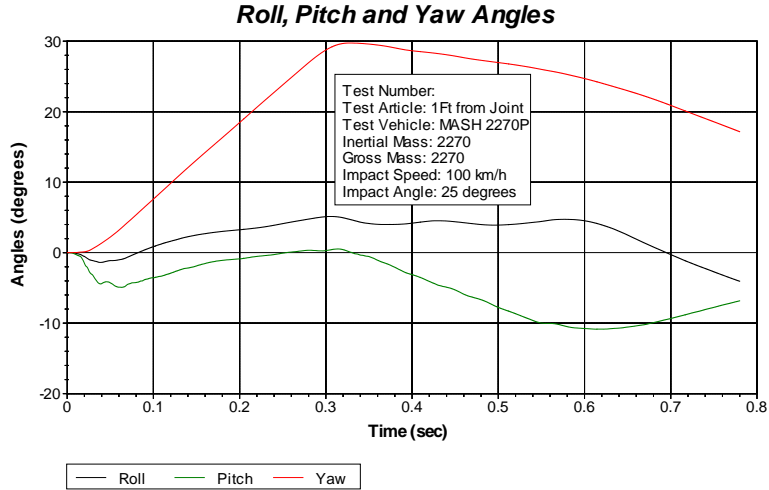


Figure 4.69. Vehicle Roll, Pitch, and Yaw Angles-1-ft Offset.

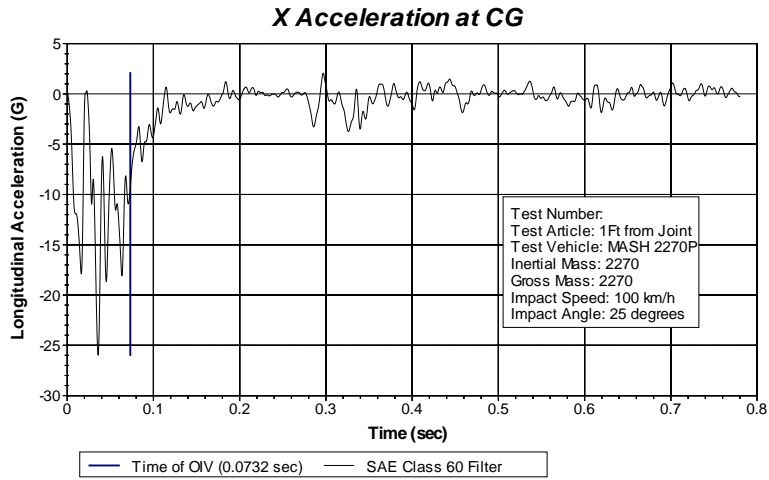


Figure 4.70. Vehicle Longitudinal Acceleration-1-ft Offset.

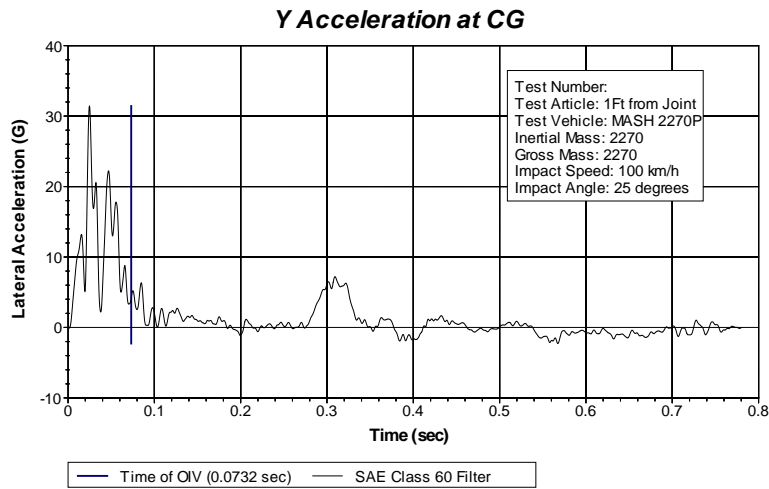


Figure 4.71. Vehicle Lateral Acceleration-1-ft Offset.

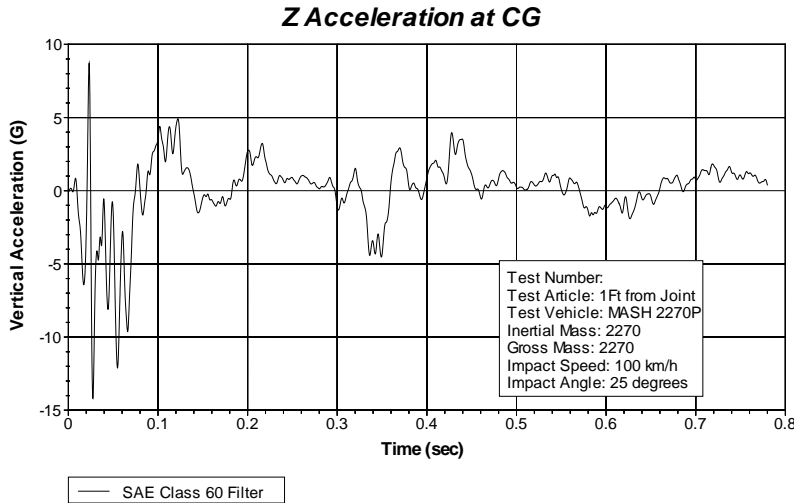


Figure 4.72. Vehicle Vertical Acceleration-1-ft Offset.

4.3.2 Simulation: Critical Impact Point 3-Ft Offset

4.3.2.1 Configuration: 3-ft Offset

The second simulation impacts barrier number one at a distance of 3 ft upstream of the joint. For this simulation all barriers are 60 ft long and each barrier has two rubber fenders. The rubber fenders are mounted a distance of 15 ft from the joints. Figures 4.73 and 4.74 show the 3-ft offset configuration in more detail.



Figure 4.73. Plan View of Impact Configuration with 3-ft Offset.

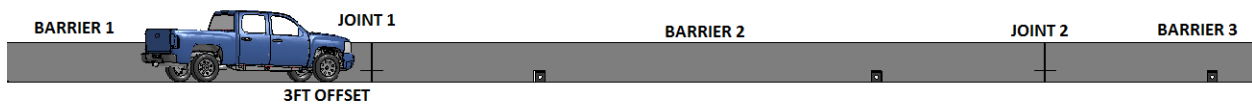


Figure 4.74. Elevation View of Impact Configuration with 3-ft Offset.

4.3.2.2 Maximum Deflection: 3-ft Offset

Figure 4.75 graphs the deflection at joint number one. The maximum deflection occurred at 0.230 s and deflected a distance of 5.10 inches. Figure 4.76 shows the simulation at time of maximum deflection.

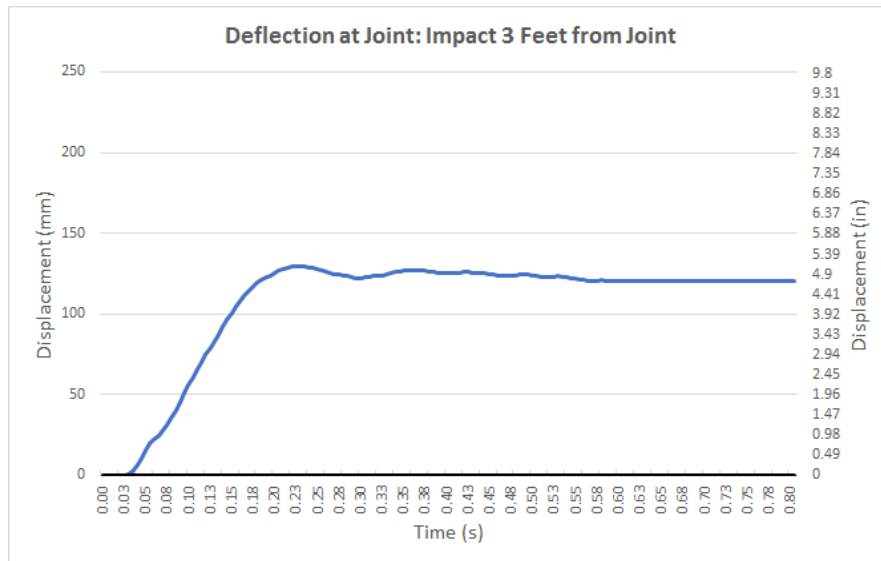


Figure 4.75. Deflection at Joint: Impact 3 ft from Joint.

Time = 0.23

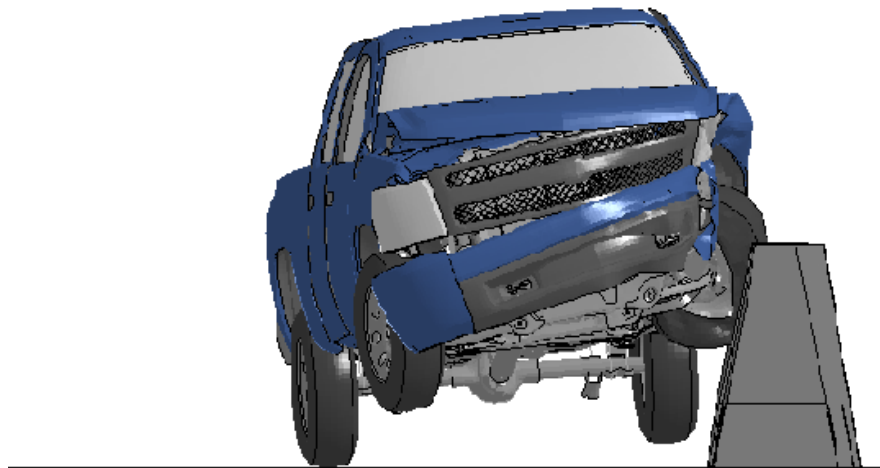


Figure 4.76. Simulation Maximum Deflection at 0.023 s.

4.3.3.3 Occupant Risk: 3-ft Offset

Accelerations at the vehicle center of gravity were tracked for evaluation of occupant risk. Table 4.9 presents the resulting occupant risk evaluation according to TRAP. Figure 4.77 shows vehicle angular displacements, and Figures 4.78 through 4.80 show vehicle acceleration versus time traces.

Table 4.9. TRAP Summary Data of 3-ft Offset Simulation.

TRAP Results: Truck Median Barrier	
<i>Impact Velocity, mi/h</i>	62.1
<i>Impact Angle (degrees)</i>	25
Occupant Risk Factors	
Impact Velocity (m/s)	
x-direction	9.2
y-direction	-6.4
Ridedown Accelerations (g's)	
x-direction	-6.3
y-direction	6.3
Max Roll, Pitch, and Yaw Angles (degrees)	
Roll	5.1
Pitch	-9.4
Yaw	29.1

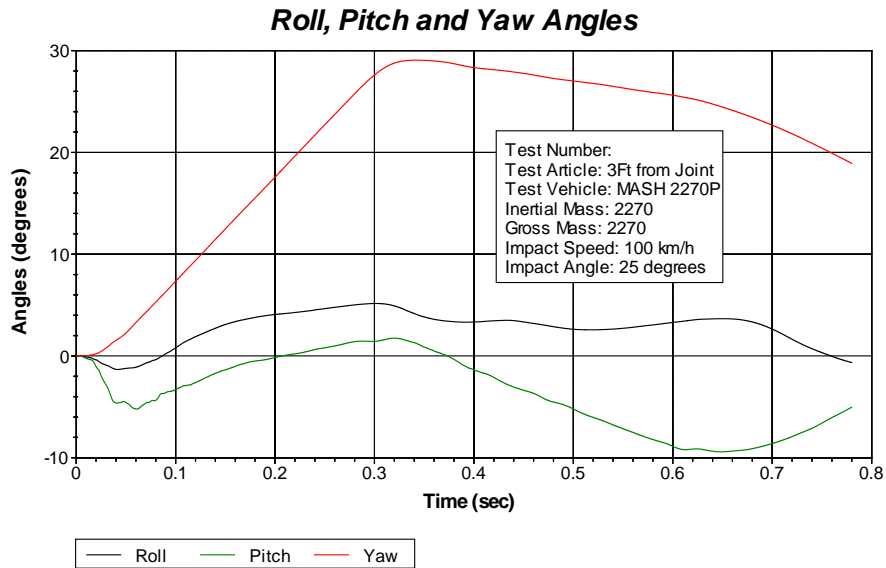


Figure 4.77. Vehicle Roll, Pitch, and Yaw Angles-3-ft Offset.

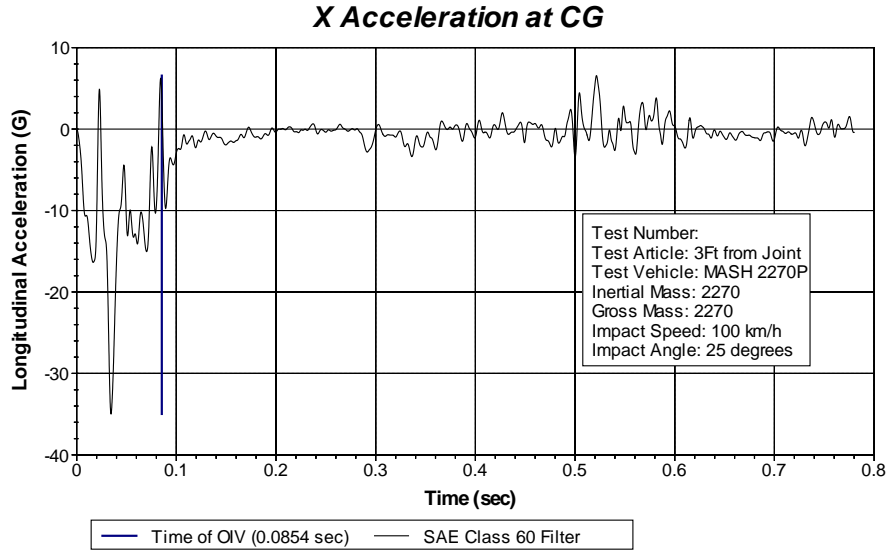


Figure 4.78. Vehicle Longitudinal Acceleration-3-ft Offset.

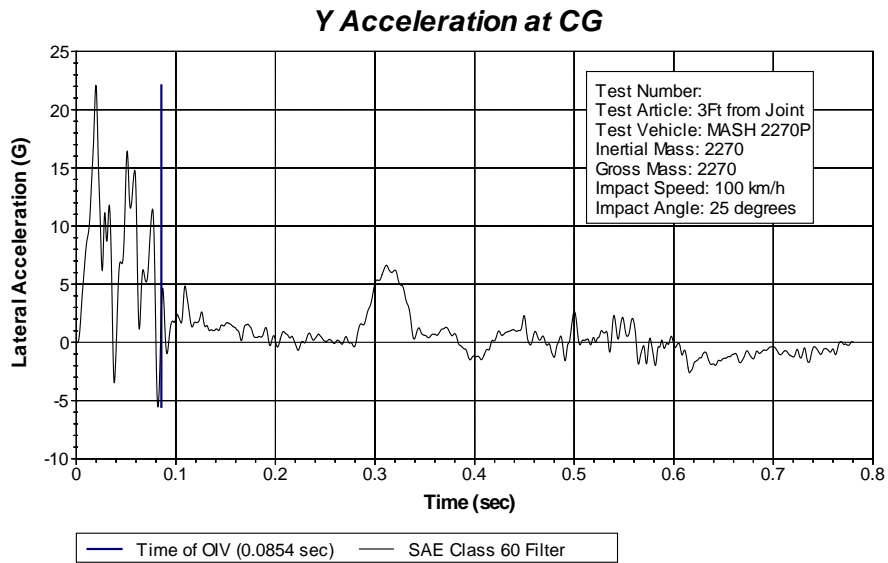


Figure 4.79. Vehicle Lateral Acceleration-3-ft Offset.

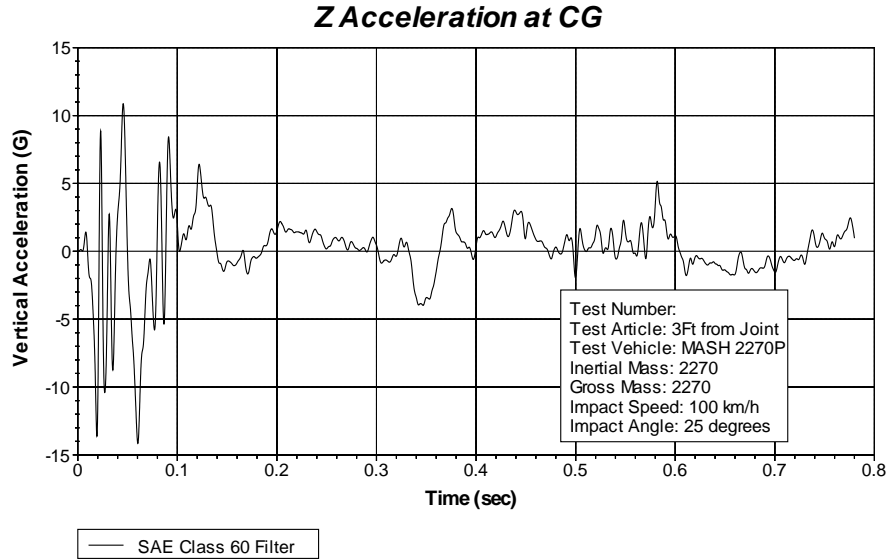


Figure 4.80. Vehicle Vertical Acceleration-3-ft Offset.

4.3.3 Simulation: Critical Impact Point 5-Ft Offset

4.3.3.1 Configuration: 5-ft Offset

The third simulation impacts barrier number one a distance of 5 ft upstream of the joint. For this simulation, all barriers are 60 ft long and each barrier has two rubber fenders. The rubber fenders are mounted a distance of 15 ft from the joints. Figure 4.81 and Figure 4.82 show the 5-ft offset configuration in more detail.



Figure 4.81. Plan View of Impact Configurations with 5-ft Offset.

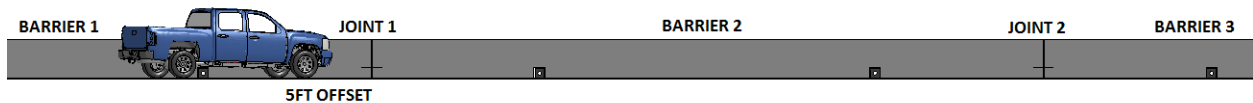


Figure 4.82. Elevation View of Impact Configuration with 5-ft Offset.

4.3.3.2 Maximum Deflection: 5-ft Offset

Figure 4.83 graphs the deflection at joint number one. The maximum deflection occurred at 0.245 s and deflected a distance of 5.33 inches. Figure 4.84 shows the simulation at time of maximum deflection.

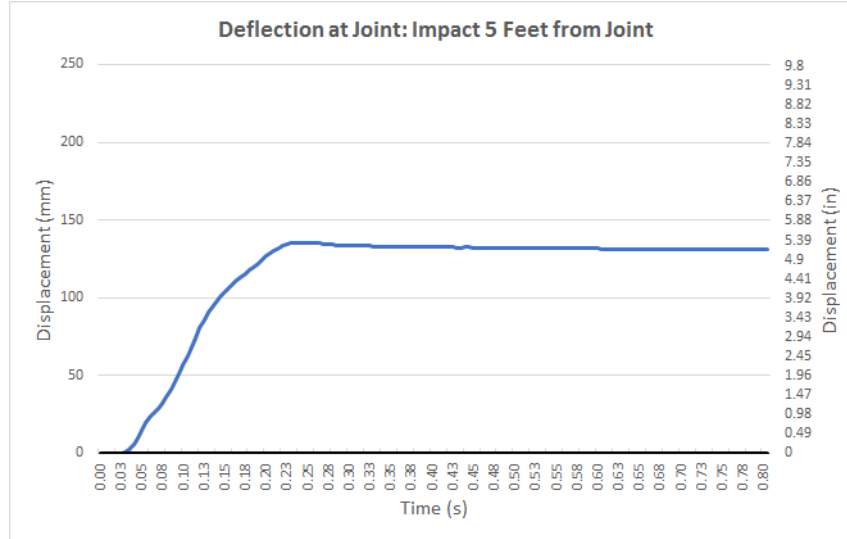


Figure 4.83. Deflection at Joint 1: Impact 5 ft from Joint.

Time = 0.245

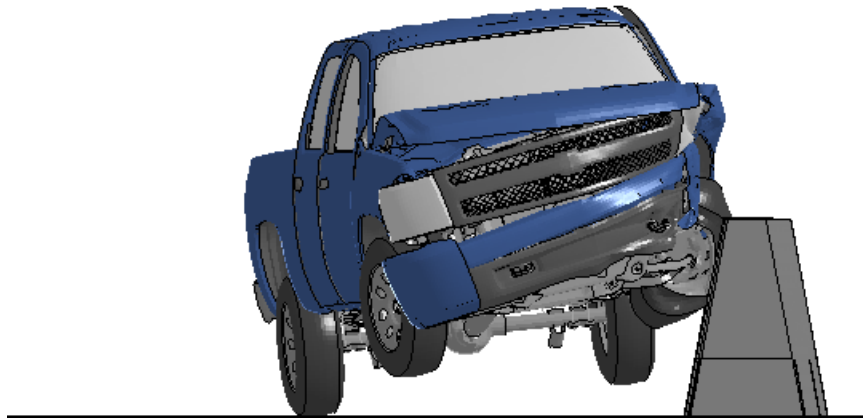


Figure 4.84. Simulation Maximum Deflection at 0.245 s.

4.3.3.3 Occupant Risk: 5-ft Offset

Accelerations at the vehicle center of gravity were tracked for evaluation of occupant risk. Table 4.10 presents the resulting occupant risk evaluation according to TRAP. Figure 4.85 shows vehicle angular displacements, and Figures 4.86 through 4.88 show vehicle acceleration versus time traces.

Table 4.10. TRAP Summary Data of 5-ft Offset Simulation.

TRAP Results: Truck Median Barrier	
<i>Impact Velocity, mi/h</i>	62.1
<i>Impact Angle (degrees)</i>	25
Occupant Risk Factors	
Impact Velocity (m/s)	
x-direction	8.6
y-direction	-6.5
Ride down Accelerations (g's)	
x-direction	-13.4
y-direction	10.0
Max Roll, Pitch, and Yaw Angles (degrees)	
Roll	-8.7
Pitch	-4.7
Yaw	34

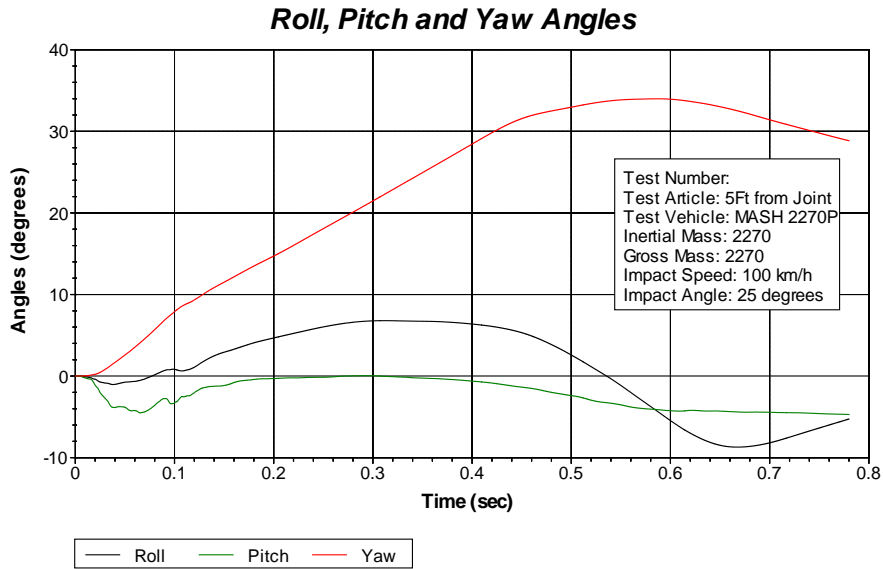


Figure 4.85. Vehicle Roll, Pitch, and Yaw Angles-5-ft Offset.

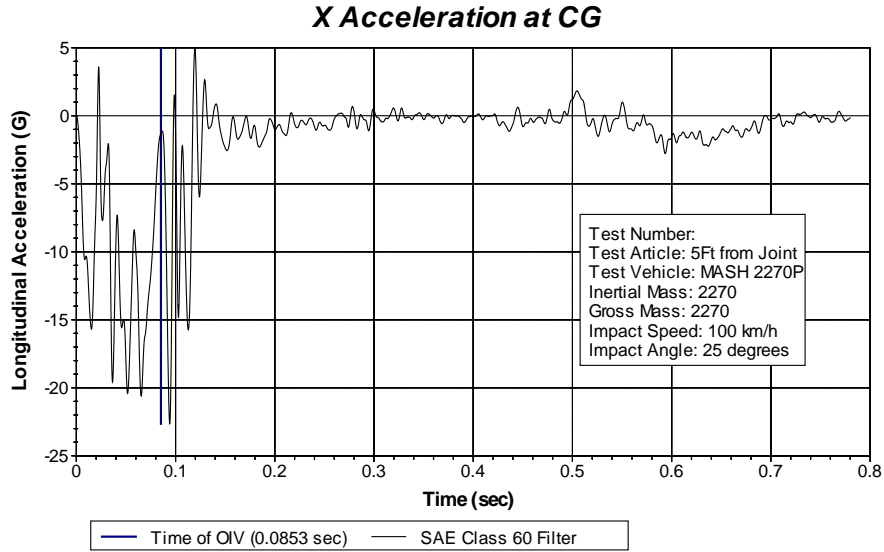


Figure 4.86. Vehicle Longitudinal Acceleration-5-ft Offset.

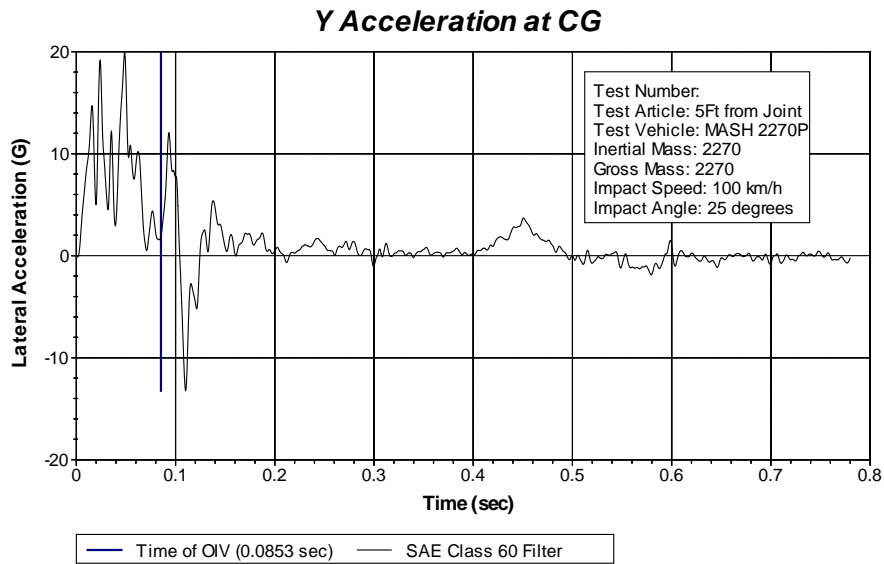


Figure 4.87. Vehicle Lateral Acceleration-5-ft Offset.

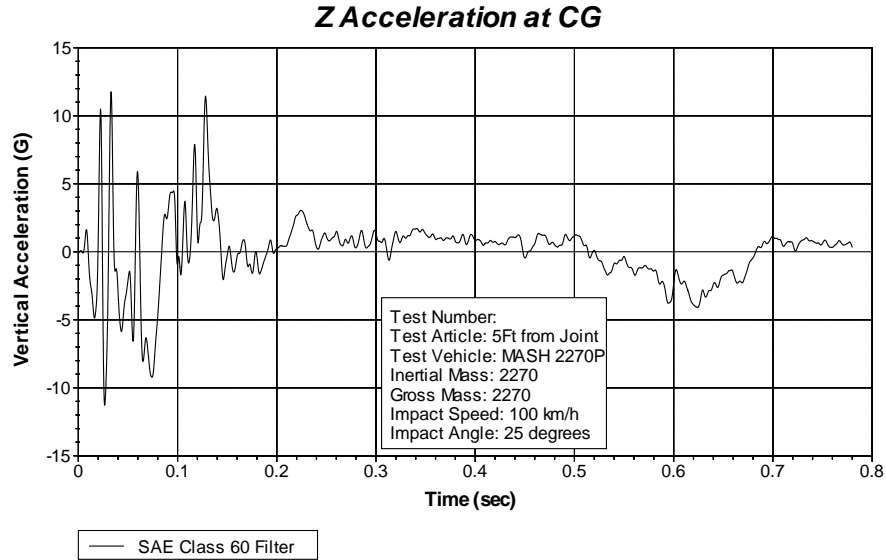


Figure 4.88. Vehicle Vertical Acceleration-5-ft Offset.

4.4 SUMMARY OF CRITICAL IMPACT SIMULATIONS

In each simulation the impact vehicle was successfully contained and redirected. The OIV and ridedown accelerations were all below the maximum limits as specified in *MASH*. Table 4.11 shows the results for the three different simulations that were conducted to determine critical impact point.

Table 4.11. Summary of Critical Impact Point Configurations.

Case	Vehicle	Max Deflection (inches)	OIV (ft/s)	Ride down Acceleration (g's)
#1 1-ft Offset	Pickup Truck	4.71	X= 25.3	X= -5.7
			Y= -27.2	Y= 6.6
#2 3-ft Offset	Pickup Truck	5.10	X= 30.2	X= -6.3
			Y= -20.9	Y= 6.3
#3 5-ft Offset	Pickup Truck	5.33	X= 28.2	X= -13.4
			Y= -21.3	Y= 10.0

4.5 RECOMMENDED SYSTEM DESIGN

The simulations conducted has indicated a comparable performance outcome based on the deflections and the occupant risk values. Hence, a 60-ft barrier segment was recommended to reduce the frequency of joints from a construction aspect. The details for the recommended design for testing is described in Chapter 6.

CHAPTER 5: BOGIE TESTING

Researchers conducted bogie impact tests to accomplish these key objectives:

- Understand the performance of the rubber fenders under impact load. This will aid in the design of the median barrier by selecting the adequate number of rubber fender for the full scale crash tests.
- Validate the rubber model for the rubber fenders so the validated model can be used in the full scale simulation with the desired confidence.
- Understand and quantify the performance of different concrete mixes including the standard TxDOT Class C (3600 psi).
- Enhance the validity of the 5000-lb bogie model to increase the confidence in subsequent bogie simulations.

5.1 BOGIE TESTING – PHASE I

5.1.1 Test Article Design and Construction

The test installation consisted of two modified standard TxDOT Single Slope Concrete Barriers (SSCB, Type 1), each was 20 ft in length, and contained a rubber/elastomer shear fender attached at each end. The barriers were separated by a 40-inch gap between the ends of the adjacent barriers. The barriers were installed on and along the edge of an abandoned out-of-service, 6-inch thick concrete runway apron.

The single slope barriers were cast in place (CIP) at the Proving Ground site. Each barrier was 42 inches tall and 24 inches wide at the base, tapering to 8 inches wide at the top with symmetrical 79.2° slopes on both faces. The top longitudinal edges were cast with a ¾-inch chamfer. A box and steel anchor plate (for securing the shear fender) was cast into each lower end of the barriers. A 3-ft long × 3-inch tall drainage relief slot was cast, and symmetrically centered, at the midpoint in the bottom side of each barrier.

Each end of each barrier incorporated a BorgWarner BJ Neolastic™ shear fender (Part No. 54-6496)¹ that measured 10-inches wide × 11⁵/₈-inches tall × 15³/₄-inches long, with a 4-inch diameter hole. Each shear fender was secured to the box in the end of the barrier with four ¾ inch × 2-inch hex bolts and USS flat washers, and to the apron with four Hilti screw anchor bolts (KH-EZ ¾-inch × 7-inch) according to the manufacturer's instructions. An 11-inch × 10¹/₂-inch × ½-inch thick plywood pad was installed between the bottom of the shear fender and the concrete apron. Bolting was located on a 4-inch × 14¹/₈-inch pattern as dictated by the shear fender specifications. Refer to Appendix B.1 for shear fender details.

The fabricated anchor plates were ¼-inch thick and each measured 11-inches deep × 12⁵/₈-inches tall × 24-inches to 19¹/₄-inches wide to conform to the profile of the barrier. Four Nelson studs (H4L, ½-inch diameter × 6-inches long) were secured to each outside face. Each horizontal (top) plate contained four ¾-inch coupling nuts centered and welded to the plate

¹ Dwg calls for Morse Rubber shear fender (Model #E46496) instead of BorgWarner Neolastic.

above $1\frac{3}{16}$ -inch diameter holes located on a 4-inch \times $14\frac{1}{8}$ -inch pattern. Refer to Appendix B.1 for anchor plate details.

Internal steel reinforcement was comprised of 23 #4 V bars ($\frac{1}{2}$ -inch diameter) longitudinally spaced at 12-inches, except for 2 shortened #4 bars at 6-inch and 4-inch spacing at each end to further reinforce the box and allow for 2-inches of concrete cover. These 23 V bars were also inclusive of 3 shorter V bars located over the drainage relief. A large and a small U bar on each end provided additional reinforcement at the boxes. Ten #5 longitudinal bars ($\frac{5}{8}$ -inch diameter), five on each side, were vertically spaced on 8-inch centers. Refer to Appendix B.1, Sheets 2, 3, and 4 of 6 for reinforcement details. See Figure 5.1 for the completed installation.



Figure 5.1. Single-Slope Median Barrier with Shear Fender Anchor Plate before Test No. 468957-B4.

Other than the two shear fenders and their bolting, there were no additional bolts, pins, or adhesives that secured the barriers to the concrete apron. Each barrier was cast on plastic film on top of the clean runway apron. To facilitate ease of construction, the shear fenders were positioned within the formwork, secured to the apron, and bolted to the installed anchor plates prior to concrete placement.

Tests B-4 and B-5 were performed on the northernmost of the two barriers. Tests B-6 and B-7 were performed on the southernmost of the two barriers.

The shear fender anchor plate was fabricated from ASTM A36 steel. Bolting met ASTM A325 specifications. Reinforcing steel was specified to meet ASTM A615 Grade 60. Concrete

for the barriers was specified as TxDOT Class C (3600 PSI minimum). Test cylinder samples were taken at the time of casting on September 9, 2016, resulting in an average compressive strength of 3313 psi on September 20, 2016, (11 days). Appendix B.2 provides the cert sheet for the fender and the concrete strength testing results for the test installation.

5.1.2 Weather Conditions:

Weather conditions on September 20, 2016, during the time of testing were: wind speed: 1-3 mi/h; wind direction: 105–196° (vehicle was traveling in a westerly direction); temperature: 85–98°F; relative humidity: 47–76 percent.

5.1.3 Test Vehicle

The tests were performed using the 4960-lb bogie impacting the barriers at 90° with the centerline of the bogie aligned with the centerline of the impact face of the center barrier segment. The bogie was equipped with a rigid nose with three pipe cylinders attached to the nose. Figure 5.2 shows photographs of the bogie vehicle used during Test Nos. 468957 B4-B7, and Appendix C provides details of the pipe cylinders.

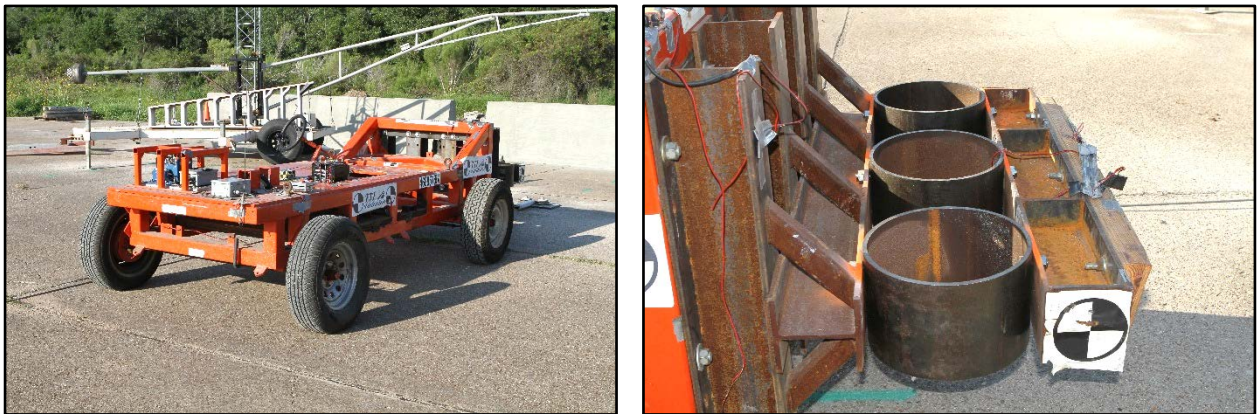


Figure 5.2. Bogie Vehicle before Test No. 468957-B4.

5.1.4 Test No. 468957-B4

5.1.4.1 Brief Test Description:

While the bogie was traveling at 18.3 mi/h, the nose of the bogie impacted the barrier at 90° with the centerline of the bogie aligned with the centerline of the barrier. The bogie ceased forward motion at 0.337 s.

5.1.4.2 Test Article Damage

Maximum deflection of the barrier was 22.3 inches and maximum permanent deflection was 1¼ inches. Three vertical cracks (one at centerline and two 12 inches to each side of centerline) were noted on the field side. Figures 5.3 through 5.7 show damage to the barrier.



Figure 5.3. Right Traffic Side of Barrier after Test No. 468957-B4.



Figure 5.4. Center and Left Traffic Side of Barrier after Test No. 468957-B4.



Figure 5.5. Traffic Face of Barrier after Test No. 468957-B4.

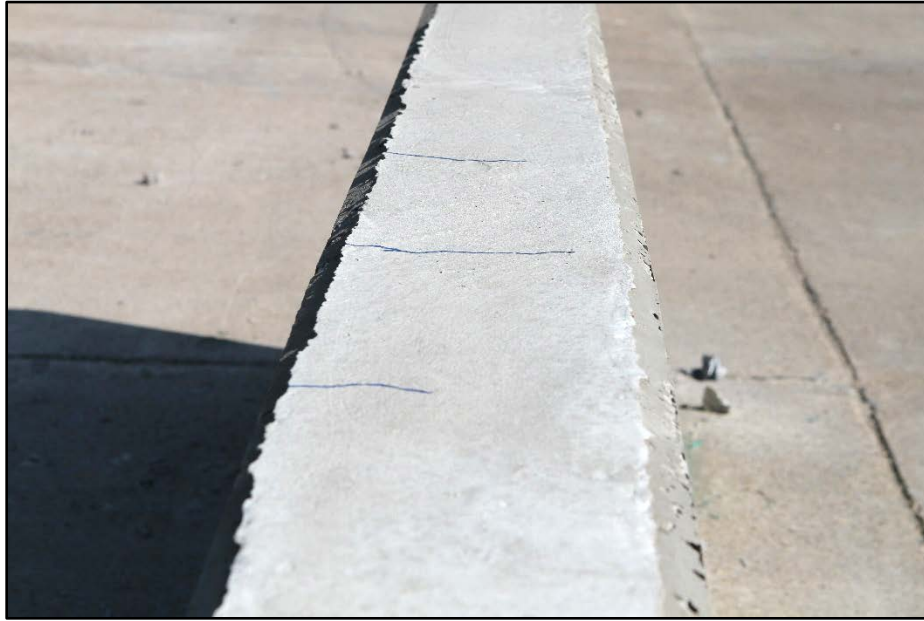


Figure 5.6. Top of Barrier after Test No. 468957-B4.



Figure 5.7. Field Side-Center of Barrier after Test No. 468957-B4.

5.1.4.3 Test Vehicle Damage

Figure 5.8 shows damage to the bogie vehicle. The pipe shapes crushed 8.9 inches. The vehicle rebounded 24 ft from the traffic face of the barrier.

5.1.4.4 Occupant Risk Factors

Data from the accelerometer, located near the vehicle center of gravity, were digitized for evaluation of occupant risk. In the longitudinal direction, the OIV was 24.6 ft/s at 0.115 s, the highest 0.010-s occupant ridedown acceleration was 4.3 g from 0.402 to 0.412 s, and the

maximum 0.050-s average acceleration was -14.2 g between 0.004 and 0.054 s. Figures 5.9 and 5.10 show longitudinal acceleration and impact force during the test.



Figure 5.8. Bogie Vehicle after Test No. 468957-B4.

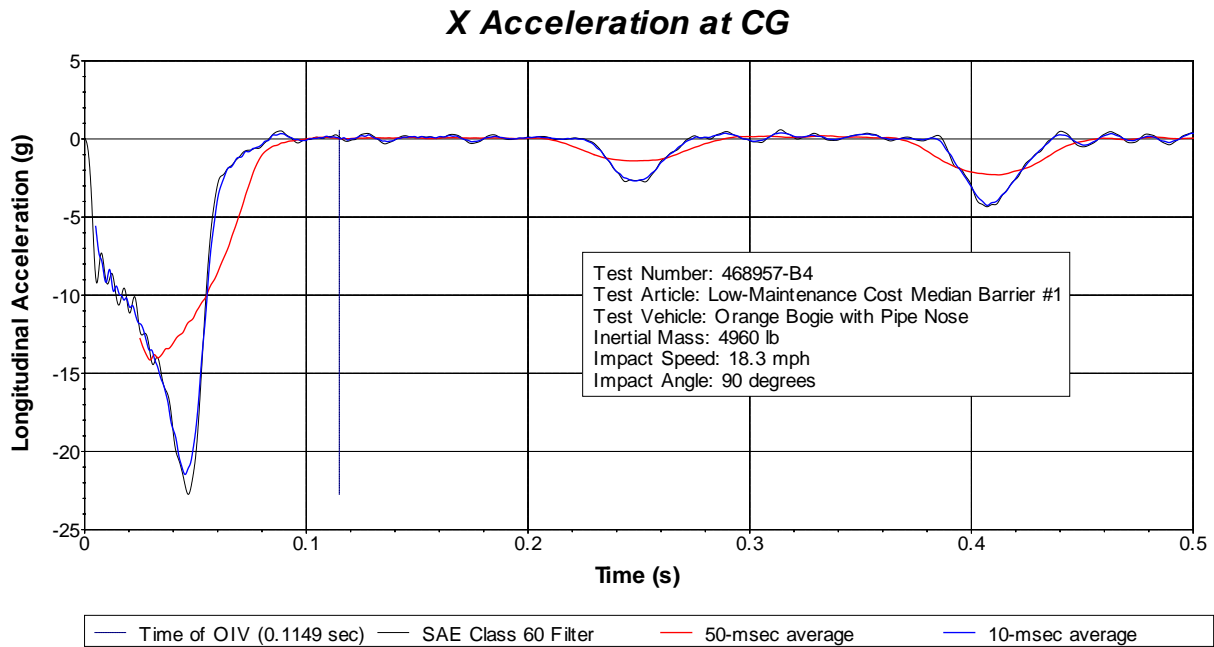


Figure 5.9. Longitudinal Accelerometer Trace during Test No. 468957-B4.

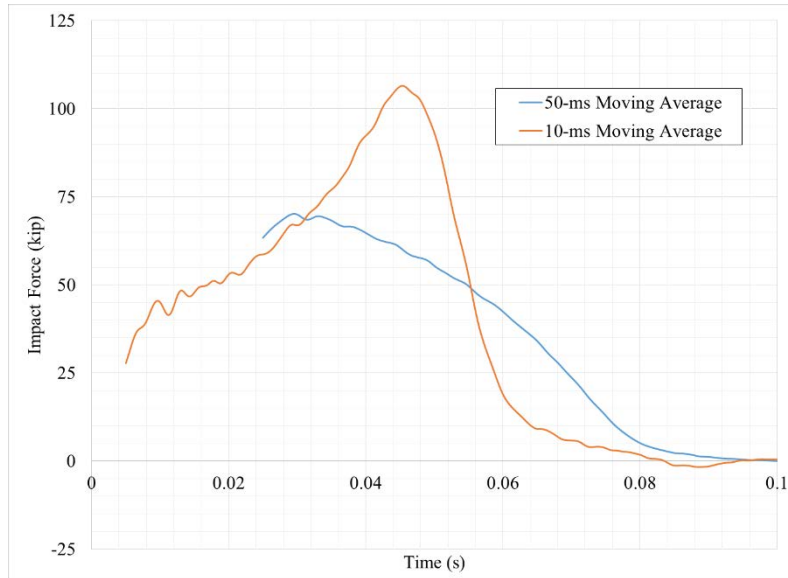


Figure 5.10. Impact Forces during Test No. 468957-B4.

5.1.5 Test No. 468957-B5

5.1.5.1 Brief Test Description:

While the bogie was traveling at 22.3 mi/h, the nose of the bogie impacted the barrier at 90° with the centerline of the bogie aligned with the centerline of the barrier. The bogie ceased forward motion at 0.430 s.

5.1.5.2 Test Article Damage

Maximum deflection of the barrier was 29.3 inches and maximum permanent deflection was 0.5 inch. The barrier had been used for the previous test, and there were two additional cracks 24 inches to both sides of the centerline. Figures 5.11 and 5.12 show damage to the barrier.



Figure 5.11. Impact Side of Barrier after Test No. 468957-B5.



Figure 5.12. Field Side-Center of Barrier after Test No. 468957-B5.

5.1.5.3 Test Vehicle Damage

The pipes had been replaced from the previous test. Figure 5.13 shows damage to the bogie vehicle. Maximum crush of the pipe shapes in the nose was 10 inches. The vehicle rebounded 30 ft from the traffic face of the barrier.



Figure 5.13. Bogie Vehicle after Test No. 468957-B5.

5.1.5.4 Occupant Risk Factors

Data from the accelerometer, located at the vehicle center of gravity, were digitized for evaluation of occupant risk. In the longitudinal direction, the OIV was 25.9 ft/s at 0.107 s, the highest 0.010-s occupant ridedown acceleration was 5.9 g from 0.333 to 0.343 s, and the maximum 0.050-s average acceleration was -15.9 g between 0.004 and 0.054 s. Figures 5.14 and 5.15 show longitudinal acceleration and impact forces during the test.

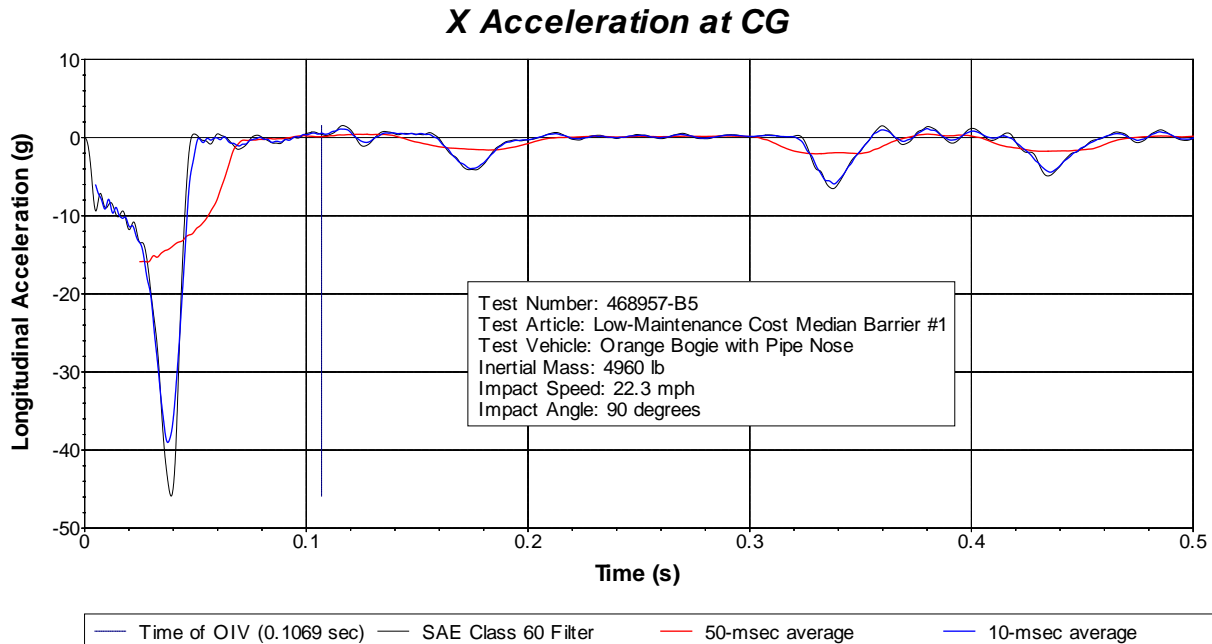


Figure 5.14. Longitudinal Acceleration during Test No. 468957-B5.

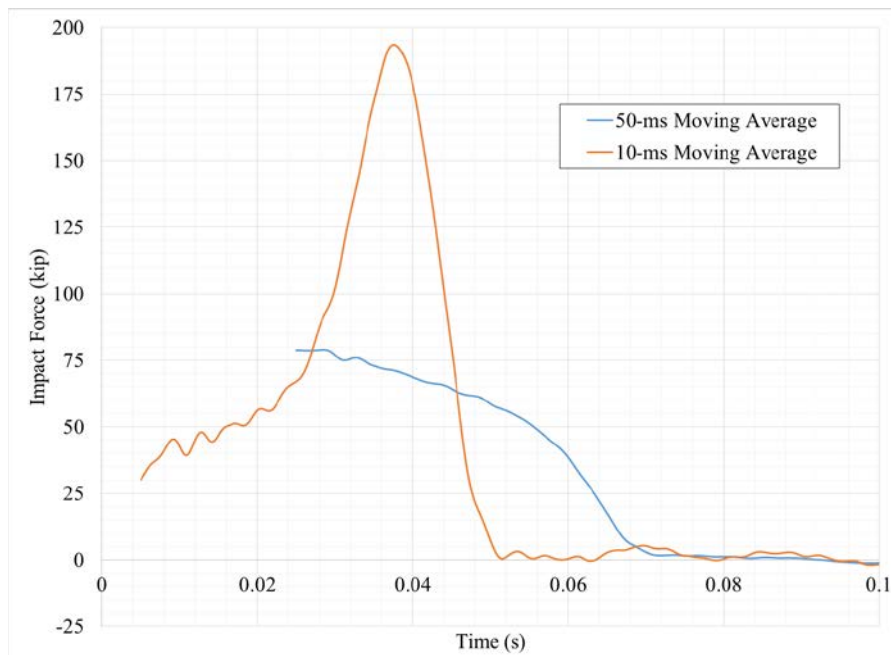


Figure 5.15. Impact Force during Test No. 468957-B5.

5.1.6 Test No. 468957-B6

5.1.6.1 Brief Test Description

While the bogie was traveling at 18.5 mi/h, the nose of the bogie impacted the barrier at 90° with the centerline of the bogie aligned with the centerline of the barrier. The bogie ceased forward motion at 0.390 s.

5.1.6.2 Test Article Damage

Maximum deflection of the barrier was 21.0 inches, and there was no measureable maximum permanent deflection. On the field side of the barrier, three cracks radiated from the base of the barrier. Figures 5.16 and 5.17 show damage to the barrier.



Figure 5.16. Impact Side of Barrier after Test No. 468957-B6.



Figure 5.17. Field Side of Barrier after Test No. 468957-B6.

5.1.6.3 Test Vehicle Damage

The pipe shapes had been replaced from the previous test. Figure 5.18 shows damage to the bogie vehicle. Maximum crush of the pipe shapes in the nose was 7 inches. The vehicle rebounded 26 ft from the traffic face of the barrier.



Figure 5.18. Bogie Vehicle after Test No. 468957-B6.

5.1.6.4 Occupant Risk Factors

Data from the accelerometer, located at the vehicle center of gravity, were digitized for evaluation of occupant risk. In the longitudinal direction, the OIV was 26.6 ft/s at 0.119 s, the highest 0.010-s occupant ridedown acceleration was 3.9 g from 0.392 to 0.402 s, and the maximum 0.050-s average acceleration was -13.8 g between 0.004 and 0.054 s. Figures 5.19 and 5.20 show longitudinal acceleration and impact force during the test.

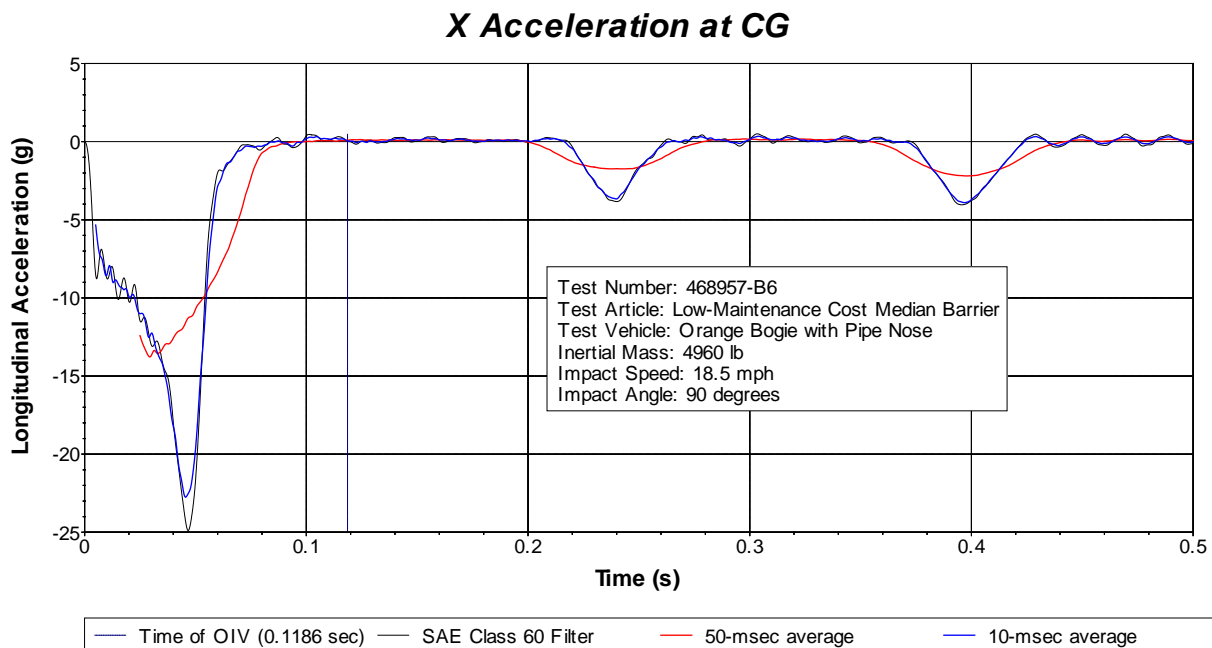


Figure 5.19. Longitudinal Acceleration during Test No. 468957-B6.

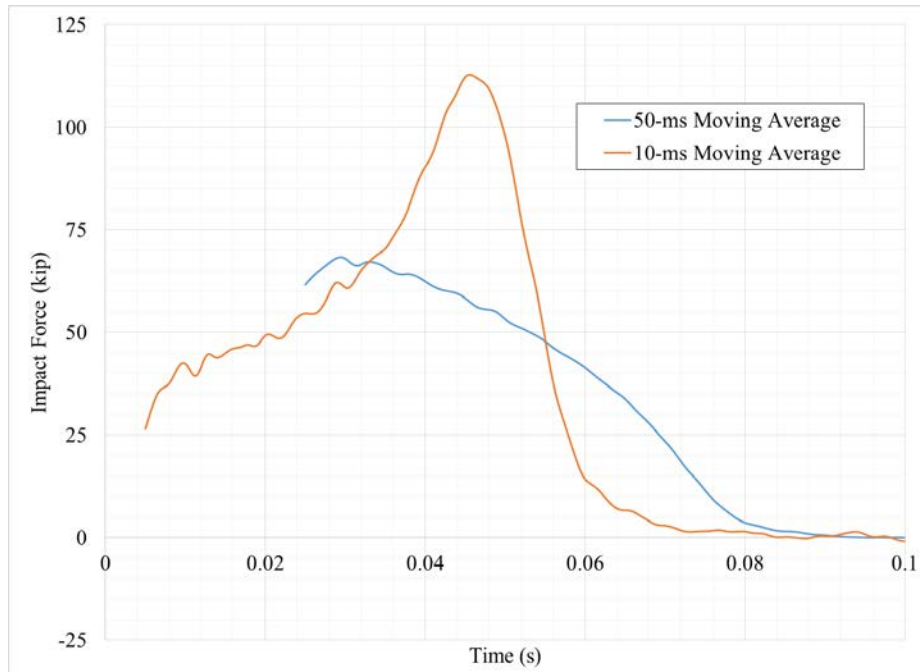


Figure 5.20. Impact Force during Test No. 468957-B6.

5.1.7 Test No. 468957-B7

5.1.7.1 Brief Test Description:

While the bogie was traveling at 22.1 mi/h, the nose of the bogie impacted the barrier at 90° with the centerline of the bogie aligned with the centerline of the barrier. The bogie ceased forward motion at 0.434 s.

5.1.7.2 Test Article Damage

Maximum deflection of the barrier was 30.5 inches, and maximum permanent deflection was 0.75 inch. The barrier used in Test No. 468957-B6 was used on this test. On the field side of the barrier, four additional cracks (two on each side) were noted to both sides of the center of the barrier. Figures 5.21 and 5.22 show damage to the barrier. Figure 4.23 shows a crack near the center of the block on the impact side.



Figure 5.21. Impact Side of Barrier after Test No. 468957-B7.



Figure 5.22. Field Side of Barrier after Test No. 468957-B7.



Figure 5.23. Crack in Block after Test No. 468957-B7.

5.1.7.3 Test Vehicle Damage

The pipe shapes had been replaced from the previous test. Figure 5.24 shows damage to the bogie vehicle. Maximum crush of the pipe shapes in the nose was 10 inches. The vehicle rebounded 26 ft from the traffic face of the barrier.



Figure 5.24. Bogie Vehicle after Test No. 468957-B7.

5.1.7.4 Occupant Risk Factors

Data from the accelerometer, located at the vehicle center of gravity, were digitized for evaluation of occupant risk. In the longitudinal direction, the OIV was 25.6 ft/s at 0.109 s, the highest 0.010-s occupant ridedown acceleration was 4.6 g from 0.328 to 0.338 s, and the maximum 0.050-s average acceleration was -15.7 g between 0.004 and 0.054 s. Figures 5.25 and 5.26 show longitudinal acceleration and impact force during the test.

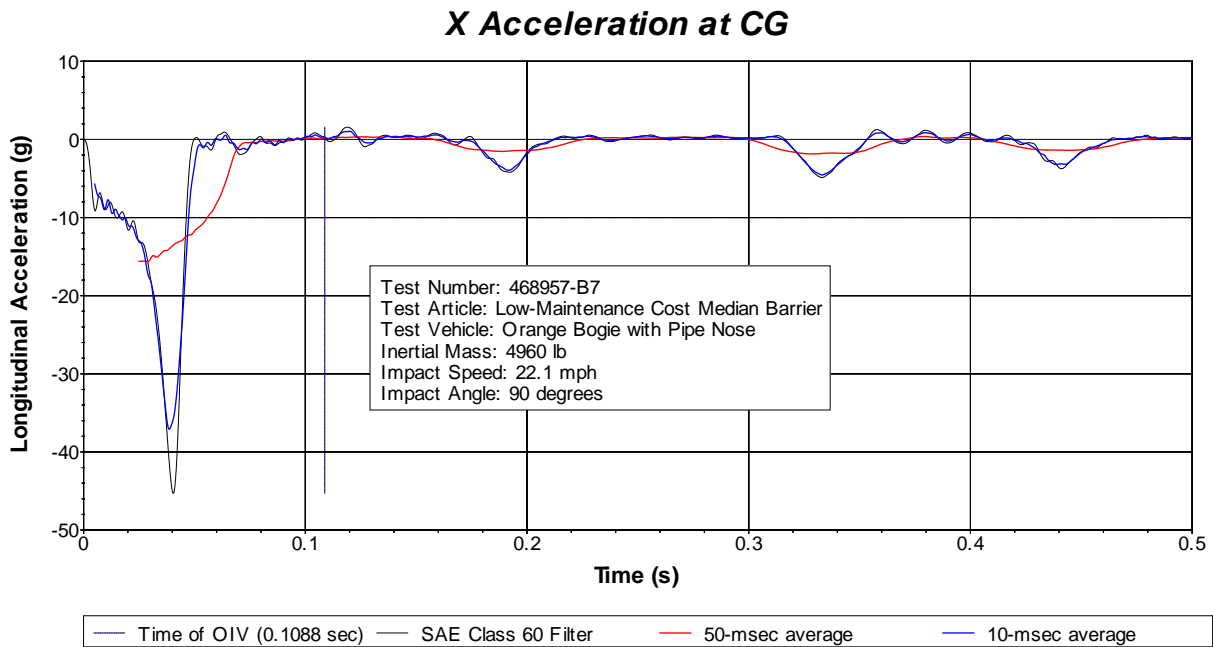


Figure 5.25. Longitudinal Acceleration during Test No. 468957-B7.

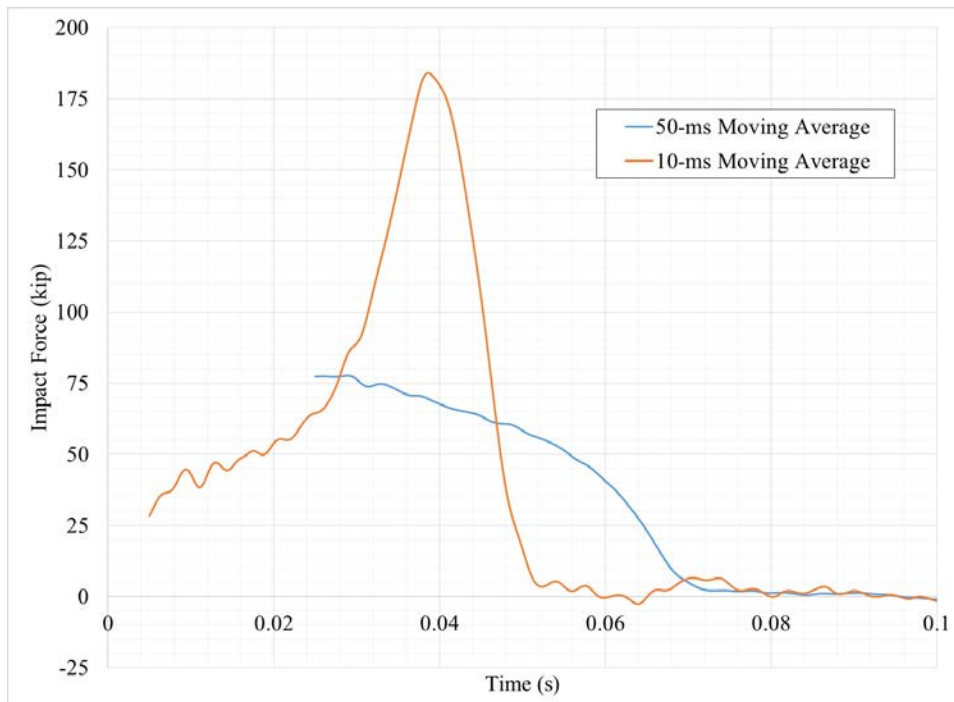


Figure 5.26. Impact Force during Test No. 468957-B7.

5.1.8 Summary – Bogie Testing Phase I

Tables 5.1 through 5.4 summarize the pertinent information from these four bogie tests.

Table 5.1. Summary of Results for Test No. 468957-B4.





 <p>0.000 s</p>	<p>General Information Test Agency Texas A&M Transportation Institute Test No. 468957-B4 Date 2016-09-20</p> <p>Test Article Type Median Barrier with Shear Fender Name TxDOT Single-Slope Traffic Railing (SSTR) Installation Dimensions 42 inches tall x 20 ft long</p> <p>Soil Type Placed on Concrete Apron</p> <p>Test Vehicle Type Bogie Test Inertia Mass 4960 lb</p> <p>Impact Conditions Speed 18.3 mi/h Angle 90°</p> <p>Occupant Risk Values Longitudinal Occupant Impact Velocity 24.6 ft/s Longitudinal Ridedown Acceleration 4.3 g Longitudinal Average 50-ms Acceleration -14.2 g</p> <p>Dynamic Deflection 22.3 inches Permanent Deflection 1.25 inch</p> <p>Vehicle Nose Crush 8.9 inches Vehicle Rebound 24 ft</p> <p>Maximum Impact Force 10-ms Moving Average 107 kips 50-ms Moving Average 70 kips</p>
 <p>0.200 s</p>	
 <p>0.400 s</p>	
 <p>0.600 s</p>	

Table 5.2. Summary of Results for Test No. 468957-B5.





 <p>0.000 s</p>	<p>General Information Test AgencyTexas A&M Transportation Institute Test No.468957-B5 Date2016-09-20</p>
 <p>0.020 s</p>	<p>Test Article Type..... Median Barrier with Shear Fender Name TxDOT Single-Slope Traffic Railing (SSTR) Installation Dimensions 42 inches tall x 20 ft long</p>
 <p>0.400 s</p>	<p>Soil Type Placed on Concrete Apron</p> <p>Test Vehicle Type.....Bogie Test Inertia Mass 4960 lb</p>
 <p>0.600 s</p>	<p>Impact Conditions Speed 22.3 mi/h Angle..... 90°</p> <p>Occupant Risk Values Longitudinal Occupant Impact Velocity..... 25.9 ft/s Longitudinal Ridedown Acceleration 5.9 g Longitudinal Average 50-ms Acceleration -15.9 g</p> <p>Dynamic Deflection29.3 inches Permanent Deflection 0.5 inch</p> <p>Vehicle Nose Crush10.0 inches Vehicle Rebound 30 ft</p> <p>Maximum Impact Force 10-ms Moving Average194 kips 50-ms Moving Average79 kips</p>

Table 5.3. Summary of Results for Test No. 468957-B6.









 <p>0.000 s</p>	<p>General Information Test AgencyTexas A&M Transportation Institute Test No.468957-B6 Date2016-09-20</p>
 <p>0.200 s</p>	<p>Test Article Type.....Median Barrier with Shear Fender Name TxDOT Single-Slope Traffic Railing (SSTR) Installation Dimensions 42 inches tall x 20 ft long</p>
 <p>0.400 s</p>	<p>Soil Type Placed on Concrete Apron</p> <p>Test Vehicle Type.....Bogie Test Inertia Mass 4960 lb</p>
 <p>0.060 s</p>	<p>Impact Conditions Speed 18.5 mi/h Angle..... 90°</p> <p>Occupant Risk Values Longitudinal Occupant Impact Velocity..... 26.6 ft/s Longitudinal Ridedown Acceleration 3.9 g Longitudinal Average 50-ms Acceleration -13.8 g</p> <p>Dynamic Deflection21.0 inches Permanent Deflection 0.5 inch</p> <p>Vehicle Nose Crush7 inches Vehicle Rebound26 ft</p> <p>Maximum Impact Force 10-ms Moving Average113 kips 50-ms Moving Average68 kips</p>

Table 5.4. Summary of Results for Test No. 468957-B7.

 <p>0.000 s</p>	<p>General Information Test Agency Texas A&M Transportation Institute Test No. 468957-B7 Date 2016-09-20</p> <p>Test Article Type Median Barrier with Shear Fender Name TxDOT Single-Slope Traffic Railing (SSTR) Installation Dimensions 42 inches tall x 20 ft long</p> <p>Soil Type Placed on Concrete Apron</p> <p>Test Vehicle Type Bogie Test Inertia Mass 4960 lb</p> <p>Impact Conditions Speed 22.1 mi/h Angle 90°</p> <p>Occupant Risk Values Longitudinal Occupant Impact Velocity 25.6 ft/s Longitudinal Ridedown Acceleration 4.6 g Longitudinal Average 50-ms Acceleration -15.7 g</p> <p>Dynamic Deflection 30.5 inches Permanent Deflection 0.75 inch</p> <p>Vehicle Nose Crush 10 inches Vehicle Rebound 26 ft</p> <p>Maximum Impact Force 10-ms Moving Average 184 kips 50-ms Moving Average 78 kips</p>
 <p>0.02 s</p>	
 <p>0.040 s</p>	
 <p>0.060 s</p>	

5.2 BOGIE TESTING – PHASE II

5.2.1 Test Article Design and Construction

Each test installation consisted of a standard TxDOT Single Slope Concrete Barrier (SSCB, Type 1), each 20-ft in length. The barriers were separated by a 39-inch gap between the ends of the adjacent barriers. The barriers were installed along the edge of the aforementioned 6-inch thick concrete runway apron.

The single slope barriers were cast-in-place at the Proving Ground site. Each barrier was 42 inches tall and 24 inches wide at the base, tapering to 8 inches wide at the top with symmetrical 79.2° slopes on both faces. The top longitudinal edges were cast with a 3/4-inch

chamfer. A 3-ft long × 3-inch tall drainage relief scupper was cast, and symmetrically centered, at the midpoint in the bottom side of each barrier.

Internal steel reinforcement was comprised of welded wire mesh (D19.7 × D9.4; 0.501 inch × 0.346 inch). Seven horizontal D19.7 bars were on each face, each vertically spaced at 6 inches. There were 30 D9.4 V bars, each longitudinally spaced at 8 inches.

A total of 18 #6 (¾-inch diameter) anchor bars (9 on each end on a 3-by-3 pattern) secured each barrier to the apron. The bars were located in three columns located 3 inches, 15 inches, and 27 inches from each barrier end. The three rows of bars were located on the centerline of the barrier and at 7-inches fore and aft. Six bent hook bars were located on the impact side, projecting 26 inches into the center of the barrier. Six hook bars were located on the centerline, projecting 16 inches into the barrier. Lastly, six straight bars were located on the protected side, projecting 6 inches into the barrier. The hooks were oriented to the protected side. Each anchor bar was embedded 12-inches deep in drilled holes in the apron and secured with Hilti RE-500 V3 epoxy according to the manufacturer's instructions.

Each barrier was cast with 4-mil thick poly sheeting on top of the clean runway apron to prevent adhesion to the existing concrete apron. There were no additional bolts or adhesives that secured the barriers to the concrete apron. Refer to Sheet 2 of 2 for reinforcement and anchorage details in Appendix D.

Welded wire mesh met ASTM A497/A1064 specifications. Reinforcing steel was specified to meet ASTM A615 Grade 60.

5.2.2 Test Vehicle

The tests were performed using the 4960-lb bogie impacting the barriers at 90° with the centerline of the bogie aligned with the centerline of the impact face of the center barrier segment. The bogie was equipped with a rigid nose with three pipe cylinders attached to the nose. Figure 5.27 shows photographs of the bogie vehicle used during Test Nos. 468957 B8-B10, and Appendix C provides details of the pipe cylinders.

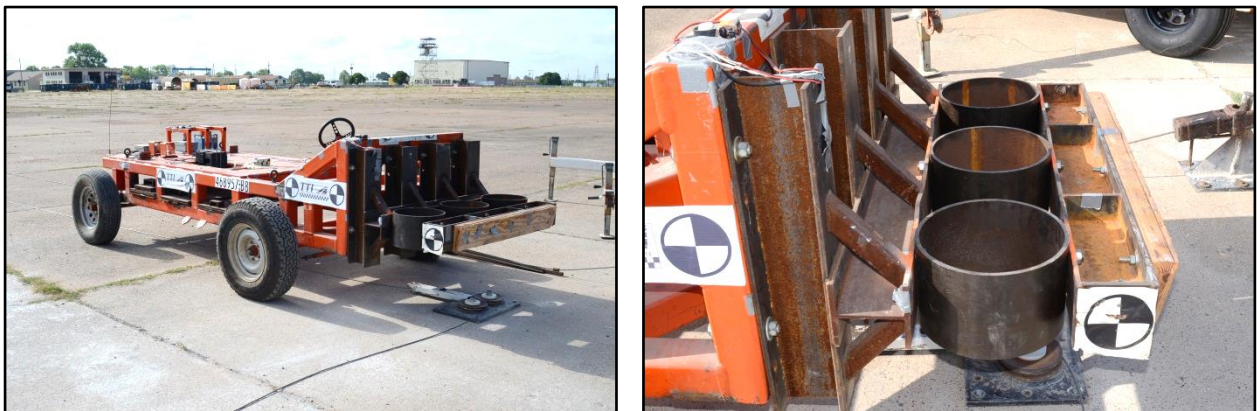


Figure 5.27. Bogie Vehicle before Testing.

5.2.3 Test No. 468957-B8 – Class C Concrete

5.2.3.1 Concrete Mix/Strength

Concrete for barrier test B8 was specified as TxDOT Class C (3600 PSI minimum). Test cylinder samples were taken at the time of casting, resulting in an average compressive strength of 4822 psi on May 31, 2017 (7 days). Figure 5.28 shows the barrier before the test.

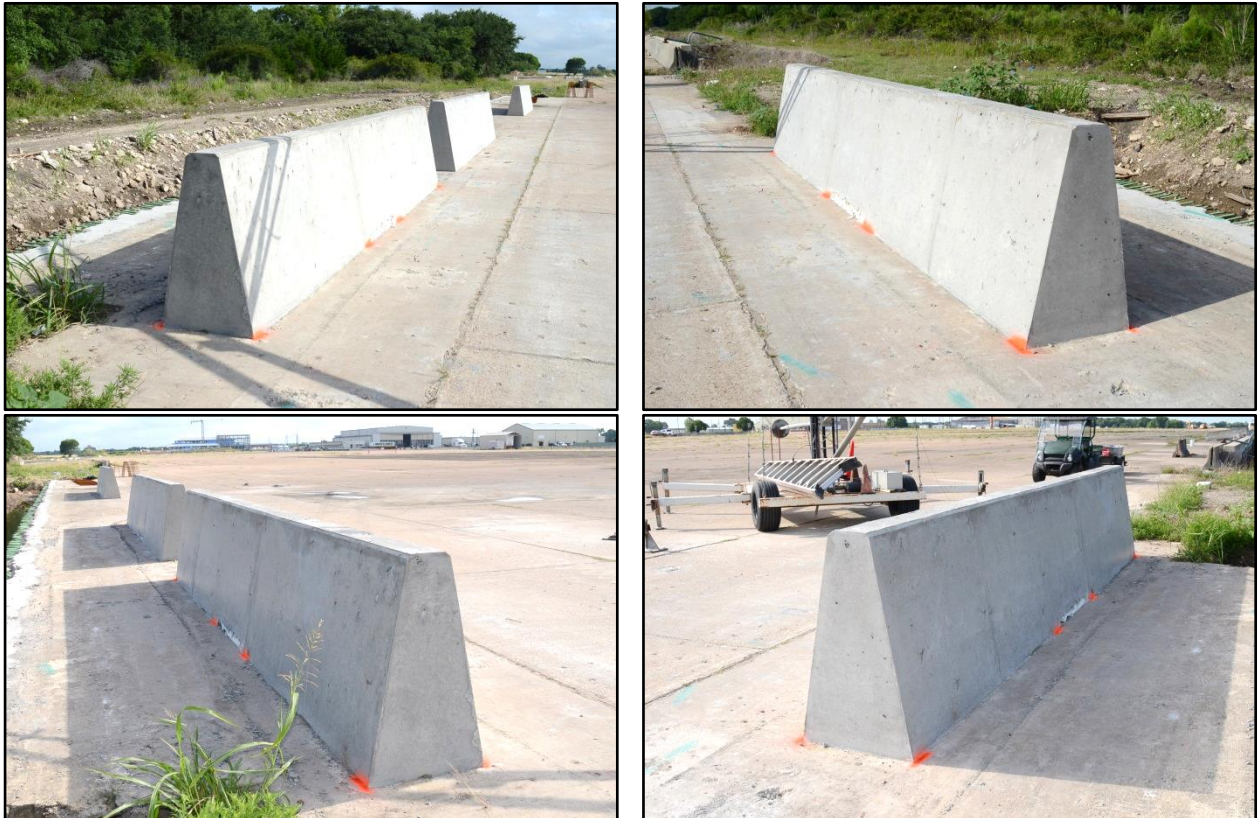


Figure 5.28. TxDOT Class C Concrete Barrier before Test No. 468957-B8.

5.2.3.2 Brief Test Description:

While the bogie was traveling at 22.5 mi/h, the nose of the bogie impacted the barrier at 90° with the centerline of the bogie aligned with the centerline of the barrier. At 0.024 s, a crack formed on the field side at approximately centerline of the bogie, and a second crack formed 15 inches to the right of the first crack. The bogie ceased forward motion at 0.063 s.

5.2.3.3 Test Article Damage

Maximum deflection of the barrier was 2.14 inches and maximum permanent deflection was 0.88 inch. Multiple vertical cracks radiated 3.5 ft to both sides of impact on the traffic side. Cracks on the field side were noted at center and 15 inches to the right of the crack at center. A crack was also noted in the ends on the field side corners of the barrier, as shown in Figures 5.29 and 5.30. Figures 5.29 through 5.33 show damage to the barrier.



Figure 5.29. Right End and Field Side of Barrier after Test No. 468957-B8.

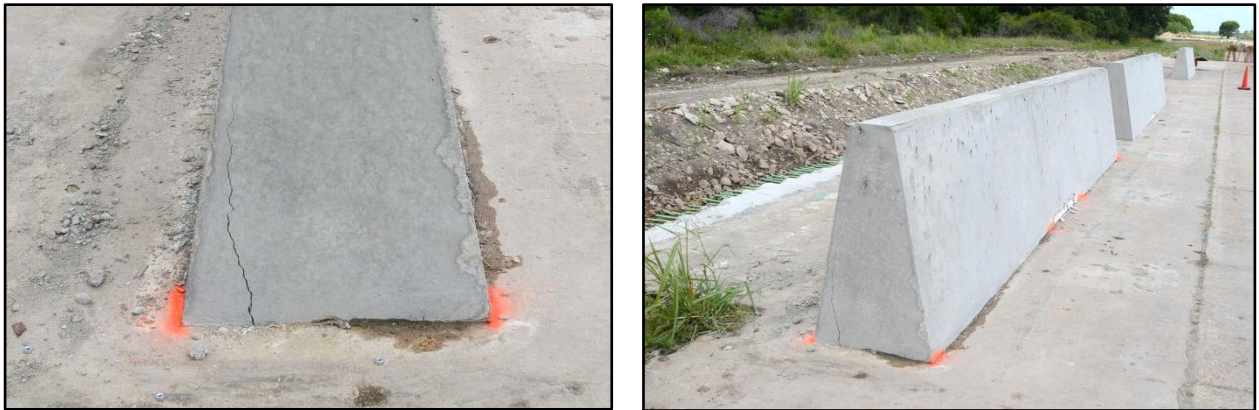


Figure 5.30. Left End and Traffic Side of Barrier after Test No. 468957-B8.



Figure 5.31. Traffic Face of Barrier after Test No. 468957-B8.

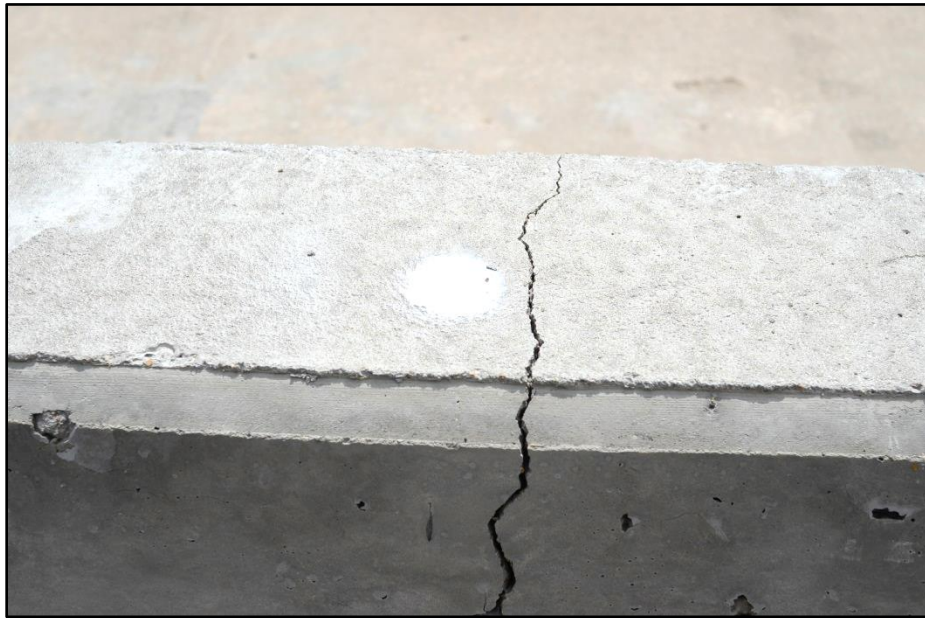


Figure 5.32. Top of Barrier after Test No. 468957-B8.



Figure 5.33. Field Side-Center of Barrier after Test No. 468957-B8.

5.2.3.4 Test Vehicle Damage

Figure 5.34 shows damage to the bogie vehicle. The pipe shapes crushed 10.8 inches. The vehicle rebounded 4.3 ft from the traffic face of the barrier.

5.2.3.5 Occupant Risk Factors

Data from the accelerometer, located near the vehicle center of gravity, were digitized for evaluation of occupant risk, which are shown in Table 5.5. Figures 5.35 and 5.36 show longitudinal acceleration and impact force during the test.



Figure 5.34. Bogie Vehicle after Test No. 468957-B8.

Table 5.5. Occupant Risk Factors for Test No. 468957-B8.

Occupant Risk Factor	Value	Time
Impact Velocity		
Longitudinal	35.8 ft/s	At 0.0910 s on front interior
Lateral	0 ft/s	
Ridedown Accelerations		
Longitudinal	0.8 g	0.1047–0.1147 s
Lateral	0.8 g	0.0941–0.1041 s
THIV	39.6 km/h	At 0.0912 s on front interior
PHD	0.9 g	0.1076–0.1176 s
ASI	1.88	0.0334–0.0834 s
Maximum 50-ms Moving Average		
Longitudinal	-18.5 g	0.0000–0.0500 s
Lateral	-0.7 g	0.0447–0.0947 s
Vertical	-1.6 g	0.0070–0.0570 s
Maximum Roll-Pitch-Yaw Angles		
Roll	4.5°	0.0887 s
Pitch	6.0°	0.0727 s
Yaw	4.8°	0.9946 s

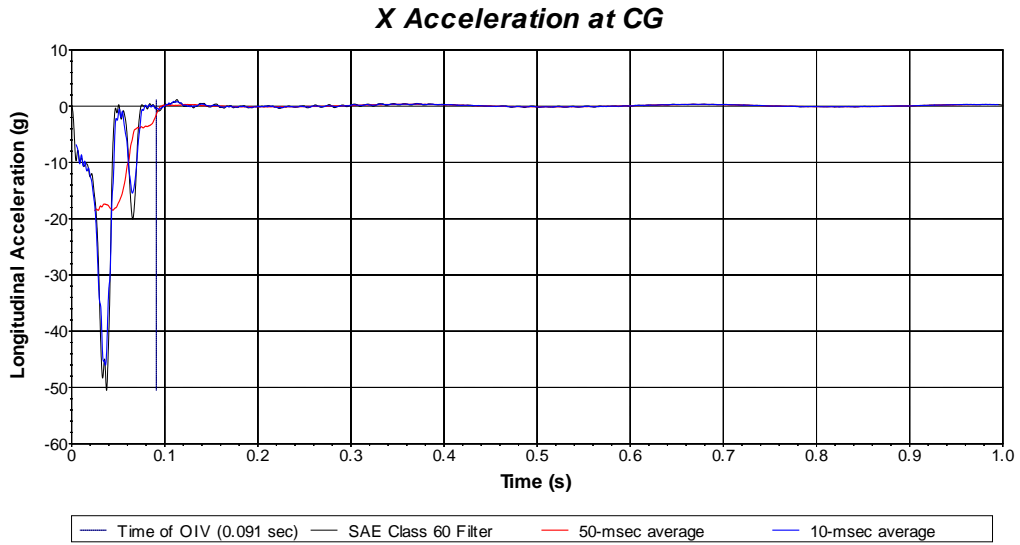


Figure 5.35. Longitudinal Accelerometer Trace during Test No. 468957-B8.

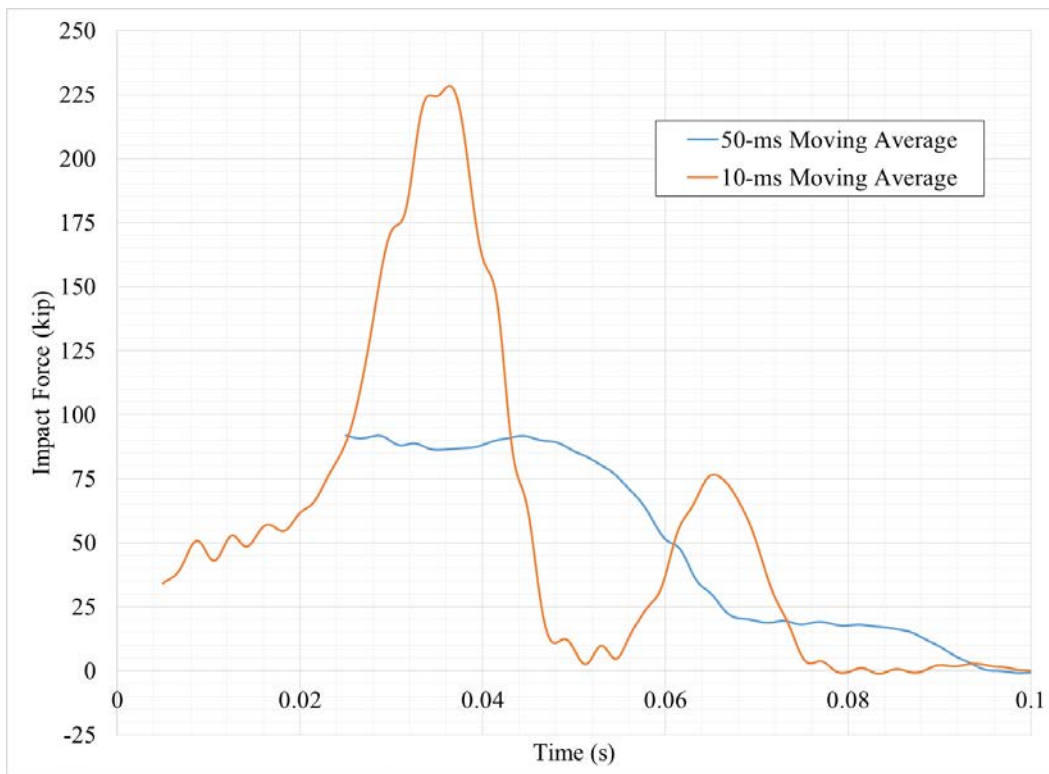


Figure 5.36. Impact Forces during Test No. 468957-B8.

5.2.4 Test No. 468957-B9 – PR5FCR5F Concrete

5.2.4.1 Concrete Mix/Strength

Concrete for barrier test B9 was specified as PR5FCR5F (3600 PSI minimum). Test cylinder samples were taken at the time of casting, resulting in an average compressive strength of 3985 psi on June 23, 2017 (30 days). Figure 4.37 shows the barrier before the test.

5.2.4.2 Brief Test Description:

While the bogie was traveling at 21.9 mi/h, the nose of the bogie impacted the barrier at 90° with the centerline of the bogie aligned with the centerline of the barrier. At 0.036 s, three cracks formed on the field side propagating from the top edge at approximately centerline. The bogie ceased forward motion at 0.064 s.

5.2.4.3 Test Article Damage

Maximum deflection of the barrier was 2.58 inches and maximum permanent deflection was 0.62 inch. Multiple vertical cracks radiated from the top over an area of 5.5 ft at impact on the field side. Cracks on the traffic side were noted at center and each end. Figures 5.38 through 5.42 show damage to the barrier.



Figure 5.37. PR5FCR5F Mix Concrete Barrier before Test No. 468957-B9.



Figure 5.38. Right End and Field Side of Barrier after Test No. 468957-B9.



Figure 5.39. Left End and Traffic Side of Barrier after Test No. 468957-B9.



Figure 5.40. Traffic Face of Barrier after Test No. 468957-B9.



Figure 5.41. Top Field Side of Barrier after Test No. 468957-B9.



Figure 5.42. Field Side-Center of Barrier after Test No. 468957-B9.

5.2.4.4 Test Vehicle Damage

Figure 5.43 shows damage to the bogie vehicle. The pipe shapes crushed 10.25 inches. The vehicle rebounded 18.5 ft from the traffic face of the barrier.



Figure 5.43. Bogie Vehicle after Test No. 468957-B9.

5.2.4.5 Occupant Risk Factors

Data from the accelerometer, located near the vehicle center of gravity, were digitized for evaluation of occupant risk, which are shown in Table 5.6. Figures 5.44 and 5.45 show longitudinal acceleration and impact force during the test.

Table 5.6. Occupant Risk Factors for Test No. 468957-B9.

Occupant Risk Factor	Value	Time
Impact Velocity		
Longitudinal	36.1 ft/s	At 0.0921 s on front interior
Lateral	1.0 ft/s	
Ridedown Accelerations		
Longitudinal	0.6 g	0.1061–0.1161 s
Lateral	0.5 g	0.1022–0.1122 s
THIV	40.6 km/h	At 0.0924 s on front interior
PHD	0.7 g	0.1065–0.1165 s
ASI	1.83	0.0348–0.0848 s
Maximum 50-ms Moving Average		
Longitudinal	-18.3 g	0.0037–0.0537 s
Lateral	-0.6 g	0.0275–0.0775 s
Vertical	2.5 g	0.0396–0.0896 s
Maximum Roll-Pitch-Yaw Angles		
Roll	11.1°	0.1251 s
Pitch	9.1°	1.0000 s
Yaw	11.3°	0.1389 s

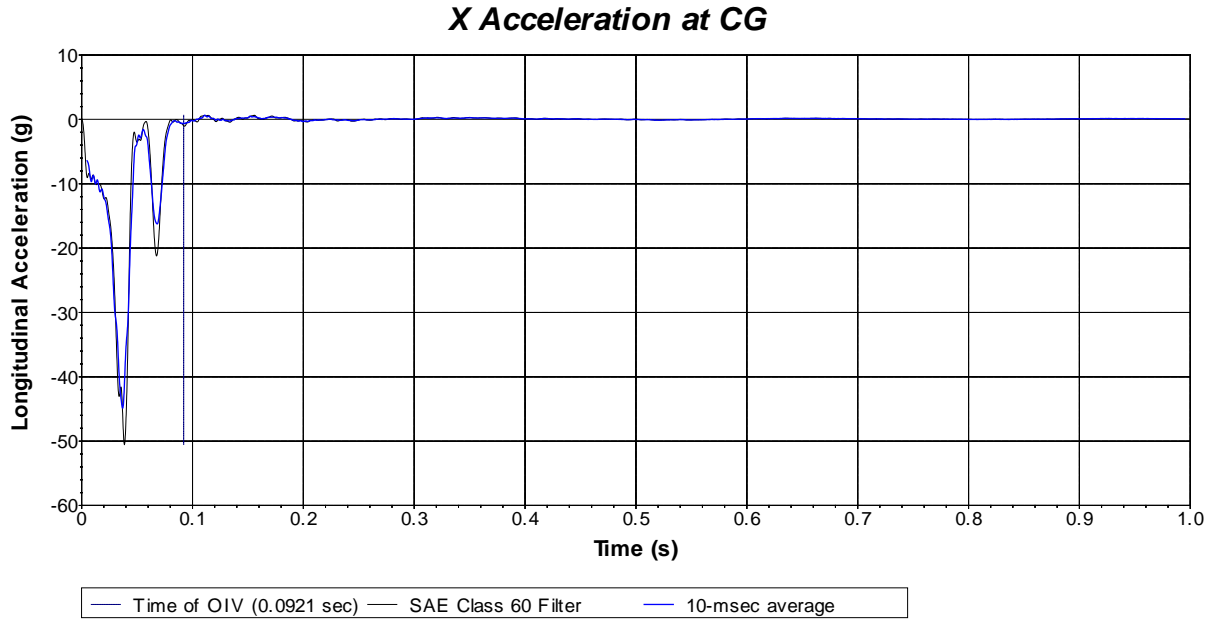


Figure 5.44. Longitudinal Accelerometer Trace during Test No. 468957-B9.

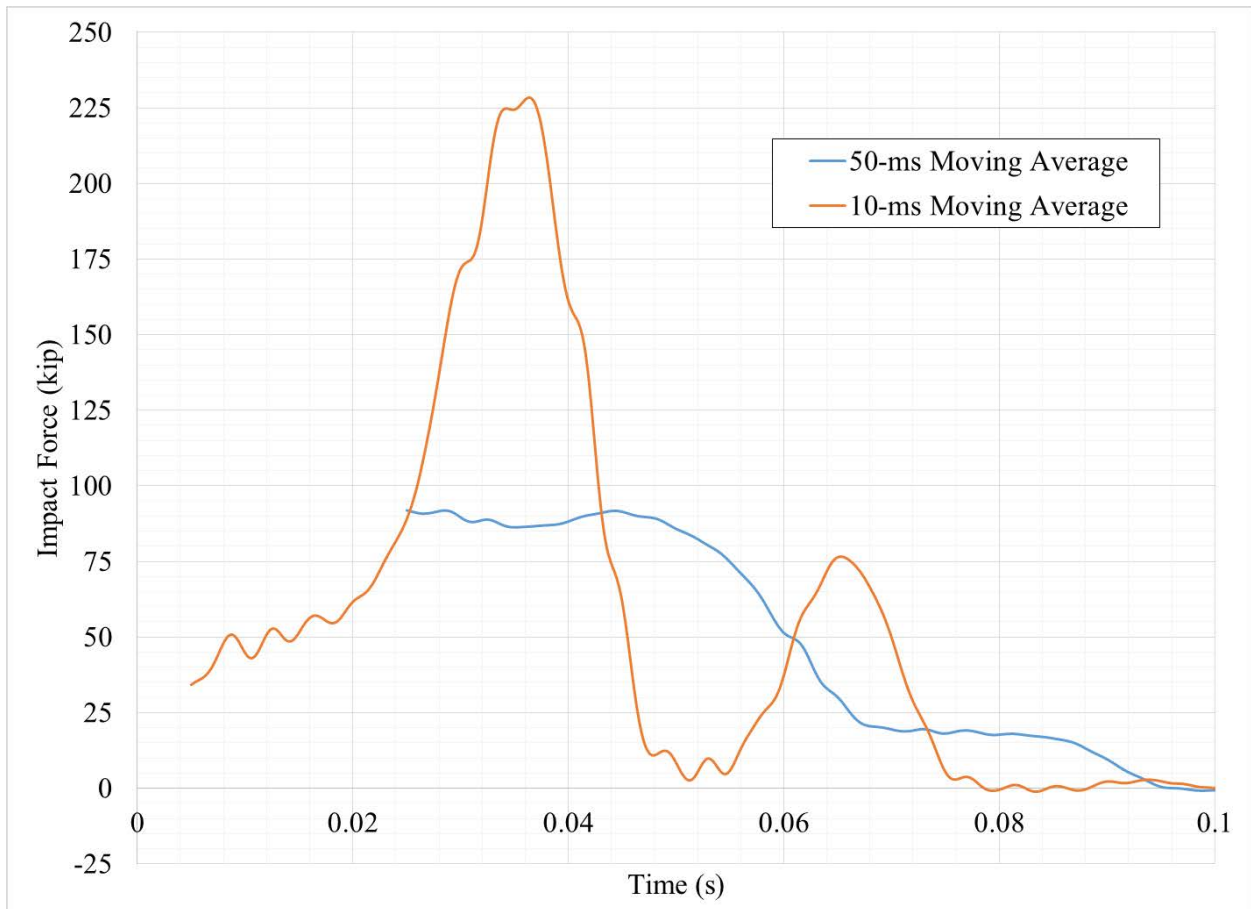


Figure 5.45. Impact Forces during Test No. 468957-B9.

5.2.5 Test No. 468957-B10 – CR10F-Gnet Mix Concrete

5.2.5.1 Concrete Mix/Strength

Concrete for barrier test B10 was specified as CR10F-Gnet Mix Concrete. Test cylinder samples were taken at the time of casting, resulting in an average compressive strength of 3602 psi on June 23, 2017 (30 days). Figure 5.46 shows the barrier before the test.



Figure 4.46. CR10F-Gnet Mix Concrete Barrier before Test No. 468957-B10.

5.2.5.2 Brief Test Description:

While the bogie was traveling at 21.8 mi/h, the nose of the bogie impacted the barrier at 90° with the centerline of the bogie aligned with the centerline of the barrier. At 0.033 s, one large crack and two small cracks formed on the field side propagating from the top edge at approximately 3 inches to the right of centerline of the bogie. The bogie ceased forward motion at 0.068 s.

5.2.5.3 Test Article Damage

Maximum deflection of the barrier was 2.31 inches, and maximum permanent deflection was 0.88 inch. Multiple small vertical cracks radiated from the top over an area of 2.7 ft at impact on the field side, with a larger vertical crack down the center. Hairline cracks on the traffic side were noted at center. Figures 5.47 through 5.51 show damage to the barrier.



Figure 5.47. Right End and Field Side of Barrier after Test No. 468957-B10.



Figure 5.48. Left End and Traffic Side of Barrier after Test No. 468957-B10.



Figure 5.49. Traffic Face of Barrier after Test No. 468957-B10.



Figure 5.50. Top of Barrier after Test No. 468957-B10.



Figure 5.51. Field Side-Center of Barrier after Test No. 468957-B10.

5.2.5.4 Test Vehicle Damage

Figure 5.52 shows damage to the bogie vehicle. The pipe shapes crushed 10.5 inches. The vehicle rebounded 6.0 ft from the traffic face of the barrier.



Figure 4.52. Bogie Vehicle after Test No. 468957-B10.

5.2.5.5 Occupant Risk Factors

Data from the accelerometer, located near the vehicle center of gravity, were digitized for evaluation of occupant risk, which are shown in Table 5.7. Figures 5.53 and 5.54 show longitudinal acceleration and impact force during the test.

Table 5.7. Occupant Risk Factors for Test No. 468957-B10.

Occupant Risk Factor	Value	Time
Impact Velocity		
Longitudinal	34.8 ft/s	At 0.0950 s on front interior
Lateral	0.7 ft/s	
Ridedown Accelerations		
Longitudinal	0.7 g	0.1094–0.1194 s
Lateral	0.4 g	0.1169–0.1269 s
THIV	38.2 km/h	At 0.0955 s on front interior
PHD	0.8 g	0.1094–0.1194 s
ASI	1.73	0.0340–0.0840 s
Maximum 50-ms Moving Average		
Longitudinal	-17.2 g	0.0037–0.0537 s
Lateral	-0.5 g	0.0058–0.0558 s
Vertical	2.4 g	0.0413–0.0913 s
Maximum Roll-Pitch-Yaw Angles		
Roll	12.8°	0.2500 s
Pitch	9.2°	0.2021 s
Yaw	11.3°	0.1424 s

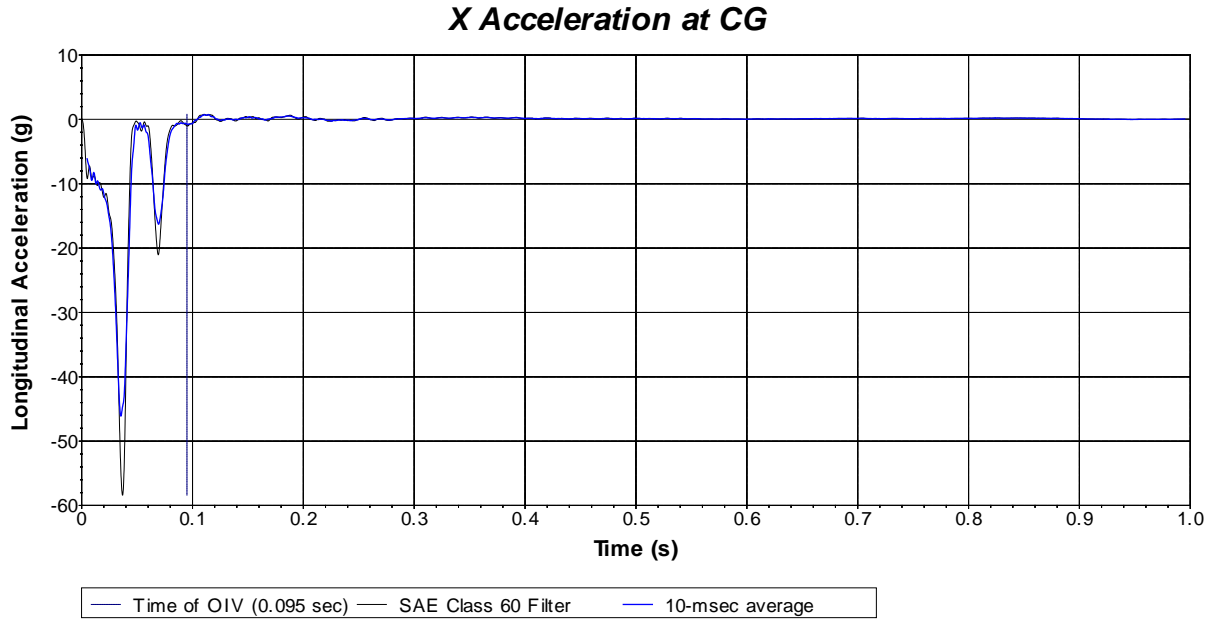


Figure 5.53. Longitudinal Accelerometer Trace during Test No. 468957-B10.

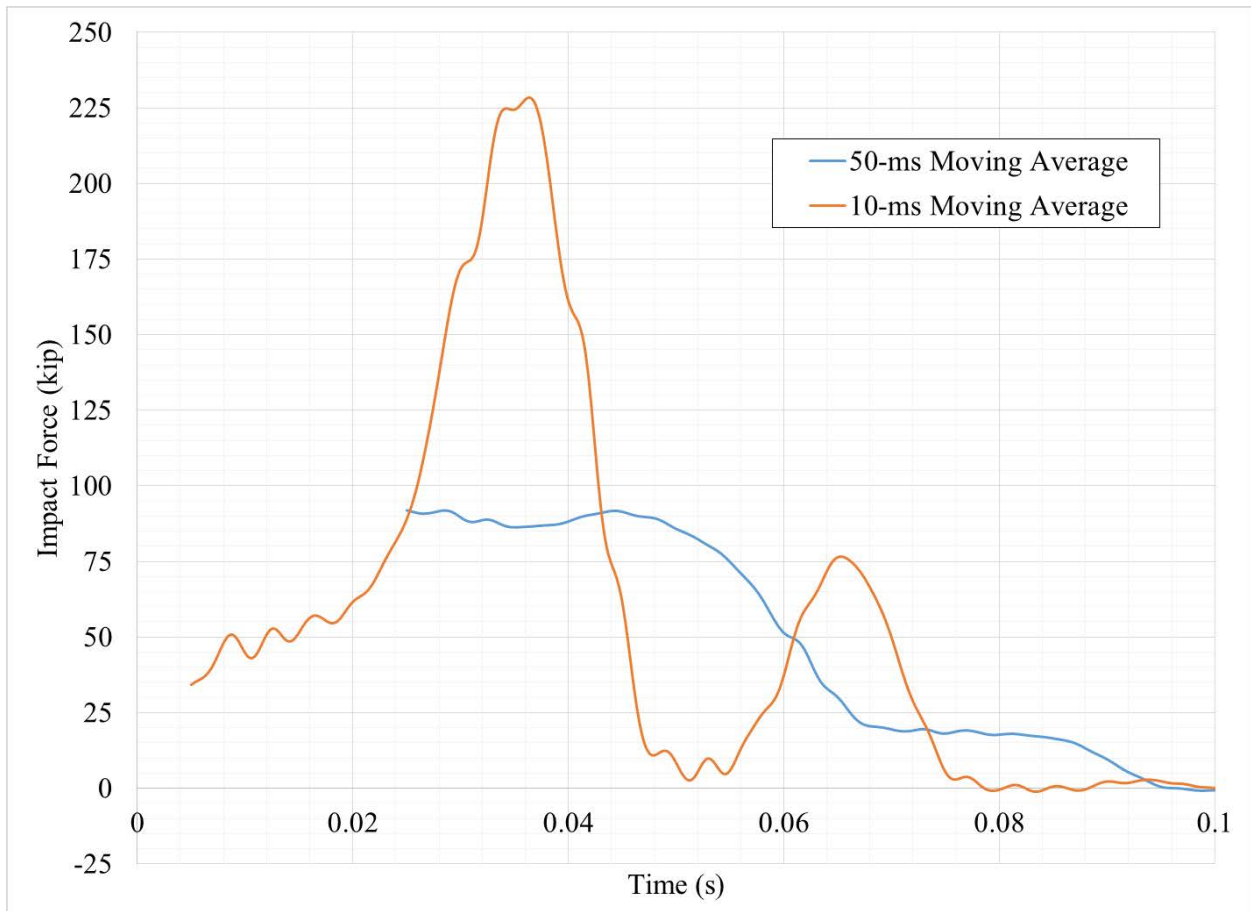


Figure 5.54. Impact Forces during Test No. 468957-B10.

5.2.6 Summary – Bogie Testing Phase II

Tables 5.8 through 5.10 summarize the pertinent information from these four bogie tests.

Table 5.8. Summary of Results for Test No. 468957-B8.





 <p>0.000 s</p>	<p>General Information Test AgencyTexas A&M Transportation Institute Test No.468957-B8 Date2017-05-31</p> <p>Test Article Type.....Median Barrier with Class C Concrete Name TxDOT Single-Slope Traffic Railing (SSTR) Installation Dimensions 42 inches tall x 20 ft long</p>
 <p>0.200 s</p>	<p>Soil Type Pinned to Concrete Apron</p> <p>Test Vehicle Type.....Bogie Test Inertia Mass..... 4960 lb</p> <p>Impact Conditions Speed 22.5 mi/h Angle..... 90°</p>
 <p>0.400 s</p>	<p>Occupant Risk Values Longitudinal Occupant Impact Velocity..... 36.1 ft/s Longitudinal Ridedown Acceleration..... 0.6 g Longitudinal Average 50-ms Acceleration -18.3 g</p> <p>Dynamic Deflection2.14 inches Permanent Deflection 0.88 inch</p>
 <p>0.600 s</p>	<p>Vehicle Nose Crush10.8 inches Vehicle Rebound 4.3 ft</p> <p>Maximum Impact Force 10-ms Moving Average228 kips 50-ms Moving Average92 kips</p>

Table 5.9. Summary of Results for Test No. 468957-B9.









 <p>0.000 s</p>	<p>General Information Test Agency Texas A&M Transportation Institute Test No. 468957-B9 Date 2017-06-23</p>
 <p>0.200 s</p>	<p>Test Article Type Median Barrier with PR5FCR5F Concrete Name TxDOT Single-Slope Traffic Railing (SSTR) Installation Dimensions 42 inches tall x 20 ft long</p> <p>Soil Type Pinned to Concrete Apron</p> <p>Test Vehicle Type Bogie Test Inertia Mass 4960 lb</p>
 <p>0.400 s</p>	<p>Impact Conditions Speed 21.9 mi/h Angle 90°</p> <p>Occupant Risk Values Longitudinal Occupant Impact Velocity 34.8 ft/s Longitudinal Ridedown Acceleration 0.8 g Longitudinal Average 50-ms Acceleration -18.5 g</p>
 <p>0.600 s</p>	<p>Dynamic Deflection 2.58 inches Permanent Deflection 0.62 inch</p> <p>Vehicle Nose Crush 10.25 inches Vehicle Rebound 18.5 ft</p> <p>Maximum Impact Force 10-ms Moving Average 223 kips 50-ms Moving Average 91 kips</p>

Table 5.10. Summary of Results for Test No. 468957-B10.

 <p>0.000 s</p>	<p>General Information Test Agency Texas A&M Transportation Institute Test No. 468957-B10 Date 2017-06-23</p> <p>Test Article Type Median Barrier with CR10F-Gnet Mix Concrete Name TxDOT Single-Slope Traffic Railing (SSTR) Installation Dimensions 42 inches tall x 20 ft long</p>
 <p>0.200 s</p>	<p>Soil Type Pinned to Concrete Apron</p> <p>Test Vehicle Type Bogie Test Inertia Mass 4960 lb</p> <p>Impact Conditions Speed 21.8 mi/h Angle 90°</p>
 <p>0.400 s</p>	<p>Occupant Risk Values Longitudinal Occupant Impact Velocity 36.1 ft/s Longitudinal Ridedown Acceleration 0.7 g Longitudinal Average 50-ms Acceleration -17.2 g</p> <p>Dynamic Deflection 2.31 inches Permanent Deflection 0.88 inch</p>
 <p>0.600 s</p>	<p>Vehicle Nose Crush 10.5 inches Vehicle Rebound 6.0 ft</p> <p>Maximum Impact Force 10-ms Moving Average 229 kips 50-ms Moving Average 85 kips</p>

5.3 SUMMARY AND CONCLUSIONS

Based on the tests conducted in this chapter, the following main conclusions were drawn:

- a) Bogie testing was conducted on the two recommended engineered concrete mixtures (a rubberized-fiber hybrid mixture and a rubberized mixture), as well as the control mixture. Similar impact resistance behavior was observed amongst the engineered concrete mixtures. The crack widths and cracking pattern of the rubberized-fiber hybrid mixture was comparable to the control mixture. This could be due to excess

- water (25 gallons) that was added to the concrete in the field, which would have considerably reduced the strength of the barrier. This is further supported by the fact that the laboratory and field compressive strength data for the rubberized-fiber mixture were not similar. Furthermore, evaluation of cores collected from that barrier depicted some consolidation issues.
- b) It is recommended that the bogie test on the rubberized-fiber hybrid mixture is repeated since due to time and testing restraint, only one bogie test was performed. For the repeat test, a water-reducer should be incorporated instead of additional water if the workability needs to be increased in the field.
 - c) ***The barrier mixture containing only the rubber particles displayed smaller, more distributed cracks than the control barrier, which indicates that the rubber performed well in arresting the crack propagation and that the toughness of the concrete was improved through the rubber inclusions.***
 - d) Since rubber is hydrophobic, further research was conducted to examine whether the bonding between the rubber and cement matrix could be improved since improved bonding should further enhance the mechanical strength properties of rubberized concrete. As such, a two-step chemical process was performed to increase hydrophilicity of the rubber particles and adhesion bonding between the surface of rubber particles and paste. Compressive strength testing on mortar samples with treated and untreated rubbers and contact angle measurement on the surface of treated and untreated rubbers were used as a measure to determine changes in bonding energy. The results showed increase in compressive strength and decrease in contact angle after treatment; both of these trends support the premise that the chemical treatment improved the cement-rubber bond. Thus, chemical functionalization of the rubber can be used to increase the compressive strength of the resultant composites.
 - e) Further study is required to evaluate the effectiveness of treatment of rubber in enhancing other mechanical properties of rubberized composite.

CHAPTER 6: SYSTEM DETAILS

6.1 TEST ARTICLE AND INSTALLATION DETAILS

The test installation consisted of four sections of modified standard TxDOT Single Slope Concrete Barriers (SSCB, Type 1), and each was 60-ft in length and contained a rubber/elastomer shear fender attached at the two quarter points of each section. The barriers were separated by a 1¾-inch wide expansion joint gap between the sections. Each joint was doweled with three #8 rebar. The overall length of the test installation was 240 ft-5¼ inches. The barriers were constructed on an abandoned out-of-service, 6-inch thick concrete runway apron.

The single slope barriers were cast in place at the Texas A&M Transportation Institute Proving Ground site. Each barrier was 42 inches tall and 24 inches wide at the base, tapering to 8 inches wide at the top with symmetrical 11° (1H:5¼V, 10.8° actual) slope on both the traffic side and the field side faces. A steel anchor box (for securing the shear fender) was cast into each lower quarter point of each of the barriers.

Each barrier incorporated a Morse Rubber Company “Neolastic” shear fender (Part No. 54.6496) that measured 10-inches wide × 11⅝-inches tall × 15¾-inches long, with a 4-inch diameter hole. Each shear fender was secured to the box in the end of the barrier with four ¾-inch × 2½-inch hex bolts and USS flat washers, and to the apron with four Hilti screw anchor bolts (KH-EZ ⅝-inch × 6½-inch) according to the manufacturer’s instructions. A 17-inch × 10¼-inch × ½-inch thick HDPE pad was installed between the bottom of the shear fender and the concrete apron. Bolting was located on a 4-inch × 14⅛-inch pattern as dictated by the shear fender specifications.

The fabricated anchor boxes were ¼-inch thick and each measured 16½-inches wide × 12⅜-inches tall × 20½-inches to 15¾-inches deep to conform to the profile of the barrier. Six Nelson studs (H4L, ½-inch diameter × 6-inches long) were secured to the outside faces of each box. Each horizontal (top) plate contained four ¾-inch coupling nuts centered and welded to the plate above 13/16-inch diameter holes located on a 4-inch × 14⅛-inch pattern. Refer to Appendix E for anchor box details.

Internal steel reinforcement was steel welded wire mesh comprised of D9.4 (0.346-inch diameter) welded wire reinforcement (WWR) lateral stirrup bars spaced at 8-inch centers along the length of the barrier. The stirrup bars were bent to conform to the profile of the barrier and provide a minimum 1¾-inch concrete cover. Longitudinal reinforcement of the SSCB was comprised of seven D19.7 bars (0.501-inch diameter) equally spaced (approximately 6 inches) along the slope of each face and located inside the lateral stirrups. The WWR was coped around the anchor boxes. Three 1-inch diameter (#8), 36-inch long reinforcing bars were cast into one end of each barrier section, and sleeved into the mating section end with 1¼-inch schedule 80 polyvinyl chloride (PVC) pipe. Refer to Appendix E for reinforcement details.

Other than the two shear fenders and their bolting per section, there were no additional bolts, pins, or adhesives that secured the barriers to the concrete apron. Each barrier was cast on 4-mil plastic film on top of the clean runway apron. To facilitate ease of construction, the shear fenders were positioned within the formwork, secured to the apron, and bolted to the installed anchor boxes prior to concrete placement.

For *MASH* Test 4-12 (Test No. 468958-1) only, two ¼-inch thick × 4-inch wide × 9-ft long steel straps were added to the impact side of each barrier segments 2 and 3 above the two shear fenders either side of joint #2 near the 10000s impact point. Each strap was secured to the SSCB with four screw anchors (Hilti KH ¾ × 7 #434452) installed per the manufacturer's instructions through 1-inch diameter holes in the strap. The screw anchors and holes were located 15 and 27 inches below the top of the barrier, and symmetrically spaced at 28½ and 52½ inches either side of the centerline of the barrier. Refer to Appendix E for details.

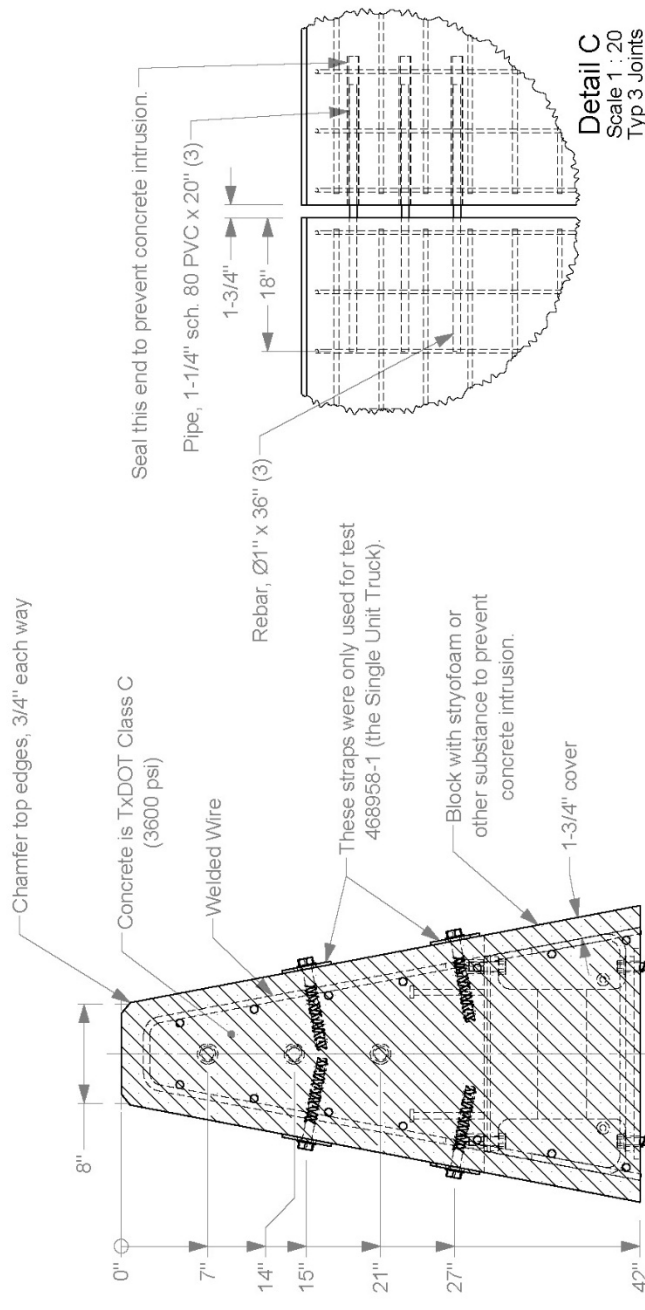
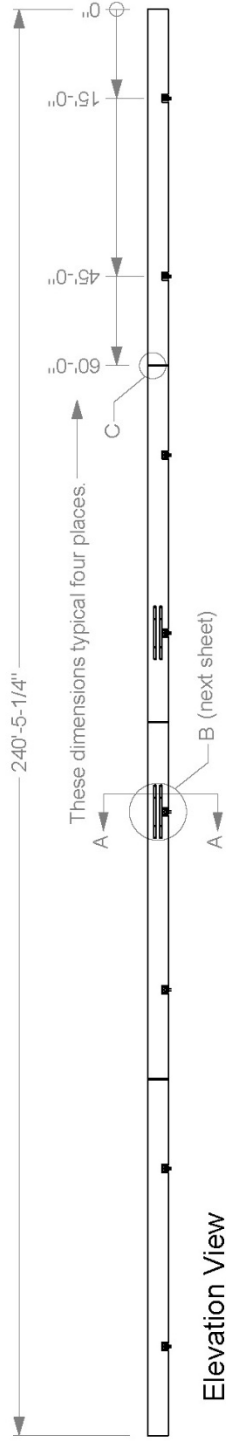
Figure 6.1 presents overall information on the TxDOT Rubber Mounted Single Slope Barrier, and Figure 6.2 provides photographs of the installation. The metal straps added for *MASH* Test 4-12 are shown in Figure 6.3. Appendix E provides further details of the TxDOT Rubber Mounted Single Slope Barrier.

6.2 MATERIAL SPECIFICATIONS

The shear fender anchor box was fabricated from ASTM A36 steel. Bolting met ASTM A325 specifications. Reinforcing steel was specified to meet ASTM A615 Grade 60. The welded wire mesh met Grade 70 specifications. The steel reinforcing straps met ASTM A529 Grade 50 specifications. Concrete for the barriers was specified as TxDOT Class C (3600 psi minimum). Test cylinder samples were taken at the time of casting on November 28, December 4, December 11, and December 13, 2017, resulting in an average compressive strength on December 18, 2017, of 4822 psi, 4780 psi, 3635 psi, and 3883 psi, respectively. Appendix F provides the concrete strength testing results for the test installation.

Appendix F also provides material certification documents for the materials used to install/construct the TxDOT Rubber Mounted Single Slope Barrier.

Test Installation



Texas A&M Transportation Institute

Project 468958 Low Maintenance Single Slope Barrier 2017-12-21

Drawn By GES Scale 1:300 Sheet 1 of 4 Test Installation

Roadside Safety and Physical Security Division - Proving Ground

Figure 6.1. Overall Details of the TxDOT Rubber Mounted Single Slope Barrier.



Figure 6.2. TxDOT Rubber Mounted Single Slope Barrier prior to MASH Tests 4-10 and 4-11.



Figure 6.3. Straps Used on TxDOT Rubber Mounted Single Slope Barrier prior to *MASH* Test 4-12.

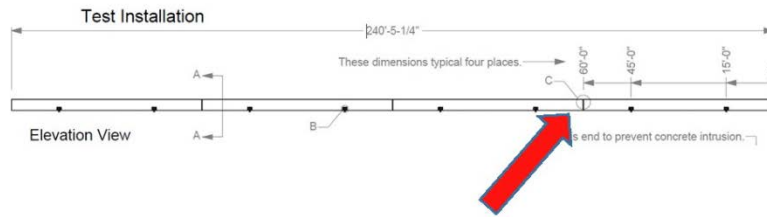
CHAPTER 7: TEST REQUIREMENTS AND EVALUATION CRITERIA

7.1 CRASH TEST MATRIX

Table 6.1 shows the test conditions and evaluation criteria for *MASH* Test Level 4 (TL-4). The target CIPs selected for the tests were determined according to the information provided in *MASH* Section 2.2.1 and Section 2.3 and FEA, and are shown in Figures 7.1 through 7.3.

Table 7.1. Test Conditions and Evaluation Criteria Specified for *MASH* TL-4.

Test Article	Test Designation	Test Vehicle	Impact Conditions		Evaluation Criteria
			Speed	Angle	
Longitudinal Barrier	4-10	1100C	62 mi/h	25°	A, D, F, H, I
	4-11	2270P	62 mi/h	25°	A, D, F, H, I
	4-12	10000S	56 mi/h	15°	A, D, G



CIP: small car (4-10) @ 42.5 inches upstream of joint # 3 (last joint of the installation)

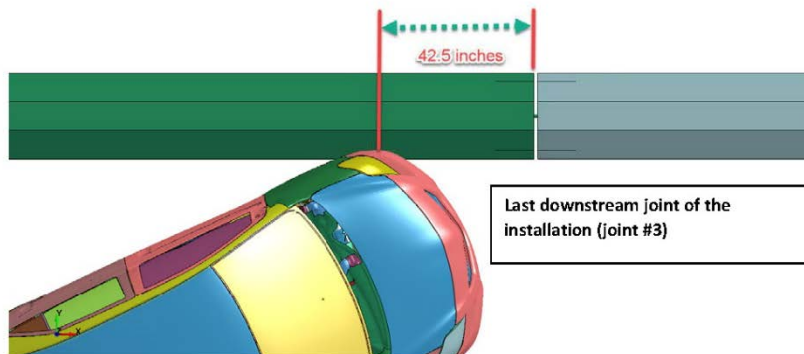
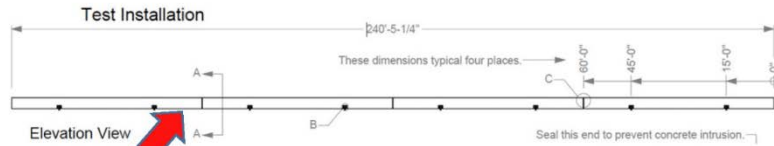
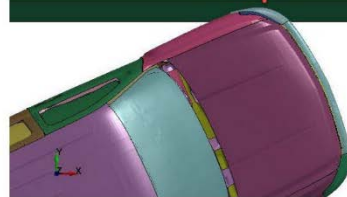
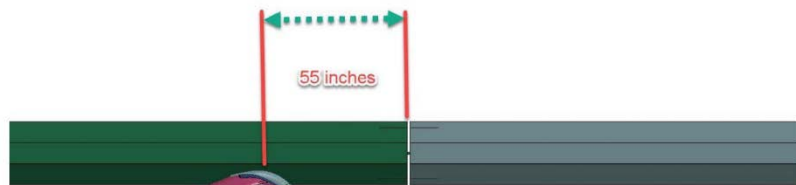


Figure 7.1. Target CIP for *MASH* Test 4-10 (Test No. 468958-3) on the TxDOT Rubber Mounted Single Slope Barrier.

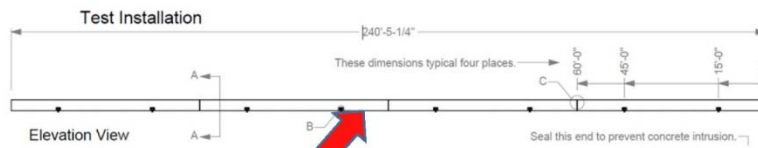


CIP: Pick Up (4-11) @ 55 inches upstream of joint # 1 (first joint of the installation)

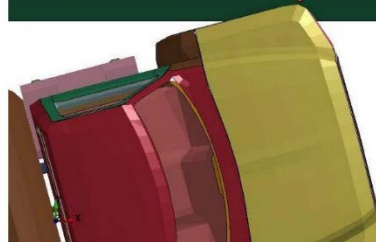
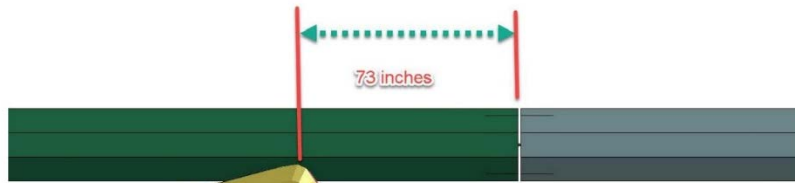


First joint of the installation (joint #1)

Figure 7.2. Target CIP for MASH Test 4-11 (Test No. 468958-2) on the TxDOT Rubber Mounted Single Slope Barrier.



CIP: SUT (4-12) @ 73 inches upstream of joint # 2 (middle joint of the installation)



Middle joint of the installation (joint #2)

Figure 7.3. Target CIP for MASH Test 4-12 (Test No. 468958-1) on the TxDOT Rubber Mounted Single Slope Barrier.

The crash tests and data analysis procedures were in accordance with guidelines presented in *MASH*. Chapter 4 presents brief descriptions of these procedures.

7.2 EVALUATION CRITERIA

The appropriate safety evaluation criteria from Tables 2-2A and 5-1A through 5-1C of *MASH* were used to evaluate the crash test(s) reported herein. The test conditions and evaluation criteria required for *MASH* Test TL-4 are listed in Table 7.1, and the substance of the evaluation criteria in Table 7.2. An evaluation of the crash test results is presented in detail under the section Assessment of Test Results.

Table 7.2. Evaluation Criteria Required for *MASH* TL-4 Tests.

Evaluation Factors	Evaluation Criteria	Applicable Tests
Structural Adequacy	A. <i>Test article should contain and redirect the vehicle or bring the vehicle to a controlled stop; the vehicle should not penetrate, underride, or override the installation although controlled lateral deflection of the test article is acceptable.</i>	4-10, 4-11, 4-12
Occupant Risk	D. <i>Detached elements, fragments, or other debris from the test article should not penetrate or show potential for penetrating the occupant compartment, or present undue hazard to other traffic, pedestrians, or personnel in a work zone. Deformations of, or intrusions into, the occupant compartment should not exceed limits set forth in Section 5.2.2 and Appendix E of MASH.</i>	4-10, 4-11, 4-12
	F. <i>The vehicle should remain upright during and after collision. The maximum roll and pitch angles are not to exceed 75 degrees.</i>	4-10, 4-11
	G. <i>It is preferable, although not essential, that the vehicle remain upright during and after the collision.</i>	4-12
	H. <i>Occupant impact velocities (OIV) should satisfy the following limits: Preferred value of 30 ft/s, or maximum allowable value of 40 ft/s.</i>	4-10, 4-11
	I. <i>The occupant ridedown accelerations should satisfy the following: Preferred value of 15.0 g, or maximum allowable value of 20.49 g.</i>	4-10, 4-11

CHAPTER 8: TEST CONDITIONS

8.1 TEST FACILITY

The full-scale crash tests reported herein were performed at TTI Proving Ground, an International Standards Organization (ISO) 17025-accredited laboratory with American Association for Laboratory Accreditation (A2LA) Mechanical Testing Certificate 2821.01. The full-scale crash tests were performed according to TTI Proving Ground quality procedures, and according to the *MASH* guidelines and standards.

The test facilities of the TTI Proving Ground are located on the Texas A&M University RELLIS Campus, which consists of a 2000-acre complex of research and training facilities situated 10 miles northwest of the flagship campus of Texas A&M University. The site, formerly a United States Army Air Corps base, has large expanses of concrete runways and parking aprons well suited for experimental research and testing in the areas of vehicle performance and handling, vehicle-roadway interaction, durability and efficacy of highway pavements, and evaluation of roadside safety hardware and perimeter protective devices. The site selected for construction and testing of the barrier was along the edge of an out-of-service apron. The apron consists of an unreinforced jointed-concrete pavement in 12.5-ft × 15-ft blocks nominally 6 inches deep. The aprons were built in 1942, and the joints have some displacement, but are otherwise flat and level.

8.2 VEHICLE TOW AND GUIDANCE SYSTEM

Each test vehicle was towed into the test installation using a steel cable guidance and reverse tow system. A steel cable for guiding the test vehicle was tensioned along the path, anchored at each end, and threaded through an attachment to the front wheel of the test vehicle. An additional steel cable was connected to the test vehicle, passed around a pulley near the impact point, through a pulley on the tow vehicle, and then anchored to the ground such that the tow vehicle moved away from the test site. A 2:1 speed ratio between the test and tow vehicle existed with this system. Just prior to impact with the installation, the test vehicle was released and ran unrestrained. The vehicle remained freewheeling (i.e., no steering or braking inputs) until it cleared the immediate area of the test site (no sooner than 2 s after impact), after which the brakes were activated, if needed, to bring the test vehicle to a safe and controlled stop.

8.3 DATA ACQUISITION SYSTEMS

8.3.1 Vehicle Instrumentation and Data Processing

Each test vehicle was instrumented with a self-contained, on-board data acquisition system. The signal conditioning and acquisition system is a 16-channel, Tiny Data Acquisition System (TDAS) Pro produced by Diversified Technical Systems, Inc. The accelerometers, which measure the x, y, and z axis of vehicle acceleration, are strain gauge type with linear millivolt output proportional to acceleration. Angular rate sensors, measuring vehicle roll, pitch, and yaw rates, are ultra-small, solid state units designed for crash test service. The TDAS Pro hardware

and software conform to the latest SAE J211, Instrumentation for Impact Test. Each of the 16 channels is capable of providing precision amplification, scaling, and filtering based on transducer specifications and calibrations. During the test, data are recorded from each channel at a rate of 10,000 values per second with a resolution of one part in 65,536. Once data are recorded, internal batteries back these up inside the unit should the primary battery cable be severed. Initial contact of the pressure switch on the vehicle bumper provides a time zero mark and initiates the recording process. After each test, the data are downloaded from the TDAS Pro unit into a laptop computer at the test site. The Test Risk Assessment Program (TRAP) software then processes the raw data to produce detailed reports of the test results.

Each of the TDAS Pro units is returned to the factory annually for complete recalibration and all instrumentation used in the vehicle conforms to all specifications outlined by SAE J211. All accelerometers are calibrated annually by means of an ENDEVCO® 2901, precision primary vibration standard. This standard and its support instruments are checked annually and receive a National Institute of Standards Technology (NIST) traceable calibration. The rate transducers used in the data acquisition system receive a calibration via a Genisco Rate-of-Turn table. The subsystems of each data channel are also evaluated annually, using instruments with current NIST traceability, and the results are factored into the accuracy of the total data channel, per SAE J211. Calibrations and evaluations are also made any time data are suspect. Acceleration data are measured with an expanded uncertainty of ± 1.7 percent at a confidence factor of 95 percent ($k=2$).

TRAP uses the data from the TDAS Pro to compute occupant/compartment impact velocities, time of occupant/compartment impact after vehicle impact, and the highest 10-millisecond (ms) average ridedown acceleration. TRAP calculates change in vehicle velocity at the end of a given impulse period. In addition, maximum average accelerations over 50-ms intervals in each of the three directions are computed. For reporting purposes, the data from the vehicle-mounted accelerometers are filtered with a 60-Hz low-pass digital filter, and acceleration versus time curves for the longitudinal, lateral, and vertical directions are plotted using TRAP.

TRAP uses the data from the yaw, pitch, and roll rate transducers to compute angular displacement in degrees at 0.0001-s intervals, then plots yaw, pitch, and roll versus time. These displacements are in reference to the vehicle-fixed coordinate system with the initial position and orientation of the vehicle-fixed coordinate systems being initial impact. Rate of rotation data is measured with an expanded uncertainty of ± 0.7 percent at a confidence factor of 95 percent ($k=2$).

8.3.2 Anthropomorphic Dummy Instrumentation

An Alderson Research Laboratories Hybrid II, 50th percentile male anthropomorphic dummy, restrained with lap and shoulder belts, was placed in the front seat on the impact side of the 1100C vehicle. The dummy was not instrumented.

According to *MASH*, use of a dummy in the 2270P vehicle is optional. However, it is recommended a dummy be used when testing “any longitudinal barrier with a height greater than or equal to 33 inches.” Use of the dummy in the 2270P vehicle is recommended for tall rails to evaluate the “potential for an occupant to extend out of the vehicle and come into direct contact with the test article.” Although this information is reported, it is not part of the impact performance evaluation. Since the rail height of the TxDOT Rubber Mounted Single Slope

Barrier was 42 inches, a dummy was placed in the front seat of the 2270P vehicle on the impact side and restrained with lap and shoulder belts.

MASH does not recommend or require use of a dummy in the 10000S vehicle.

8.3.3 Photographic Instrumentation and Data Processing

Photographic coverage of the test included three high-speed cameras:

- One overhead with a field of view perpendicular to the ground and directly over the impact point.
- One placed behind the installation at an angle.
- A third placed to have a field of view parallel to and aligned with the installation at the downstream end.

A flashbulb on the impacting vehicle was activated by a pressure-sensitive tape switch to indicate the instant of contact with the TxDOT Rubber Mounted Single Slope Barrier. The flashbulb was visible from each camera. The video files from these digital high-speed cameras were analyzed to observe phenomena occurring during the collision and to obtain time-event, displacement, and angular data. A digital camera recorded and documented conditions of each test vehicle and the installation before and after the test.

CHAPTER 9: MASH TEST 4-10 (CRASH TEST NO. 468958-3)

9.1 TEST DESIGNATION AND ACTUAL IMPACT CONDITIONS

MASH Test 4-10 involves an 1100C vehicle weighing 2420 lb \pm 55 lb impacting the CIP of the barrier at an impact speed of 62 mi/h \pm 2.5 mi/h and an angle of 25° \pm 1.5°. The target CIP for *MASH* Test 4-10 on the TxDOT Rubber Mounted Single Slope Barrier was 3.5 ft \pm 1 ft upstream of the third construction joint in the barrier.

The 2011 Kia Rio used in the test weighed 2456 lb, and the actual impact speed and angle were 62.4 mi/h and 24.5°, respectively. The actual impact point was 2.9 ft upstream of the third joint in the barrier. Minimum target impact severity (IS) was 51 kip-ft, and actual IS was 55 kip-ft.

9.2 WEATHER CONDITIONS

The test was performed on the afternoon of December 18, 2017. Weather conditions at the time of testing were as follows: wind speed: 1 mi/h; wind direction: 194° (vehicle was traveling in a northwesterly direction); temperature: 62°F; relative humidity: 91 percent.

9.3 TEST VEHICLE

The 2011 Kia Rio, shown in Figures 9.1 and 9.2, was used for *MASH* Test 4-10. The vehicle's test inertia weight was 2456 lb, and its gross static weight was 2621 lb. The height to the lower edge of the vehicle bumper was 7.75 inches, and height to the upper edge of the bumper was 21.0 inches. Table G.1 in Appendix G.1 gives additional dimensions and information on the vehicle. The vehicle was directed into the installation using the cable reverse tow and guidance system, and was released to be freewheeling and unrestrained just prior to impact.



Figure 9.1. TxDOT Rubber Mounted Single Slope Barrier/Test Vehicle Geometrics for Test No. 468958-3.

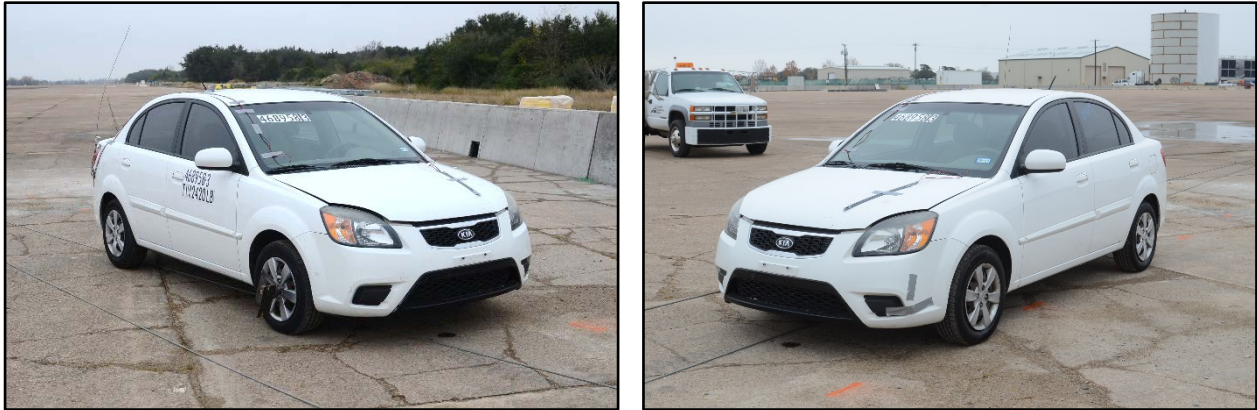


Figure 9.2. Test Vehicle before Test No. 468958-3.

9.4 TEST DESCRIPTION

The test vehicle, traveling at an impact speed of 62.4 mi/h, contacted the barrier 2.9 ft upstream of the third construction joint in the barrier at an impact angle of 24.5°. Table 9.1 lists times and significant events that occurred during Test No. 468958-3. Figures G.1 and G.2 in Appendix G.1 present sequential photographs during the test.

Table 9.1. Events during Test No. 468958-3.

TIME (s)	EVENT
0.012	Vehicle begins to redirect
0.024	Left front tire begins to climb traffic face of barrier
0.041	Barrier begins to deflect toward field side
0.076	Right front tire loses contact with ground
0.141	Vehicle begins traveling parallel with barrier
0.158	Rear of vehicle contacts barrier
0.265	Vehicle loses contact with barrier while traveling 52.7 mi/h and 1.8°
0.355	Left front tire touches ground

For longitudinal barriers, it is desirable that the vehicle redirects and exits the barrier within the exit box criteria (not less than 32.8 ft downstream from impact for cars and pickups). The 1100C vehicle exited within the exit box criteria defined in *MASH*. After loss of contact with the barrier, the vehicle came to rest 220 ft downstream of the impact and 7 ft toward traffic lanes.

9.5 DAMAGE TO TEST INSTALLATION

Figure 9.3 shows the barrier sustained relatively minor damage. Vertical cracks were noted at each corner of the recess on the traffic face of the barrier. Working width was 26.1 inches at the field side toe of the barrier. Maximum dynamic deflection during the test was 3.7 inches, and maximum permanent deformation was 1.0 inch.



Figure 9.3. TxDOT Rubber Mounted Single Slope Barrier after Test No. 468958-3.

9.6 DAMAGE TO TEST VEHICLE

Figure 9.4 shows the damage that the vehicle had sustained. The front bumper, grill, hood, left front tire and rim, left front fender, left front and rear doors, left rear tire and rim, left rear quarter panel, and rear bumper were damaged. Maximum exterior crush to the vehicle was 8.0 inches in the side plane at the left front corner at bumper height. Maximum occupant compartment deformation was 1.5 inches in the left side instrument panel area and left front floor pan/firewall. Figure 9.5 shows the interior of the vehicle. Tables G.2 and G.3 in Appendix G.1 provide exterior crush and occupant compartment measurements.



Figure 9.4. Test Vehicle after Test No. 468958-3.



Before Test



After Test

Figure 9.5. Interior of Test Vehicle for Test No. 468958-3.

9.7 OCCUPANT RISK FACTORS

Data from the accelerometer, located at the vehicle center of gravity, were digitized for evaluation of occupant risk and are shown in Table 9.2. Figure 9.6 summarizes these data and other pertinent information from the test. Figure G.3 in Appendix G.3 shows the vehicle angular displacements, and Figures G.4 through G.9 in Appendix G.4 show accelerations versus time traces.

Table 9.2. Occupant Risk Factors for Test No. 468958-3.

Occupant Risk Factor	Value	Time
Occupant Impact Velocity (OIV) Longitudinal Lateral	18.4 ft/s 28.9 ft/s	at 0.0736 s on left side of interior
Occupant Ridedown Accelerations Longitudinal Lateral	4.5 g 16.6 g	0.1539–0.1639 s 0.1563–0.1663 s
Theoretical Head Impact Velocity (THIV)	37.2 km/h 10.3 m/s	at 0.0718 s on left side of interior
Post Head Deceleration (PHD)	17.0 g	0.1561–0.1661 s
Acceleration Severity Index (ASI)	2.43	0.0399–0.0899 s
Maximum 50-ms Moving Average Longitudinal Lateral Vertical	-10.5 g 17.2 g -4.3 g	0.0103–0.0603 s 0.0168–0.0668 s 0.0327–0.0827 s
Maximum Roll, Pitch, and Yaw Angles Roll Pitch Yaw	24.7° 4.1° 47.6°	0.4859 s 0.1750 s 0.9497 s



<p>General Information</p> <p>Test Agency..... Texas A&M Transportation Institute (TTI)</p> <p>Test Standard Test No..... MASH Test 4-10</p> <p>TTI Test No..... 468958-3</p> <p>Test Date..... 2017-12-18</p> <p>Test Article</p> <p>Type..... Median Barrier</p> <p>Name..... TxDOT Rubber Mounted Single Slope</p> <p>Installation Length..... 240 ft 5/4 inches</p> <p>Material or Key Elements ... Three 60-ft long segments of 42-inch tall single slope reinforced concrete barrier mounted on rubber shear fender</p> <p>Soil Type and Condition Placed on existing concrete surface, damp</p> <p>Test Vehicle</p> <p>Type/Designation..... 1100C</p> <p>Make and Model..... 2011 Kia Rio</p> <p>Curb..... 2468 lb</p> <p>Test Inertial..... 2456 lb</p> <p>Dummy..... 165 lb</p> <p>Gross Static..... 2651 lb</p>	<p>Impact Conditions</p> <p>Speed..... 62.4 mi/h</p> <p>Angle..... 24.5°</p> <p>Location/Orientation..... 2.9 ft upstream of joint</p> <p>Impact Severity..... 55 kip-ft</p> <p>Exit Conditions</p> <p>Speed..... 52.7 mi/h</p> <p>Angle..... 1.8°</p> <p>Occupant Risk Values</p> <p>Longitudinal OIV..... 18.4 ft/s</p> <p>Lateral OIV..... 28.9 ft/s</p> <p>Longitudinal Ridedown..... 4.5 g</p> <p>Lateral Ridedown..... 8.8 g</p> <p>THIV..... 37.2 km/h</p> <p>PHD..... 17.0 g</p> <p>ASI..... 2.43</p> <p>Max. 0.050-s Average</p> <p>Longitudinal..... -10.5 g</p> <p>Lateral..... 17.2 g</p> <p>Vertical..... -4.3 g</p>	<p>Post-Impact Trajectory</p> <p>Stopping Distance..... 220 ft downstream</p> <p>..... 7 ft twd traffic lanes</p> <p>Vehicle Stability</p> <p>Maximum Yaw Angle..... 48°</p> <p>Maximum Pitch Angle..... 4°</p> <p>Maximum Roll Angle..... 25°</p> <p>Vehicle Snagging..... No</p> <p>Vehicle Pocketing..... No</p> <p>Test Article Deflections</p> <p>Dynamic..... 3.7 inches</p> <p>Permanent..... 1.0 inch</p> <p>Working Width..... 26.1 inches</p> <p>Height of Working Width..... Field side toe</p> <p>Vehicle Damage</p> <p>VDS..... 11LFQ3</p> <p>CDC..... 11FLEW3</p> <p>Max. Exterior Deformation..... 8.0 inches</p> <p>OCDI..... FS0000000</p> <p>Max. Occupant Compartment Deformation..... 1.5 inches</p>
---	---	--

Figure 9.6. Summary of Results for MASH Test 4-10 on the TxDOT Rubber Mounted Single Slope Barrier.

CHAPTER 10: MASH TEST 4-11 (CRASH TEST NO. 468958-2)

10.1 TEST DESIGNATION AND ACTUAL IMPACT CONDITIONS

MASH Test 4-11 involves a 2270P vehicle weighing 5000 lb \pm 110 lb impacting the CIP of the barrier at an impact speed of 62 mi/h \pm 2.5 mi/h and an angle of 25° \pm 1.5°. The target CIP for *MASH* Test 4-11 on the TxDOT Rubber Mounted Single Slope Barrier was 4.6 ft \pm 1 ft upstream of the first construction joint of the barrier.

The 2011 Dodge RAM 1500 pickup truck used in the test weighed 5024 lb, and the actual impact speed and angle were 62.6 mi/h and 24.9°, respectively. The actual impact point was 3.8 ft upstream of the first construction joint. Minimum target impact severity was 106 kip-ft, and actual IS was 117 kip-ft.

10.2 WEATHER CONDITIONS

The test was performed on the morning of December 20, 2017. Weather conditions at the time of testing were as follows: wind speed: 5 mi/h; wind direction: 179° (vehicle was traveling in a northwesterly direction); temperature: 66°F; relative humidity: 90 percent.

10.3 TEST VEHICLE

The 2011 Dodge RAM 1500 pickup truck, shown in Figures 10.1 and 10.2, was used for *MASH* Test 4-12. The vehicle's test inertia weight was 5024 lb, and its gross static weight was 5189 lb. The height to the lower edge of the vehicle bumper was 11.75 inches, and height to the upper edge of the bumper was 27.35 inches. The height to the vehicle's center of gravity was 28.38 inches. Tables H.1 and H.2 in Appendix H.1 give additional dimensions and information on the vehicle. The vehicle was directed into the installation using the cable reverse tow and guidance system, and was released to be freewheeling and unrestrained just prior to impact.



Figure 10.1. TxDOT Rubber Mounted Single Slope Barrier/Test Vehicle Geometrics for Test No. 468958-2.



Figure 10.2. Test Vehicle before Test No. 468958-2.

10.4 TEST DESCRIPTION

The test vehicle, traveling at an impact speed of 62.6 mi/h, contacted the barrier 3.8 ft upstream of the first construction joint at an impact angle of 24.9°. Table 10.1 lists times and significant events that occurred during Test No. 468958-2. Figures H.1 and H.2 in Appendix H.2 present sequential photographs during the test.

Table 10.1. Events during Test No. 468958-2.

TIME (s)	EVENT
0.028	Vehicle begins to redirect
0.031	Joint 1-2 begins to deflect toward the field side
0.079	Concrete dust blows out of field side Joint 1-2
0.100	Crack forms on upstream end of recess 1B on barrier #1
0.135	Crack forms on downstream end of recess 2A on barrier #2
0.195	Vehicle becomes parallel with barrier
0.499	Vehicle loses contact with barrier

For longitudinal barriers, it is desirable that the vehicle redirects and exits the barrier within the exit box criteria (not less than 32.8 ft downstream from impact for cars and pickups). The 2270P vehicle exited within the exit box criteria defined in *MASH*. After loss of contact with the barrier, the vehicle came to rest 320 ft downstream of the impact and 27 ft toward the field side.

10.5 DAMAGE TO TEST INSTALLATION

Figures 10.3 through 10.5 show the damage to the barrier. A crack radiated upward from each side of recess 1B through barrier #1. Recess 2A on barrier #2 had a small crack radiating from the upstream side of the recess and a larger through crack radiating upward on the downstream end. Working width was 55.0 inches at the height of the field side toe of the barrier. Maximum dynamic deflection during the test was 32.2 inches, and maximum permanent deformation was 27.0 inches.



Figure 10.3. TxDOT Rubber Mounted Single Slope Barrier after Test No. 468958-2.



Figure 10.4. Damage to Barrier #1 after Test No. 468958-2.



Figure 10.5. Damage to Barrier #2 after Test No. 468958-2.

10.6 DAMAGE TO TEST VEHICLE

Figure 10.6 shows the damage the vehicle sustained. The front bumper, grill, hood, radiator and support, left front fender, left front tire and rim, left front upper and lower A-arms, left front outer tie rod end, left front and rear doors, left exterior bed, left rear tire and rim, tail gate, and rear bumper were damaged. Maximum exterior crush to the vehicle was 8.0 inches in the side plane at the left front corner at bumper height. No occupant compartment deformation or intrusion was noted. Figure 10.7 shows the interior of the vehicle. Tables H.3 and H.4 in Appendix H.1 provide exterior crush and occupant compartment measurements.

10.7 OCCUPANT RISK FACTORS

Data from the accelerometer, located at the vehicle center of gravity, were digitized for evaluation of occupant risk and are shown in Table 10.2. Figure 10.8 summarizes these data and other pertinent information from the test. Figure H.3 in Appendix H.3 shows the vehicle angular displacements, and Figures H.4 through H.9 in Appendix H.4 show accelerations versus time traces.



Figure 10.6. Test Vehicle after Test No. 468958-2.



Before Test

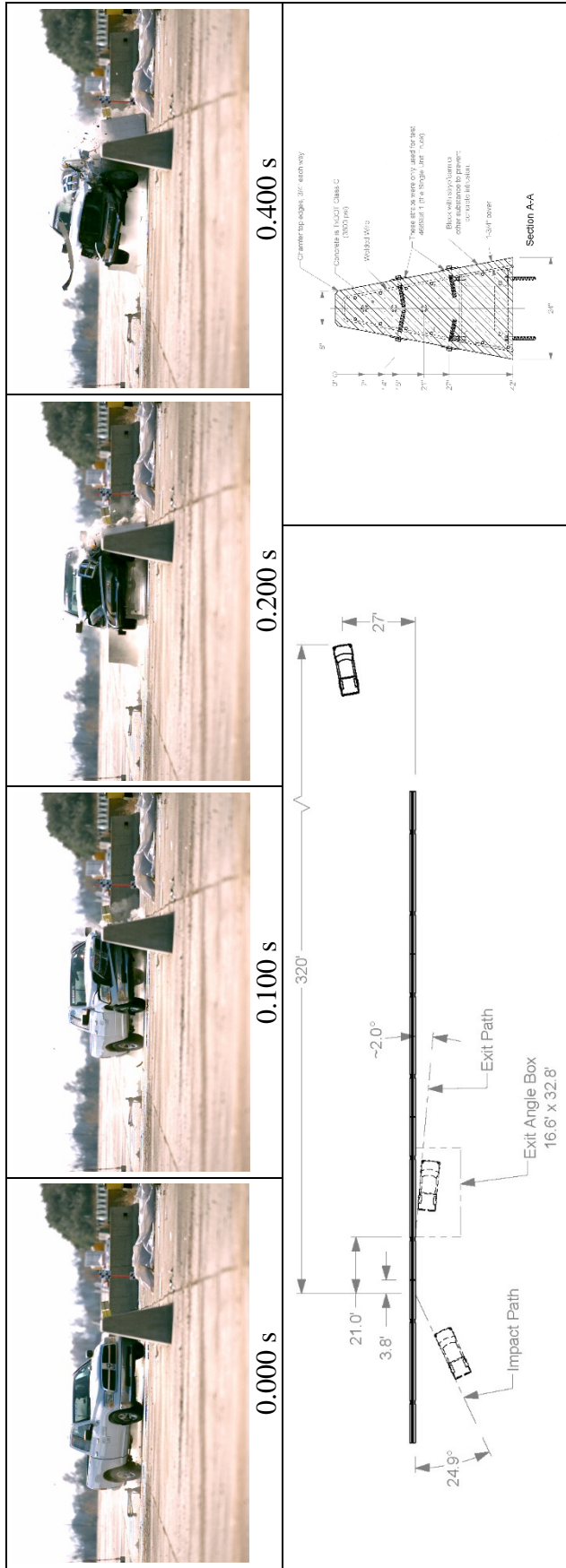


After Test

Figure 10.7. Interior of Test Vehicle for Test No. 568958-2.

Table 10.2. Occupant Risk Factors for Test No. 468958-2.

Occupant Risk Factor	Value	Time
OIV Longitudinal Lateral	14.4 ft/s 23.0 ft/s	at 0.0993 s on left side of interior
Occupant Ridedown Accelerations Longitudinal Lateral	6.4 g 12.3 g	0.2217–0.2317 s 0.2155–0.2255 s
THIV	30.7 km/h 8.5 m/s	at 0.0960 s on left side of interior
PHD	13.3 g	0.2157–0.2257 s
ASI	1.70	0.0564–0.1064 s
Maximum 50-ms Moving Average Longitudinal Lateral Vertical	–9.6 g 12.7 g –3.9 g	0.0122–0.0622 s 0.0359–0.0859 s 0.0268–0.0768 s
Maximum Roll, Pitch, and Yaw Angles Roll Pitch Yaw	21.5° 6.9° 32.8°	0.6565 s 0.2113 s 0.6210 s



General Information	Texas A&M Transportation Institute (TTI)	Impact Conditions	Post-Impact Trajectory
Test Agency.....	Texas A&M Transportation Institute (TTI)	Speed.....	Stopping Distance.....
Test Standard Test No.....	MASH Test 4-11	Angle.....	320 ft downstream
TTI Test No.....	468958-2	Location/Orientation.....	27 ft twd field side
Test Date.....	2017-12-20	Impact Severity.....	
Test Article		Angle.....	
Type.....	Median Barrier	Exit Conditions	
Name.....	TxDOT Rubber Mounted Single Slope	Speed.....	
Installation Length.....	240 ft 5/4 inches	Angle.....	
Material or Key Elements ...	Three 60-ft long segments of 42-inch tall single slope reinforced concrete barrier mounted on rubber shear fender	Occupant Risk Values	
	Placed on existing concrete surface, damp	Longitudinal OIV.....	
Soil Type and Condition	2270P	Lateral OIV.....	
Test Vehicle	2011 Dodge RAM 1500 Pickup	Longitudinal Ridedown.....	
Type/Designation.....	4875 lb	Lateral Ridedown.....	
Make and Model.....	5024 lb	THIV.....	
Curb.....	165 lb	PHD.....	
Test Inertial.....	5189 lb	ASI.....	
Dummy.....		Max. 0.050-s Average	
Gross Static.....		Longitudinal.....	
		Lateral.....	
		Vertical.....	

Figure 10.8. Summary of Results for MASH Test 4-11 on the TxDOT Rubber Mounted Single Slope Barrier.

CHAPTER 11: MASH TEST 4-12 (CRASH TEST NO. 468958-1)

11.1 TEST DESIGNATION AND ACTUAL IMPACT CONDITIONS

MASH Test 4-12 involves a 10000S vehicle weighing 22,046 lb \pm 660 lb impacting the CIP of the barrier at an impact speed of 56 mi/h \pm 2.5 mi/h and an angle of 15° \pm 1.5°. The target CIP for *MASH* Test 4-12 on the TxDOT Rubber Mounted Single Slope Barrier was 6.1 ft \pm 1 ft upstream of the middle construction joint in the barrier.

The 2003 International 4200 single-unit box-van truck used in the test weighed 22,300 lb, and the actual impact speed and angle were 58.3 mi/h and 14.4°, respectively. The actual impact point was 6.3 ft upstream of the middle construction joint in the barrier. Minimum target IS was 142 kip-ft, and actual IS was 157 kip-ft.

11.2 WEATHER CONDITIONS

The test was performed on the morning of December 21, 2017. Weather conditions at the time of testing were as follows: wind speed: 5 mi/h; wind direction: 179° (vehicle was traveling in a northwesterly direction); temperature: 66°F; relative humidity: 90 percent.

11.3 TEST VEHICLE

The 2003 International 4200 single-unit box-van truck, shown in Figures 11.1 and 11.2, was used for *MASH* Test 4-12. The vehicle's test inertia weight was 22,300 lb, and its gross static weight was 22,300 lb. The height to the lower edge of the vehicle bumper was 20.0 inches, and height to the upper edge of the bumper was 35.0 inches. Table I.1 in Appendix I.1 gives additional dimensions and information on the vehicle. The vehicle was directed into the installation using the cable reverse tow and guidance system, and was released to be freewheeling and unrestrained just prior to impact.



Figure 11.1. TxDOT Rubber Mounted Single Slope Barrier/Test Vehicle Geometrics for Test No. 468958-1.



Figure 11.2. Test Vehicle before Test No. 468958-1.

11.4 TEST DESCRIPTION

The test vehicle, traveling at an impact speed of 58.3 mi/h, contacted the barrier 6.3 ft upstream of the middle construction joint in the barrier at an impact angle of 14.4°. Table 11.1 lists times and significant events that occurred during Test No. 468958-1. Figure I.1 in Appendix I.1 presents sequential photographs during the test.

Table 11.1. Events during Test No. 468958-1.

TIME (s)	EVENT
0.030	Cab of vehicle begins to redirect
0.032	Bottom strap on rear of barrier #3 begins to bow outward at center
0.037	Right front wheel begins to steer counterclockwise
0.062	Bottom strap on rear of barrier #2 begins to bow outward at center
0.780	Top strap on rear of barrier #3 begins to bow outward at center
0.106	Left front corner of box contacts barrier
0.109	Box of vehicle begins to redirect
0.284	Rear of vehicle contacts barrier
0.289	Cab of vehicle becomes parallel with barrier
0.303	Box of vehicle becomes parallel with barrier

For longitudinal barriers, it is desirable that the vehicle redirects and exits the barrier within the exit box criteria (not less than 65.6 ft downstream from impact for heavy vehicles). The 10000S vehicle exited within the exit box criteria defined in *MASH*. After loss of contact with the barrier, the vehicle came to rest 255 ft downstream of the impact and 18 ft toward the field side.

11.5 DAMAGE TO TEST INSTALLATION

Figures 11.3 through 11.6 show the damage the barrier sustained. Numerous vertical cracks were noted on barriers #2 and #3. Working width was 74.3 inches at the field side toe of

the barrier. Maximum dynamic deflection during the test was 39.9 inches, and maximum permanent deformation was 21.0 inches.



Figure 11.3. TxDOT Rubber Mounted Single Slope Barrier/Test Vehicle after Test No. 468958-3.



Figure 11.4. Damage to Barrier #2 after Test No. 468958-3.



Figure 11.5. Damage to Barrier #3 after Test No. 468958-3.



Figure 11.6. Damage to Field Side of Barrier after Test No. 468958-3.

11.6 DAMAGE TO TEST VEHICLE

Figure 11.7 shows the damage that the vehicle had sustained. The front bumper, hood, grill, left front tire and rim, left front axle, left side of box, left rear tire and rim, and floor pan were damaged. Maximum exterior crush to the vehicle was 18.0 inches in the front plane at the left front corner at bumper height. Maximum occupant compartment deformation was 8.0 inches in the left side of the floor pan where the seam adjacent to the door frame was pushed upward. Figure 11.8 shows the interior of the vehicle.



Figure 11.7. Test Vehicle after Test No. 468958-3.



Before Test

After Test

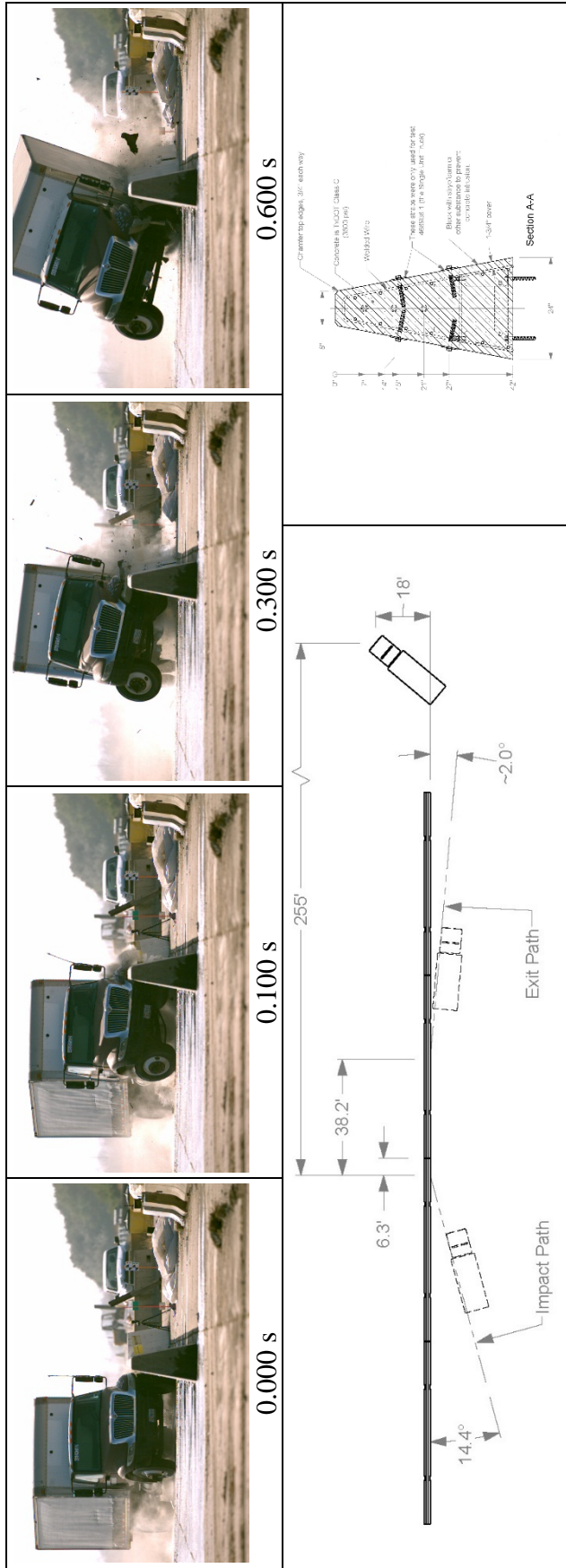
Figure 11.8. Interior of Test Vehicle for Test No. 468958-3.

11.7 OCCUPANT RISK FACTORS

Occupant risk factors are not required for *MASH* Test 4-12. However, the data from the accelerometers were digitized for informational purposes only and are shown in Table 11.2. Figure 11.9 summarizes these data and other pertinent information from the test. Figure I.2 in Appendix I.3 shows the vehicle angular displacements, and Figures I.3 through I.8 in Appendix I.4 show accelerations versus time traces.

Table 11.2. Occupant Risk Factors for Test No. 468958-1.

Occupant Risk Factor	Value	Time
OIV Longitudinal Lateral	5.6 ft/s 9.8 ft/s	at 0.2269 s on left side of interior
Occupant Ridedown Accelerations Longitudinal Lateral	3.4 g 9.2 g	0.2873–0.2973 s 0.2723–0.2823 s
THIV	12.4 km/h 3.4 m/s	at 0.2183 s on left side of interior
PHD	9.4 g	0.2723–0.2823 s
ASI	0.46	0.2744–0.3244 s
Maximum 50-ms Moving Average Longitudinal Lateral Vertical	-1.6 g 4.2 g -2.6 g	0.2714–0.3214 s 0.2489–0.2989 s 0.0437–0.0937 s
Maximum Roll, Pitch, and Yaw Angles Roll Pitch Yaw	17.2° 7.8° 26.0°	0.8227 0.8354 1.2260



General Information	Texas A&M Transportation Institute (TTI)	Impact Conditions	Speed	58.3 mi/h	Post-Impact Trajectory	Stopping Distance.....	255 ft downstream 18 ft twd field side	
Test Agency.....	TTI	Angle	14.4°	Location/Orientation	6.3 ft upstream of joint	Vehicle Stability	Maximum Yaw Angle	26°
Test Standard Test No.	468958-1	Impact Severity	157 kip-ft	Exit Conditions	Speed	Maximum Pitch Angle	8°	
TTI Test No.	2017-12-21	Angle	Not obtainable	Speed	Not obtainable	Maximum Roll Angle	17°	
Test Date	2017-12-21	Occupant Risk Values	Longitudinal OIV	5.6 ft/s	Longitudinal OIV	Vehicle Snagging	No	
Test Article	Median Barrier	Lateral OIV	9.8 ft/s	Lateral OIV	3.4 g	Vehicle Pocketing	No	
Type	TxDOT Rubber Mounted Single Slope	Longitudinal Ridedown	3.4 g	Lateral Ridedown	9.2 g	Test Article Deflections	Dynamic.....	39.9 inches
Name	240 ft 5¼ inches	Lateral Ridedown	9.2 g	THIV	12.4 km/h	Permanent.....	21.0 inches	
Installation Length.....	Three 60-ft long segments of 42-inch tall single slope reinforced concrete barrier	PHD	9.4 g	ASI	0.46	Working Width.....	74.4 inches	
Material or Key Elements ...	Mounted on rubber shear fender placed on existing concrete surface, damp	Max. 0.050-s Average	Longitudinal	-1.6 g	Longitudinal	Height of Working Width	At toe of barrier	
Soil Type and Condition	10000S	Lateral	4.2 g	Vertical.....	-2.6 g	Vehicle Damage	VDS.....	NA
Test Vehicle	2003 International 4200 Truck	Vertical.....	-2.6 g			CDC.....	11FLEW5	
Type/Designation.....	12,570 lb					Max. Exterior Deformation.....	18.0 inches	
Make and Model	22,300 lb					OCDI.....	NA	
Curb	No dummy					Max. Occupant Compartment Deformation	8.0 inches	
Test Inertial	22,300 lb							
Dummy.....	No dummy							
Gross Static	22,300 lb							

Figure 11.9. Summary of Results for MASH Test 4-10 on the TxDOT Rubber Mounted Single Slope Barrier.

CHAPTER 12: STUDIES OF COATINGS

In this phase of the project, the suitability of using titanium dioxide (TiO₂) based coatings to increase water penetration resistance and improve the sight visibility of median barriers was examined. This chapter provides background overview, sample preparation, performance measures and assessment of performance of titanium dioxide based coatings in decreasing water and light absorbance.

12.1 BACKGROUND STUDY ON COATINGS

Titanium dioxide based coatings have gained much interest in the concrete industry due to its self-cleaning property with photocatalytic application. Titanium dioxide is a semiconductor and photocatalytic material. The material traps and decomposes organic and inorganic air pollutants utilizing photocatalytic property (60). Consequently, the material maintains a clean surface. The self-cleaning surface of the concrete is expected to have a brighter surface with lower light absorbance compared to that of a regular concrete surface (61). Much research has been performed to investigate the self-cleaning property of TiO₂ coating (62, 63). All the studies reported effectiveness of TiO₂ in self-cleaning. However, the performance and enhancement in brightness vary with, but not limited to, surface types (62) and outdoor environment condition (63).

TiO₂ surfaces utilize a hydrophobicity mechanism to roll away the water droplets along with dirt (64). This hydrophobic nature of TiO₂ can also be useful for concrete surfaces to reduce ingress of water in concrete. Hydrophobic surfaces increase contact angle between water droplets and the surface concrete. Consequently, the coating reduces surface affinity of water. This may aid in mitigating durability related issues with high water penetration in concrete. Shen, Burton, Jobson, and Haselbach reported decrease in infiltration rate with TiO₂ surface treatment applied to porous concrete pavements (65). Sun, Yu, Liu, Li, Lu, and Hunt applied TiO₂ on wooden surfaces and observed decrease in rate of water penetration (66). With these useful properties, TiO₂ based coatings have prospect to apply on concrete barrier surfaces in enhancing surface visibility by self-cleaning, and better durability by increasing water penetration resistance.

Two commercially available TiO₂ based coatings were evaluated in this study. Commercially available coatings were selected to eliminate the variability of performance associated with, but not limited to, mixing proportion and method of TiO₂ to a solution, dispersion of powders in solution and TiO₂ powder properties. Commercial names of the coatings are FN-nano an TPX, and were designated as FN and TPX for the sake of discussion and data analysis.

12.2 COATING PERFORMANCE EVALUATION

Slab and cube specimens were cast to conduct this study. Concrete slabs were cast for three different mixtures, including the Control mixture. The mixtures were selected based on the performance of the mixtures evaluated in the previous chapter. The mixture designations were - Control, PR5FCR5F, and CR10FGnet. The slabs were cast in a wooden formwork and cubes were prepared using steel molds.

The slabs were cured for 28 days in controlled temperature and humidity. The coatings were then applied on top of the surface of the concrete slabs as per the instructions provided by the manufacturer. Then the slabs were positioned at an angle of 30° with respect to vertical and exposed to the outdoor environment. Change in color of the concrete surface over time with and without the coatings were collected from these slabs using spectrophotometer. Four-inch concrete cubes for the same mixtures were prepared for an approach similar to ASTM C642-06. In addition, additional slabs were cast and 2-inch concrete cubes were cut and also subjected to ASTM C642-06 evaluation. The water penetration resistance of the coatings and the effect of surface types on the coating water absorbance performance was examined.

12.2.1 Water Absorption

Water absorption tests were performed on 2-inch cut cubes and 4-inch cast cubes. Casting of 2-inch cubes was not possible due to the restriction of the minimum volume of concrete specimens associated with maximum aggregate size. Aggregate used for the study has 1-inch maximum aggregate size and required a minimum volume to meet the ASTM requirement for concrete mold for the particular aggregate size. Therefore, 4-inch concrete cubes were prepared.

A similar approach as ASTM C642-06 was implemented to observe change in water absorption of concrete with or without coatings. Four-inch cube samples were prepared for three mixtures: Control, PR5FCR5F, and CR10FGnet. Slabs were cast and cured for 28 days. Similar to ASTM C642-06, the samples were oven dried at 110°C for 24 hours. The samples were cooled at room temperature for 2 hours and then the coatings were applied on all surfaces of the cube samples. After coating, samples were cured in the laboratory indoor environment for 7 days. After curing, initial weights of the samples were recorded and then submerged in water. Samples were taken out from water, wiped to attain saturated surface dry condition and weighed at discrete time intervals (1, 7, 14, 24, and 31 days) to obtain water absorption data. Two-inch concrete cube samples were also made to observe effect of concrete surface on coating performance in terms of water absorption. To obtain 2-inch cut concrete cube samples, concrete slabs were cast, cured for 28 days and cut into 2-inch cubes. Afterward, a similar process as for the 4-inch cubes were adopted for the 2-inch cut cubes.

Percent absorbance was determined to compare water absorption at discrete times for the three mixtures and three graphs were plotted to observe the trend (See Figure 12.1). The plots showed that PR5FCR5F samples started with very low absorption at day 1 (Figure 12.1b), then absorbed water at a high rate after day 1 until day 7, and then reduced the rate of absorption to a very low value. This low initial absorption could be due to weak bonding between the rubber and the cement matrix and non-conformity of the rubber with gradation of replaced fine aggregates, and could be two of the possible reasons to get higher values percent absorbance for rubber cement blend compared to the Control mixture (67). After 31 days, Control showed the lowest, and CR10FGnet showed the highest percent absorbance. Comparing performance of the coatings for all three samples, researchers observed that the TPX coating had lower absorption compared to no coating and FN-coated samples. In addition, the plots revealed the difference between percent absorbance of no-coat and TPX-coated samples was higher (0.47) for PR5FCR5F compared to that of the other two mixtures (0.21 and 0.15 for Control and CR10FGnet, respectively). This signified that in comparison to no-coat, TPX reduced percent water absorption of PR5FCR5F by 11 percent, Control by 5.5 percent, and CR10FGnet by 3 percent at day 31.

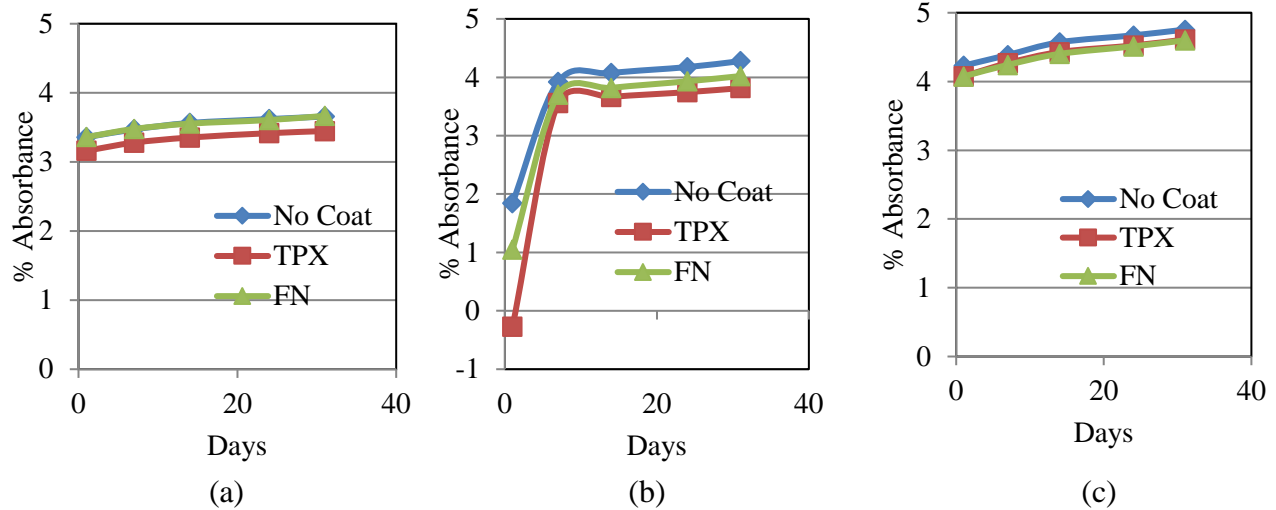


Figure 12.1. Plots for Percent Absorbance at Discrete Time Intervals in Days for Samples (a) Control, (b) PR5FCR5F, and (c) CR10FGnet.

Control concrete (Figure 12.1a) and CR10FGnet (Figure 12.1c) attained around 3-4 percent absorption at day 1 and maintained a very low rate of increase in absorbance, regardless of whether the concrete was coated or not. Overall, the Control mix displayed the lowest absorbance percent and CR10FGnet the highest.

After 31 days, Control showed the lowest and CR10FGnet the highest percent absorbance. Comparing performance of coatings for all three samples, it was observed that TPX coating had lower absorption compared to no coating and FN-coated samples. In addition, the plots revealed that the difference between percent absorbance of No-Coat and TPX-coated samples was higher (0.47) for PR5FCR5F compared to that of other two mixtures (0.21 and 0.15 for Control and CR10FGnet respectively). This signified that in comparison to the No-Coat mixture, TPX reduced percent water absorption of PR5FCR5F by 11 percent, Control by 5.5 percent and CR10FGnet by 3 percent at day 31.

Bulk resistivity test was performed on concrete cube samples at day 31, and a bar chart was plotted to observe percent increase in bulk resistivity of samples with coatings compared to the No-Coat samples (See Figure 12.2). It was notable that the bulk resistivity trend supported the trend in percent water absorption. The data revealed that, Control had the highest bulk resistivity and CR10FGnet the lowest (See Table 12.1). TPX-coated samples demonstrated highest percent increase in bulk resistivity for PR5FCR5F samples. It was expected that increase in bulk resistivity of CR10FGnet would be lower compared to Control based on the percent water absorption data at day 31 for TPX and No-Coat. However, the opposite trend was observed.

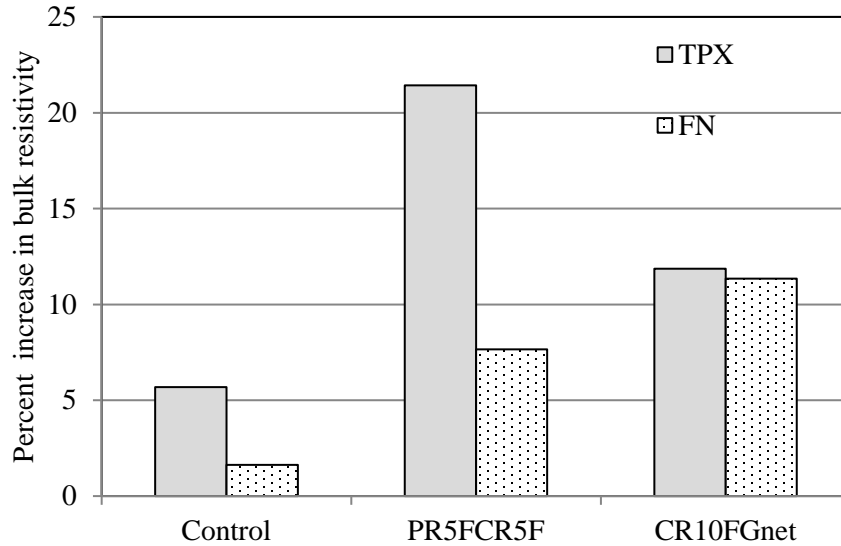


Figure 12.2. Change in Percent Bulk Resistivity of Coated Samples Compared to No-Coat Samples at Day 31.

Table 12.1. Bulk Resistivity at Day 31 Measured at 10kH.

	Bulk resistivity, kΩ-cm at 10kH		
	Control	PR5FCR5F	CR10FGnet
No-Coat	2.46	1.96	1.94
TPX	2.6	2.38	2.17
FN	2.5	2.11	2.16

12.2.2 Surface Color Measurement

The surface color measurement test provides an evaluation process to determine light reflectance or absorbance, as well as to assess the self-cleaning property of TiO₂ based coatings. A spectrophotometer was utilized to obtain color data on the surface of the slabs coated with two different coatings and no coating for Control, PR5FCR5F and CR10FGnet mixtures. The spectrophotometer used CIE L*a*b* colorimetric system to measure color. Here L* varies between black to white (0 to 100), a* between red and green (-128 to 127) and b* between blue and yellow (-128 to 127). Difference in L values provides a comparison of lighter or darker surface. In another way, it gives a contrast between samples in terms of light absorbance or reflectance. This method was also adopted by Motohashi and Inukai (63) to evaluate change of brightness, and Crain et al. (61) incorporated this method to observe change in color of concrete surfaces with the application of several coatings.

A probe attached to a light source and spectrometer was used to obtain color data for at least eight locations on the concrete surfaces with and without coatings at discrete time intervals. The average of L* was compared to determine the change in color after 7 days of application to 60 days after coating application. A summary of the data is tabulated in Table 12.2. Time interval data revealed that there is no or very subtle change in L value with time for both coated and non-coated samples. This may be due to several reasons, e.g., not enough time, winter weather conditions with low temperature, heavy rainfall, and fog. TiO₂ coatings require sun or

ultraviolet ray exposure to react with the dirt to perform the self-cleaning mechanism. In addition, heavy rainfall and fog stay on the surface and leaves less surface area to be in contact with contaminants and pollutants. Therefore, with low reactivity, surface color did not change over the two-month period. It was observed that, FN coating provided a white stain on the surface of the concrete and did not wash away after washing with water at day 7. From visual inspection, the section coated with FN could be identified due to its white stain. As the FN-coated surface was brighter, those FN-coated surfaces demonstrated higher L^* values compared to TPX and non-coated samples. Color measurement visual interpretation is shown in Figure 12.3. It was observed that non-coated and TPX-coated surfaces maintained similar brightness, whereas FN coated surfaces provided a little higher brightness compared to the other two surface types. A similar trend was obtained for all three mixtures surfaces. However, the color of the surface of CR10FGnet samples was found to be a somewhat yellowish-grey with a higher b^* value. According to the study performed by Chen et al., the yellowish color was manifested by samples with higher photocatalytic activity (62).

Table 12.2. L^* Values at Day 60.[Error! Not a valid link.](#)

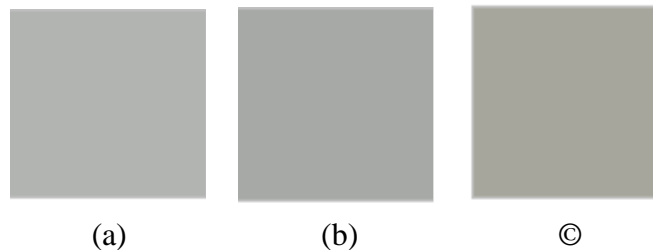


Figure 12.3. Visual Interpretation of Colors Measured on (a) FN Coated, (b) TPX Coated, and (c) Non-Coated PR5FCR5F Mixture Slab Surfaces.

12.3 CONCLUSION ON STUDIES ON COATINGS

Two commercially available TiO_2 based coatings were evaluated in the interest of improving sight visibility and decrease water penetration of the concrete barrier surface. Slabs and cube specimens were cast to assess sight visibility in terms of change in color on the surface of slabs exposed to outdoor environment, and water penetration with the water absorbance test using the cubes. Overall, TPX performed better in resisting water penetration and reduced percent water absorbance about 11 percent at day 31 compared to non-coated samples. The bulk resistivity test was also performed, which supported the trend of water absorbance. However, color change data revealed no variation with time. The FN coating leaves a white stain on the surface after application. Therefore, FN coating demonstrated a higher brightness value throughout the color data collection period. Color data was collected over a short period of time and clustered in between winter days with less sun exposure, heavy rainfall, and moist weather conditions. These conditions might have impacted the performance of the coatings in the photocatalytic application for self-cleaning. Further study is required on different weather periods to validate the behavior trend of this study.

CHAPTER 13: SUMMARY AND CONCLUSIONS

13.1 ASSESSMENT OF CRASH TEST RESULTS

Three full-scale crash tests were performed on the TxDOT Rubber Mounted Single Slope Barrier. The results of these crash tests were detailed in Chapters 9 through 11, and assessments of the tests based on the applicable safety evaluation criteria for *MASH* TL-4 are provided in Tables 13.1 through 13.3.

13.2 CONCLUSIONS

Table 13.4 shows the TxDOT Rubber Mounted Single Slope Barrier performed acceptably for *MASH* TL-4.

Table 13.1. Performance Evaluation Summary for MASH Test 4-10 on the TxDOT Rubber Mounted Single Slope Barrier.

Test Agency: Texas A&M Transportation Institute		Test No.: 468958-3	Test Date: 2017-12-18
<u>MASH Test 4-10 Evaluation Criteria</u>		Test Results	Assessment
<u>Structural Adequacy</u>			
A. <i>Test article should contain and redirect the vehicle or bring the vehicle to a controlled stop; the vehicle should not penetrate, underride, or override the installation although controlled lateral deflection of the test article is acceptable</i>		The barrier contained and redirected the 1100C vehicle. The vehicle did not penetrate, underride, or override the installation. Maximum dynamic deflection during the test was 3.7 inches.	Pass
<u>Occupant Risk</u>			
D. <i>Detached elements, fragments, or other debris from the test article should not penetrate or show potential for penetrating the occupant compartment, or present an undue hazard to other traffic, pedestrians, or personnel in a work zone.</i>		No detached elements, fragments, or other debris were present to penetrate or to show potential for penetrating the occupant compartment, or to present undue hazard to others in the area.	Pass
<i>Deformations of, or intrusions into, the occupant compartment should not exceed limits set forth in Section 5.3 and Appendix E of MASH.</i>		Maximum occupant compartment deformation was 1.5 inches in the left front firewall/toe pan area and left front instrument panel area.	
F. <i>The vehicle should remain upright during and after collision. The maximum roll and pitch angles are not to exceed 75 degrees.</i>		The 1100C vehicle remained upright during and after the collision event. Maximum roll and pitch angles were 25° and 4°, respectively.	Pass
H. <i>Occupant impact velocities (OIV) should satisfy the following limits: Preferred value of 30 ft/s, or maximum allowable value of 40 ft/s.</i>		Longitudinal OIV was 18.4 ft/s, and lateral OIV was 28.9 ft/s.	Pass
I. <i>The occupant ridedown accelerations should satisfy the following limits: Preferred value of 15.0 g, or maximum allowable value of 20.49 g.</i>		Maximum longitudinal occupant ridedown acceleration was 4.5 g, and maximum lateral occupant ridedown acceleration was 8.8 g.	Pass

Table 13.2. Performance Evaluation Summary for MASH Test 4-11 on the TxDOT Rubber Mounted Single Slope Barrier.

Test Agency: Texas A&M Transportation Institute		Test No.: 468958-2	Test Date: 2014-12-20
MASH Test 4-11 Evaluation Criteria		Test Results	
<u>Structural Adequacy</u>			
A.	<i>Test article should contain and redirect the vehicle or bring the vehicle to a controlled stop; the vehicle should not penetrate, underride, or override the installation although controlled lateral deflection of the test article is acceptable</i>	The barrier contained and redirected the 2270P vehicle. The vehicle did not penetrate, underride, or override the installation. Maximum dynamic deflection during the test was 32.2 inches.	Pass
<u>Occupant Risk</u>			
D.	<i>Detached elements, fragments, or other debris from the test article should not penetrate or show potential for penetrating the occupant compartment, or present an undue hazard to other traffic, pedestrians, or personnel in a work zone.</i>	No detached elements, fragments, or other debris were present to penetrate or to show potential for penetrating the occupant compartment, or to present undue hazard to others in the area.	Pass
	<i>Deformations of, or intrusions into, the occupant compartment should not exceed limits set forth in Section 5.3 and Appendix E of MASH.</i>	No occupant compartment deformation or intrusion was noted.	
F.	<i>The vehicle should remain upright during and after collision. The maximum roll and pitch angles are not to exceed 75 degrees.</i>	The 2270P vehicle remained upright during and after the collision event. Maximum roll and pitch angles were 22° and 7°, respectively.	Pass
H.	<i>Occupant impact velocities (OIV) should satisfy the following limits: Preferred value of 30 ft/s, or maximum allowable value of 40 ft/s.</i>	Longitudinal OIV was 14.4 ft/s, and lateral OIV was 23.0 ft/s.	Pass
I.	<i>The occupant ridedown accelerations should satisfy the following limits: Preferred value of 15.0 g, or maximum allowable value of 20.49 g.</i>	Maximum longitudinal occupant ridedown acceleration was 6.4 g, and maximum lateral occupant ridedown acceleration was 12.3 g.	Pass

Table 13.3. Performance Evaluation Summary for MASH Test 4-12 on the TxDOT Rubber Mounted Single Slope Barrier.

Test Agency: Texas A&M Transportation Institute

Test No.: 468958-1

Test Date: 2017-12-21

MASH Test 4-12 Evaluation Criteria	Test Results	Assessment
<p><u>Structural Adequacy</u></p> <p>A. <i>Test article should contain and redirect the vehicle or bring the vehicle to a controlled stop; the vehicle should not penetrate, underride, or override the installation although controlled lateral deflection of the test article is acceptable</i></p>	<p>The barrier contained and redirected the 10000S vehicle. The vehicle did not penetrate, underride, or override the installation. Maximum dynamic deflection during the test was 39.9 inches.</p>	<p>Pass</p>
<p><u>Occupant Risk</u></p> <p>D. <i>Detached elements, fragments, or other debris from the test article should not penetrate or show potential for penetrating the occupant compartment, or present an undue hazard to other traffic, pedestrians, or personnel in a work zone.</i></p> <p><i>Deformations of, or intrusions into, the occupant compartment should not exceed limits set forth in Section 5.3 and Appendix E of MASH.</i></p>	<p>No detached elements, fragments, or other debris were present to penetrate or to show potential for penetrating the occupant compartment, or to present undue hazard to others in the area.</p>	<p>Pass</p>
<p>G. <i>It is preferable, although not essential, that the vehicle remain upright during and after collision.</i></p>	<p>Maximum occupant compartment deformation was 8.0 inches in the left front floor pan area adjacent to the door frame.</p> <p>The 10000S vehicle remained upright during and after the collision event.</p>	<p>Pass</p>

**Table 13.4. Assessment Summary for *MASH* TL-4 Testing
on the TxDOT Rubber Mounted Single Slope Concrete Barrier.**

Evaluation Factors	Evaluation Criteria	Test No. 468958-3	Test No. 468958-2	Test No. 468958-1
Structural Adequacy	A	S*	S	S
Occupant Risk	D	S	S	S
	F	S	S	S
	G	N/A	N/A	S
	H	S	S	N/A
	I	S	S	N/A
Test No.		<i>MASH</i> Test 4-10	<i>MASH</i> Test 4-11	<i>MASH</i> Test 4-12
Pass/Fail		Pass	Pass	Pass

* S = Satisfactory
 U = Unsatisfactory
 N/A = Not applicable

CHAPTER 14: IMPLEMENTATION STATEMENT[†]

A new generation, rubber-mounted single-slope concrete median barrier was successfully developed and tested under this project. The new barrier is a 42-inch tall concrete median barrier that is consistent with TxDOT's standard single-slope concrete median barrier except it was modified to include a rubber mounting system in the place of the continuous use of interface reinforcing bars between the barrier and the road deck. This system consisted of four 60-ft long segments. The joint between any two adjacent segments has dowels per TxDOT standards. There are two rubber fenders per each segment. One is placed 15 ft from the upstream end and the other is placed 15-ft from the downstream end. Hence, there are placed 30 ft apart. There is a thin polymer sheath on the ground to prevent the barrier concrete from developing a cold joint with the ground.

The rubber-mounted anchoring system increases the flexibility of the barrier and allows the system to behave more like a semi-flexible barrier system when impacted by an errant vehicle, whereas, the typical single-slope concrete median barrier behaves like the typical rigid barrier system. It was shown that the increase in barrier flexibility decreased the risk posed to occupants of an errant vehicle when it collides with the barrier. In addition, the increase in flexibility should allow the barrier to sustain greater impact loads with less permanent damage and simply return to or be pushed back into its original position after an impact. Finally, the damage to the impacting vehicle caused by the barrier during the impact was minimized as compared to the damage caused the typical rigid single-slope concrete median barrier.

The rubber-mounted single-slope concrete median barrier was successfully crash tested as part of this project. A total of three full-scale crash tests were performed under the final phase of this project according *MASH* TL-4 conditions. The rubber-mounted single-slope concrete median barrier is considered to be a *MASH* compliant longitudinal barrier according to the *MASH* TL-4 evaluation criteria.

MASH TL-4-11 test caused the barrier to rupture at the location of the two closest rubber fenders to the impact points. This rupture was attributed to the reduction of the barrier reinforcement at the rubber sections. Subsequently, four external straps were attached at each rubber fender location to compensate for the reduced reinforcement, two on the front face of the barrier and two on the back face of the barrier. *MASH* TL-4-12 test did not cause fracture at the rubber fender location although it is considered more severe than the *MASH* TL-4-11 test. These external reinforcing straps are not intended to be implemented in the final design of the rubber-mounted single-slope median barrier.

Hence, it is recommended to add reinforcement the modified design equal to the cross-sectional areas of the straps. Also, it is recommended to reduce the moment arm at the joint to the closest rubber fender from 15 ft to 10 ft to reduce the bending moment applied at rubber fender section.

As a recommendation for further evaluation, a new rubber-mounted single-slope concrete median barrier requires the use of a Morse Rubber Company Shear Fender (#46496) placed

[†] The opinions/interpretations identified/expressed in this section are outside the scope of TTI Proving Ground's A2LA Accreditation.

every 20 ft along the length of the barrier. The barrier would have 60-ft joints with dowels per TxDOT standards. These rubber fenders should offset 10 ft from the barrier segment joint. The shear fenders anchor directly to the existing concrete deck and no stirrup reinforcing bars are used between the concrete median barrier and the concrete deck. In addition, a thin sheet of polyethylene plastic (or similar product) should be placed between the concrete median barrier and the concrete deck to prevent bonding between the two during the slip-forming process. These design details aid in allowing the barrier to move freely in the lateral direction. The width of the anchor box, which houses the shear fender is approximately 3.5 inches more narrow than and matches the slope of the barrier. This allows each face of the anchor box to be sealed with a plastic, foam, or plywood cover to prevent concrete intrusion as the slip-forming machine passes over the anchor box. These covers should be removed after the concrete has adequately cured. The recommended design is shown in Appendix J.

The recommended design of the rubber-mounted single-slope median barrier incorporates additional internal reinforcing bars with a structural capacity similar to that used in the *MASH* Test 4-12. *MASH* Tests 4-10 and 4-11 are not considered to be negatively affected by the presence of the additional reinforcement in the installation since the vehicle was successfully redirected without the additional reinforcing. In addition, the increase in barrier stiffness due to presence of the additional reinforcement should not negatively affect the stability of the impact vehicle or the risk posed to its occupants due to the fact that the rubber-mounted single-slope concrete median barrier is more flexible than the TxDOT single-slope concrete median barrier, which has been successfully full-scale crash tested to *MASH* TL-3 (68).

In addition to modifying the structural design of a single-slope concrete median barrier, this study also explored the development of new concrete mixtures for concrete barriers that demonstrate improved performance in toughness and impact resistance so that the reaction of the barrier material in a crash event imparts less safety threat to occupant and vehicle.

With the specific goal to enhance concrete barrier composite performance, researchers searched for low cost alternate material series to be incorporated in concrete mixtures to improve toughness and impact resistance. Researchers selected five materials series to investigate the suitability of the material series for concrete barrier use. The material series were geogrids, fiber, reclaimed asphalt pavement (RAP), recycled tire rubber, and high-volume Class F fly ash. Each material series included a suit of materials. As such, data on physical properties and characteristics of materials were gathered and used to narrow down the design matrix.

Initial screening study was performed to understand the behavior of the different material series. The screening study eliminated the high-volume fly ash series and geogrid from the further testing. A net-like synthetic polypropylene fiber was chosen based on its enhanced overall performance on concrete properties as compared to the other fiber types evaluated. Concrete containing 25 percent coarse RAP performed well and was selected for final evaluation. Rubber series performance was also satisfactory. Based on the likely synergy between rubbers and fibers to address the shortcomings of one another while used as a combination blend, fiber rubberized concrete with different mixture proportions were also evaluated. Considering all the material series testing performance, RAP concrete, fiber rubberized reinforced concrete, rubberized concrete, and fiber reinforced concrete mixtures were evaluated to select two optimized performance concretes. Concrete mixtures containing 5 percent crumb and 5 percent powdered rubber as a 10 percent volume replacement of fine aggregate and a concrete blend containing 10 percent crumb rubber as volume replacement of fine aggregate

with the addition of 0.25 percent fiber showed better overall performance and are recommended for barrier use and field bogie testing.

Bogie testing was conducted on the two recommended engineered concrete mixtures (a rubberized-fiber hybrid mixture and a rubberized mixture) and the control mixture. Similar impact resistance behavior was observed among the engineered concrete mixtures. The crack widths and cracking pattern of the rubberized-fiber hybrid mixture was comparable to the control mixture. This could be due to excess water (25 gallons) that was added to the concrete in the field, which would have considerably reduced the strength of the barrier. This is further supported by the fact that the laboratory and field compressive strength data for the rubberized-fiber mixture were not similar. Furthermore, evaluation of cores collected from that barrier depicted some consolidation issues.

As such, it is recommended that the bogie test on the rubberized-fiber hybrid mixture be repeated since due to time and testing restraint, only one bogie test was performed. For the repeat test, a water-reducer should be incorporated instead of additional water if the workability needs to be increased in the field.

However, the barrier mixture containing only the rubber particles displayed smaller, more distributed cracks than the control barrier, which indicates that the rubber performed well in arresting the crack propagation and that the toughness of the concrete was improved through the rubber inclusions. Since rubber is hydrophobic, further research was conducted to examine whether the bonding between the rubber and cement matrix could be improved since improved bonding should further enhance the mechanical strength properties of rubberized concrete. As such, a two-step chemical process was performed to increase hydrophilicity of the rubber particles and adhesion bonding between the surface of rubber particles and paste. The results showed that chemical functionalization of the rubber can be used to increase the compressive strength of the resultant composites.

The use of photocatalytic coatings as a novel way to improve sight visibility of the barrier and reduce water penetration was also evaluated. Increased water resistance was determined in the coated specimens as compared to the control. In the period of time in which the color change of the concrete was evaluated, no variation with time was observed between the control and the specimen with coatings. Since the color data were collected on a short time period (2-month duration) and clustered in winter days with less sun exposure and heavy rainfall, it is recommended that a longer evaluation period (at least 1 year) be conducted.

In this research, a control concrete mixture was used and the engineered mixtures were based on that control. It is recommended that optimization of the concrete mixture proportions (e.g., w/c ratio, aggregate gradation) is also examined. As a recommendation for further evaluation, research should be conducted to evaluate the impact of the treated rubber in other mechanical tests and in larger sized specimens. Finally, one of the challenging aspects is scaling up the impact tests from laboratory scale to that of what occurred in the bogie test. Thus, researchers recommend development of a laboratory experimental test that can simulate impact loading in *MASH* crash tests.

REFERENCES

1. TxDOT. (2014). *Roadway Design Manual. Roadway Design Manual*.
2. Bligh, R., Miaou, S.-P., Lord, D., & Cooner, S. (2006). *Median Barrier Guidelines For Texas*. (Vol. 7).
3. Bligh, R. P., Sheikh, N. M., Menges, W. L., & Haug, R. R. (2005). *Development of Low-Deflection Precast Concrete Barrier*. (Vol. 7).
4. Cantisani, G., Di Mascio, P. D., & Polidori, C. (2017). New research opportunities for roadside safety barriers improvement. *IOP Conference Series: Materials Science and Engineering*, 236(1). <https://doi.org/10.1088/1757-899X/236/1/012097>.
5. Topçu, I. B., & Avcular, N. (1997a). Collision behaviours of rubberized concrete. *Cement and Concrete Research*, 27(12), 1893–1898. [https://doi.org/10.1016/S0008-8846\(97\)00204-4](https://doi.org/10.1016/S0008-8846(97)00204-4)
6. Topçu, I. B., & Avcular, N. (1997b). Collision behaviours of rubberized concrete. *Cement and Concrete Research*, 27(12), 1893–1898. [https://doi.org/10.1016/S0008-8846\(97\)00204-4](https://doi.org/10.1016/S0008-8846(97)00204-4).
7. Grzebieta, R. H., Zou, R., Corben, B., Judd, R., Kulgren, A., Tingval, C., & Powell, C. (2002). Roadside Crash Barrier Testing. In *3rd International Crashworthiness Conference*.
8. Jjhooks.com, *Jersey, F-Shape, Constant Slope, & Other Barrier Profiles*, 2015. [Online]. Available: <http://www.jjhooks.com/profiles.shtml>. [Accessed: 09- Oct- 2015].
9. AASHTO. *Manual for Assessing Roadside Safety Hardware*. Second Edition, 2016, American Association of State Highway and Transportation Officials: Washington, D.C.
10. H.E. Ross, Jr., D.L. Sicking, R.A. Zimmer and J.D. Michie, *Recommended Procedures for the Safety Performance Evaluation of Highway Features*, National Cooperative Highway Research Program Report 350, Transportation Research Board, National Research Council, Washington, D.C., 1993.
11. LS-DYNA KEYWORD USER'S MANUAL, LIVERMORE SOFTWARE TECHNOLOGY CORPORATION (LSTC), Livermore, California, August 2016.
12. Schmidt, Jennifer D., *Development of a New Energy-Absorbing Roadside/Median Barrier System with Restorable Elastomer Cartridges*. Final Report to the Nebraska Department of Roads and the Federal Highway Administration – Nebraska Division, MwRSF Research Report No. TRP-03-281-13, Midwest Roadside Safety Facility, University of Nebraska-Lincoln, Lincoln, Nebraska, July 16, 2013.
13. Cuelho, E., Perkins, S., & Morris, Z. (2014). *Relative Operational Performance of Geosynthetics Used As Subgrade Stabilization*. FHWA.
14. Chidambaram, S. R., & Agarwal, P. (2014). The confining effect of geo-grid on the mechanical properties of concrete specimens with steel fiber under compression and flexure. *Construction and Building Materials*, 71, 628–637. <https://doi.org/10.1016/j.conbuildmat.2014.08.059>.
15. Kim, S., Tang, X., & Chehab, G. (2008). Laboratory study of geogrid reinforcement in Portland cement concrete. In *Pavement Cracking : Mechanisms, Modeling, Detection, Testing and Case Histories*. CRC Press.

16. Chidambaram, S. R., & Agarwal, P. (2014). The confining effect of geo-grid on the mechanical properties of concrete specimens with steel fiber under compression and flexure. *Construction and Building Materials*, 71, 628–637.
<https://doi.org/10.1016/j.conbuildmat.2014.08.059>.
17. Meski, F. El, & Chehab, G. R. (2014). Flexural Behavior of Concrete Beams Reinforced with Different Types of Geogrids. *Journal of Materials in Civil Engineering*, 26(8), 1–8.
[https://doi.org/10.1061/\(ASCE\)MT.1943-5533.0000920](https://doi.org/10.1061/(ASCE)MT.1943-5533.0000920).
18. Zakaria, Muda, C., Sharif, S. F. A., & Jun hongHong, N. (2012). FLEXURAL BEHAVIOR OF LIGHTWEIGHT OIL PALM SHELLS CONCRETE SLAB REINFORCED WITH GEOGRID 1- Introduction 2- Background. *International Journal of Scientific & Engineering Research*, 3(11), 1–18.
19. Oikonomou, N., & Mavridou, S. (2009). The use of waste tyre rubber in civil engineering works. *Sustainability of Construction Materials*, 213–238.
<https://doi.org/10.1533/9781845695842.213>.
20. Eldin, N. N., & Senouci, A. B. (1994). Measurement and prediction of the strength of rubberized concrete. *Cement and Concrete Composites*, 16(4), 287–298.
[https://doi.org/10.1016/0958-9465\(94\)90041-8](https://doi.org/10.1016/0958-9465(94)90041-8).
21. Huang, B., Li, G., Pang, S.-S., & Eggers, J. (2004). Investigation into Waste Tire Rubber-Filled Concrete. *Journal of Materials in Civil Engineering*, 16(3), 187–194.
[https://doi.org/10.1061/\(ASCE\)0899-1561\(2004\)16:3\(187\)](https://doi.org/10.1061/(ASCE)0899-1561(2004)16:3(187)).
22. Siddique, R., & Naik, T. R. (2004a). Properties of concrete containing scrap-tire rubber - An overview. *Waste Management*, 24(6), 563–569.
<https://doi.org/10.1016/j.wasman.2004.01.006>.
23. Siddique, R., & Naik, T. R. (2004b). Properties of concrete containing scrap-tire rubber - An overview. *Waste Management*, 24(6), 563–569.
<https://doi.org/10.1016/j.wasman.2004.01.006>.
24. Taha, M. M. R., El-Dieb, A. S., El-wahab, M. A. A., & Abdel-Hameed, M. E. (2009). Mechanical , Fracture , and Microstructural Investigations, 20(10), 640–649.
25. Topçu, I. B. (1995). The properties of rubberized concretes. *Cement and Concrete Research*, 25(2), 304–310. [https://doi.org/10.1016/0008-8846\(95\)00014-3](https://doi.org/10.1016/0008-8846(95)00014-3).
26. Al-Tayeb, M. M., Bakar, B. H. A., Ismail, H., & Akil, H. M. (2012). Impact Resistance of Concrete with Partial Replacements of Sand and Cement by Waste Rubber. *Polymer-Plastics Technology and Engineering*, 51(12), 1230–1236.
<https://doi.org/10.1080/03602559.2012.696767>.
27. Savas, B., Ahmad, S., & Fedroff, D. (1997). Freeze-Thaw Durability of Concrete with Ground Waste Tire Rubber. *Transportation Research Record: Journal of the Transportation Research Board*, 1574(970050), 80–88. <https://doi.org/10.3141/1574-11>.
28. Thomas, B. S., Gupta, R. C., Kalla, P., & Cseteneyi, L. (2014). Strength, abrasion and permeation characteristics of cement concrete containing discarded rubber fine aggregates. *Construction and Building Materials*, 59, 204–212.
<https://doi.org/10.1016/j.conbuildmat.2014.01.074>.

29. Gupta, T., Sharma, R. K., & Chaudhary, S. (2015). Impact resistance of concrete containing waste rubber fiber and silica fume. *International Journal of Impact Engineering*, 83, 76–87. <https://doi.org/10.1016/j.ijimpeng.2015.05.002>.
30. Tantala, M. W., Lepore, J. A., & Zandi, I. (1996). Quasi-elastic behaviour of rubber included concrete using waste rubber tyres. In *12th International Conference on Solid Waste Technology and Management*. Philadelphia: University of Philadelphia Press, USA.
31. Hernández-Olivares, F., Barluenga, G., Bollati, M., & Witoszek, B. (2002). Static and dynamic behaviour of recycled tyre rubber-filled concrete. *Cement and Concrete Research*, 32(10), 1587–1596. [https://doi.org/10.1016/S0008-8846\(02\)00833-5](https://doi.org/10.1016/S0008-8846(02)00833-5).
32. Siddique, R. (2004). Performance characteristics of high-volume Class F fly ash concrete. *Cement and Concrete Research*, 34(3), 487–493. <https://doi.org/10.1016/j.cemconres.2003.09.002>.
33. Mehta, P. K., & Langley, W. S. (2000). Monolith Foundation: Built to Last a 1000 Years. *ACI Concrete International*, 22(7), 27–32.
34. Malhotra, V. M., & Mehta, P. K. (2008). *High-performance, high-volume fly ash concrete for building sustainable and durable structures* (3rd ed.). Ottawa, Canada: Asphalt Institute, 2014.
35. Hansen and Copeland, 2016.
36. Hossiney, N., Tia, M., & Bergin, M. (2010). Concrete Containing Recycled Concrete Aggregate for Use in Concrete Pavement. *International Journal of Pavement Research*, 3(5), 251–258. <https://doi.org/10.3141/2164-15>.
37. Delwar, M., Mostafa, F., & Ramzi, T. (1997). Use of Reclaimed Asphalt Pavement as an Aggregate in Portland Cement Concrete. *ACI Materials Journal*, 94(3). Retrieved from <http://www.concrete.org/publications/internationalconcreteabstractsportal.aspx?m=details&i=306>.
38. Hassan, K. E., Brooks, J. J., & Erdman, M. (2000). The use of reclaimed asphalt pavement (RAP) aggregates in concrete. *Waste Management Series*, 1(C), 121–128. [https://doi.org/10.1016/S0713-2743\(00\)80024-0](https://doi.org/10.1016/S0713-2743(00)80024-0).
39. Huang, B., Shu, X., & Li, G. (2005). Laboratory investigation of portland cement concrete containing recycled asphalt pavements. *Cement and Concrete Research*, 35(10), 2008–2013. <https://doi.org/10.1016/j.cemconres.2005.05.002>.
40. Jenq, Y. S., & Shah, S. P. (1986). Crack propagation in fiber-reinforced concrete. *Journal of Structural Engineering*, 112(1), 19–34.
41. Naaman, a, & Gopalratnam, V. (1983). Impact properties of steel fibre reinforced concrete in bending. *International Journal of Cement Composites and Lightweight Concrete*, 5(4), 225–233. [https://doi.org/10.1016/0262-5075\(83\)90064-7](https://doi.org/10.1016/0262-5075(83)90064-7).
42. Banthia, N., Yan, C., & Sakai, K. (1998). Impact resistance of fiber reinforced concrete at subnormal temperatures. *Cement and Concrete Composites*, 20(5), 393–404. [https://doi.org/10.1016/S0958-9465\(98\)00015-8](https://doi.org/10.1016/S0958-9465(98)00015-8).
43. Gopalratnam, V. S., Shah, S. P., Batson, G. B., Criswell, M. E., Ramakrishnan, V., & Wecharatana, M. (1991). Fracture toughness of fiber reinforced concrete. *ACI Materials Journal*, 88(4), 339–353.

45. Kim, H., Kim, G., Gucunski, N., Nam, J., & Jeon, J. (2015). Assessment of flexural toughness and impact resistance of bundle-type polyamide fiber-reinforced concrete. *Composites Part B: Engineering*, 78, 431–446. <https://doi.org/10.1016/j.compositesb.2015.04.011>.
46. Lok and Zhao, P.J., T. S. (2004). Impact response of steel fiber-reinforced concrete using a split Hopkinson pressure bar. *Journal of Materials in Civil Engineering*, 16(February), 1–6. [https://doi.org/10.1061/\(ASCE\)0899-1561\(2004\)16:1\(54\)](https://doi.org/10.1061/(ASCE)0899-1561(2004)16:1(54)).
47. Song, P. S., & Hwang, S. (2004). Mechanical properties of high-strength steel fiber-reinforced concrete. *Construction and Building Materials*, 18(9), 669–673. <https://doi.org/10.1016/j.conbuildmat.2004.04.027>,
48. Cominoli, L., Failla, C., & Plizzari, G. A. (2007). Steel and synthetic fibres for enhancing concrete toughness and shrinkage behaviour. *Sustainable Construction Materials and Technologies*, 231–240.
49. Hamoush, S., Abu-Lebdeh, T., & Cummins, T. (2010). Deflection behavior of concrete beams reinforced with PVA micro-fibers. *Construction and Building Materials*, 24(11), 2285–2293. <https://doi.org/10.1016/j.conbuildmat.2010.04.027>.
50. Wang, Y. (1998). Toughness Characteristics of Synthetic Fibre-Reinforced Cementitious Composites. *Fatigue & Fracture of Engineering Materials & Structures*, 21(4), 521–532. <https://doi.org/10.1046/j.1460-2695.1998.00045>.
51. Bindiganavile, V., & Banthia, N. (2005). Impact response of the fiber-matrix bond in concrete. *Canadian Journal of Civil Engineering*, 32(5), 924–933.
52. Nia, A. A., Hedayatian, M., Nili, M., & Sabet, V. A. (2012). An experimental and numerical study on how steel and polypropylene fibers affect the impact resistance in fiber-reinforced concrete. *International Journal of Impact Engineering*, 46, 62–73. <https://doi.org/10.1016/j.ijimpeng.2012.01.009>.
53. Konsta-Gdoutos, M., & , Shah, SP, Z. S. (2009). *Crack free concrete made with nanofiber reinforcement. Developing a Research Agenda for Transportation Infrastructure Preservation and Renewal Conference*.
54. Zhang, P., Zhao, Y.-N., Li, Q.-F., Wang, P., & Zhang, T.-H. (2014). Flexural Toughness of Steel Fiber Reinforced High Performance Concrete Containing Nano-SiO₂ and Fly Ash. *The Scientific World Journal*, 2014, 1–11. <https://doi.org/10.1155/2014/403743>.
55. Tyson, B. M., Abu Al-Rub, R. K., Yazdanbakhsh, A., & Grasley, Z. (2011). Carbon Nanotubes and Carbon Nanofibers for Enhancing the Mechanical Properties of Nanocomposite Cementitious Materials. *Journal of Materials in Civil Engineering*, 23(7), 1028–1035.
56. Huang, B., Shu, X., & Cao, J. (2013). A two-staged surface treatment to improve properties of rubber modified cement composites. *Construction and Building Materials*, 40, 270–274. <https://doi.org/10.1016/j.conbuildmat.2012.11.014>.
57. Bilodeau, A., & Malhotra, V. M. (2000). High-Volume Fly Ash System : Concrete Solution for Sustainable Development, (97), 41–48.
58. Dalvand, A., Sharbatdar, M. K., Kheyroddin, A., & Nikui, A. (2014). Assessment of statistical variations in experimental impact resistance and mechanical properties of silica fume concrete, 21, 1577–1591.

59. Mohammadi, Y., Carkon-Azad, R., Singh, S. P., & Kaushik, S. K. (2009). Impact resistance of steel fibrous concrete containing fibres of mixed aspect ratio. *Construction and Building Materials*, 23(1), 183–189.
<https://doi.org/10.1016/j.conbuildmat.2008.01.002>.
60. Fujishima, A., Zhang, X., & Tryk, D. A. (2008). TiO₂ photocatalysis and related surface phenomena. *Surface Science Reports*, 63(12), 515–582.
<https://doi.org/10.1016/j.surfrep.2008.10.001>.
61. Crain, N., Juenger, M., Cros, C., Terpeluk, A., Burris, L., McDonald-Buller, E., ... Rung, M. (2016). *Laboratory and Field Studies of Photocatalytic NO_x and O₃ Removal by Coatings on Concrete*. Retrieved from <http://library.ctr.utexas.edu/ctr-publications/0-6636-1.pdf>.
62. Chen, J., Kou, S. cong, & Poon, C. Sun. (2011). Photocatalytic cement-based materials: Comparison of nitrogen oxides and toluene removal potentials and evaluation of self-cleaning performance. *Building and Environment*, 46(9), 1827–1833.
<https://doi.org/10.1016/j.buildenv.2011.03.004>.
63. Motohashi, K., & Inukai, T. (2007). Self-cleaning performance evaluation of commercial photocatalyst coating materials through 5 years of outdoor exposure. In *International RILEM Symposium on Photocatalysis, Environment and Construction Materials* (pp. 307–313).
64. Agrios, A. G., & Pichat, P. (2005). State of the art and perspectives on materials and applications of photocatalysis over TiO₂. *Journal of Applied Electrochemistry*, 35(7–8), 655–663. <https://doi.org/10.1007/s10800-005-1627-6>.
65. Shen, S., Burton, M., Jobson, B., & Haselbach, L. (2012). Pervious concrete with titanium dioxide as a photocatalyst compound for a greener urban road environment. *Construction and Building Materials*, 35(509), 874–883.
<https://doi.org/10.1016/j.conbuildmat.2012.04.097>.
66. Sun, Q., Yu, H., Liu, Y., Li, J., Lu, Y., & Hunt, J. F. (2010). Improvement of water resistance and dimensional stability of wood through titanium dioxide coating. *Holzforschung*, 64(6), 757–761. <https://doi.org/10.1515/HF.2010.114>.
67. Bignozzi, M. C., & Sandrolini, F. (2006). Tyre rubber waste recycling in self-compacting concrete. *Cement and Concrete Research*, 36(4), 735–739.
<https://doi.org/10.1016/j.cemconres.2005.12.011>.
68. Williams, William F., Bligh, Roger P., and Menges, Wanda L. *MASH Test 3-11 of the TxDOT single Slope Bridge Rail (Type SSRT) on Pan-Formed Bridge Deck*. Texas Department of Transportation. March 2011.

APPENDIX A. MATERIAL SOURCE, TYPE, AND PHYSICAL PROPERTIES

Table A.1. Material Nomenclature, Distributor, and Oxide Analysis.

Material	Distributor	SiO ₂	Al ₂ O ₃	Fe ₂ O ₃	CaO	MgO	SO ₃	Na ₂ O	K ₂ O
		mass %	mass %	mass %	mass %	mass %	mass %	mass %	mass %
Cement-PC I/II	Texas Lehigh	21.0	4.7	3.2	63.7	1.2	3.0	0.5	
Cement-PC III	Texas Lehigh	-	-	-	-	1.3	3.9	0.8	
Fly ash-Class F	Headwaters Resources Inc	54.3	24.6	4.7	10.3	2.5	0.5	0.3	0.9

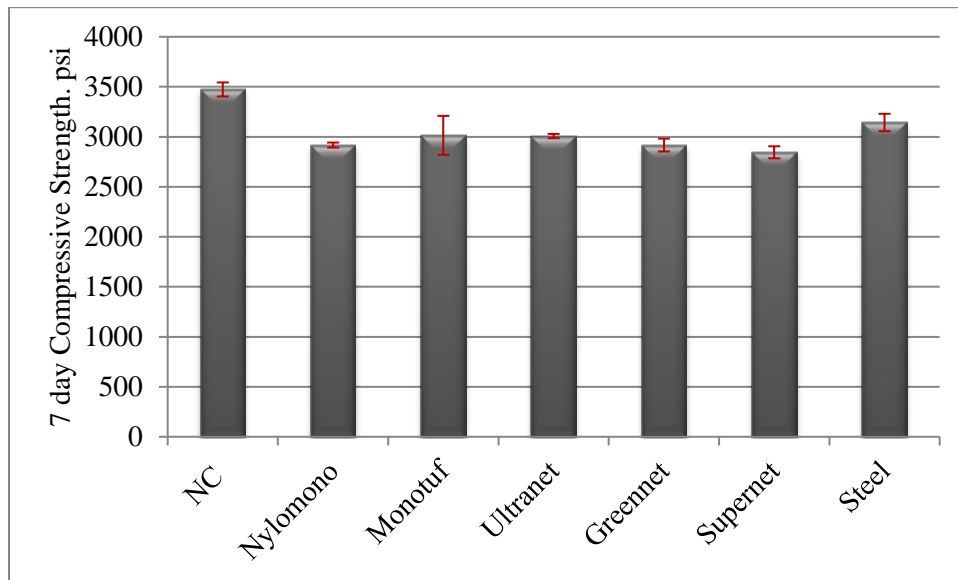


Figure A.1. Impact of Fiber Type on 7 Day Compressive Strength.

Table A.2. Material Source, Type, and Physical Properties of Aggregates.

Material	Source/Type	Specific Gravity	Absorption Capacity
Coarse aggregate	Martin Marietta #67 gravel	2.59	1.08
Fine aggregate	Martin Marietta Concrete sand	2.58	0.91

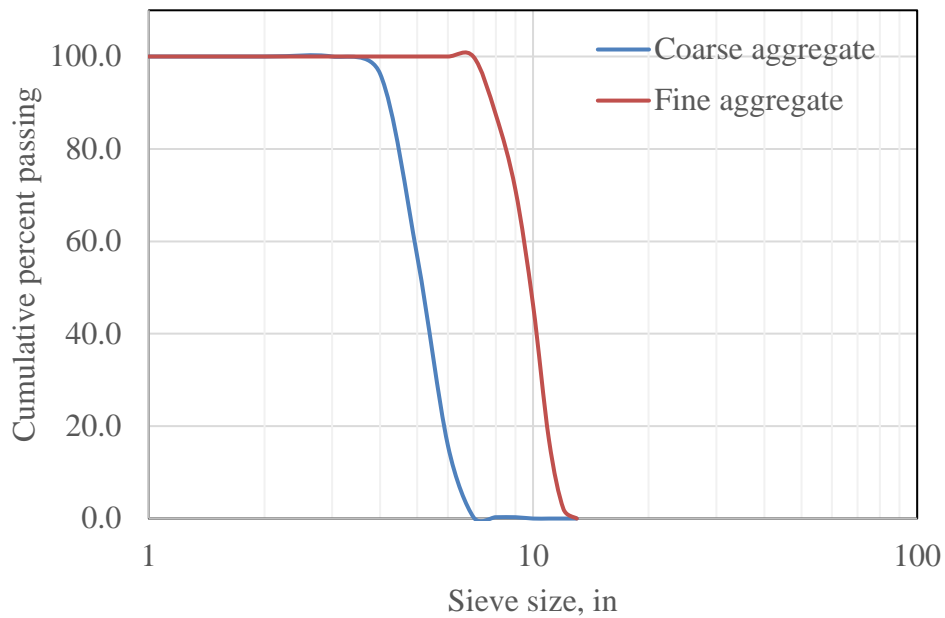


Figure A.2. Sieve Analysis of Coarse and Fine Aggregate.

Table A.3. Performance of PVA Fibers at Dosage of 0.25% by Volume of Mixtures in Concrete.

	Compressive strength, psi	Flexural strength, psi	Flexural toughness, lbf-in	Number of blows for initial crack to occur	Number of blows for failure to occur
Control	6094	788	17	14	15
PVA.25	6135	762	50	16	21

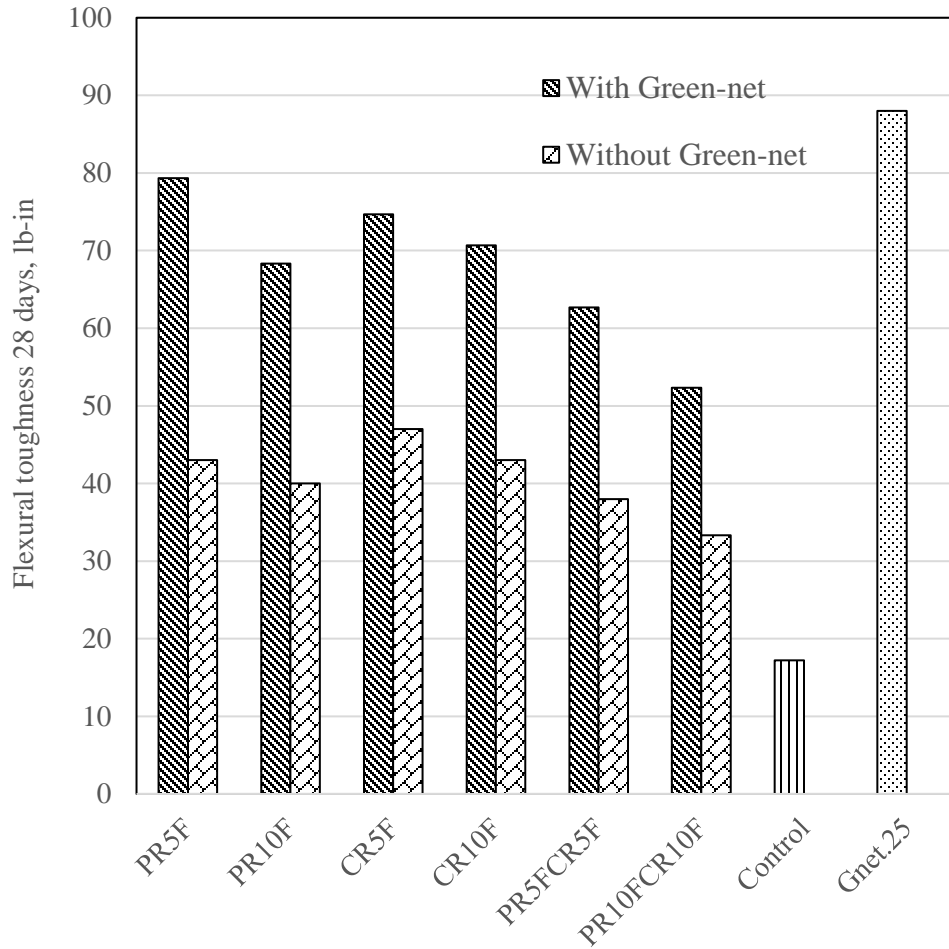


Figure A.3. Flexural Toughness Comparison between Rubberized Concrete Mixtures with and without Green-Net Fiber.

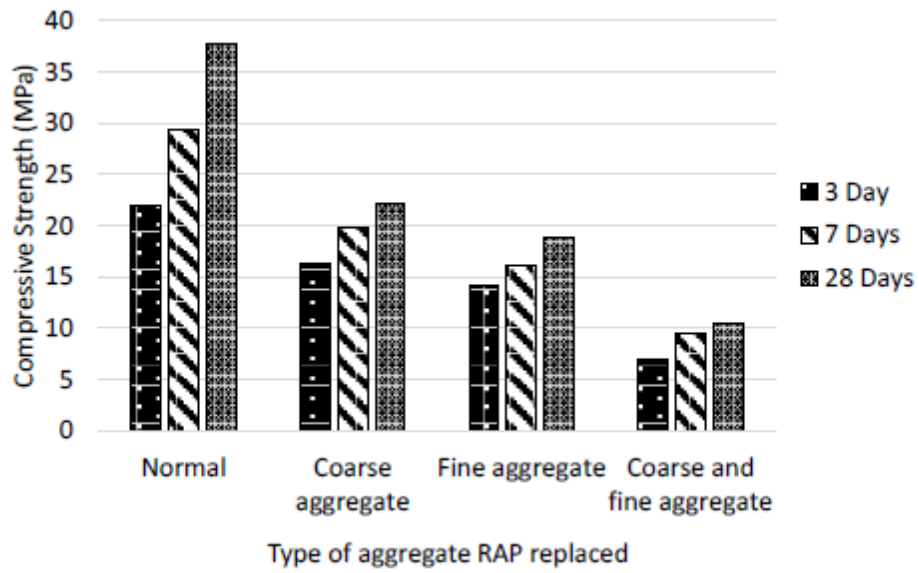
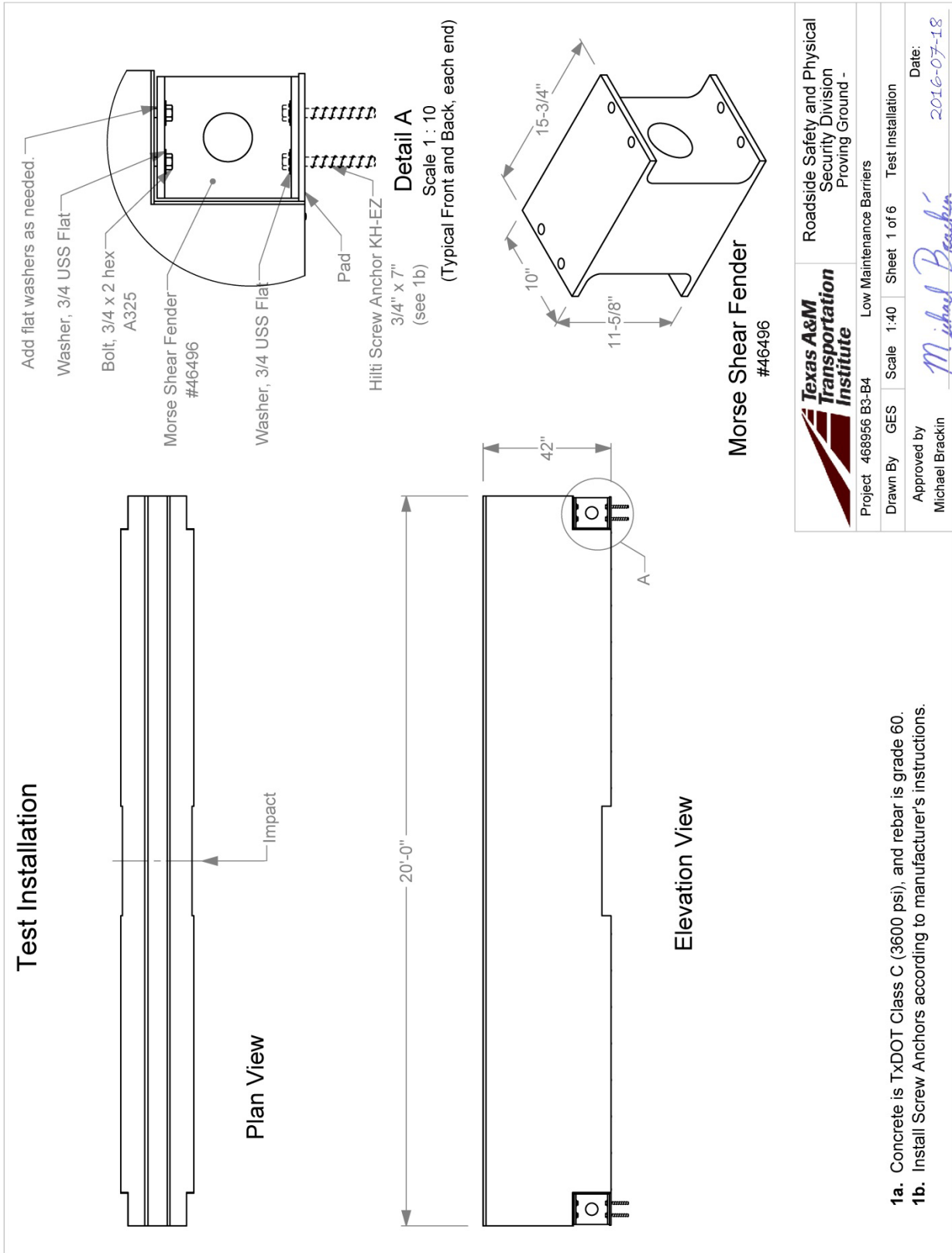


Figure A.4. Effect of RAP Aggregate Size on Compressive Strength (from Huang et al. 2005).

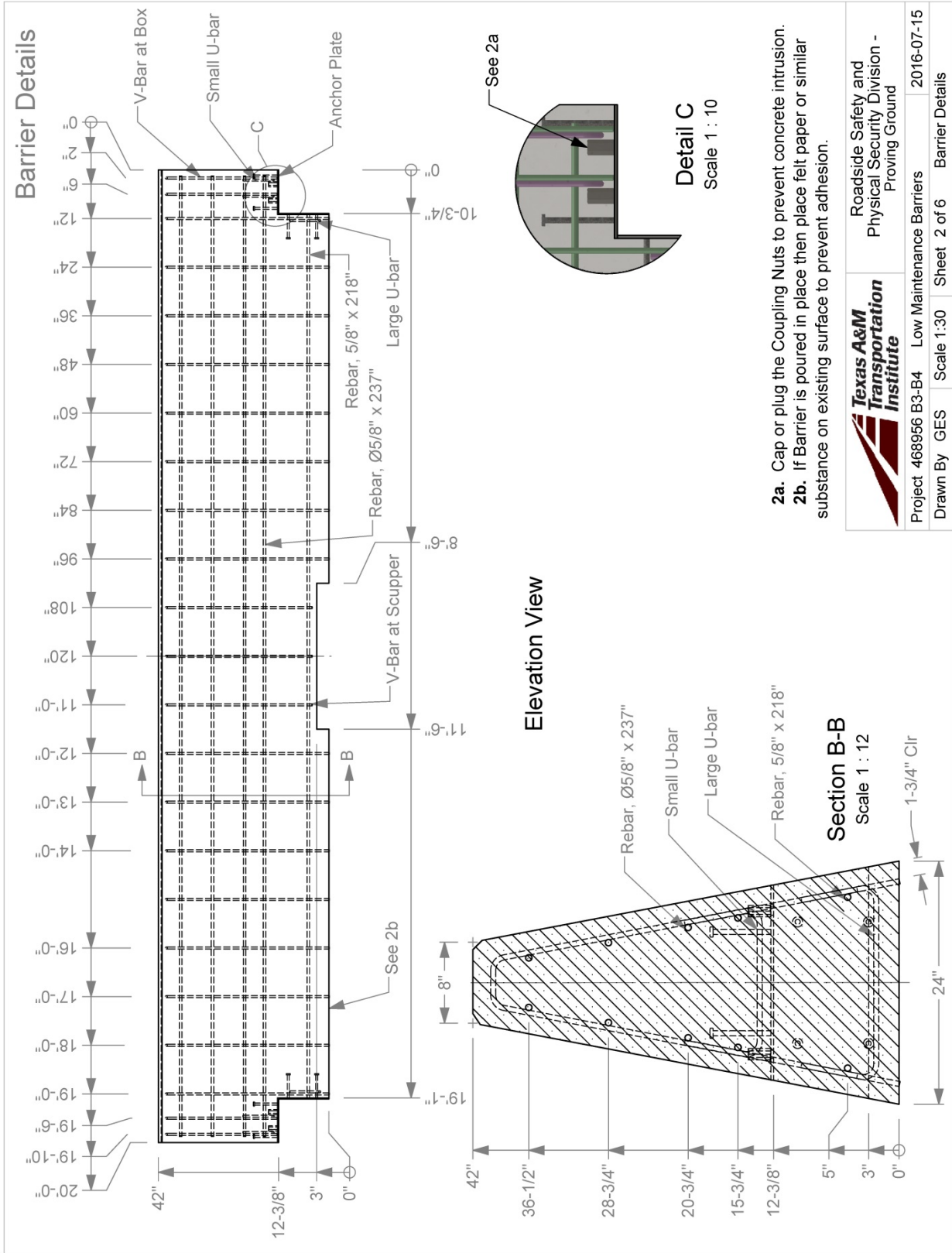
APPENDIX B: BOGIE TESTING PHASE I

B.1 TEST ARTICLE DETAILS

T:\1-ProjectFiles\468956-TxDOT-Low-MaintenanceCostMedianBarriers\468956-B-3\Drafting\468956-B3 Drawing

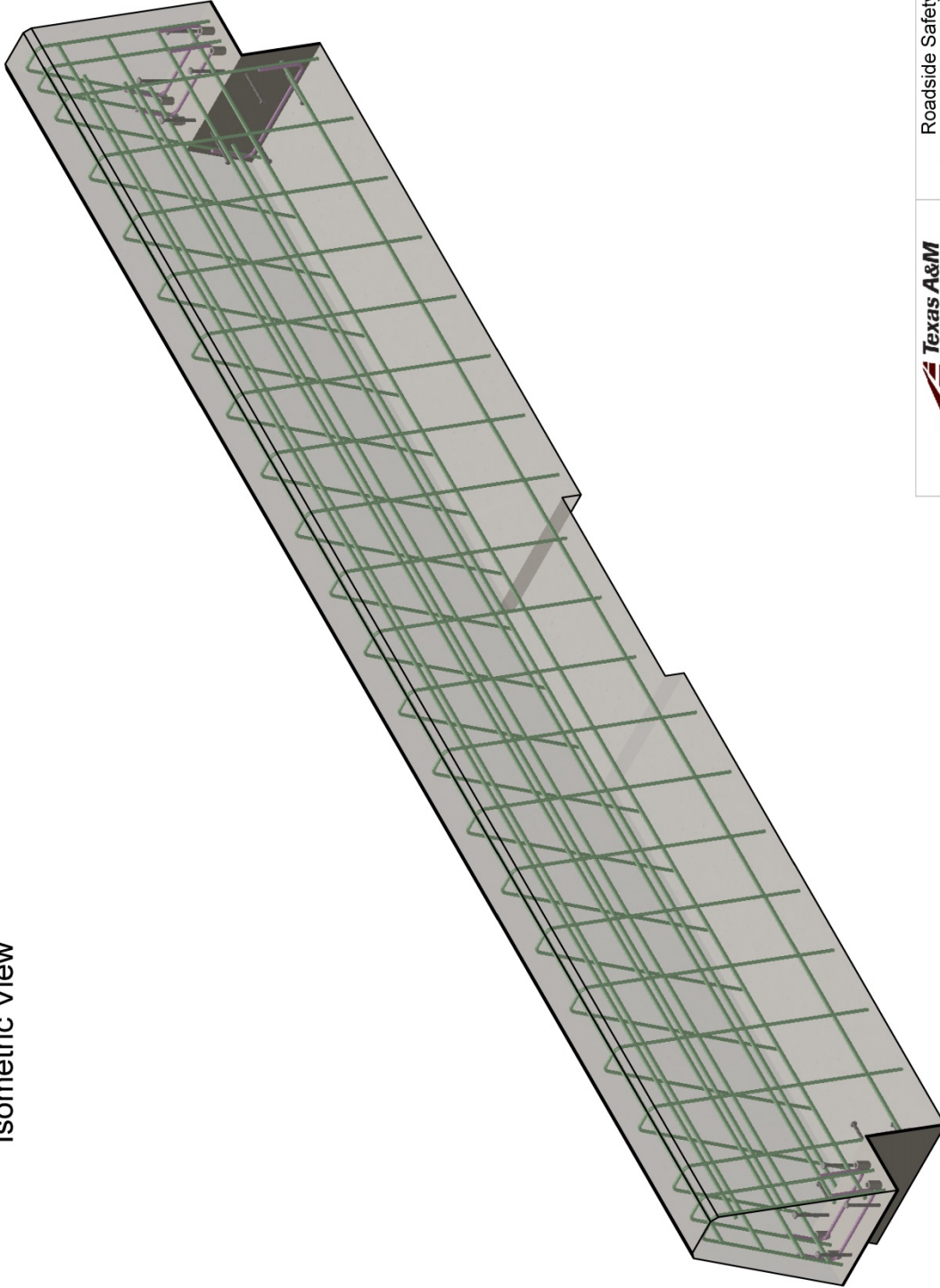


- 1a. Concrete is TxDOT Class C (3600 psi), and rebar is grade 60.
- 1b. Install Screw Anchors according to manufacturer's instructions.

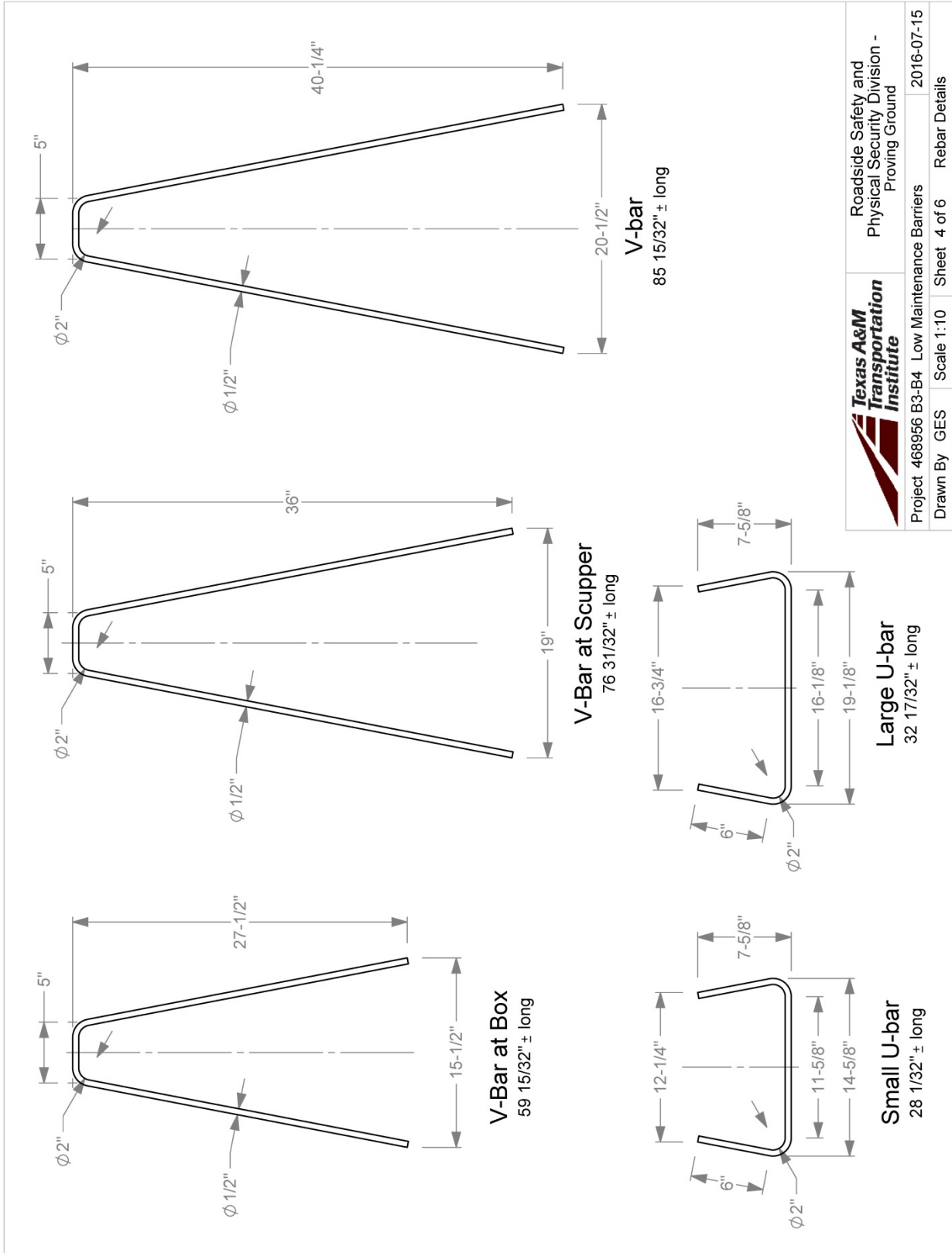


	Roadside Safety and Physical Security Division - Proving Ground		2016-07-15
	Project 468956 B3-B4	Low Maintenance Barriers	Barrier Details
Drawn By GES	Scale 1:30	Sheet 2 of 6	

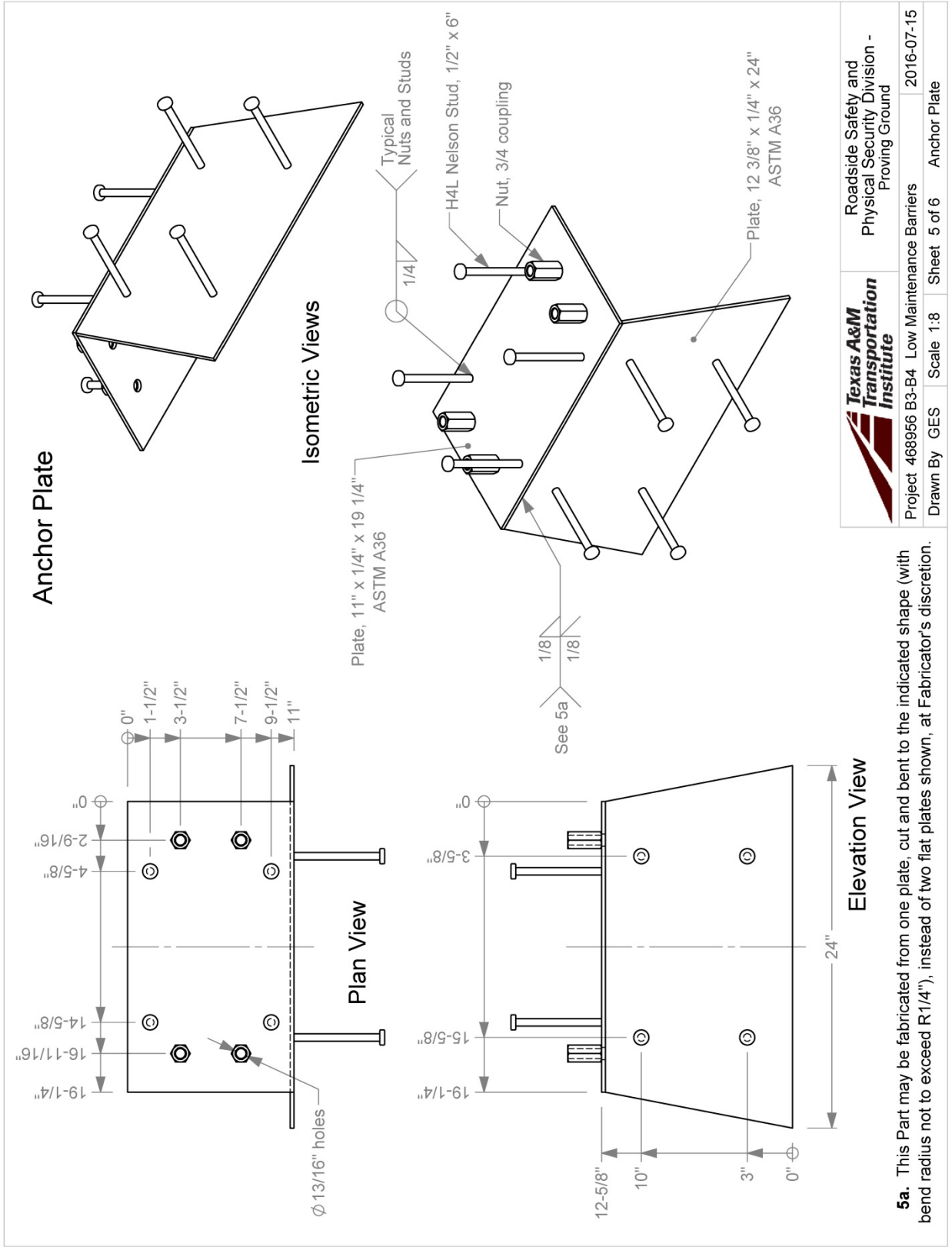
Isometric View



	Roadside Safety and Physical Security Division - Proving Ground		2016-07-15
	Project 468956 B3-B4	Low Maintenance Barriers	Sheet 3 of 6
Drawn By GES	Scale 1:20		Isometric View

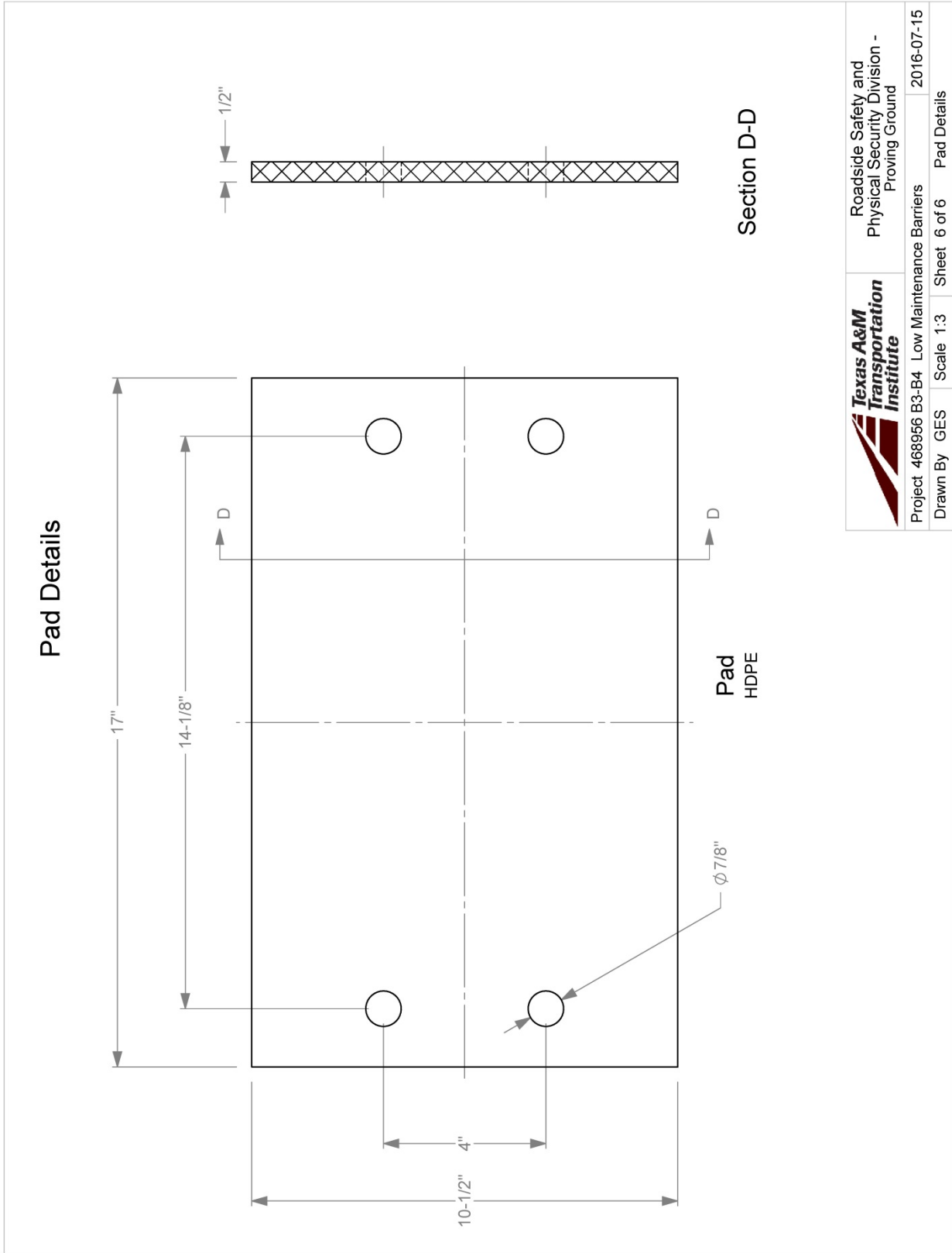


	Roadside Safety and Physical Security Division - Proving Ground		
	Project 468956 B3-B4 Low Maintenance Barriers	Sheet 4 of 6	Rebar Details
Drawn By GES	Scale 1:10	2016-07-15	



T:\1-ProjectFiles\468956-TXDOT-Low-MaintenanceCost\MedianBarriers\468956-B-3\Drafting\468956-B3 Drawing

	Roadside Safety and Physical Security Division - Proving Ground		
	Project 468956 B3-B4 Low Maintenance Barriers	2016-07-15	
Drawn By GES	Scale 1:8	Sheet 5 of 6	Anchor Plate

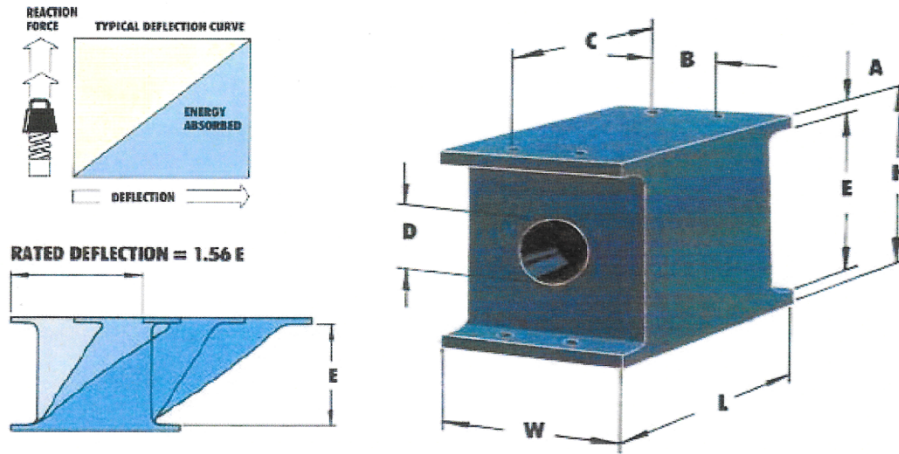


	Roadside Safety and Physical Security Division - Proving Ground	2016-07-15
Project 468956 B3-B4	Low Maintenance Barriers	Sheet 6 of 6
Drawn By GES	Scale 1:3	Pad Details

B.2 MATERIAL CERTIFICATION DOCUMENTS

468 957-B4-7

MORSE SHEAR FENDER



Dimensions (Inches)							
Part No.	W	H	L	A	B	C	D
E46496	10	11 5/8	15 3/4	5/8	4	14 1/8	4
E46498	12	13 7/8	18 7/8	11/16	5	16 15/16	5
E46500	14	16	22	3/4	5 1/2	19 3/4	6
E46502	16	18 9/16	25 1/8	15/16	7	22 5/8	7
E46504	18	20 15/16	28 1/4	1 1/16	8	25 3/8	8
E46506	20	22 15/16	31 3/8	1 1/16	9	28 1/4	9
E46508	22	25 3/8	34 1/2	1 1/4	10	31	10
E46510	24	27 3/4	37 3/4	1 3/8	11	33 7/8	11

Part No.	Shear				Compression			
	Energy Absorbed		Reaction		Energy Absorbed		Reaction	
	Ton-M	Ft.-Kips	Tonnes	Kips	Ton-M	Ft.-Kips	Tonnes	Kips
E46496	0.87	6.3	4.3	9.5	0.21	1.5	4.5	10
E46498	1.47	10.6	5.9	13	0.35	2.5	6.3	14
E46500	2.27	16.4	7.8	17.1	0.57	4.1	9.1	20
E46502	3.3	23.9	10.1	22.3	0.86	6.2	11.8	26
E46504	4.67	33.7	12.3	27.4	1.19	8.6	14.5	32
E46506	6.08	44	14.6	32.1	1.59	11.5	17.7	39
E46508	7.91	57.2	17.2	37.9	2.12	15.3	21.3	47
E46510	10.06	72.8	20.3	44.8	2.74	19.8	25.4	56

Morse Rubber LLC 3588 Main St. Keokuk, IA 52632
 T: 319 524 8430 F: 319 524 7290 info@morsrubber.com

Texas A&M Transportation Institute
 Proving Ground
 3100 SH 47, Bldg 7091
 Bryan, TX 77807
 Texas A&M University
 College Station, TX 77843
 Phone 979-845-6375

Quality Policy Form

5.7.2 Concrete Break

Revised by: G. E. Schroeder
 Approved by: C. E. But

Doc. No.	QPF 5.7.2	Revision Date:	2012-09-17
Revision:	5	Page:	1 of 1

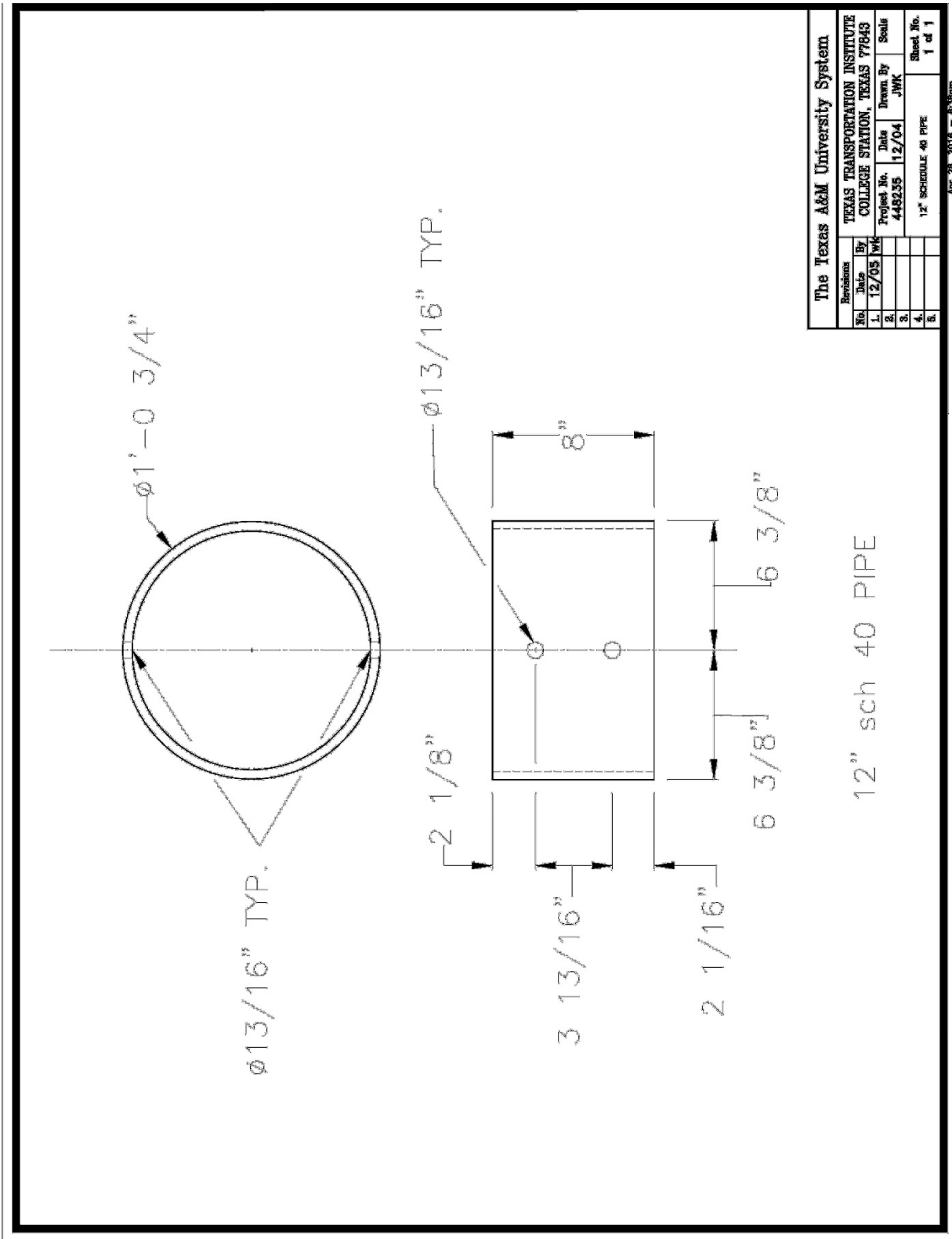
Project No.: 468956 Casting Date: 2016-09-09
 Placement: PARADE Mix Design P.S.I.: 4500

Truck No.	Batch Ticket	Yards

Printed name of Technician taking sample: Edwin Hays
 Signature of Technician taking sample: [Signature]
 Printed name of Technician breaking sample: Edwin Hays
 Signature of Technician breaking sample: [Signature]

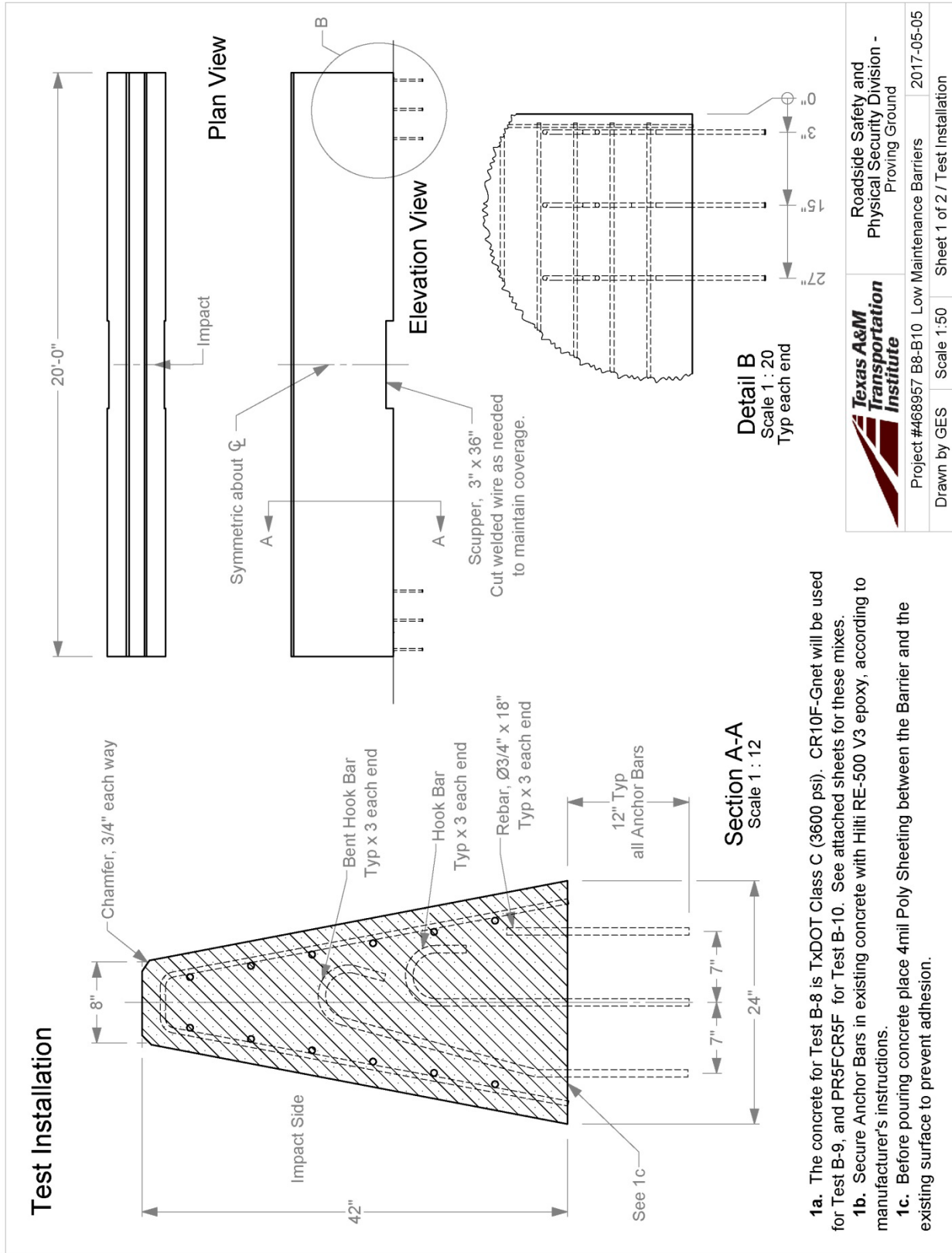
Break Date	Cylinder Age	Truck No.	Total Load (Pounds)	PSI Break	Average
2016-09-20	11 DAYS		89,000	3148	3313
			98,000	3466	
			94,000	3325	

APPENDIX C. DETAILS OF THE PIPE CYLINDERS FOR NOSE OF BOGIE

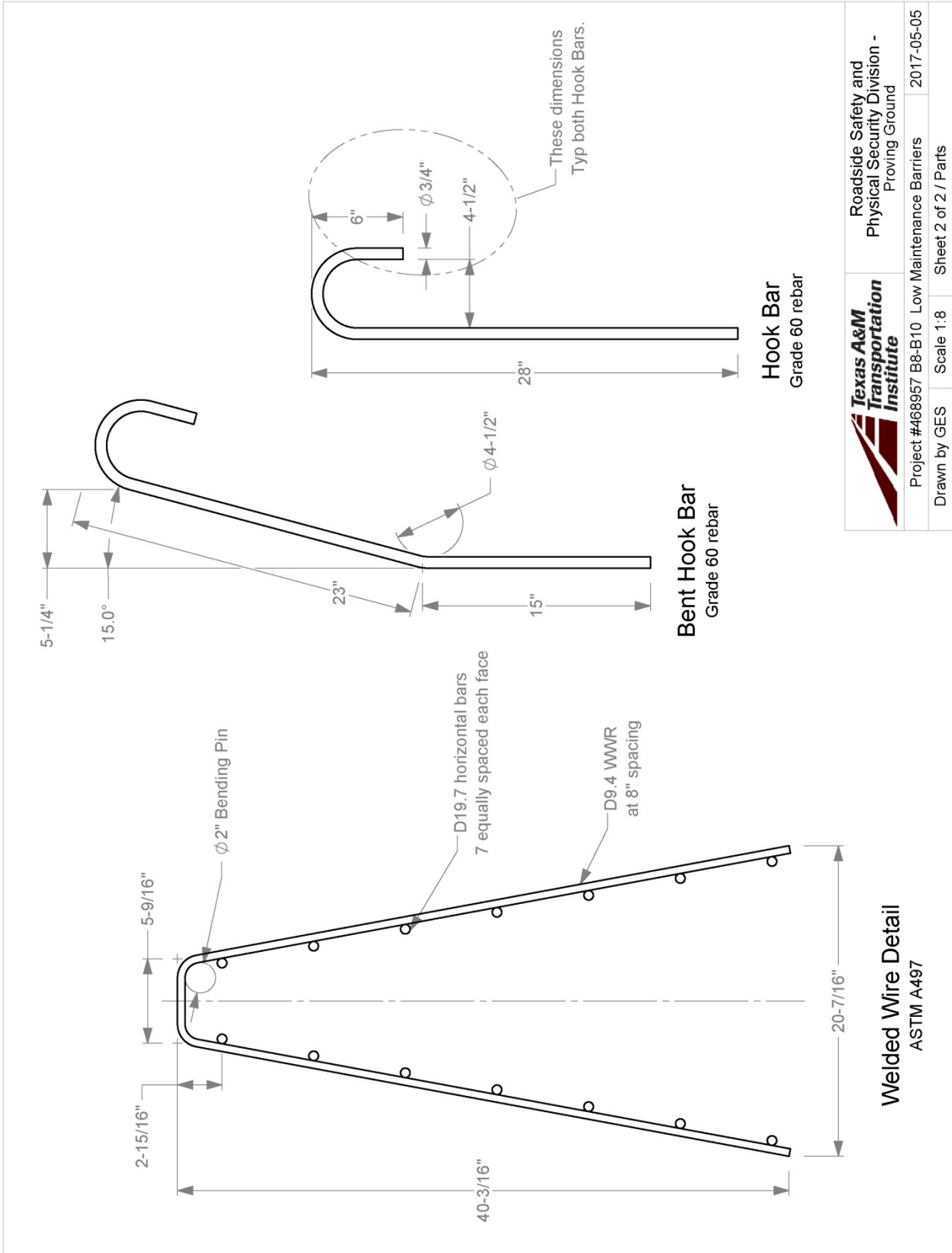


APPENDIX D. TEST ARTICLE DETAILS – BOGIE TESTING PHASE II

T:\1-ProjectFiles\468957-TxDOT-Low-MaintenanceCostMedianBarriers\468957-B-8\Drawings, 468957-B8-B10\468957-B8-B10 Drawing



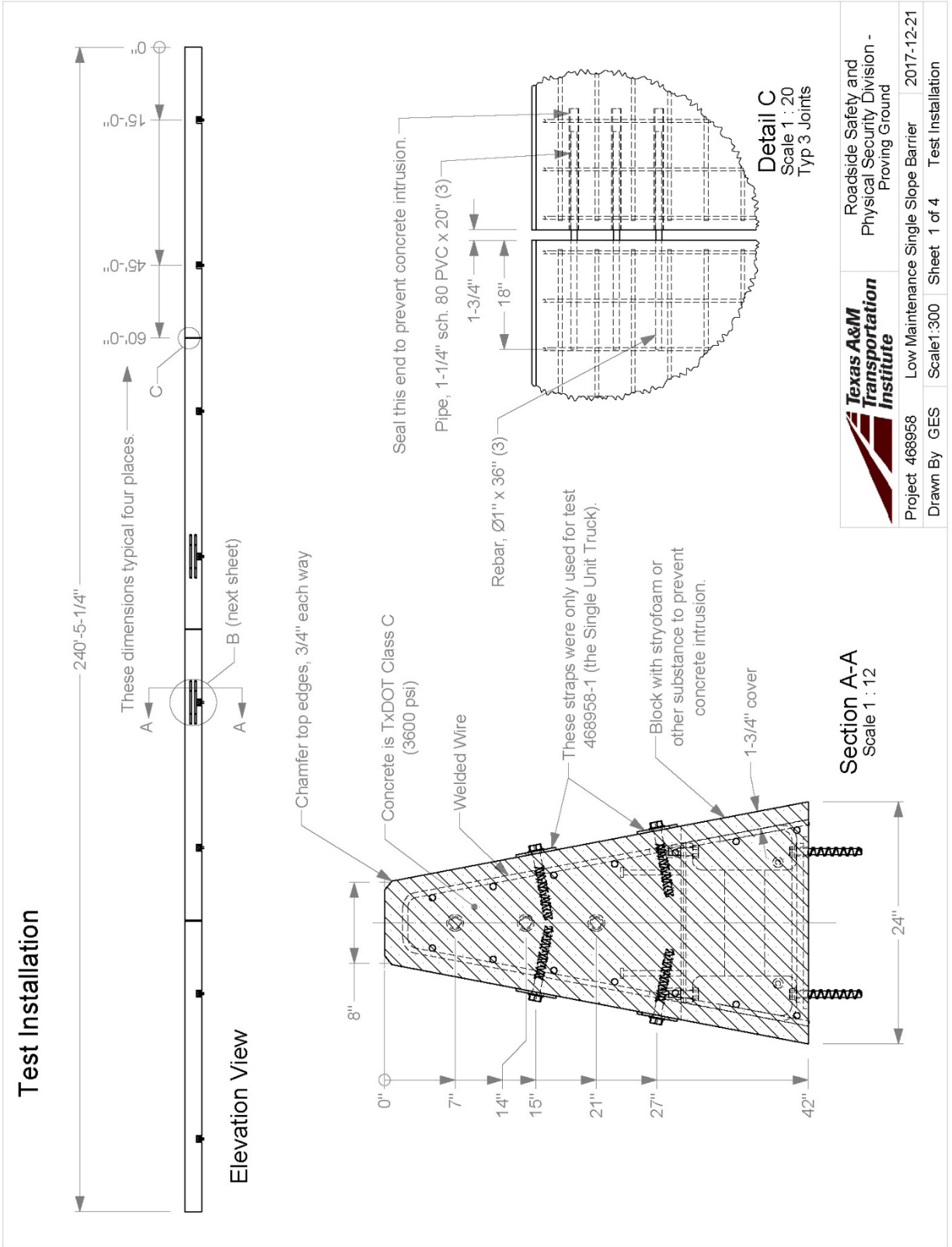
- 1a. The concrete for Test B-8 is TxDOT Class C (3600 psi). CR10F-Gnet will be used for Test B-9, and PR5FCR5F for Test B-10. See attached sheets for these mixes.
- 1b. Secure Anchor Bars in existing concrete with Hilti RE-500 V3 epoxy, according to manufacturer's instructions.
- 1c. Before pouring concrete place 4mil Poly Sheeting between the Barrier and the existing surface to prevent adhesion.



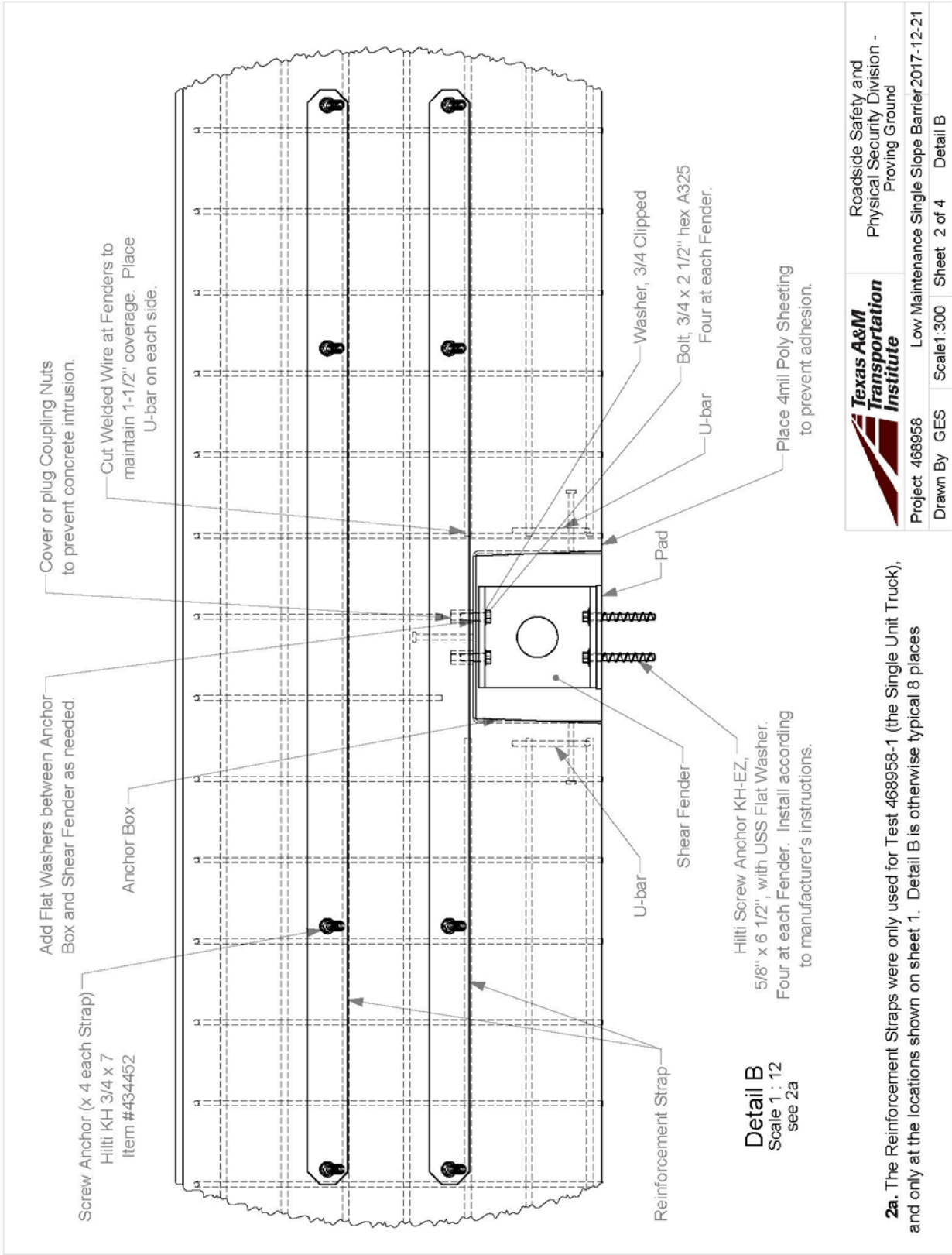
	Roadside Safety and Physical Security Division - Proving Ground	2017-05-05
	Project #468957 B8-B10 Low Maintenance Barriers	2017-05-05
Drawn by GES	Scale 1:8	Sheet 2 of 2 / Parts

APPENDIX E. DETAILS OF THE TXDOT RUBBER MOUNTED SINGLE SLOPE BARRIER

T:\M-ProjectFiles\468958-TXDOT-Low-MaintenanceCostMedianBarrier\Drawing, 468958\468958 Drawing



	Roadside Safety and Physical Security Division - Proving Ground
	Project 468958 Low Maintenance Single Slope Barrier 2017-12-21
Drawn By GES	Sheet 1 of 4
Scale: 1:300	Test Installation



Cover or plug Coupling Nuts to prevent concrete intrusion.

Cut Welded Wire at Fenders to maintain 1-1/2" coverage. Place U-bar on each side.

Add Flat Washers between Anchor Box and Shear Fender as needed.

Screw Anchor (x 4 each Strap)
Hilti KH 3/4 x 7
Item #434452

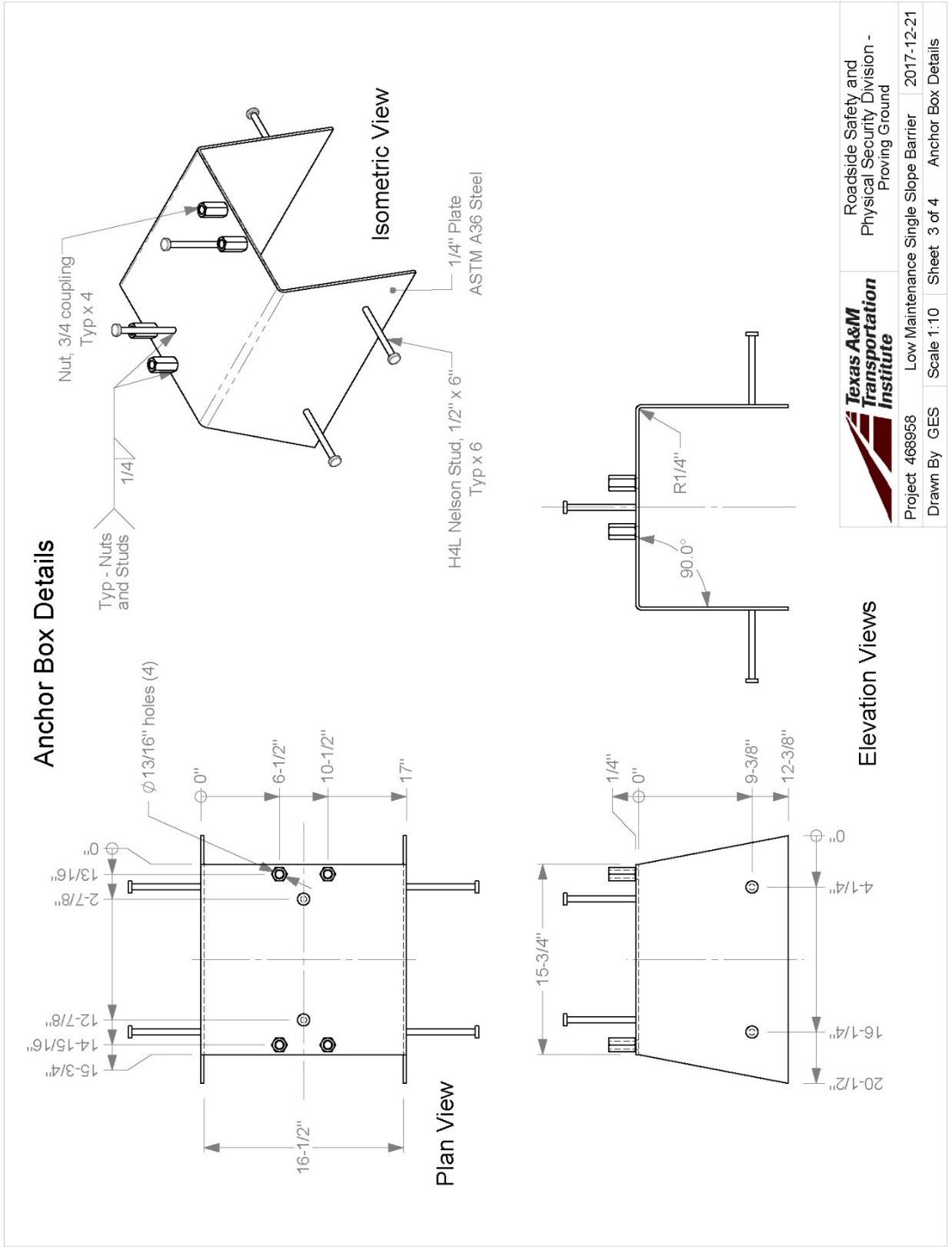
Detail B
Scale 1 : 12
see 2a

Hilti Screw Anchor KH-EZ,
5/8" x 6 1/2", with USS Flat Washer.
Four at each Fender. Install according
to manufacturer's instructions.

Place 4mil Poly Sheeting
to prevent adhesion.

2a. The Reinforcement Straps were only used for Test 468958-1 (the Single Unit Truck), and only at the locations shown on sheet 1. Detail B is otherwise typical 8 places

	Roadside Safety and Physical Security Division - Proving Ground	
	Project 468958	Low Maintenance Single Slope Barrier 2017-12-21
Drawn By GES	Scale 1:300	Sheet 2 of 4 Detail B



APPENDIX F. SUPPORTING CERTIFICATION DOCUMENTS



MATERIAL CERTIFICATION OF COMPLIANCE and TEST REPORT Dayton, TX

Insteel Wire Products hereby certifies that the Steel Welded Wire Reinforcement material identified below has been manufactured in accordance with and meets the requirements of: ASTM – A 1064 – 16.

Sales Order Number: 460662-1

BOL Number: 00226029

Job Number: 768114

Product Description: VAR X 8 D19.7/D9.4 (.501/.346) DR 82.7" (+1.375",+1.375")

Item: 53D-229768

X 31' 1" (17",4") 42" SSCB (1) or (1F) 539-270680-Epoxy

53D-229768-Bent 536-229767-Flat

TENSILE TESTS

Longitudinal	Wire Size		Test No.	Deformed Nominal Lbs/Ft	Nominal Wire DIA (Inches)	Nominal Area Sq. In.	Tensile	ROA	Bend	Heat No
	Transverse	Convolutd								
D19.7	---	---	1	0.6698	0.501	0.1970	100562	---	PASS	5314460602
D19.7	---	---	2	0.6698	0.501	0.1970	101709	---	PASS	5314460602
---	D9.4	---	1	0.3196	0.346	0.0940	103998	---	PASS	5314477302
---	D9.4	---	2	0.3196	0.346	0.0940	102069	---	PASS	5314477302

WELD SHEAR TESTS

WIRE SIZES: D19.7 / D9.4

Test Number	1	2	3	4	Average	Pass/Fail
Break Load (Lbs Of Force)	6992	11892	10445	8945	9569	PASS


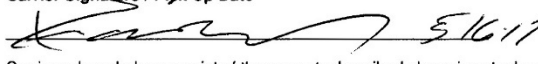

MINIMUM BREAK LOAD REQUIRED: 6895 LBS OF FORCE

The use of this product conforms with Buy America Requirements set forth in 23 CFR Subpart D, Section 635.410, Buy America Requirements and Title 49 – Transportation, Chapter VI – Federal Transit Administration, Department of Transportation Part 661 – Buy America Requirements – Surface Transportation Assistance Act of 1982, As Amended.

Quality Assurance Manager:

Nora J. Jones

Date: 12-MAY-2017

		INSTEEL WIRE PRODUCTS COMPANY UNIFORM STRAIGHT BILL OF LADING ORIGINAL - NOT NEGOTIABLE		Bill of Lading No. 00226029-7144137 Date: 16-MAY-17 Stop 1 of 1		Page 1 of 1	
SHIP FROM				CARRIER			
Name: INSTEEL WIRE PRODUCTS COMPANY Address: 500 KLEMP ROAD DAYTON, TX 77535				CUSTOMER TRUCK			
SHIP TO DESTINATION (CONSIGNEE)				FREIGHT PAYMENT METHOD			
Name: TEXAS TRANSPORTATION INSTITUTE Address: SAFETY & STRUCTURAL SYSTEMS DIV. 3100 SH 47 BLDG 7091 BRYAN TX 77807				<input type="checkbox"/> Prepaid <input checked="" type="checkbox"/> Customer Truck			
SPECIAL INSTRUCTIONS/COMMENTS							
Customer Truck							
CARGO				NOTE: Wire carriers, if used, remain Insteel's property. To return, please call 1-336-719-9000			
Hazardous Material	Units	Package Type	Sales Order No.	Unit Weight	Weight	Commodity Description, Special Marks, Exceptions	
	17 EA	SHEETS	460662	394	6690	53D-229768 VAR X 8 D19.7/D9.4 (.501/.346) DR 82.7" (+1.375",+1.375") X 31' 1" (17",4") 42" SSCB (1) or (1F) 539-270680-Epoxy 53D-229768-Bent 536-229767-Flat	
Total Weight:				6,690 LBS			
RECEIVED, subject exclusively to the Terms and Conditions stated herein to the exclusion of any rates, classifications, or tariffs established or maintained by the Carrier. The Carrier has received from the Shipper, the property described above in actual good order and condition, except as noted, at the location noted in the "SHIP FROM" Box above and will properly and carefully load, handle, carry, keep, care for, and deliver it to the destination noted in the "SHIP TO" Box above, in exchange for certain freight charges, the adequacy of which is hereby acknowledged by the Carrier. Notwithstanding the fact that Shipper may provide recommendations and personnel to assist in loading the Cargo on Carrier's vehicles, Carrier and its agents and employees remain solely responsible for proper arrangement of the Cargo on Carrier's vehicles. It is mutually agreed by and between the Shipper and Carrier that every service to be performed hereunder is subject to the Terms and Conditions hereof. The Carrier hereby certifies that it is familiar with all of those Terms and Conditions and that it irrevocably agrees to them for itself and its assigns.				NOTE QUANTITY & QUALITY EXCEPTIONS AT DESTINATION HERE			
				NOTE: Failure to specify exceptions at destination here does not affect the Shipper's rights against the Carrier.			
				Carrier Signature / Pick Up Date  5/16/17 Carrier acknowledges receipt of the property described above in actual good order and condition, except as noted. By signing this form, the driver accepts the Shipper's Terms and Conditions as provided. A Driver copy of the Terms and Conditions page may be requested from the Shipper, if desired.			
Shipper Signature / Date  5-16-17 Shipper certifies that the property described above is properly packaged, marked, and labeled and in proper condition for transportation according to the applicable regulations of the DOT.				Customer Signature / Delivery Date _____ Customer acknowledges receipt of the property described above in actual good order and condition, except as noted.			



5.7.2 Concrete Break
 Revised by: G. E. Schroeder
 Approved by: C. E. But

Doc. No. QPF 5.7.2
 Revision: 5
 Page: 1 of 1
 Revision Date: 2012-09-17

Quality Policy Form

Project No.: 468958 Casting Date: 2017-11-28
 Placement: SINGLE SLOPE Mix Design P.S.I.: CLASS C

Truck No.	Batch Ticket	Yards
1		6
2		6

Printed name of Technician taking sample: GREG FRITTE
 Signature of Technician taking sample: [Signature]
 Printed name of Technician breaking sample: GREG FRITTE
 Signature of Technician breaking sample: [Signature]

Break Date	Cylinder Age	Truck No.	Total Load (Pounds)	PSI Break	Average
2017-12-18	20 DAYS	1	131500	4650	
		1	139500	4935	4875
		1	142500	5040	
		2	126500	4475	
		2	134500	4760	4770
		2	143500	5075	



Quality Policy Form

5.7.2 Concrete Break

Revised by: G. E. Schroeder
 Approved by: C. E. But

Doc. No.	QPF 5.7.2	Revision:	5	Page:	1 of 1
Revision Date:	2012-09-17				

Project No.: 468958 Casting Date: 2017-12-4

Placement: SINGLE SLOPE Mix Design P.S.I.: CLASS C

Truck No.	Batch Ticket	Yards
1		6
2		6

Printed name of Technician taking sample: GREG FRITZ
 Signature of Technician taking sample: [Signature]
 Printed name of Technician breaking sample: GREG FRITZ
 Signature of Technician breaking sample: [Signature]

Break Date	Cylinder Age	Truck No.	Total Load (Pounds)	PSI Break	Average
2017-12-18	14 DAYS	1	133500	4720	
		1	130000	4600	4750
		1	139500	4935	
		2	129500	4580	
		2	138500	4900	4810
		3	140000	4950	



Quality Policy Form Proving Ground 3102 S8447, Bldg 7051 Bryan, TX 77807	Revised by: G. E. Schroeder Approved by: C. E. But	5.7.2 Concrete Break	Doc. No. QPF 5.7.2	Revision Date: 2012-09-17
	Casting Date: 2017-12-11	Revision: 5	Revision: 5	Page: 1 of 1

Project No.: **468958** Placement: **SINGLE SLOPE** Casting Date: **2017-12-11**
 Mix Design P.S.I.: **CLASS C**

Truck No.	Batch Ticket	Yards
1		6
2		6

Printed name of Technician taking sample: **GREG FRITZ**
 Signature of Technician taking sample: *[Signature]*
 Printed name of Technician breaking sample: **GREG FRITZ**
 Signature of Technician breaking sample: *[Signature]*

Break Date	Cylinder Age	Truck No.	Total Load (Pounds)	PSI Break	Average
2017-12-18	7 days	1	120000	4245	
		1	117000	4140	4220
		1	121000	4280	
		2	87,000	3080	
		2	81,500	2880	3050
		2	90,000	3185	



Quality Policy Form

5.7.2 Concrete Break

Revised by: G. E. Schroeder
 Approved by: C. E. But

Doc. No.	QPF 5.7.2	Revision Date:	2012-09-17
Revision:	5	Page:	1 of 1

Project No.: **468958**

Casting Date: **2017-12-13**

Placement: **SINGLE SLOPE**

Mix Design P.S.I.: **CLASS C**

Truck No.	Batch Ticket	Yards
1		6
2		6

Printed name of Technician taking sample: **GREG FRITZ**
 Signature of Technician taking sample: *[Signature]*
 Printed name of Technician breaking sample: **GREG FRITZ**
 Signature of Technician breaking sample: *[Signature]*

Break Date	Cylinder Age	Truck No.	Total Load (Pounds)	PSI Break	Average
2017-12-18	50±15	1	113,500	4015	
		1	96,500	3415	3760
		1	109,000	3855	
		2	108,000	3820	
		2	112,500	3980	4005
		2	119,000	4210	

APPENDIX G. MASH TEST 4-10 (CRASH TEST NO. 468958-3)

G.1 VEHICLE PROPERTIES AND INFORMATION

Table G.1. Vehicle Properties for Test No. 468958-3.

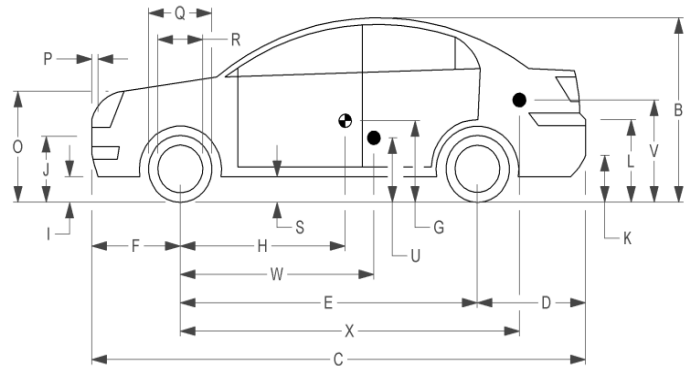
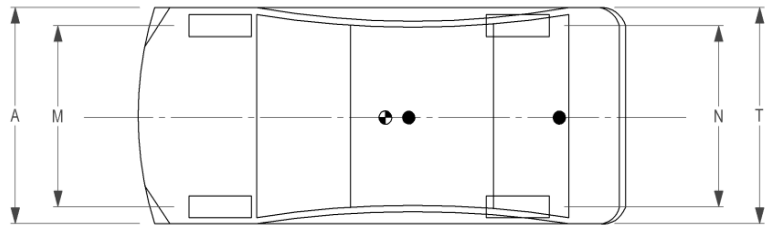
Date: 2017-12-18 Test No.: 468958-3 VIN No.: KNADH4A37B6725845
 Year: 2011 Make: Kia Model: Rio
 Tire Inflation Pressure: 32 psi Odometer: 168958-3 Tire Size: 185/65R14
 Describe any damage to the vehicle prior to test: None

• Denotes accelerometer location.

NOTES: None

Engine Type: 4 cylinder
 Engine CID: 1.6liter
 Transmission Type:
 Auto or Manual
 FWD RWD 4WD
 Optional Equipment:
None

Dummy Data:
 Type: 50th percentile male
 Mass: 165 lb
 Seat Position: Driver



Geometry: inches

A	<u>66.38</u>	F	<u>33.00</u>	K	<u>10.50</u>	P	<u>4.12</u>	U	<u>15.00</u>
B	<u>58.00</u>	G	<u>-----</u>	L	<u>24.50</u>	Q	<u>22.50</u>	V	<u>20.50</u>
C	<u>165.75</u>	H	<u>35.74</u>	M	<u>57.75</u>	R	<u>15.50</u>	W	<u>35.70</u>
D	<u>34.00</u>	I	<u>7.75</u>	N	<u>57.75</u>	S	<u>9.00</u>	X	<u>106.25</u>
E	<u>98.75</u>	J	<u>21.00</u>	O	<u>28.00</u>	T	<u>66.25</u>		
	Wheel Center Ht Front	<u>11.00</u>		Wheel Center Ht Rear	<u>11.00</u>		W-H	<u>0</u>	

GVWR Ratings:	Mass: lb	Curb	Test Inertial	Gross Static
Front	<u>1718</u>	M_{front}	<u>1581</u>	<u>1652</u>
Back	<u>1874</u>	M_{rear}	<u>887</u>	<u>969</u>
Total	<u>3638</u>	M_{Total}	<u>1468</u>	<u>2621</u>

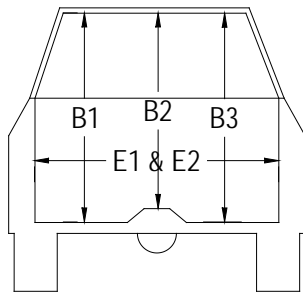
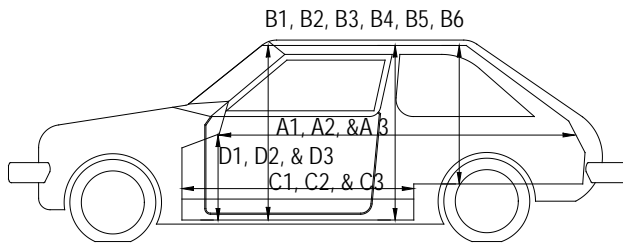
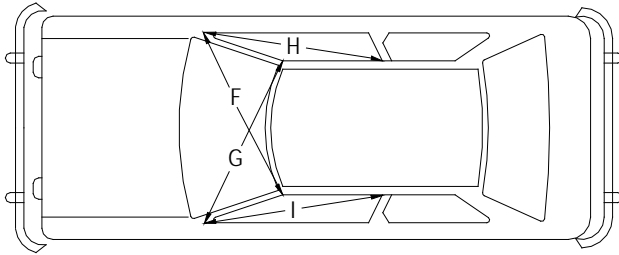
Allowable TIM = 2420 lb ±55 lb | Allowable GSM = 2585 lb ± 55 lb

Mass Distribution:

lb LF: 775 RF: 792 LR: 403 RR: 486

Table G.3. Occupant Compartment Measurements of Vehicle for Test No. 468958-3.

Date: 2017-12-18 Test No.: 468958-3 VIN No.: KNADH4A37B6725845
 Year: 2011 Make: Kia Model: Rio



OCCUPANT COMPARTMENT DEFORMATION MEASUREMENT

	Before	After (inches)	Differ.
A1	67.50	67.00	-0.50
A2	67.00	67.00	0.00
A3	67.50	67.50	0.00
B1	40.50	39.00	-1.50
B2	37.00	37.00	0.00
B3	40.50	40.50	0.00
B4	36.00	36.00	0.00
B5	35.50	35.50	0.00
B6	36.00	36.00	0.00
C1	26.00	26.00	0.00
C2	-----	-----	-----
C3	26.00	26.00	0.00
D1	9.50	8.00	-1.50
D2	-----	-----	-----
D3	9.50	9.50	0.00
E1	51.50	51.50	0.00
E2	51.25	51.25	0.00
F	51.00	51.00	0.00
G	51.00	51.00	0.00
H	37.00	37.00	0.00
I	37.00	37.00	0.00
J*	51.00	51.00	0.00

*Lateral area across the cab from driver's side kickpanel to passenger's side kickpanel.

G.2 SEQUENTIAL PHOTOGRAPHS

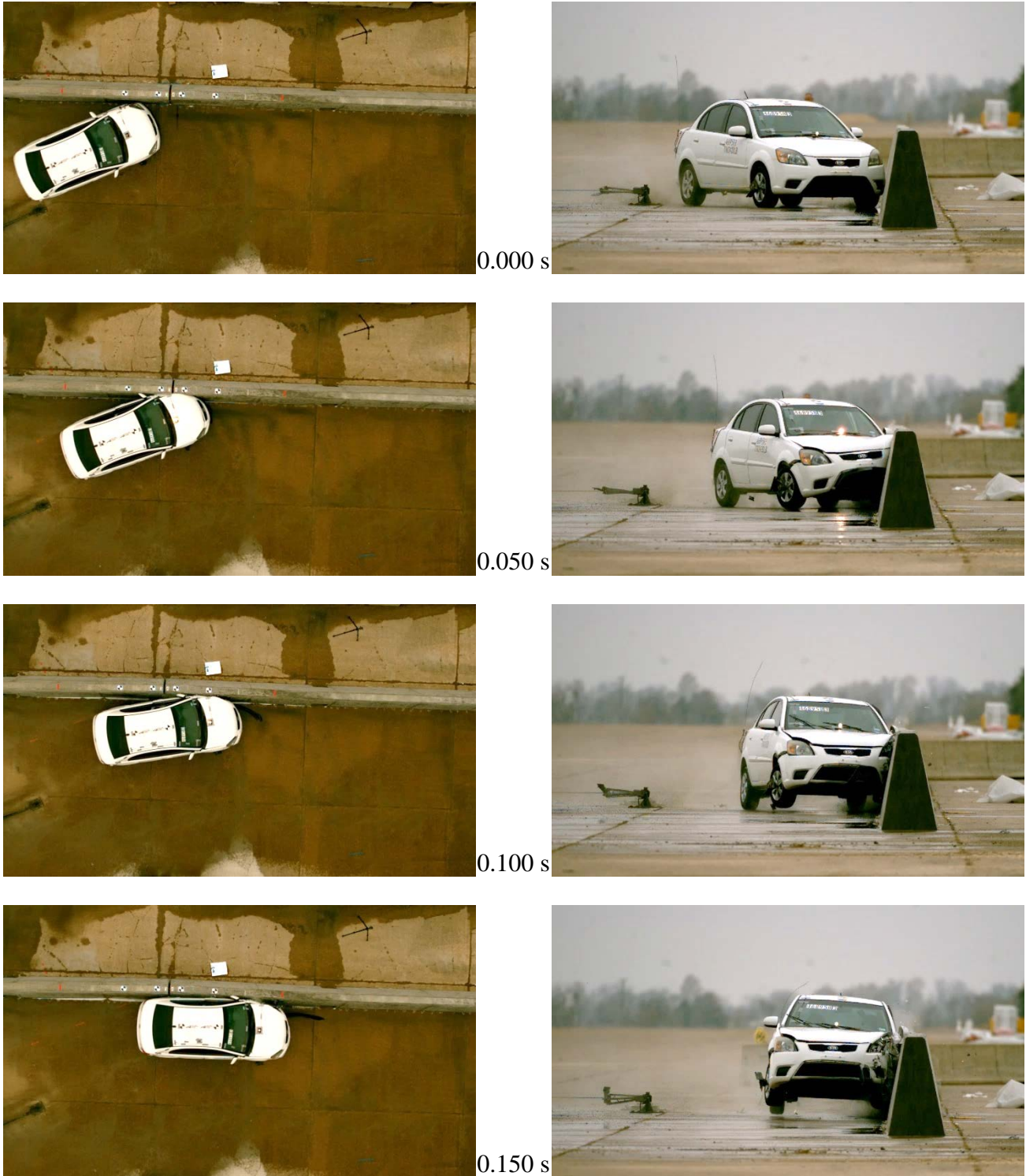
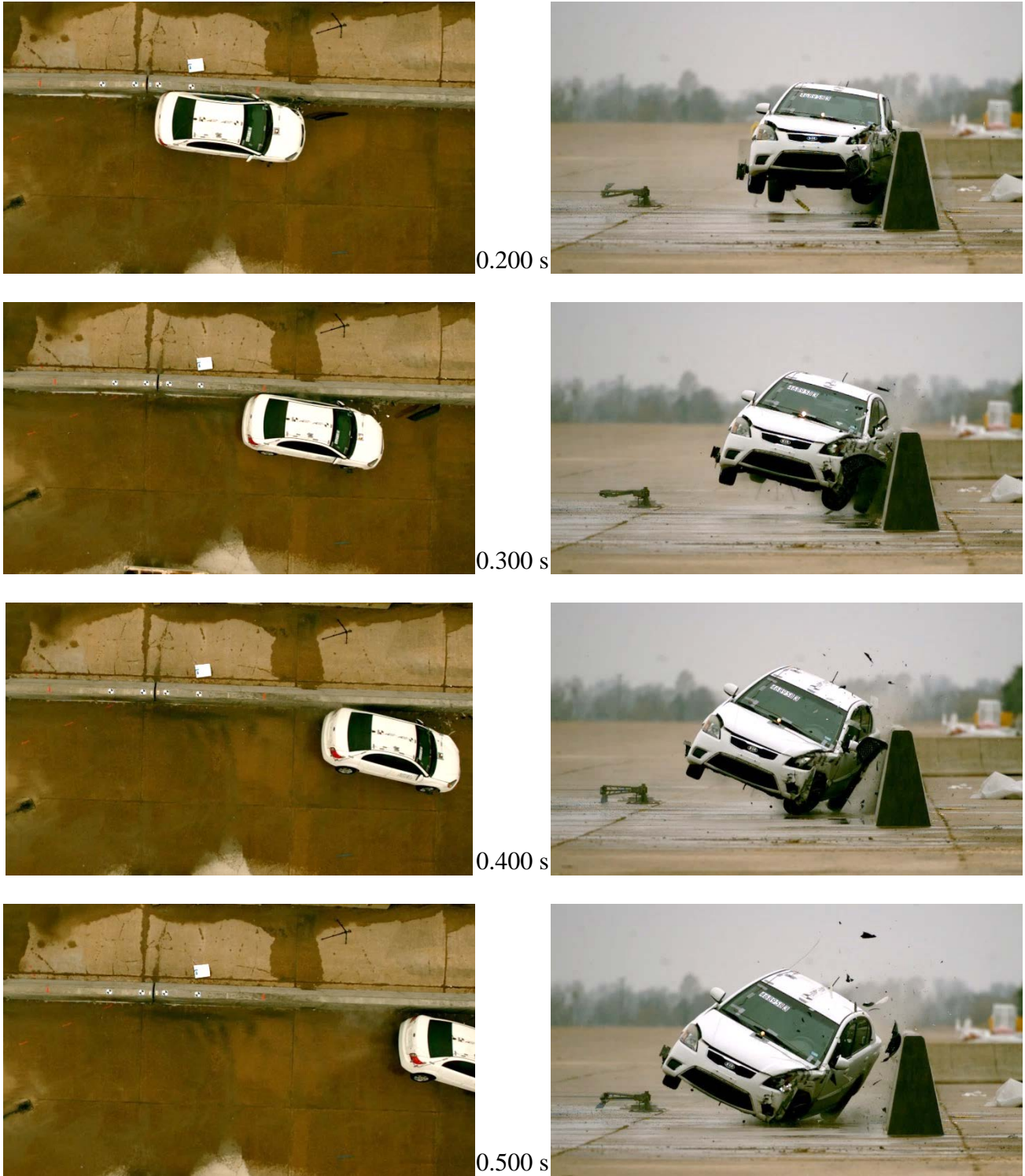


Figure G.1. Sequential Photographs for Test No. 468958-3 (Overhead and Frontal Views).



**Figure G.1. Sequential Photographs for Test No. 468958-3 (Overhead and Frontal Views)
(Continued).**



0.000 s



0.200 s



0.050 s



0.300 s



0.100 s



0.400 s



0.150 s



0.500 s

Figure G.2. Sequential Photographs for Test No. 468958-3 (Rear View).

G.3 VEHICLE ANGULAR DISPLACEMENT

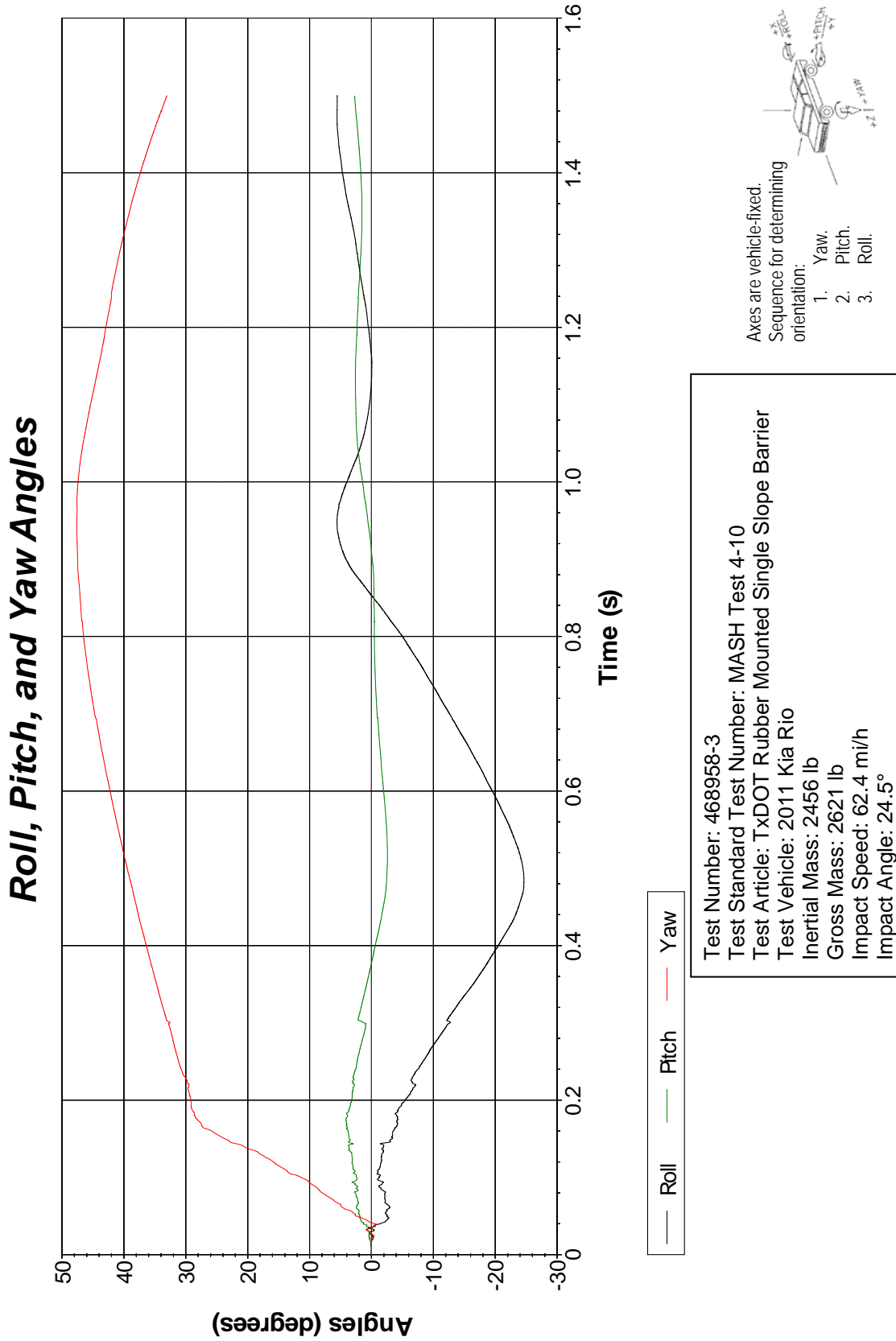


Figure G.3. Vehicle Angular Displacements for Test No. 468958-3.

G.4 VEHICLE ACCELERATIONS

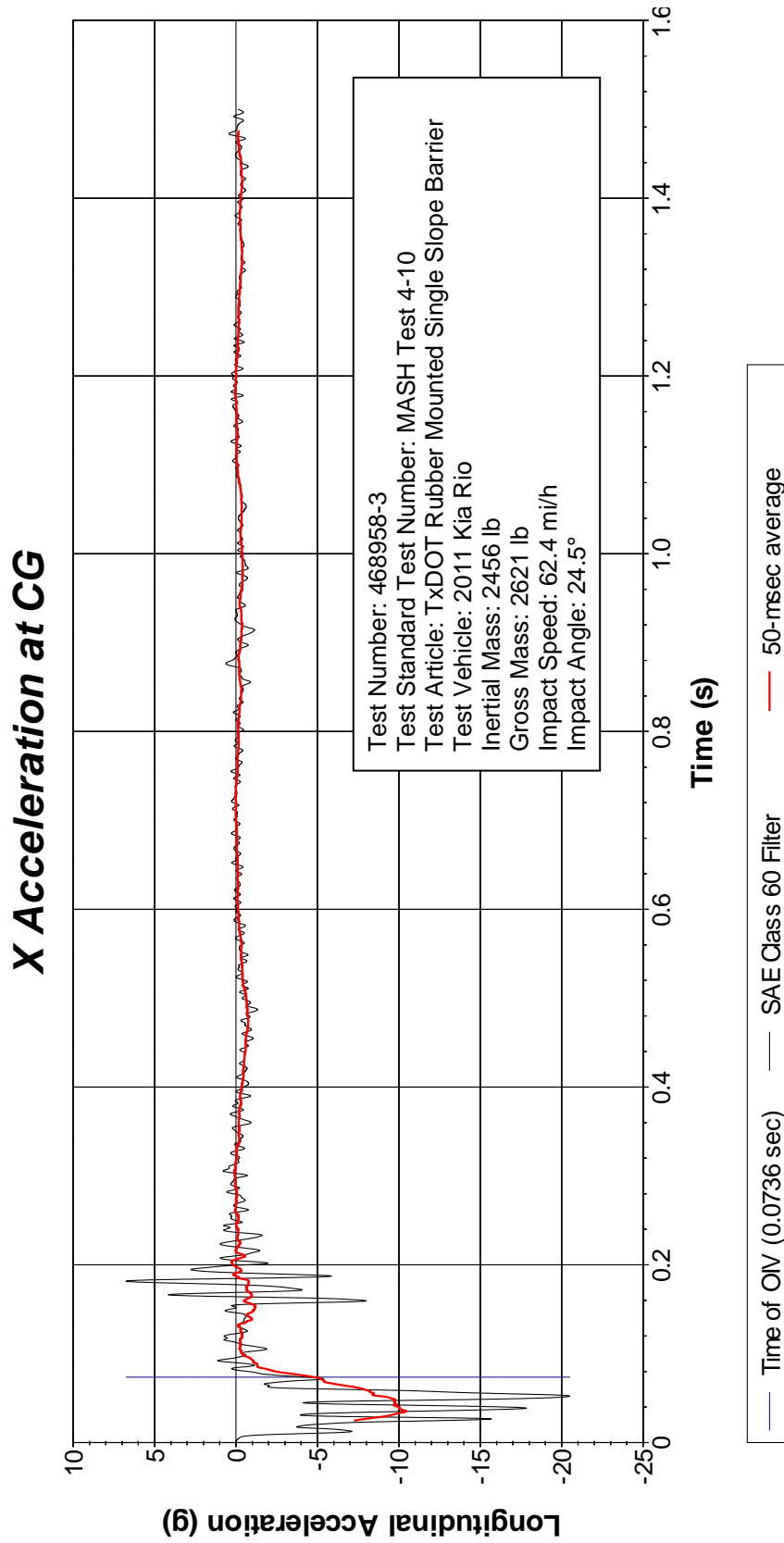


Figure G.4. Vehicle Longitudinal Accelerometer Trace for Test No. 468958-3 (Accelerometer Located at Center of Gravity).

Y Acceleration at CG

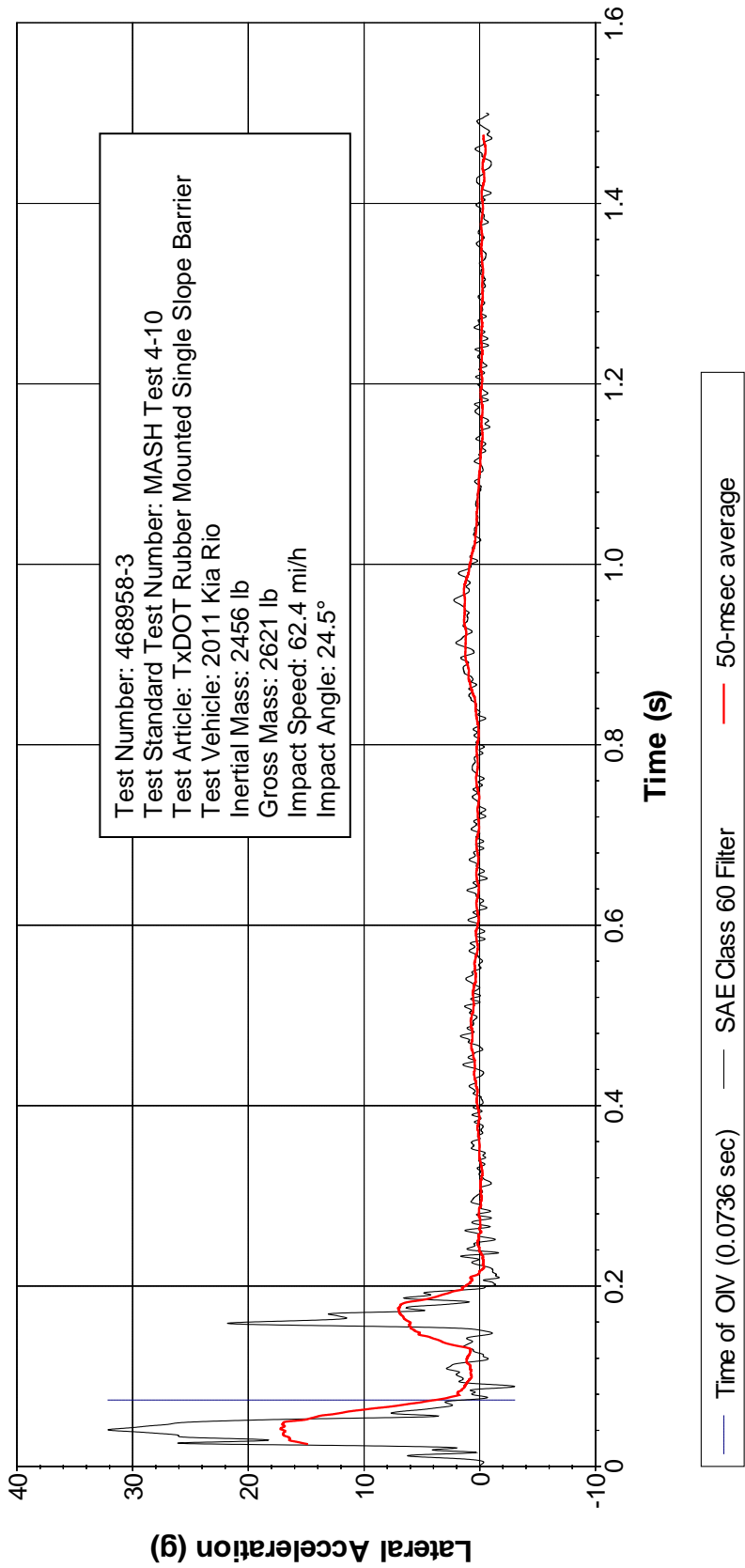


Figure G.5. Vehicle Lateral Accelerometer Trace for Test No. 468958-3 (Accelerometer Located at Center of Gravity).

Z Acceleration at CG

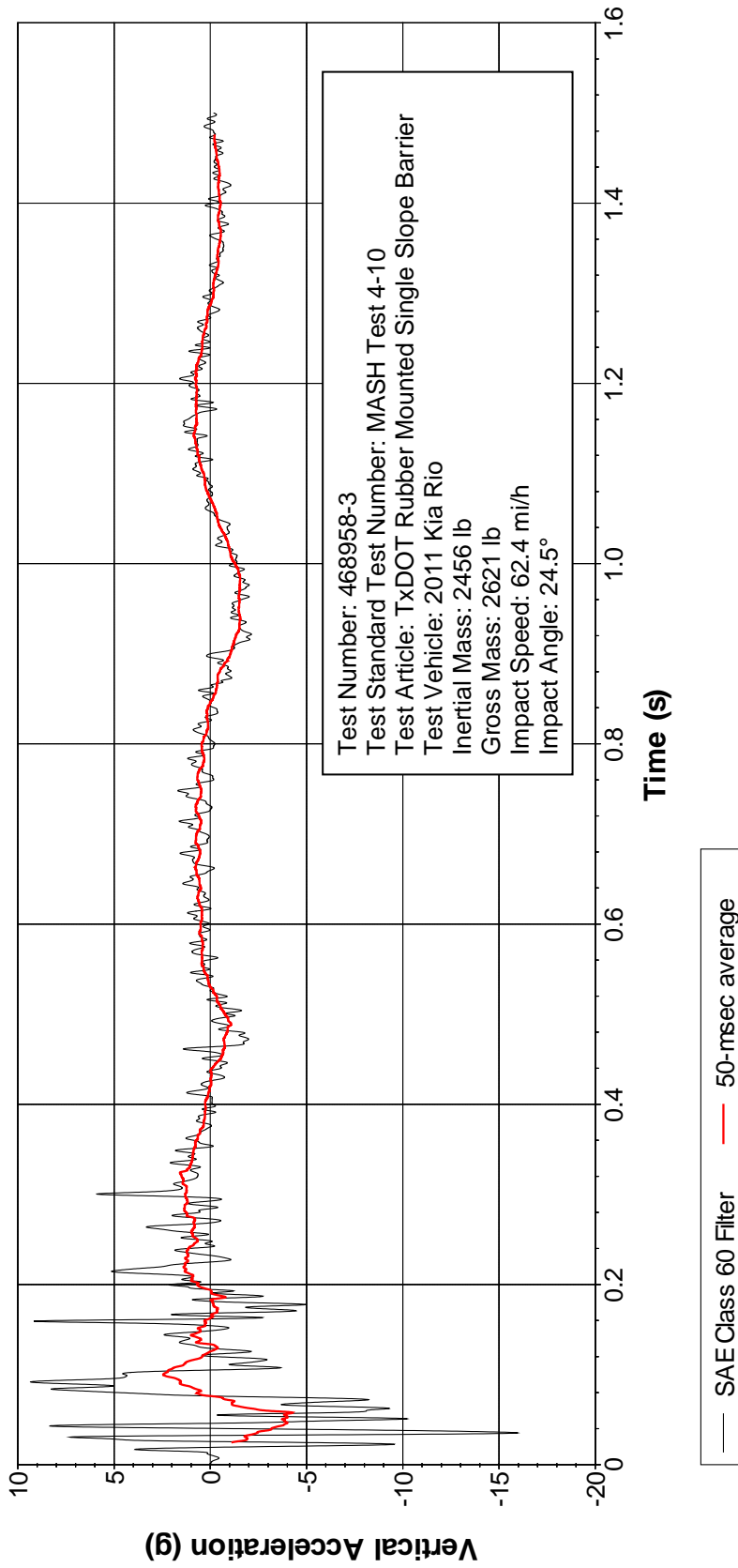


Figure G.6. Vehicle Vertical Accelerometer Trace for Test No. 468958-3 (Accelerometer Located at Center of Gravity).

X Acceleration Rear of CG

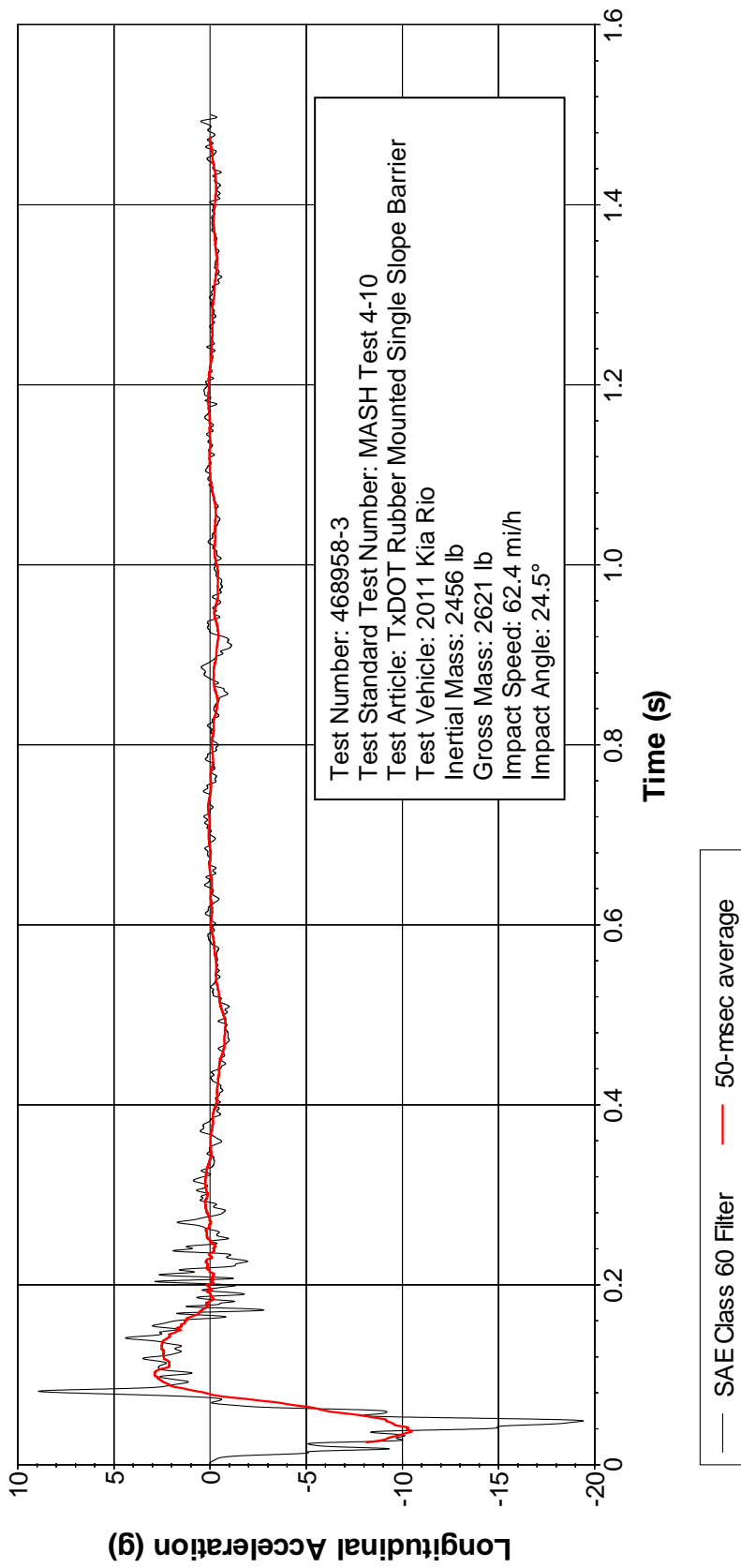


Figure G.7. Vehicle Longitudinal Accelerometer Trace for Test No. 468958-3 (Accelerometer Located Rear of Center of Gravity).

Y Acceleration Rear of CG

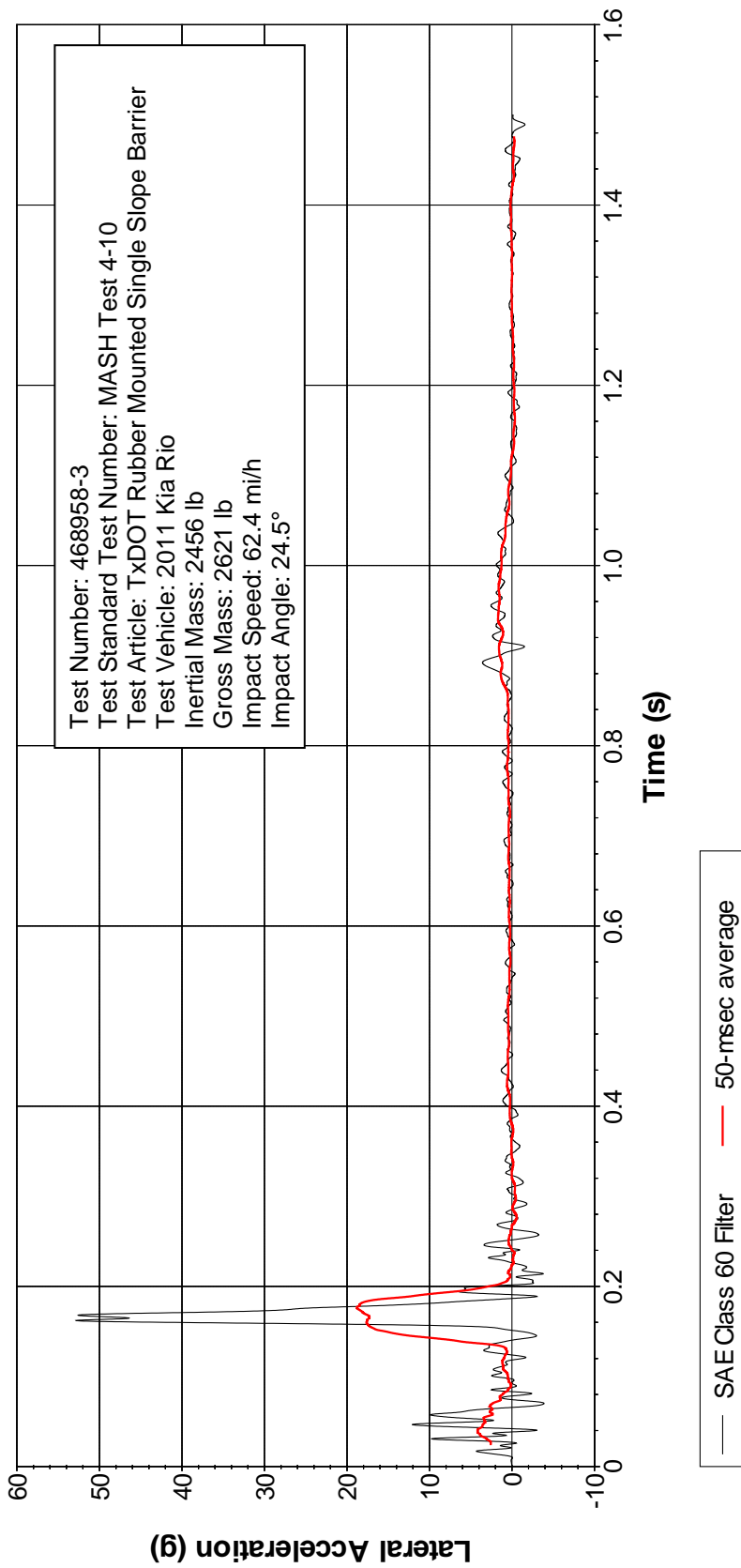


Figure G.8. Vehicle Lateral Accelerometer Trace for Test No. 468958-3 (Accelerometer Located Rear of Center of Gravity).

Z Acceleration Rear of CG

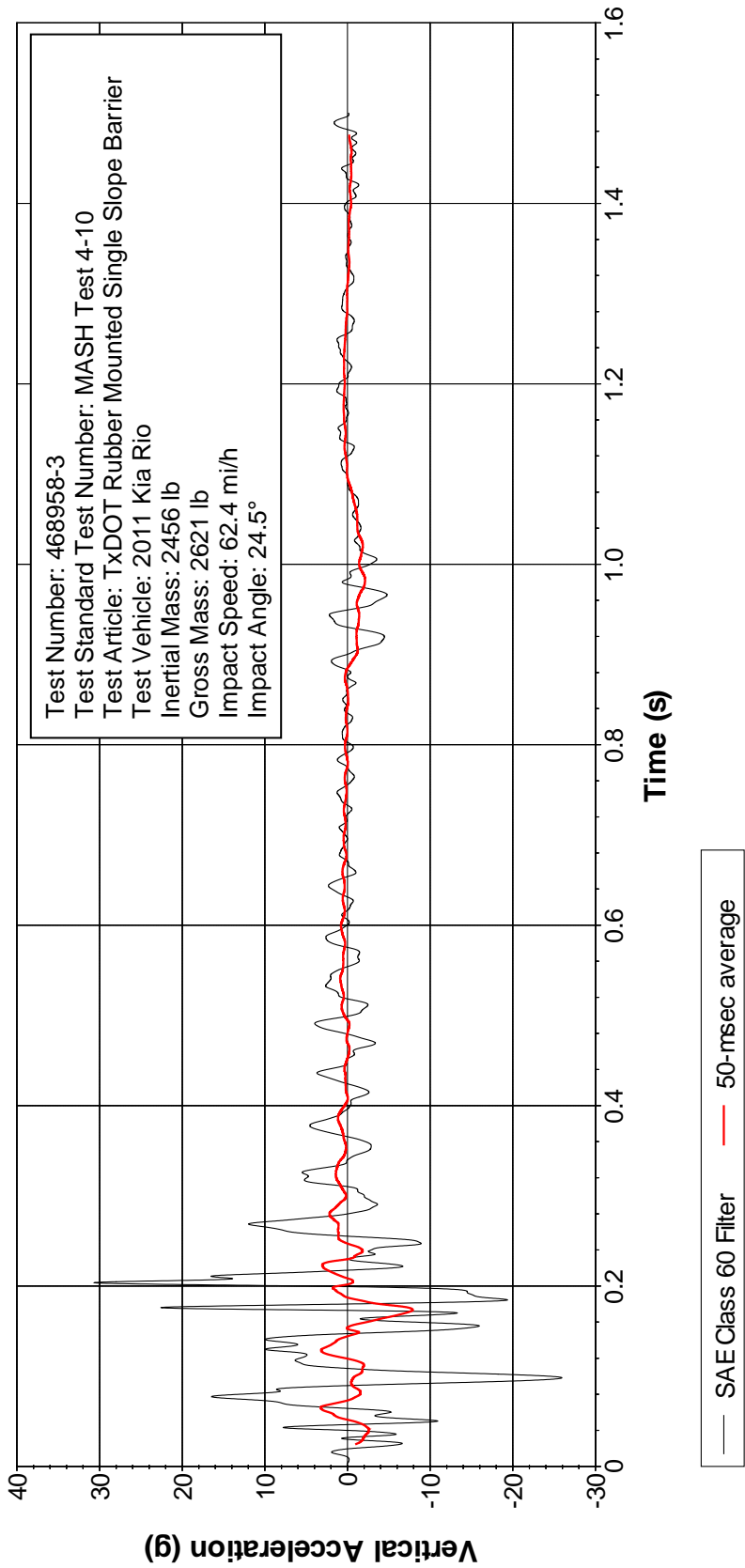


Figure G.9. Vehicle Vertical Accelerometer Trace for Test No. 468958-3 (Accelerometer Located Rear of Center of Gravity).

APPENDIX H. MASH TEST 4-11 (CRASH TEST NO. 468958-2)

H.1 VEHICLE PROPERTIES AND INFORMATION

Table H.1. Vehicle Properties for Test No. 468958-2.

Date: 2017-12-20 Test No.: 468958-2 VIN No.: 1D7RB1GP5BS651728
 Year: 2011 Make: Dodge Model: RAM 1500
 Tire Size: 265/70R17 Tire Inflation Pressure: 44 psi
 Tread Type: Highway Odometer: 153424
 Note any damage to the vehicle prior to test: None

• Denotes accelerometer location.

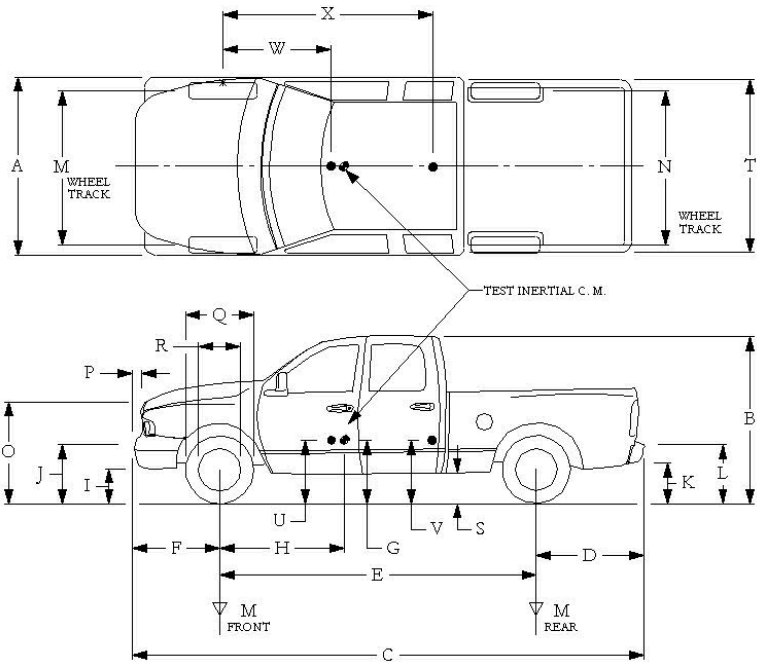
NOTES: None

Engine Type: V8
 Engine CID: 4.7 liter

Transmission Type:
 Auto or Manual
 FWD RWD 4WD

Optional Equipment:
None

Dummy Data:
 Type: 50th percentile male
 Mass: 165 lb
 Seat Position: Driver



Geometry: inches

A	<u>78.50</u>	F	<u>40.00</u>	K	<u>20.00</u>	P	<u>3.00</u>	U	<u>27.25</u>
B	<u>74.00</u>	G	<u>28.38</u>	L	<u>30.00</u>	Q	<u>30.50</u>	V	<u>29.75</u>
C	<u>227.50</u>	H	<u>61.41</u>	M	<u>68.50</u>	R	<u>18.00</u>	W	<u>61.40</u>
D	<u>44.00</u>	I	<u>11.75</u>	N	<u>68.00</u>	S	<u>12.75</u>	X	<u>77.75</u>
E	<u>140.50</u>	J	<u>27.25</u>	O	<u>46.00</u>	T	<u>77.00</u>		
Wheel Center Height Front	<u>14.75</u>	Wheel Well Clearance (Front)	<u>6.00</u>	Bottom Frame Height - Front	<u>12.00</u>				
Wheel Center Height Rear	<u>14.75</u>	Wheel Well Clearance (Rear)	<u>9.25</u>	Bottom Frame Height - Rear	<u>25.50</u>				

GVWR Ratings:

Front	<u>3700</u>
Back	<u>3900</u>
Total	<u>6700</u>

Mass: lb

M_{front}	<u>2874</u>
M_{rear}	<u>2001</u>
M_{Total}	<u>4875</u>

Curb

<u>2874</u>
<u>2001</u>
<u>4875</u>

Test Inertial

<u>2828</u>
<u>2196</u>
<u>5024</u>

Gross Static

<u>2913</u>
<u>2276</u>
<u>5189</u>

(Allowable Range for TIM and GSM = 5000 lb ±110 lb)

Mass Distribution:

lb	LF: <u>1426</u>	RF: <u>1402</u>	LR: <u>1084</u>	RR: <u>1112</u>
----	-----------------	-----------------	-----------------	-----------------

Table H.2. Measurements of Vehicle Vertical CG for Test No. 468958-2.

Date: 2017-12-20 Test No.: 468958-2 VIN: 1D7RB1GP5BS651728
 Year: 2011 Make: Dodge Model: RAM 1500
 Body Style: Quad Cab Mileage: 153424
 Engine: 4.7 liter V8 Transmission: Automatic
 Fuel Level: Empty Ballast: 180 lb (440 lb max)
 Tire Pressure: Front: 44 psi Rear: 44 psi Size: 265/70R17

Measured Vehicle Weights: (lb)			
LF:	<u>1426</u>	RF:	<u>1402</u>
Front Axle:		<u>2828</u>	
LR:	<u>1084</u>	RR:	<u>1112</u>
Rear Axle:		<u>2196</u>	
Left:	<u>2510</u>	Right:	<u>2514</u>
Total:		<u>5024</u>	
5000 ±110 lb allowed			
Wheel Base:	<u>140.5</u> inches	Track: F:	<u>68.5</u> inches
148 ±12 inches allowed		R:	<u>68</u> inches
Track = (F+R)/2 = 67 ±1.5 inches allowed			
Center of Gravity, SAE J874 Suspension Method			
X:	<u>61.41</u> inches	Rear of Front Axle	(63 ±4 inches allowed)
Y:	<u>0.03</u> inches	Left - Right +	of Vehicle Centerline
Z:	<u>28.375</u> inches	Above Ground	(mininum 28.0 inches allowed)

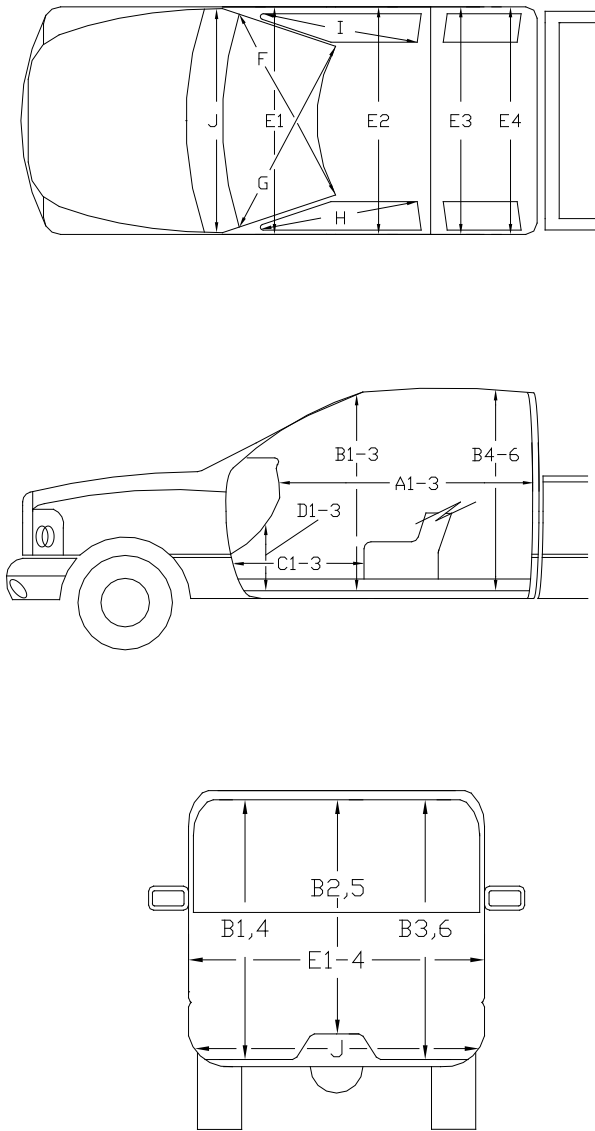
Hood Height: 46.00 inches Front Bumper Height: 27.00 inches
 43 ±4 inches allowed

Front Overhang: 40.00 inches Rear Bumper Height: 30.00 inches
 39 ±3 inches allowed

Overall Length: 227.50 inches
 237 ±13 inches allowed

Table H.4. Occupant Compartment Measurements of Vehicle for Test No. 468958-2.

Date: 2017-12-20 Test No.: 468958-2 VIN No.: 1D7RB1GP5BS651728
 Year: 2011 Make: Dodge Model: RAM 1500



OCCUPANT COMPARTMENT DEFORMATION MEASUREMENT

	Before	After (inches)	Differ.
A1	65.00	65.00	0.00
A2	63.00	63.00	0.00
A3	65.50	65.50	0.00
B1	45.00	45.00	0.00
B2	38.00	38.00	0.00
B3	45.00	45.00	0.00
B4	39.25	39.25	0.00
B5	43.00	43.00	0.00
B6	39.25	39.25	0.00
C1	26.00	26.00	0.00
C2	-----	-----	-----
C3	26.00	26.00	0.00
D1	11.00	11.00	0.00
D2	-----	-----	-----
D3	11.00	11.00	0.00
E1	58.50	58.50	0.00
E2	63.50	63.50	0.00
E3	63.50	63.50	0.00
E4	63.50	63.50	0.00
F	59.00	59.00	0.00
G	59.00	59.00	0.00
H	37.50	37.50	0.00
I	37.50	37.50	0.00
J*	23.50	23.50	0.00

*Lateral area across the cab from driver's side kickpanel to passenger's side kickpanel.

H.2 SEQUENTIAL PHOTOGRAPHS

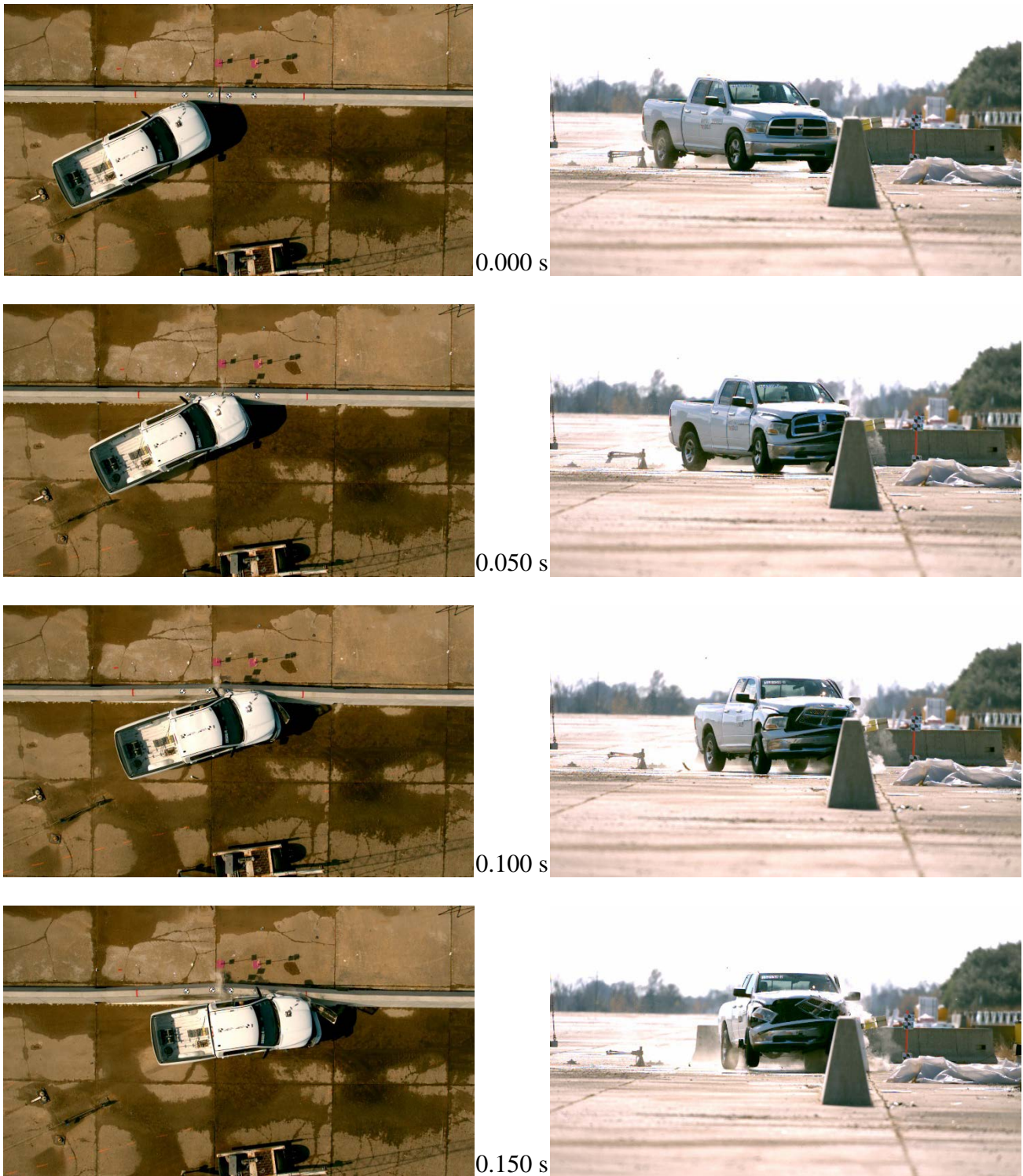


Figure H.1. Sequential Photographs for Test No. 468958-2 (Overhead and Frontal Views).



0.200 s



0.300 s



0.400 s

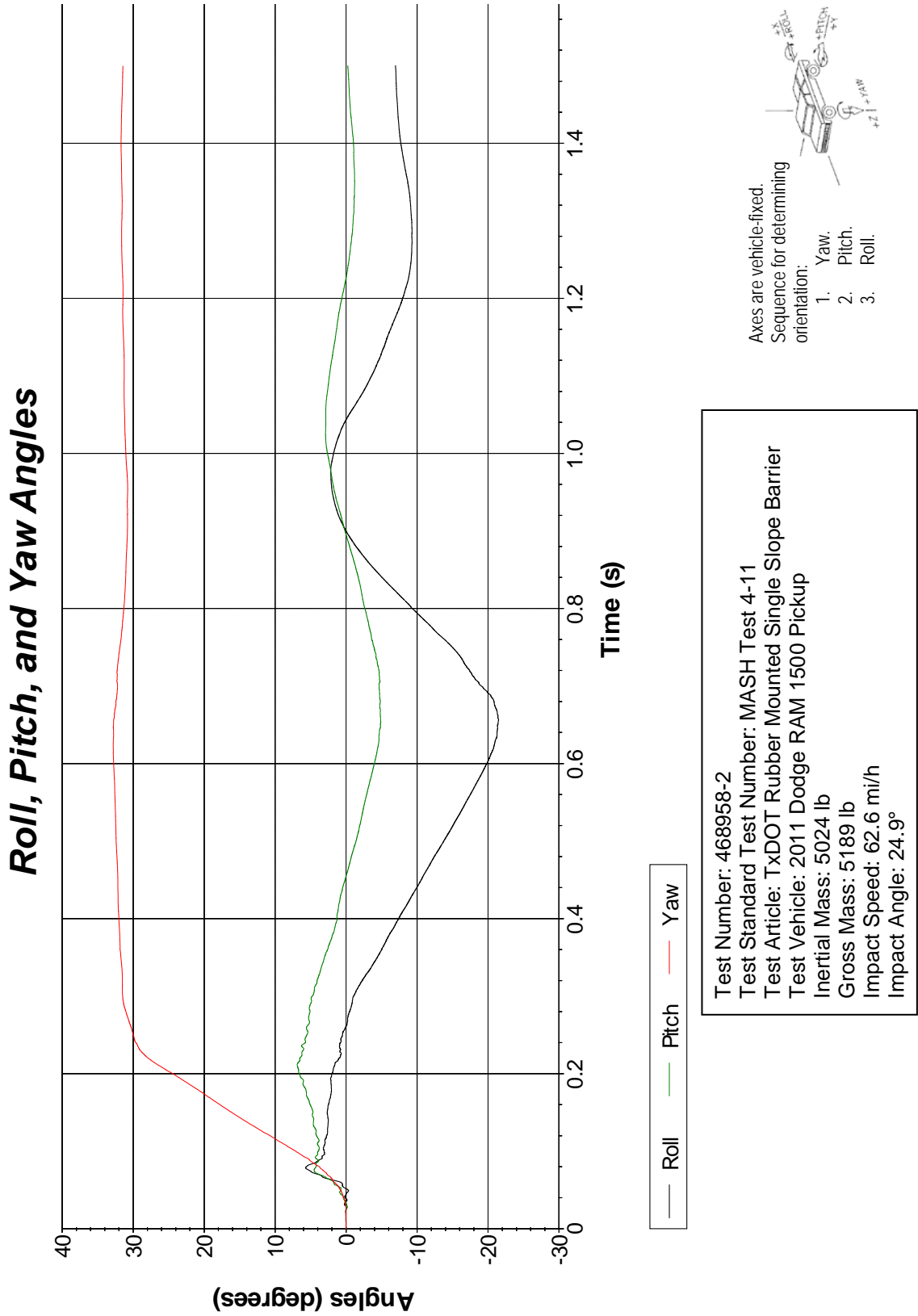


0.500 s



**Figure H.1. Sequential Photographs for Test No. 468958-2 (Overhead and Frontal Views)
(Continued).**

H.3 VEHICLE ANGULAR DISPLACEMENT



Test Number: 468958-2
 Test Standard Test Number: MASH Test 4-11
 Test Article: TxDOT Rubber Mounted Single Slope Barrier
 Test Vehicle: 2011 Dodge RAM 1500 Pickup
 Inertial Mass: 5024 lb
 Gross Mass: 5189 lb
 Impact Speed: 62.6 mi/h
 Impact Angle: 24.9°

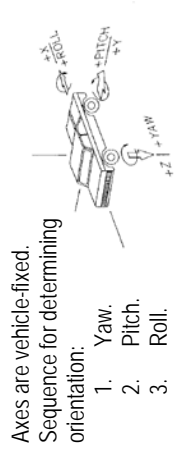


Figure H.2. Vehicle Angular Displacements for Test No. 468958-2.

H.4 VEHICLE ACCELERATIONS

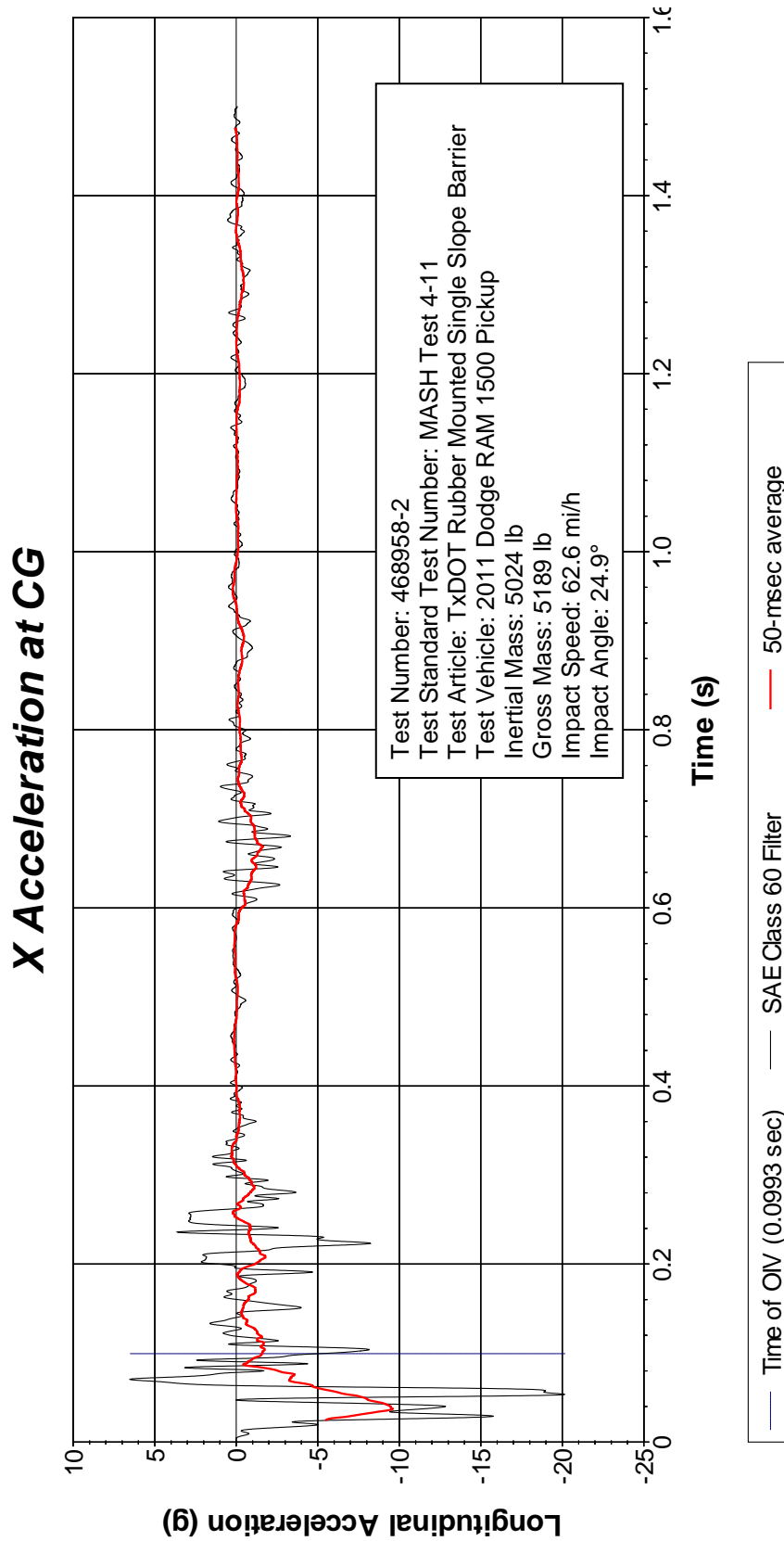


Figure H.3. Vehicle Longitudinal Accelerometer Trace for Test No. 468958-2 (Accelerometer Located at Center of Gravity).

Y Acceleration at CG

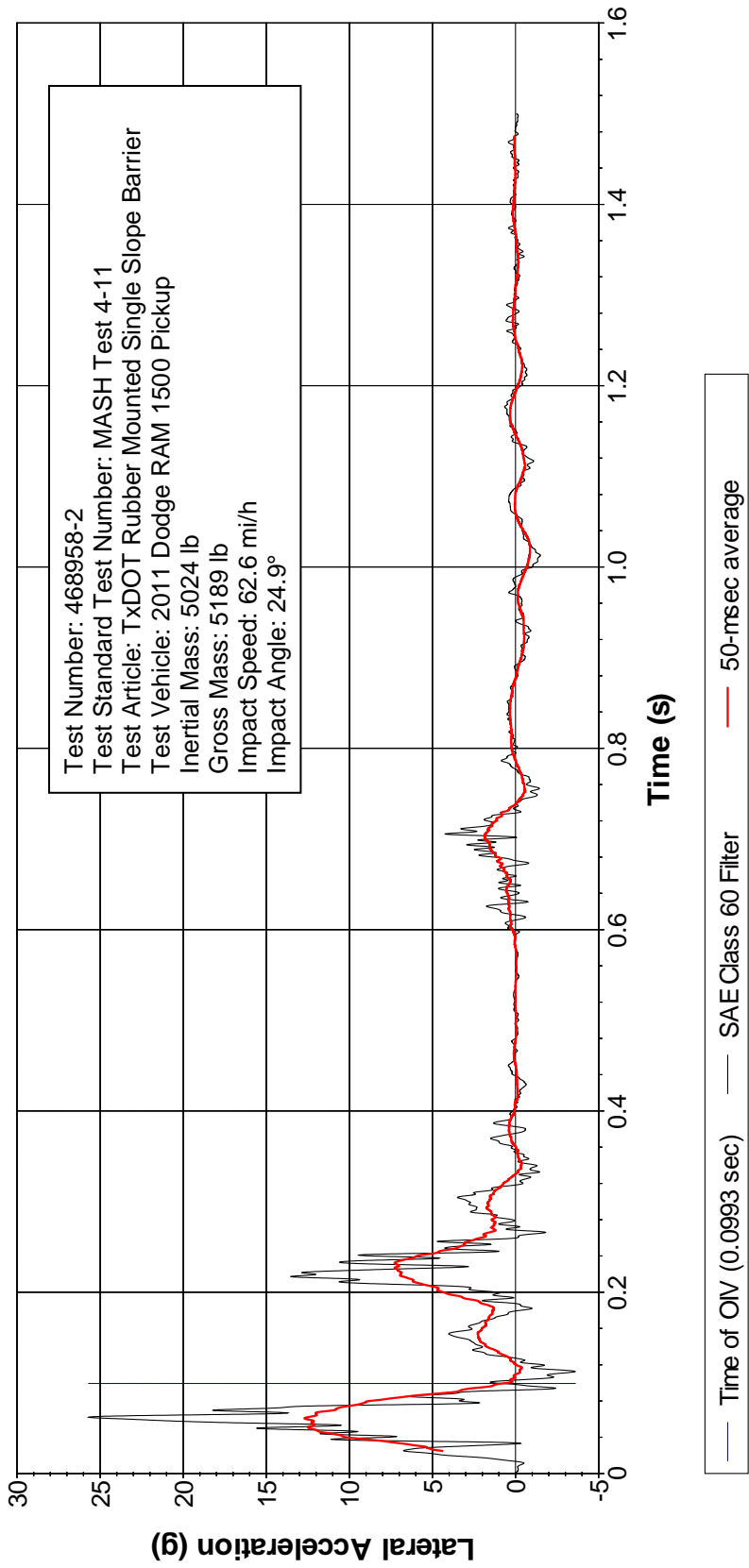


Figure H.4. Vehicle Lateral Accelerometer Trace for Test No. 468958-2 (Accelerometer Located at Center of Gravity).

Z Acceleration at CG

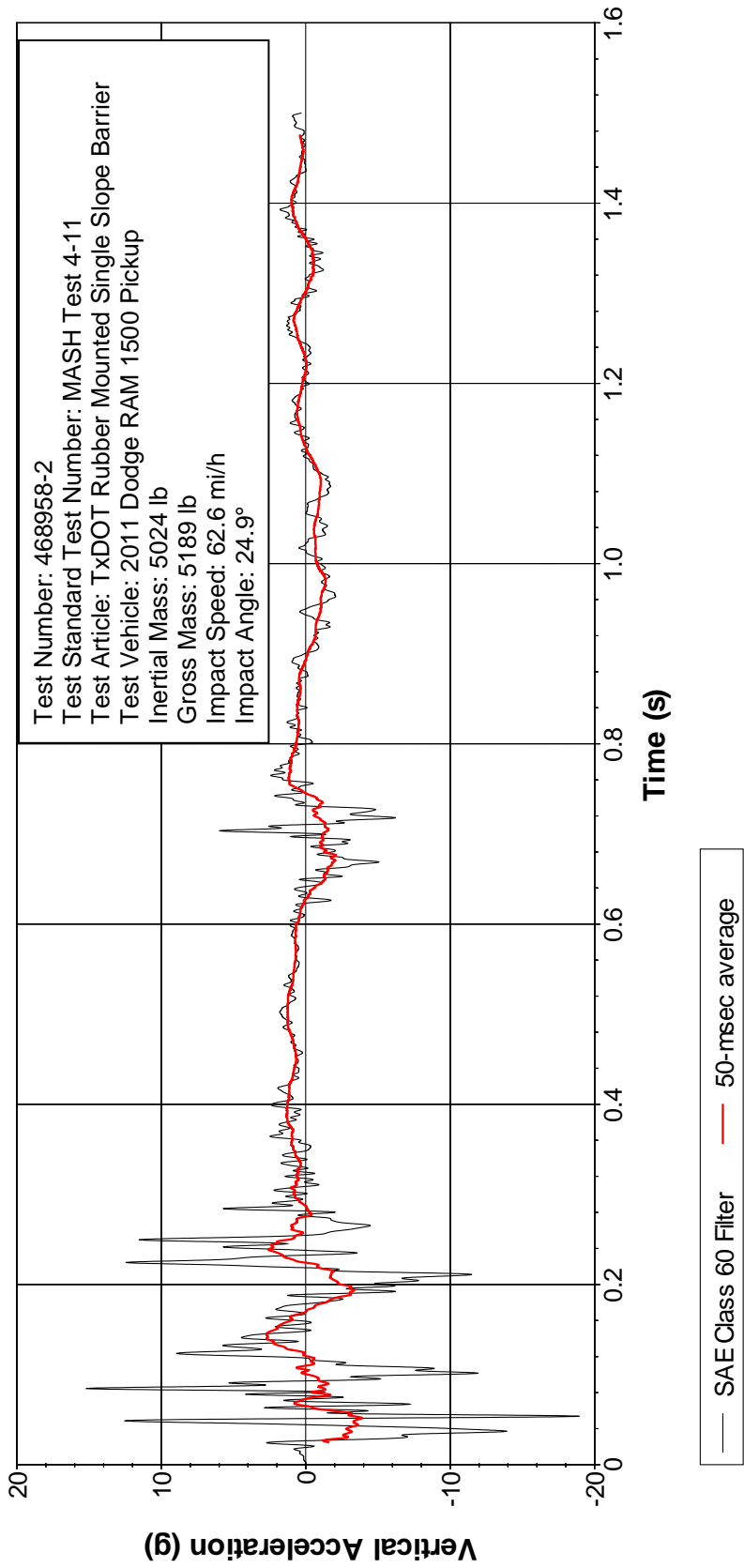


Figure H.5. Vehicle Vertical Accelerometer Trace for Test No. 468958-2 (Accelerometer Located at Center of Gravity).

X Acceleration Rear of CG

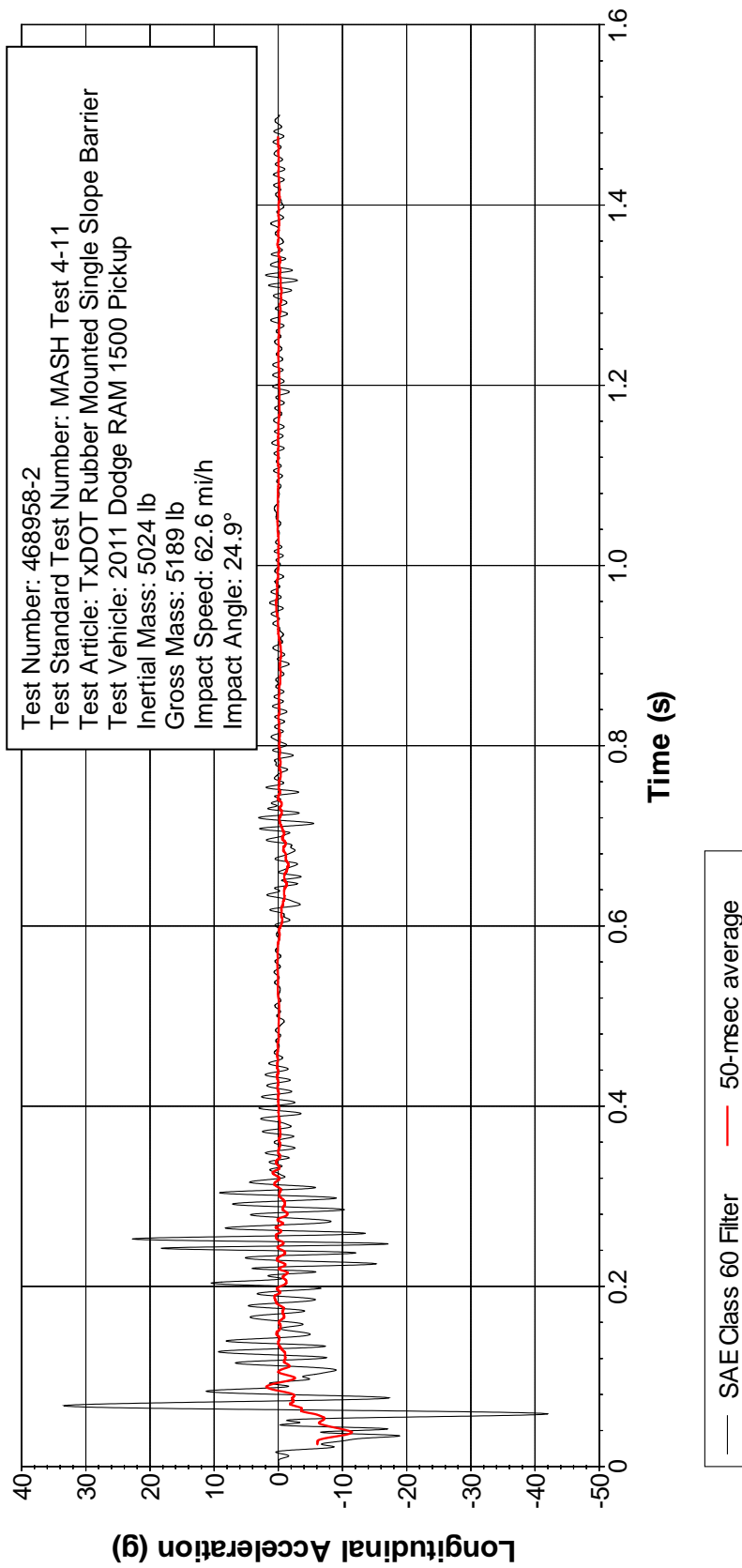


Figure H.6. Vehicle Longitudinal Accelerometer Trace for Test No. 468958-2 (Accelerometer Located Rear of Center of Gravity).

Y Acceleration Rer of CG

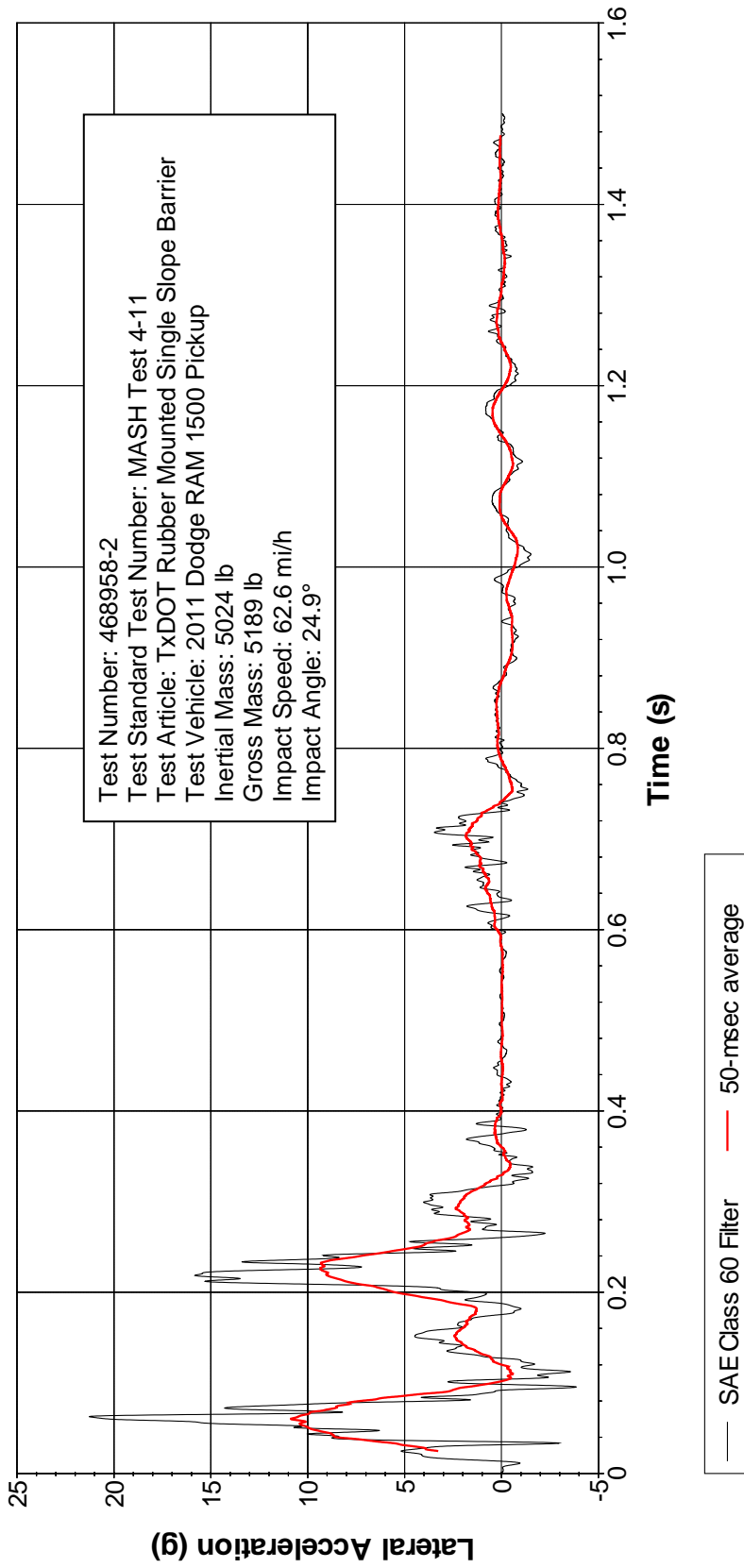


Figure H.7. Vehicle Lateral Accelerometer Trace for Test No. 468958-2 (Accelerometer Located Rear of Center of Gravity).

Z Acceleration Rear of CG

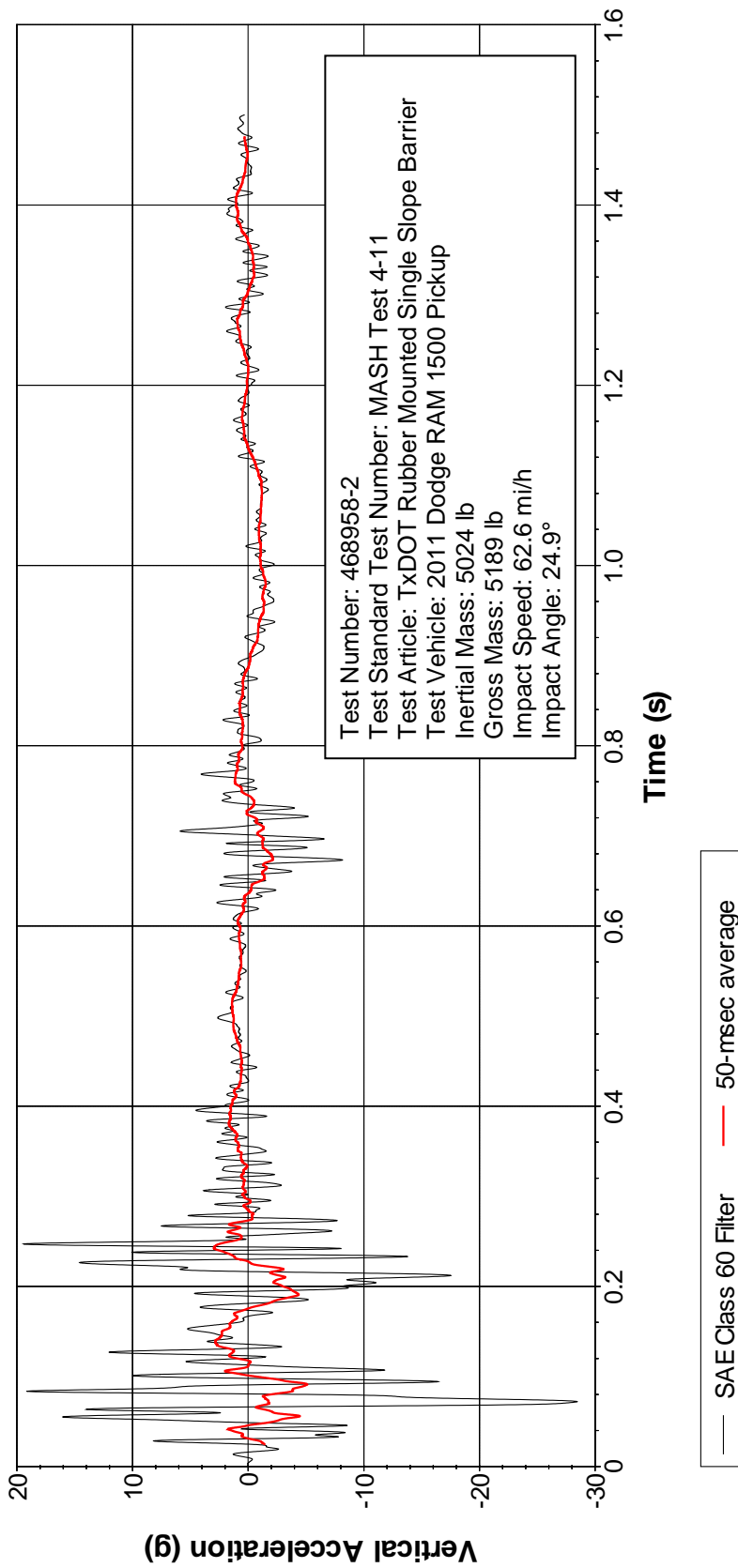


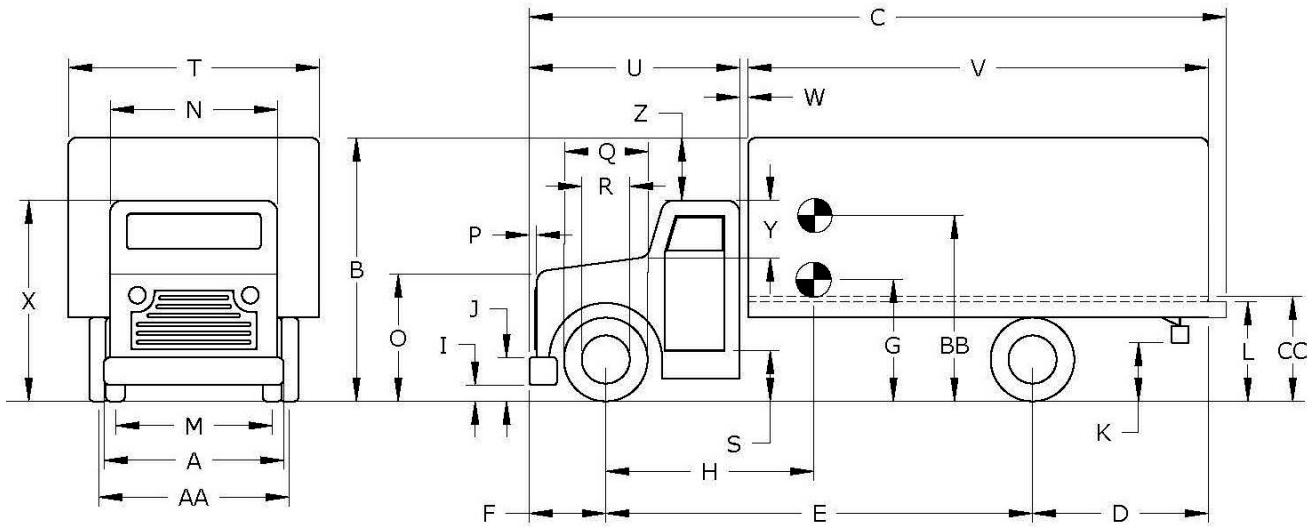
Figure H.8. Vehicle Vertical Accelerometer Trace for Test No. 468958-2 (Accelerometer Located Rear of Center of Gravity).

APPENDIX I. MASH TEST 4-10 (CRASH TEST NO. 468958-1)

I.1 VEHICLE PROPERTIES AND INFORMATION

Table I.1. Vehicle Properties for Test No. 468958-1.

Date: 2017-12-21 Test No.: 468958-1 VIN No.: 1HTMPAFN53H571935
 Year: 2003 Make: International Model: 4200
 Odometer: 262726 Tire Size Front: 295/75R22.5 Tire Size Rear: 295/75R22.5



Vehicle Geometry: inches

A Front Bumper Width:	<u>91.00</u>	K Rear Bumper Bottom:	<u>-----</u>	U Cab Length:	<u>104.00</u>
B Overall Height:	<u>131.00</u>	L Rear Frame Top:	<u>37.00</u>	V Trailer/Box Length:	<u>222.00</u>
C Overall Length:	<u>332.00</u>	M Front Track Width:	<u>79.00</u>	W Gap Width:	<u>4.50</u>
D Rear Overhang:	<u>89.00</u>	N Roof Width:	<u>60.50</u>	X Overall Front Height:	<u>97.00</u>
E Wheel Base:	<u>205.50</u>	O Hood Height:	<u>60.00</u>	Y Roof-Hood Distance:	<u>27.00</u>
F Front Overhang:	<u>36.00</u>	P Bumper Extension:	<u>7.50</u>	Z Roof-Box Height Difference:	<u>31.00</u>
G C.G. Height:	<u>-----</u>	Q Front Tire Width:	<u>40.00</u>	AA Rear Track Width:	<u>73.00</u>
H C.G. Horizontal Dist. w/Ballast:	<u>139.80</u>	R Front Wheel Width:	<u>23.00</u>	BB Ballast Center of Mass:	<u>61.50</u>
I Front Bumper Bottom:	<u>20.00</u>	S Bottom Door Height:	<u>37.00</u>	CC Cargo Bed Height:	<u>49.12</u>
J Front Bumper Top:	<u>35.00</u>	T Overall Width:	<u>95.50</u>		
Wheel Center Height Front	<u>19.00</u>	Wheel Well Clearance (Front)	<u>12.00</u>	Bottom Frame Height (Front)	<u>26.00</u>
Wheel Center Height Rear	<u>19.00</u>	Wheel Well Clearance (Rear)	<u>5.50</u>	Bottom Frame Height (Rear)	<u>27.00</u>

Table I.1. Vehicle Properties for Test No. 468958-1 (Continued).

Date: 2017-12-21 Test No.: 468958-1 VIN No.: 1HTMPAFN53H571935
 Year: 2003 Make: International Model: 4200

WEIGHTS
(lb)

	CURB	TEST INERTIAL
$W_{\text{front axle}}$	<u>6010</u>	<u>7130</u>
$W_{\text{rear axle}}$	<u>6560</u>	<u>15170</u>
W_{TOTAL}	<u>12570</u>	<u>22300</u>

Ballast: 9730 (lb)

Mass Distribution

(lb): **LF:** 3570 **RF:** 3560 **LR:** 7710 **RR:** 7460

Engine Type: International (diesel)

Accelerometer Locations (inches or mm)

Engine Size: VT 365 6 liter

x³ **y** **z⁴**

Transmission Type:

Front: _____

Auto or Manual
 FWD RWD 4WD

Center: 140.00 ----- 49.50

Rear: 227.00 ----- 49.50

Describe any damage to the vehicle prior to test: None

Other notes to include ballast type, dimensions, mass, location, center of mass, and method of attachment:

Block: height 30 inches/width 30 inches/length 30 inches

Block: height 30 inches/width 30 inches/length 30 inches

Centered in middle of bed

62 inches from ground to middle of block

Four ⁵/₁₆-inch cables per block

³ Referenced to the front axle

⁴ Above ground

I.2 SEQUENTIAL PHOTOGRAPHS



0.000 s



0.050 s



0.100 s



200



Figure I.1. Sequential Photographs for Test No. 468958-1 (Overhead and Frontal Views).



0.300 s



0.400 s



0.500 s



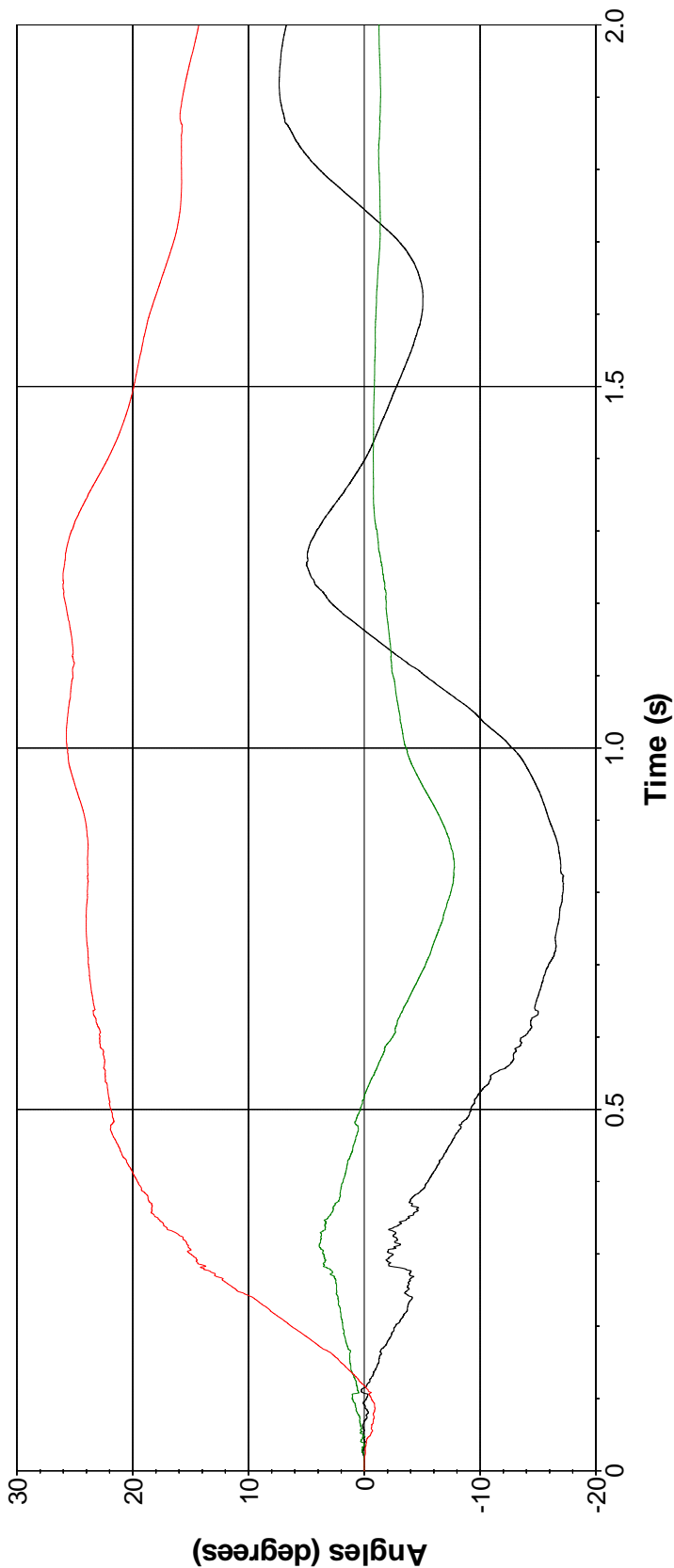
0.600 s



**Figure I.1. Sequential Photographs for Test No. 468958-1 (Overhead and Frontal Views)
(Continued).**

I.3 VEHICLE ANGULAR DISPLACEMENT

Roll, Pitch, and Yaw Angles



— Roll — Pitch — Yaw

Test Number: 468958-1
 Test Standard Test Number: MASH Test 4-12
 Test Article: TxDOT Rubber Mounted Single Slope Barrier
 Test Vehicle: 2003 International 4200 Single-Unit Truck
 Inertial Mass: 22,300 lb
 Gross Mass: 22,300 lb
 Impact Speed: 58.3 mi/h
 Impact Angle: 14.4°

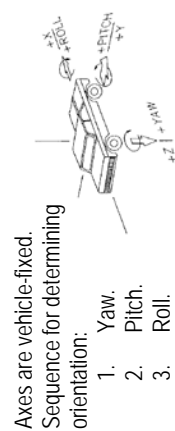
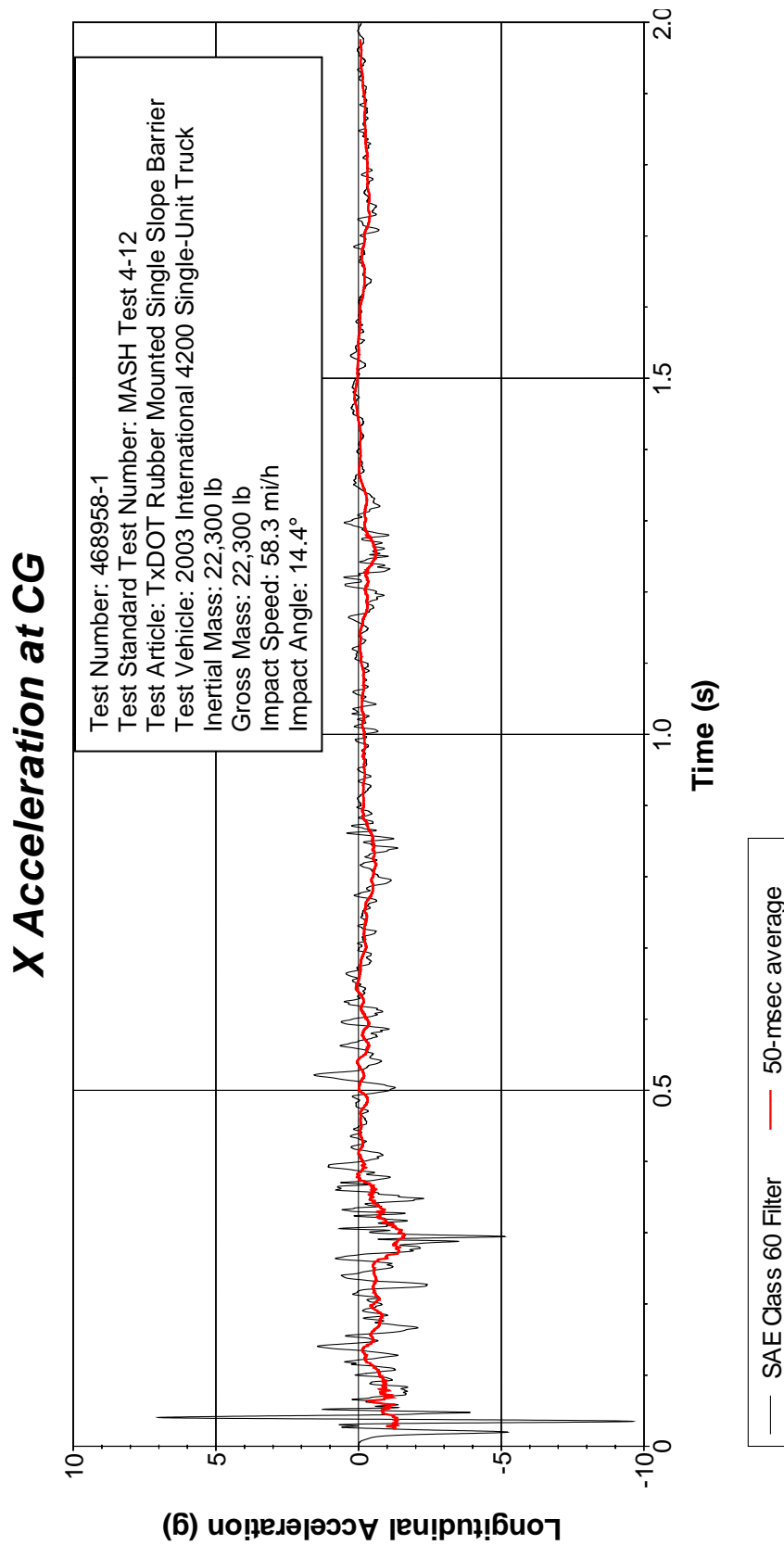


Figure I.2. Vehicle Angular Displacements for Test No. 468958-1.

I.4 VEHICLE ACCELERATIONS



**Figure I.3. Vehicle Longitudinal Accelerometer Trace for Test No. 468958-1
(Accelerometer Located at Center of Gravity).**

Y Acceleration at CG

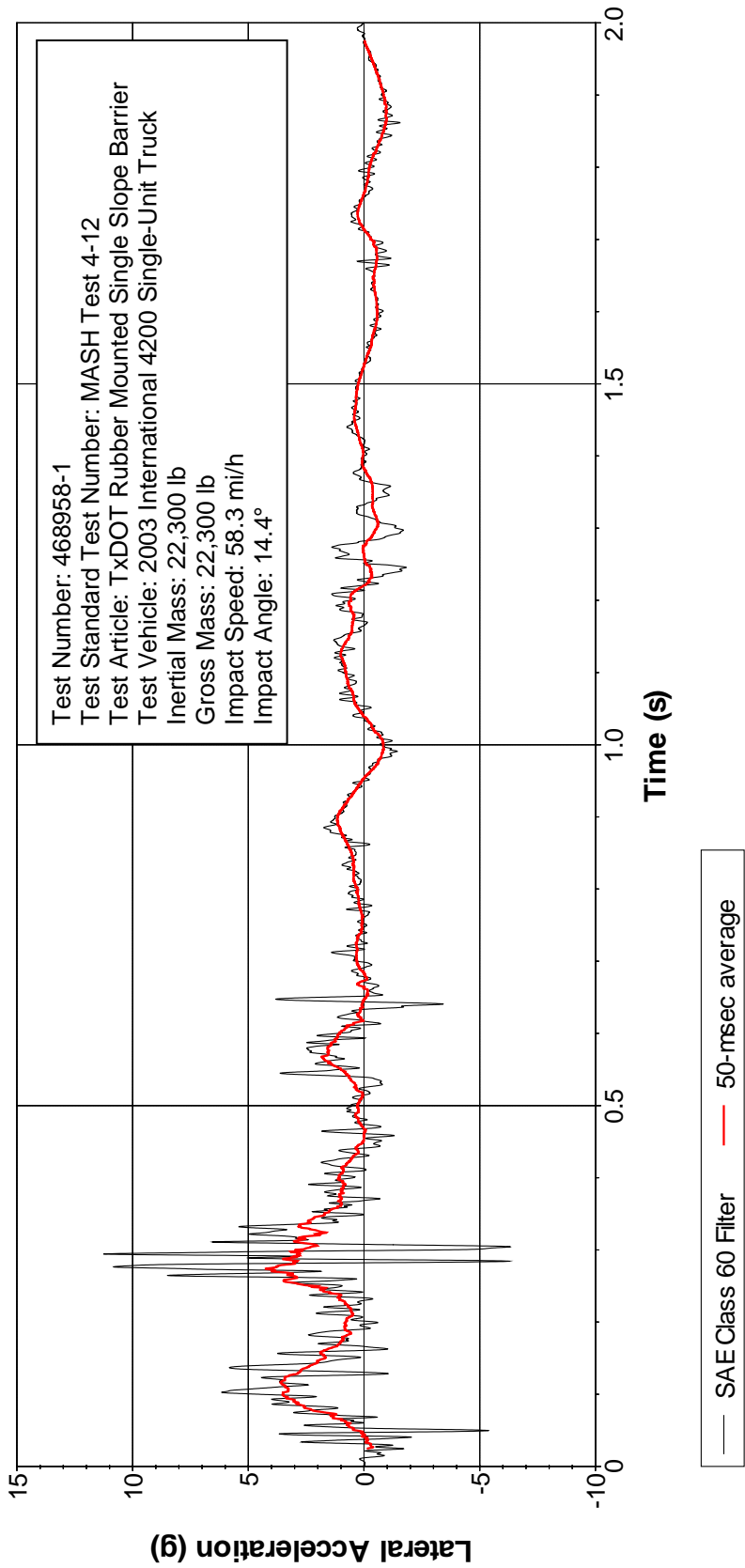


Figure I.4. Vehicle Lateral Accelerometer Trace for Test No. 468958-1 (Accelerometer Located at Center of Gravity).

Z Acceleration at CG

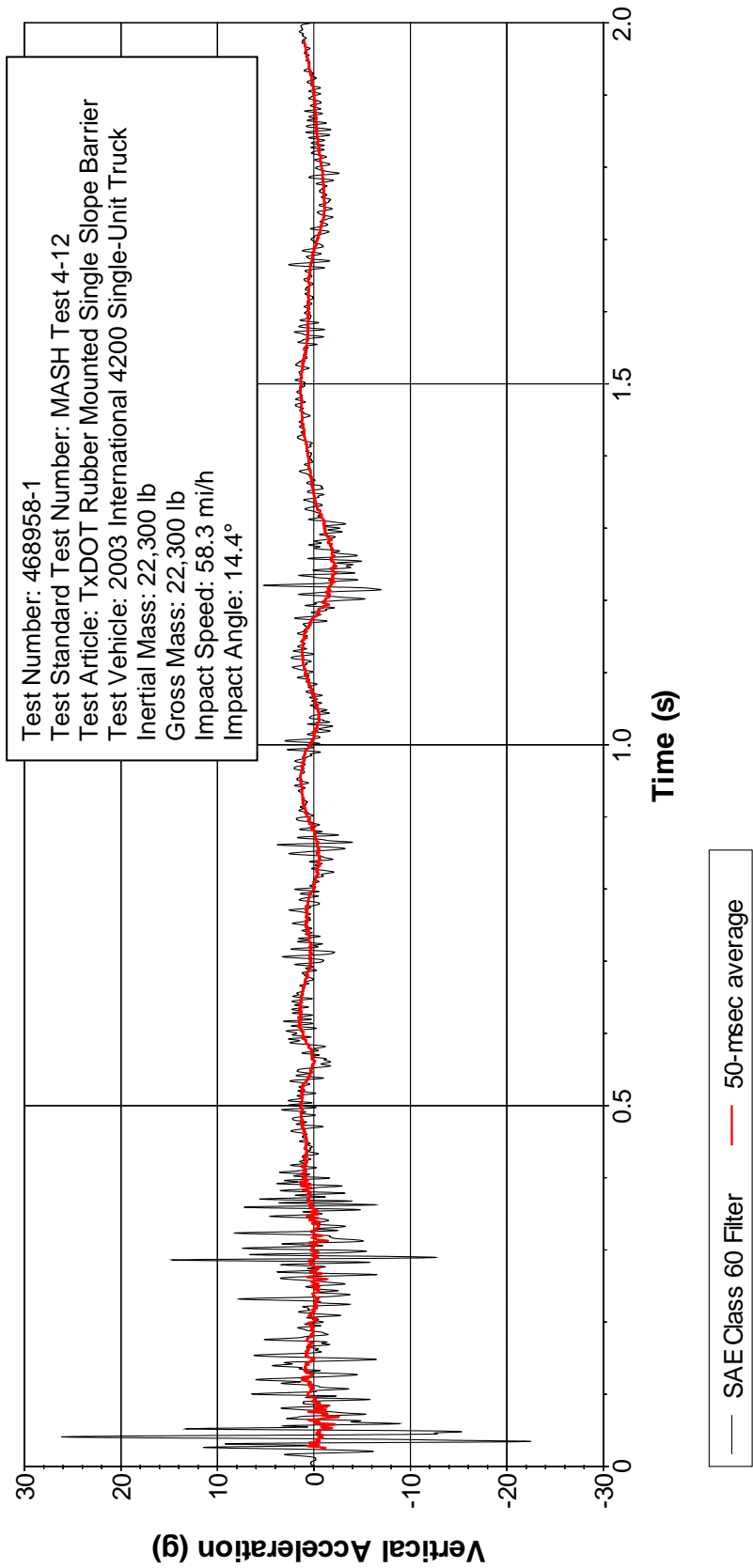


Figure I.5. Vehicle Vertical Accelerometer Trace for Test No. 468958-1
(Accelerometer Located at Center of Gravity).

X Acceleration Rear of CG

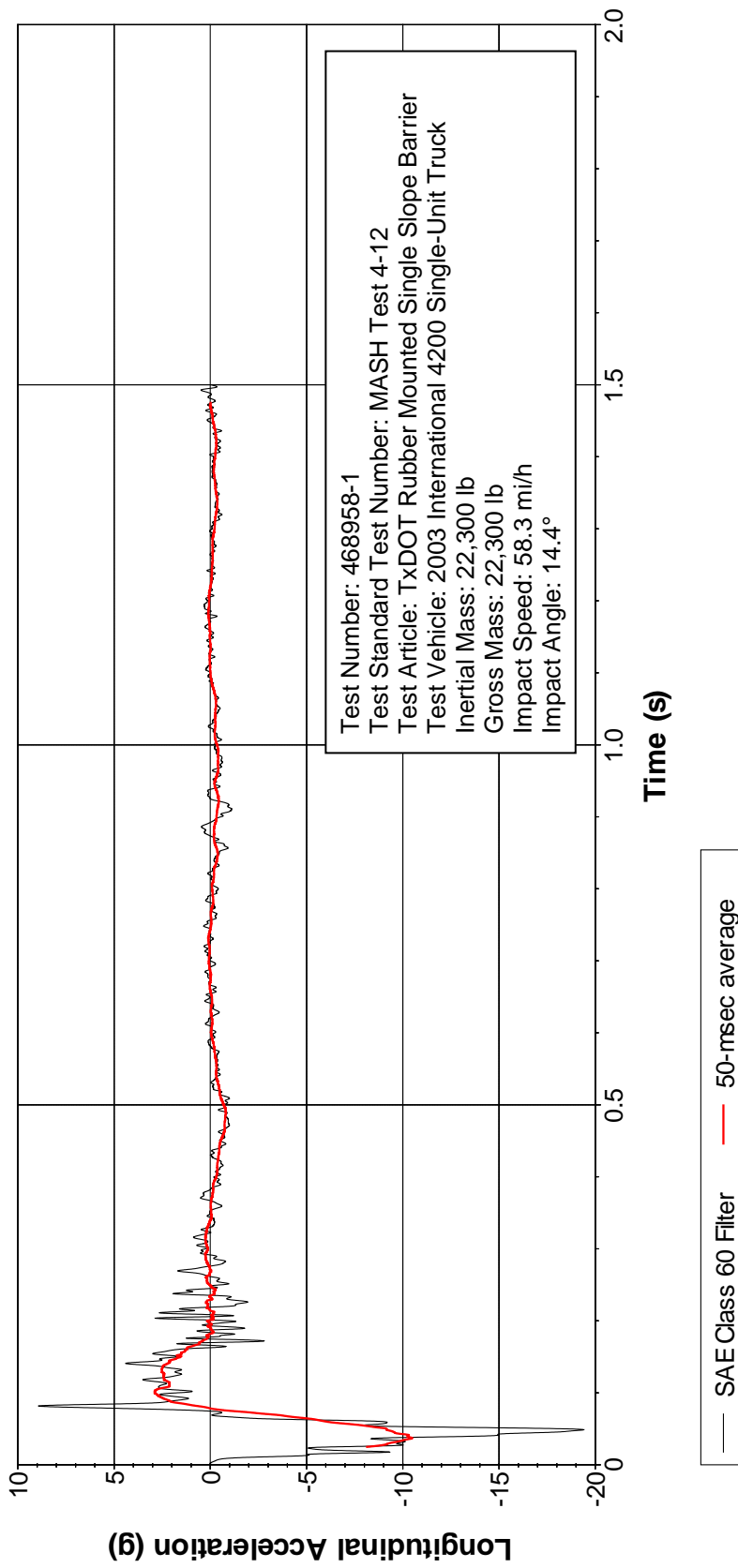


Figure I.6. Vehicle Longitudinal Accelerometer Trace for Test No. 468958-1 (Accelerometer Located Rear of Center of Gravity).

Y Acceleration Rear of CG

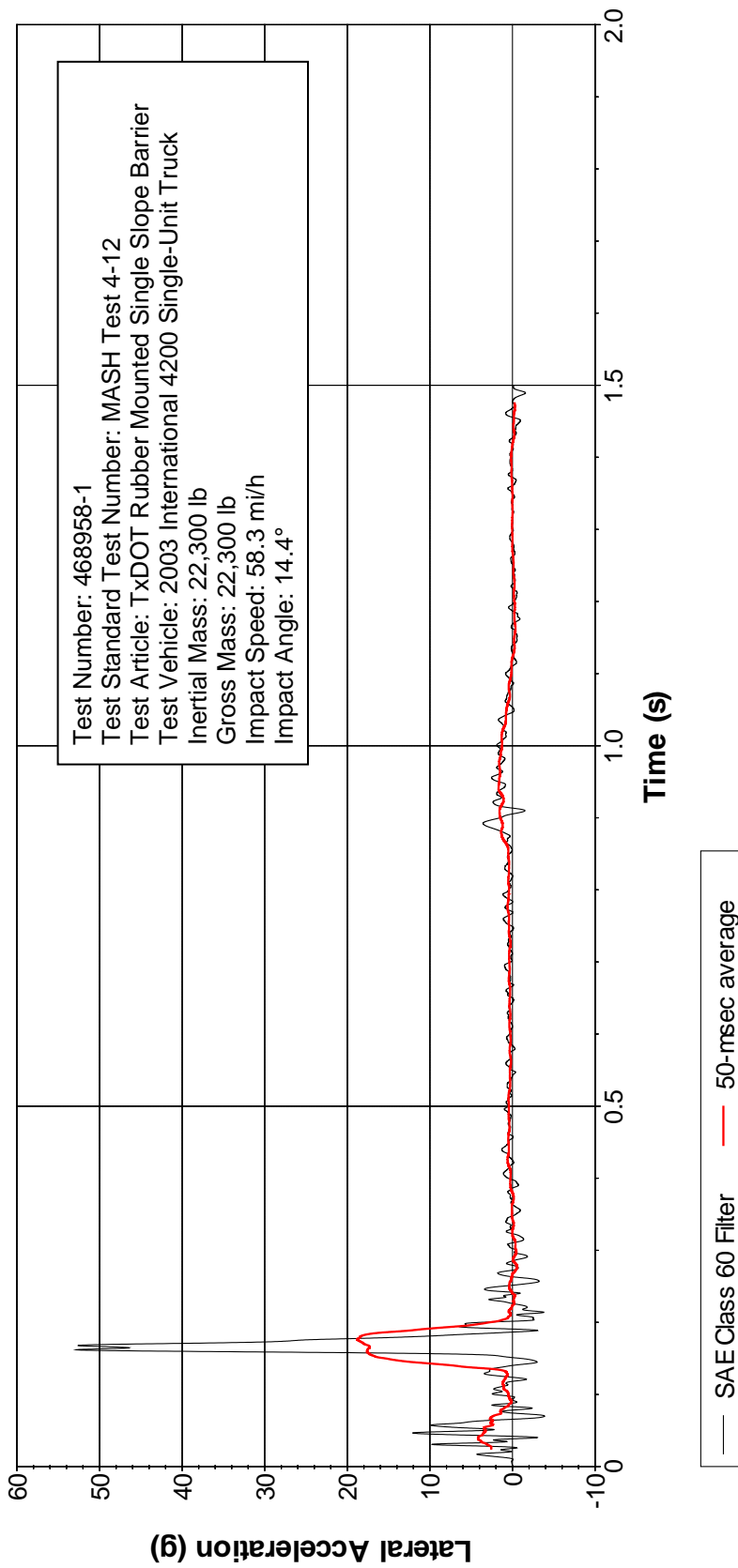


Figure I.7. Vehicle Lateral Accelerometer Trace for Test No. 468958-1 (Accelerometer Located Rear of Center of Gravity).

Z Acceleration Rear of CG

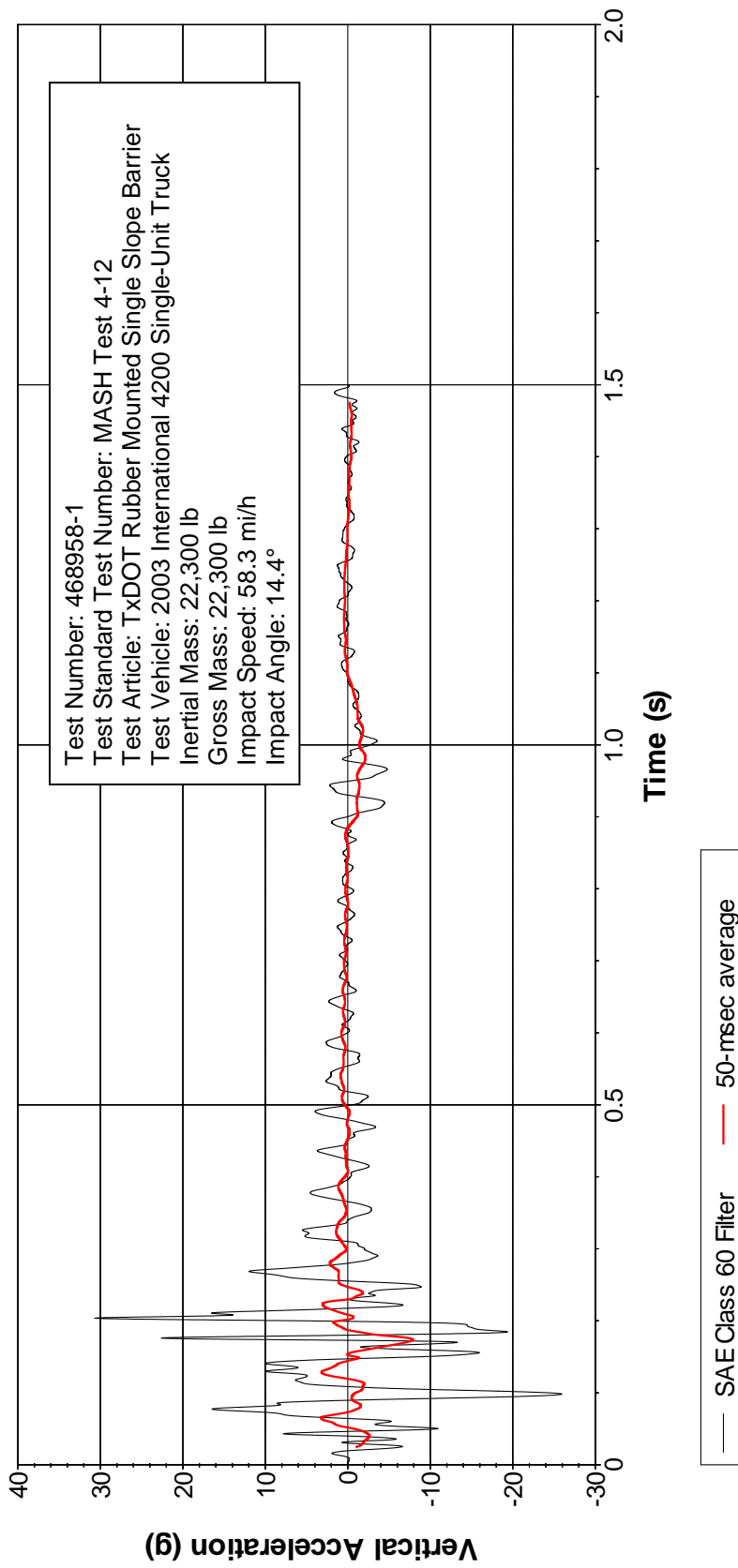
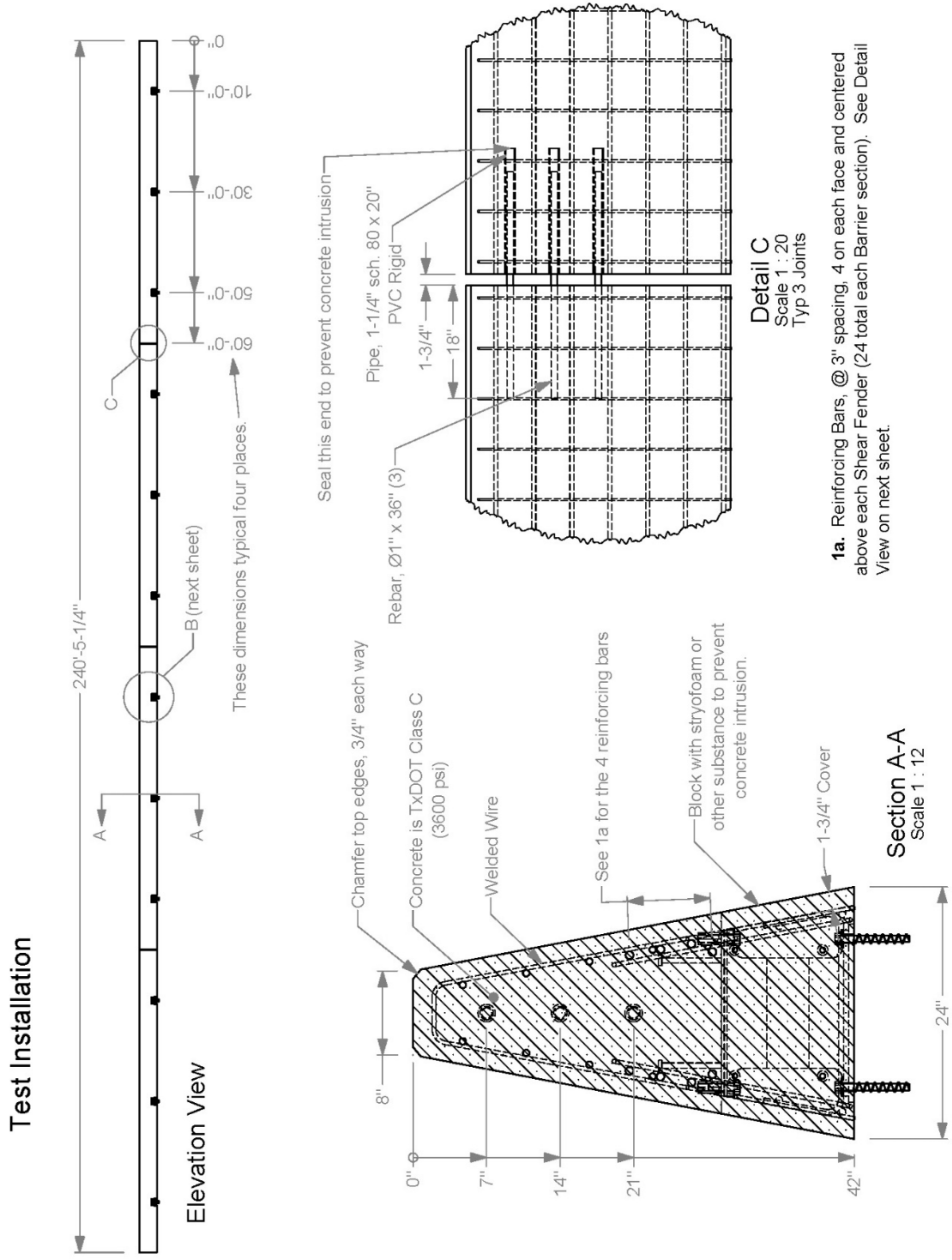
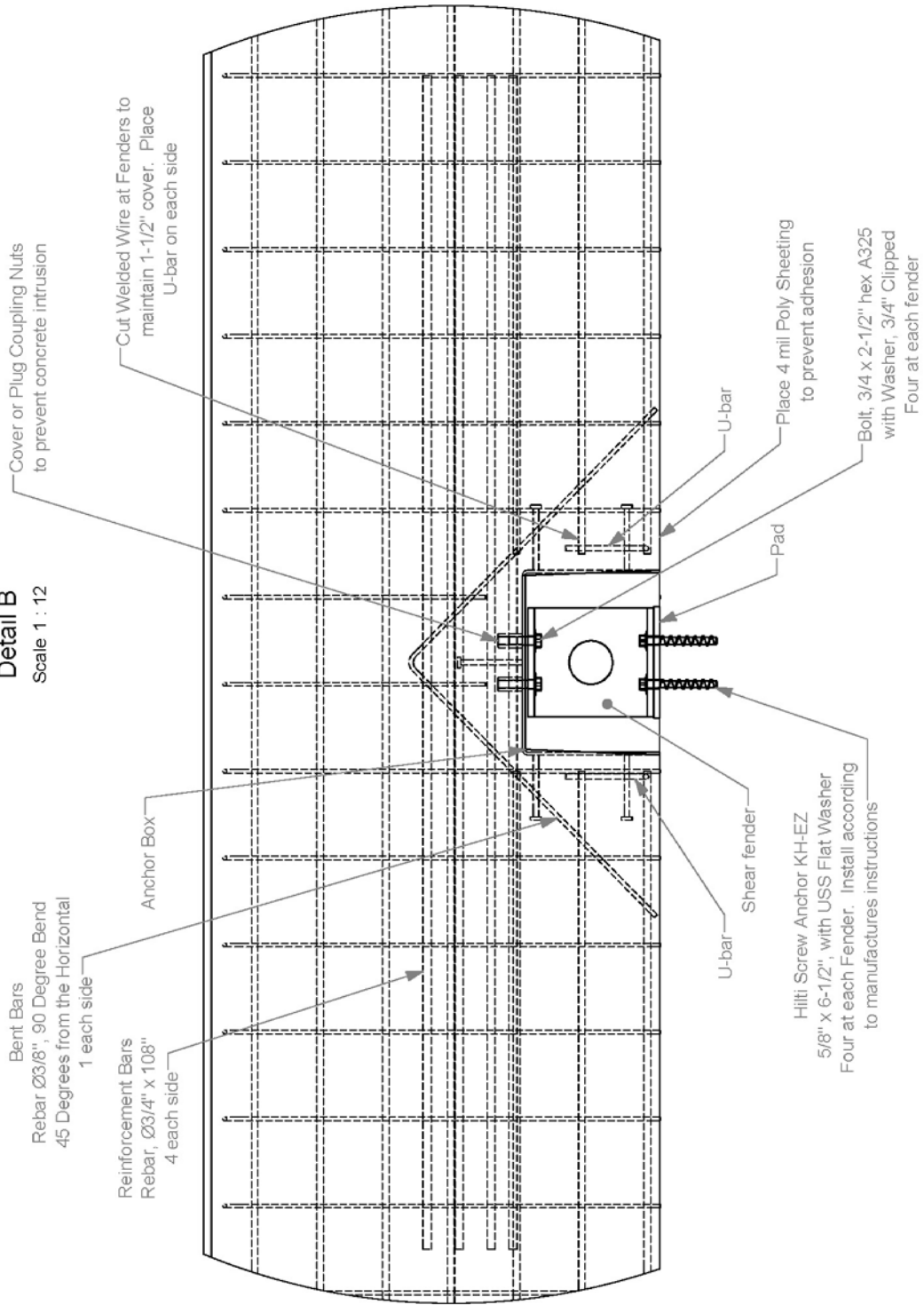


Figure I.8. Vehicle Vertical Accelerometer Trace for Test No. 468958-1 (Accelerometer Located Rear of Center of Gravity).

APPENDIX J. RECOMMENDED TXDOT RUBBER MOUNTED SINGLE SLOPE BARRIER



Detail B
Scale 1 : 12



Cover or Plug Coupling Nuts to prevent concrete intrusion

Cut Welded Wire at Fenders to maintain 1-1/2" cover. Place U-bar on each side

Bent Bars
Rebar Ø3/8", 90 Degree Bend
45 Degrees from the Horizontal
1 each side

Reinforcement Bars
Rebar, Ø3/4" x 108"
4 each side

Anchor Box

U-bar

Place 4 mil Poly Sheeting to prevent adhesion

Bolt, 3/4 x 2-1/2" hex A325
with Washer, 3/4" Clipped
Four at each fender

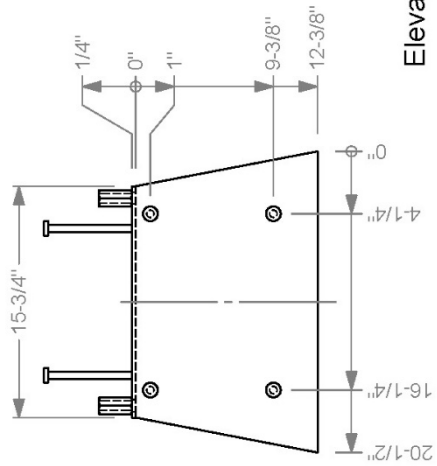
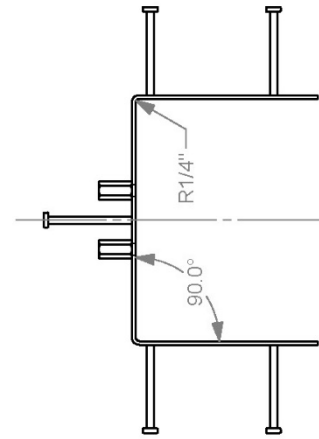
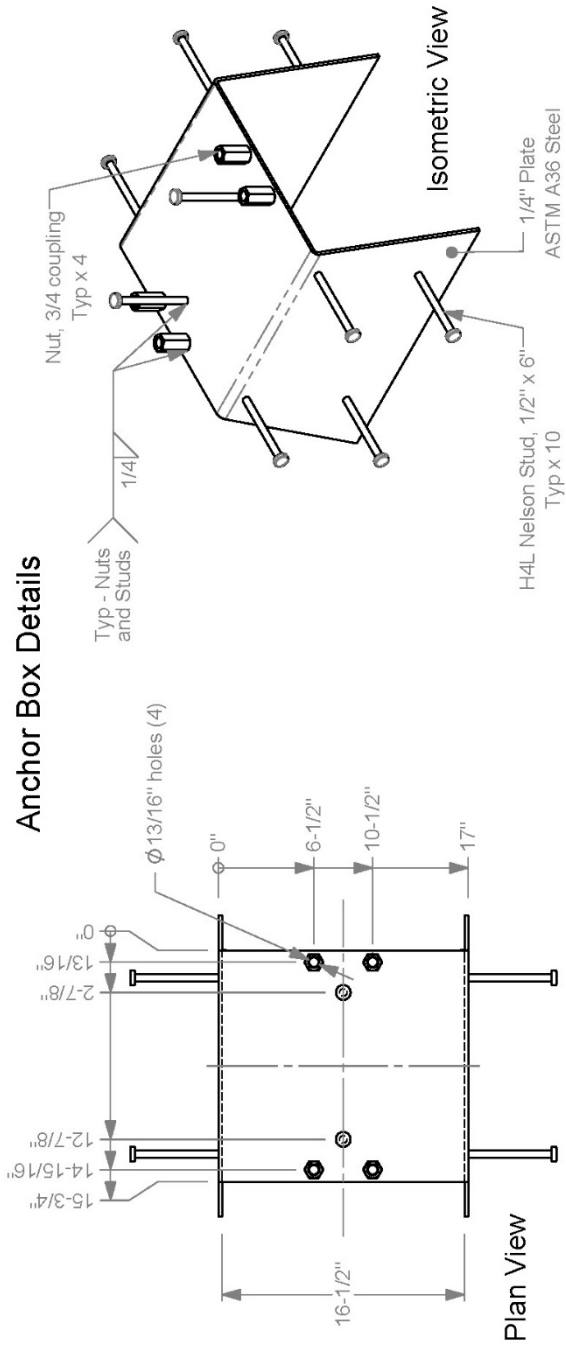
Pad

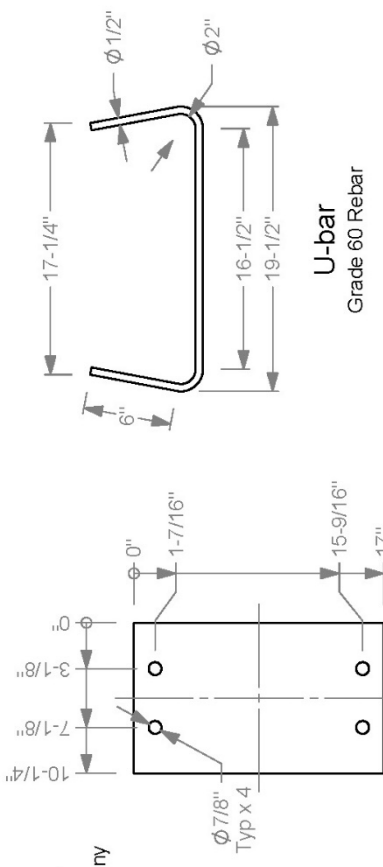
Hilti Screw Anchor KH-EZ
5/8" x 6-1/2", with USS Flat Washer
Four at each Fender. Install according to manufactures instructions

U-bar

Shear fender

Anchor Box Details

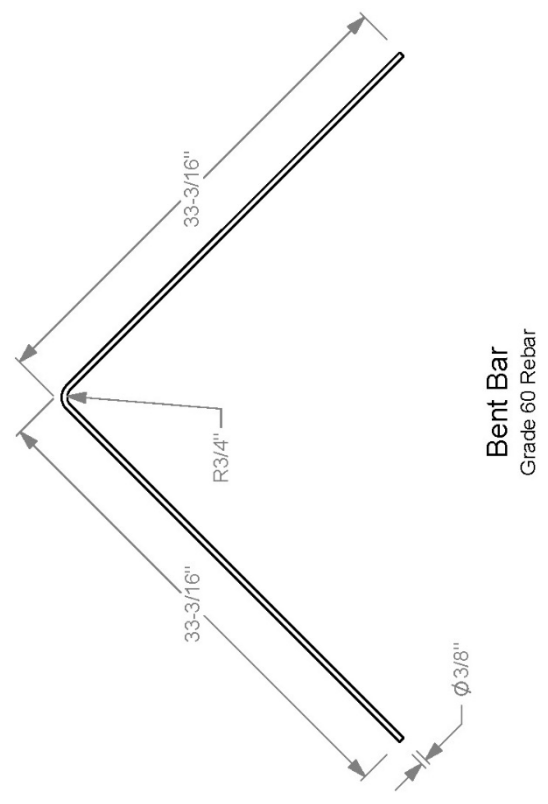




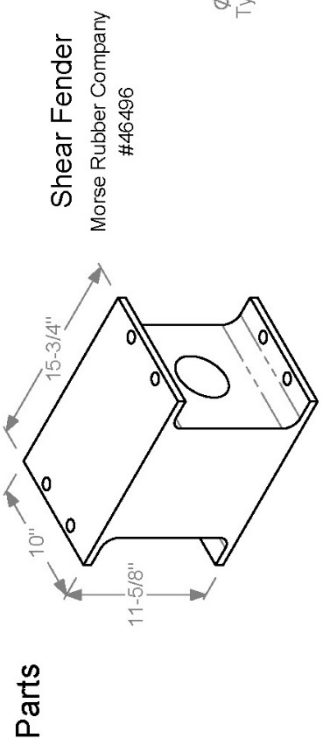
U-bar
Grade 60 Rebar

Pad

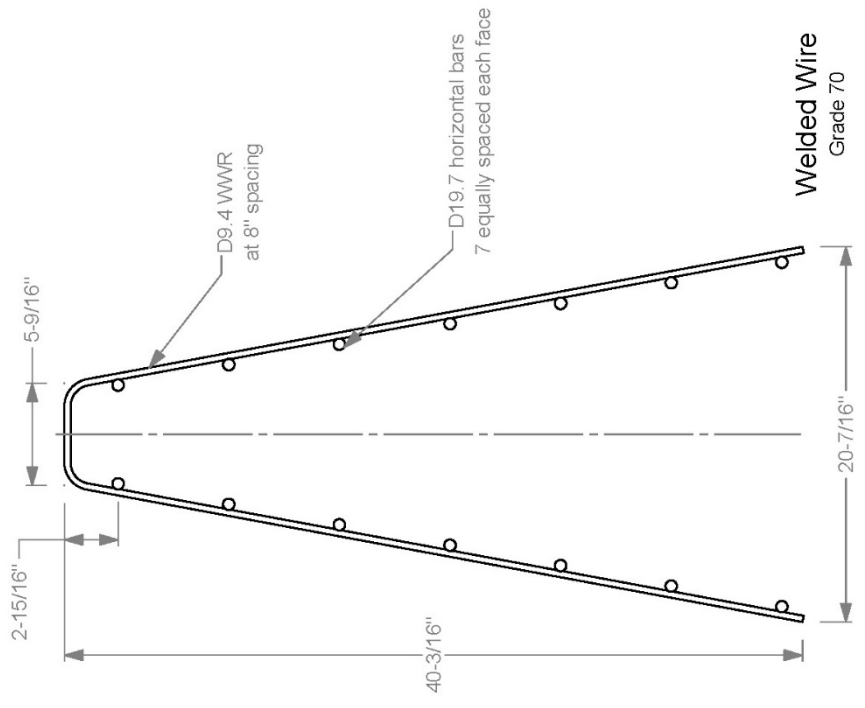
17" x 10 1/4" x 1/2"
PE High Density



Bent Bar
Grade 60 Rebar



Shear Fender
Morse Rubber Company
#46496



Welded Wire
Grade 70